

Identification and characterization of sperm-specific components required
for female meiosis in *C. elegans*

by

Rudra Prasanna Banerjee

A thesis submitted in partial fulfillment of the requirements for the degree of

Doctor of Philosophy
in
Molecular Biology and Genetics

Department of Biological Sciences
University of Alberta

© Rudra Prasanna Banerjee, 2022

Abstract

In most sexually reproducing animals, sperm entry provides the signal to initiate the final stages of female meiosis. The molecular mechanism of this process is still unclear. In *C. elegans*, three maternally-expressed paralogs, *memi-1*, 2 and 3 (meiosis-to-mitosis) are required for sensing sperm entry. Loss of all three paralogs results in a skipped meiosis II (MII) phenotype. In contrast, a hypermorphic mutation, *memi-1(sb41ts)*, results in embryonic lethality, whereby fertilized cells enter MII but are unable to exit MII properly. A previous genome-wide RNAi screen for suppressors of *memi-1(sb41)* lethality revealed two genes that encode sperm-specific PP1 phosphatases, *gsp-3* and *gsp-4*. Further EMS-based suppressor screening recovered alleles of *gsp-4* and additional genes in this pathway. One of the genes, *gskl-1*, encodes a putative GSK-3 protein kinase. Work presented in this thesis reveals that *gskl-1* is functionally redundant with another GSK-3-encoding gene, *gskl-2*, and that double mutants exhibit a range of defects, including paternal-effect embryonic lethality, abnormal sister chromatid segregation during male meiosis, and defective spermatid budding. Furthermore, sperm produced from double-mutant males exhibited defects in motility and pseudopod treadmilling. Indirect immunofluorescence experiments showed that GSKL-1 and GSKL-2 locate to the pseudopod region of activated sperm, indicating that they could play a role in regulating the dynamics of the cytoskeletal polymer, major sperm protein (MSP), possibly by phosphorylating MSP at the tip of the pseudopod. *gskl-1 gskl-2* double-mutant hermaphrodites also exhibited embryonic lethality with incomplete penetrance. Defective embryos exhibited normal MI, but MII

spindle assembly was delayed, and the second polar body failed to extrude. In addition to the double mutant phenotypes, a *gskl-1 gskl-2 gsp-4* triple mutant exhibited an increase in embryonic lethality, and some embryos displayed a skipped female MII phenotype, which is similar to *memi-1/2/3(RNAi)*. Together, this work affirms that GSK-3 kinases and PP1 phosphatases perform some similar functions with respect to sperm motility and meiosis, and that these enzymes work together for post-fertilization functions involving MEMI.

Preface

The results presented in Chapter 4 and the Appendix of this thesis are original work and have not been previously published.

The background work of the results presented in Chapter 3 was done, in part, by Jens Herzog and previously published as Jens Herzog, 2018. Shreyosi Bose and Ish Jain were involved in making the strain *mbk-2::abc56 memi-1(sb41)* which was used to generate data in Figure 3.5. The results are presented herein with permission.

Dedication

To my former mentors, Prof. Sudhansu Kumar Ghosal and Prof. Tapas Deb who inspired me to do research in Genetics.

To my family and friends, especially my grandfathers whom I lost during this journey.

Acknowledgements

I would like to extend my heartfelt gratitude to my supervisor Prof. Martin Srayko. Without his relentless guidance and tremendous support, I wouldn't have been able to successfully navigate through the trying times of my Ph.D. It was indeed one of the best phases of my life to work under his supervision. If I am able to set up my own lab someday, I will try my best to establish the kind of bond and understanding I had with Martin with my students.

I was fortunate enough to have Prof. Shelagh Campbell and Prof. David Stuart as my committee members. Their insightful comments and constructive feedback during the committee meetings guided me in my research and helped me design my experiments thoroughly.

I also want to express my sincere thanks to all my lab mates for their constant support throughout this journey. It would have been impossible to complete this journey without their encouragement and support.

Contents

1. Introduction	1
1.1 A brief history of our conception of sexual reproduction	1
1.2 The fusion of the products of meiosis give rise to the zygote.....	2
1.2.1 Sperm activation	2
1.2.2 Sperm-oocyte interactions	3
1.2.3 Egg activation	4
1.3 <i>C. elegans</i> – an excellent model to study fertilization <i>in vivo</i>	5
1.4 Spermatogenesis in <i>C. elegans</i>	9
1.4.1 Overview.....	9
1.4.2 Regulation of MSP distribution in the FB-MO complex	11
1.4.3 Post-meiotic sperm activation	14
1.4.4 Sex-specific sperm activation	17
1.4.5 Phosphorylation signalling during sperm activation in <i>C. elegans</i>	18
1.5 Oocyte meiotic maturation in <i>C. elegans</i>	20
1.5.1 Oocyte growth and development	20
1.5.2 Oocyte meiotic maturation and MSP signalling.....	22
1.5.3 Ovulation.....	25
1.6 Fertilization in <i>C. elegans</i>	27
1.6.1 Female meiotic spindle assembly	28
1.6.2 Chromosome segregation during female meiosis	30
1.6.3 Degradation of different proteins.....	32
1.7 The MEMI pathway	33
1.7.1 EMS screen to identify suppressors of <i>memi-1(sb41)</i>	35
1.8 The role of GSK-3 and PP1 phosphatases in fertilization	37
1.9 Goal of the thesis	39
1.10 Summary of the thesis	40
2. Materials and methods	42
2.1 <i>Caenorhabditis elegans</i> nomenclature	42
2.2 Strains and Maintenance	43
2.2.1 Maintenance	43

2.2.2 Mating Strategies	43
2.2.3 Making of Strains	45
2.2.5 Freezing Strains	49
2.3 PCR and Sequencing	50
2.3.1 Worm Lysis	50
2.3.2 PCR reaction	50
2.3.3 Preparation of sequencing sample	51
2.4 RNAi by feeding	52
2.5 Embryonic viability assays	53
2.6 Testing paternal-effect embryonic lethality	54
2.7. Preparation of agarose pads for <i>C. elegans</i> microinjection	54
2.8. Sperm migration assay	55
2.9 Pseudopod treadmilling rate analysis	56
2.10 <i>In vitro</i> sperm activation	57
2.11 Live imaging of male meiosis	58
2.12 CRISPR-Cas9 mediated gene editing	58
2.12.1 Identifying PAM sites	60
2.12.2 Designing crRNA	60
2.12.3 CRISPR tracrRNA	61
2.12.4 <i>In vitro</i> Cas9 digestion assay	61
2.12.5 Preparing Repair Templates	62
2.12.5.1 Preparing GFP repair template	63
2.12.5.2 Preparing repair templates for small tags	64
2.12.5.3 Preparing repair templates for creating point mutations	67
2.12.6 Making injecting cocktails	68
2.12.7 Injecting worms	68
2.12.8 Screening injected worms	69
2.12.9 Screening for edits	69
2.12.10 Isolating homozygous worm strains	70
2.13. Immunostaining	71
2.13.1 Troubleshooting Secondary antibody for false positive staining	72
2.14 Western Blotting	73

2.14.1 Preparation of sample.....	74
2.14.2 Western Blot.....	74
2.14.3 Standardization of antibodies.....	75
2.14.4 Visualizing proteins after Western blotting.....	77
2.15 <i>In utero</i> confocal imaging.....	77
2.16 Statistical analysis.....	78
3. Identification of suppressors of embryonic lethality of <i>memi-1(sb41)</i>	79
3.1 Identification of suppressor loci.....	79
3.2 <i>gsp-3</i> and <i>gsp-4</i> suppress <i>memi-1(sb41)</i> embryonic lethality.....	79
3.3 <i>gskl-1</i> suppresses <i>memi-1(sb41)</i> embryonic lethality.....	81
3.4 Towards the identification of extragenic suppressors of <i>memi-1(sb41)</i>	82
3.4.1 <i>smz-1</i> suppresses <i>memi-1(sb41)</i> embryonic lethality.....	83
3.4.2 <i>frm-8</i> is identified as a suppressor of <i>memi-1(sb41)</i> embryonic lethality.....	84
3.4.3 <i>mbk-2</i> is identified as a suppressor of <i>memi-1(sb41)</i> embryonic lethality.....	86
3.4.5 Testing candidate genes to identify the suppressor mutation <i>abc36</i>	89
3.5 Uncharacterized suppressors.....	91
3.6 Evidence for a paternal basis for suppression of <i>memi-1(sb41)</i>	91
3.7 Summary.....	92
4. Functional characterization of <i>gskl-1</i>	94
4.1 Genetic analysis of <i>gskl-1</i> suppressor alleles.....	94
4.2 <i>gskl-1</i> mutants are superficially wild-type.....	98
4.3 <i>gskl-1</i> mutant males are fertile.....	100
4.4 An RNAi-based approach to assess the function of <i>gskl-1</i>	102
4.5 Using <i>rrf-1</i> mutant background to test <i>gskl-1(RNAi)</i>	105
4.6. <i>gskl-1</i> is functionally redundant with <i>gskl-2</i>	107
4.7 <i>gskl-1 gskl-2</i> mutants exhibit paternal-effect embryonic lethality.....	112
4.8 <i>gskl-1</i> and <i>gskl-2</i> are not part of the <i>spe-8</i> pathway.....	115
4.9 <i>gskl-1</i> and <i>gskl-2</i> are required for efficient sperm migration.....	119
4.10 <i>gskl-1</i> and <i>gskl-2</i> are required for pseudopod formation and treadmilling....	120
4.11 Tagging <i>gskl-1</i> and <i>gskl-2</i> by CRISPR-cas9.....	123

4.12 <i>gskl-1</i> and <i>gskl-2</i> are expressed only in masculinized, but not feminized, worms	129
4.13 <i>gskl-1</i> and <i>gskl-2</i> are expressed in the male germline	130
4.14 GSKL-1 and GSKL-2 localize to the pseudopod in spermatozoa	131
4.15 <i>gskl-1</i> and <i>gskl-2</i> are not required for MO-MSP distribution during sperm activation.....	134
4.16 <i>gskl-1</i> and <i>gskl-2</i> are required for sister chromatid segregation and spermatid budding during male meiosis	135
4.17 <i>gskl-1</i> and <i>gskl-2</i> are required for female meiosis II	137
4.18 <i>gskl-1</i> and <i>gskl-2</i> genetically interact with <i>gsp-3/4</i> to regulate female meiosis II through the MEMI pathway	142
4.19 Summary	147
5. Discussion	148
5.1 Sperm-specific suppressors of <i>memi-1(sb41)</i>	148
5.2 Summary of sperm phenotypes associated with loss of <i>gskl-1</i> and <i>gskl-2</i>	152
5.3 <i>gskl-1</i> and <i>gskl-2</i> expression are specific to the male germline	155
5.4 The role of <i>gskl-1</i> and <i>gskl-2</i> in sperm meiosis.....	156
5.5 The role of <i>gskl-1</i> and <i>gskl-2</i> in MSP treadmilling in activated sperm	161
5.6 Testing <i>gskl-1</i> and <i>gskl-2</i> for their role in the <i>spe-8</i> pathway	164
5.7 A possible role for <i>gskl-1/gskl-2</i> during oocyte progression through the spermatheca	165
5.8 <i>gskl-1</i> and <i>gskl-2</i> are required to complete female meiosis II after fertilization	168
5.9 <i>gsp-4</i> and <i>gskl-1/gskl-2</i> work together to activate the <i>memi</i> pathway	171
References	176
Appendix	210

List of Tables

2.1: List of strains	45
4.1: Average brood size of different double-deletion combinations	109
4.2: Average brood size and percentage of dead eggs of <i>fog-2</i> hermaphrodites during en masse mating at 20°C	114
4.3 Average brood size and percentage of dead eggs of <i>fog-2</i> hermaphrodites during single male mating at 20°C.....	118
4.4: Summary of crispr injections to tag <i>gskl-1</i> with <i>gfp</i> at the 5' end.....	124
4.5: Summary of Crispr injection to tag <i>gskl-1</i> with <i>3xFLAG</i> on its 5' end.....	125
4.6: Summary of Crispr injection to tag <i>gskl-2</i> with <i>Ollas</i> on its 5' end.....	127
5.1: Summary of phenotypes displayed by <i>gskl-2(Δ); gskl-1(Δ)</i> male sperm.....	153
5.2: Summary of the phenotypes displayed by <i>gskl-2(Δ); gskl-1(Δ)</i> embryos.....	154

List of Figures

1.1: Schematic diagram of a hermaphrodite <i>C. elegans</i>	7
1.2: A schematic diagram of a single-arm of wild type male gonad	8
1.3: Schematic representation of functions of different <i>spe</i> genes in spermatogenesis and in fertilization	14
1.4: Schematic diagram of sperm activation in <i>C. elegans</i>	16
1.5: Schematic diagram showing oocyte meiotic maturation and the point of fertilization	23
1.6: Schematic diagram representing ovulation	26
1.7: Schematic representation of The MEMI pathway	34
1.8: Average percent embryonic viability from wild type, <i>memi-1(sb41)</i> and 16 suppressor strains at 25°C	36
2.1: Schematic representation of making <i>gskl-2(Δ); gskl-1(Δ)</i> strain	46
2.2: Schematic representation of the genetic cross to recover the <i>abc57</i> suppressor alleles after outcrossing.....	49
2.3: Schematic diagram of making agarose pad	55
2.4: Schematic diagram showing how pseudopod treadmilling rates were calculated	57
2.5: <i>In vitro</i> Cas9 digestion assay	62
2.6: Schematic representation of designing repair template to tag <i>gskl-1</i> with <i>gfp</i> at 5 prime end	64
2.7: Schematic representation of designing repair template to tag <i>gskl-1</i> with 3x <i>flag</i> at 5 prime end	65
2.8: Schematic representation of designing repair template to tag <i>gskl-2</i> with <i>Ollas</i> at 5 prime end	66
2.9: Schematic representation of designing repair template to create C821T point mutation on <i>mbk-2</i>	67
2.10: Schematic representation of the overview of CRISPR-Cas9 technique	70
2.11: False Positive signal from goat anti-rat antibody	72

2.12: Testing Alexa 488 goat anti-rat antibody.....	73
2.13: Testing F1804 FLAG antibody	76
3.1: <i>gsp-4</i> (Δ) and <i>gsp-3</i> (Δ) suppress <i>memi-1(sb41)</i> embryonic lethality at 25°C.....	80
3.2: <i>gskl-1</i> (Δ) suppresses <i>memi-1(sb41)</i> embryonic lethality at 25°C.....	82
3.3: <i>smz-1</i> (Δ) male suppresses MEL of <i>memi-1(sb41)</i> at 25°C.....	84
3.4: <i>frm-8</i> (Δ) male suppresses MEL of <i>memi-1(sb41)</i> at 25°C	86
3.5: <i>abc56</i> causes a missense mutation (A274V) in an evolutionary conserved Alanine residue in the MBK-2	88
3.6: <i>mbk-2::abc56</i> suppresses MEL of <i>memi-1(sb41)</i> at 25°C	88
3.7: Average percent embryonic viability of <i>ceh-18</i> (Δ)/+; +/- <i>memi-1(sb41)</i> trans heterozygous worms	90
3.8: Evidence for a paternal basis for suppression of <i>memi1(sb41)</i>	92
4.1: <i>gskl-1</i> sequence with the suppressor mutations	96
4.2: Amino acid sequence of GSKL-1	96
4.3: <i>abc59</i> resulted to a change in evolutionary conserved region of GSK-3	96
4.4: Average percent embryonic viability of <i>gskl-1(abc57)</i> and <i>gskl-1(abc41)</i> with <i>memi-1(sb41)</i>	97
4.5: Average brood size from wild type, <i>gskl-1(abc41)</i> , <i>gskl-1(abc51)</i> , <i>gskl-1(abc57)</i> and <i>gskl-1(abc59)</i> at 20°C	99
4.6: Embryonic viability from wild type, <i>gskl-1(abc41)</i> , <i>gskl-1(abc51)</i> , <i>gskl-1(abc57)</i> and <i>gskl-1(abc59)</i> at 20°C	99
4.7: Number of outcross males produced by suppressor <i>abc57</i>	101
4.8: Suppression of embryonic lethality <i>memi-1(sb41)</i> by <i>gskl-1(RNAi)</i>	103
4.9: Quantification of brood size of <i>gskl-1(abc57)</i> worms on RNAi feeding of uncharacterized members of the <i>gsk-3</i> family	104
4.10: Quantification of brood size of <i>gskl-1(abc41)</i> worms on RNAi feeding of uncharacterized members of <i>gsk-3</i> family	105
4.11: Quantification of brood size of <i>rrf-1</i> mutant worms on <i>gskl-1(RNAi)</i>	106
4.12: Quantification of brood size from wild type, <i>gskl-1</i> (Δ), <i>gskl-2</i> (Δ), <i>C44H4.6</i> (Δ), <i>Y106G6D.4</i> (Δ), <i>Y106G6E.1</i> (Δ), <i>F21F3.2</i> (Δ).....	107

4.13: <i>gskl-2</i> (Δ); <i>gskl-1</i> (Δ) displayed embryonic lethality	108
4.14: <i>gskl-2</i> suppresses embryonic lethality of <i>memi-1</i> (<i>sb41</i>) at 25°C	110
4.15: <i>gsk-3</i> (Δ) did not enhance the embryonic lethality of <i>gskl-2</i> (Δ); <i>gskl-1</i> (Δ) at 20°C	111
4.16: Embryonic lethality of <i>gskl-2</i> (Δ); <i>gskl-1</i> (Δ) was rescued by mating with wild-type males	113
4.17: Significant embryonic lethality is observed by mating <i>gskl-2</i> (Δ); <i>gskl-1</i> (Δ) males to <i>fog-2</i> (<i>q71</i>) hermaphrodites at 20°C	114
4.18: <i>spe-6</i> does not suppress the embryonic lethality of <i>gskl-2</i> (Δ); <i>gskl-1</i> (Δ) at 20°C.....	116
4.19: Embryonic lethality of <i>gskl-2</i> (Δ); <i>gskl-1</i> (Δ) hermaphrodite is rescued by mating <i>gskl-2</i> (Δ); <i>gskl-1</i> (Δ) males at 20°C	117
4.20: Significant embryonic lethality is observed by mating <i>gskl-2</i> (Δ); <i>gskl-1</i> (Δ) males to <i>fog-2</i> (<i>q71</i>) hermaphrodites at 20°C	118
4.21: DIC and fluorescence images of wild type hermaphrodites after mating to mCherry labelled wild type or <i>gskl-2</i> ; <i>gskl-1</i> males at 20°C	119
4.22: Time-lapse images of pseudopod treadmilling	120
4.23: <i>gskl-2</i> (Δ); <i>gskl-1</i> (Δ) caused a decrease in pseudopod treadmilling rates.....	121
4.24: <i>gskl-2</i> (Δ); <i>gskl-1</i> (Δ) caused a delay in sperm activation	122
4.25: Time-lapse images of different stages of male sperm activation with Pronase	123
4.26: 3xFLAG:: <i>gskl-1</i> displayed no decrease in brood size	126
4.27: 3xFLAG:: <i>gskl-1</i> males did not suppress embryonic lethality of <i>memi-1</i> (<i>sb41</i>) at 25°C	126
4.28: <i>Ollas</i> :: <i>gskl-2</i> displayed no decrease in brood size	128
4.29: <i>Ollas</i> :: <i>gskl-2</i> males did not suppress embryonic lethality of <i>memi-1</i> (<i>sb41</i>) at 25°C	128
4.30: GSKL-1 and GSKL-2 were detected only in sperm enrich worms	130

4.31: Immunostaining of endogenously tagged FLAG::GSKL-1 and Ollas::GSKL-2 in gonads of dissected males	131
4.32: Immunostaining of endogenously Flag tagged FLAG::GSKL-1 in inactive and active sperm	133
4.33: Immunostaining of endogenously Ollas tagged OLLAS::GSKL-1 in inactive and active sperm	134
4.34: Immunostaining to show MO-MSP distribution in wild type and <i>gskl-2</i> (Δ); <i>gskl-1</i> (Δ) worms	135
4.35: DIC and DAPI images of wild-type and <i>gskl-2</i> (Δ); <i>gskl-1</i> (Δ) male spermatids.....	136
4.36: Time-lapse images of Wild type and <i>gskl-2</i> ; <i>gskl-1</i> male spermatocytes expressing mCherry-histone and GFP-tubulin	137
4.37: <i>gskl-2</i> (Δ); <i>gskl-1</i> (Δ) embryos exhibit a delay from the beginning of anaphase I to metaphase II	139
4.38: <i>gskl-2</i> (Δ); <i>gskl-1</i> (Δ) embryos displayed defects in meiosis II	140
4.39: <i>gskl-2</i> (Δ); <i>gskl-1</i> (Δ) embryos displayed broken oocyte phenotypes	141
4.40: <i>gskl-1</i> and <i>gsp-4</i> genetically interact as the double-deletion combinations results in embryonic lethality	142
4.41: <i>gsp-4</i> and <i>gskl-1</i> suppress <i>memi-1</i> (<i>sb41</i>) individually and in combination	144
4.42: <i>gskl-1</i> , <i>gskl-2</i> and <i>gsp-4</i> genetically interact	145
4.43 <i>gsp-4</i> <i>gskl-2</i> ; <i>gskl-1</i> embryos displayed meiotic defects	146
5.1: A proposed model explaining how sperm-specific suppressors could rescue the embryonic lethality of <i>mem-1</i> (<i>sb41</i>)	151
5.2: Schematic representation of sperm meiosis chromosome segregation defects caused by <i>gskl-1/gskl-2</i> , <i>gsp-3/4</i> , <i>top-2</i> and <i>emb-27</i>	160
5.3: A model for GSK3 function in sperm motility and the post-fertilization signal for female meiosis II.....	174

List of Symbols, Abbreviations and Nomenclature

°C	Degrees Celsius
ABHD	α/β hydroxylase domain containing protein
2AG	2-arachidonoylglycerol
APC	Anaphase promoting complex
AIR	Aurora/Ipl1-related serine/threonine kinase
ATP	Adenosine triphosphate
BP	Base pair
CDK	Cyclin-dependent kinase
CRISPR	Clustered Regularly Interspaced Short Palindromic Repeats
crRNA	CRISPR ribonucleic acid
CUL	Cullin
DAG	Diacylglycerol
DAPI	4',6-diamidino-2-phenylindole
DIC	Differential interference contrast
DNA	Deoxyribonucleic acid
DNC	Dynactin domain-containing protein
DNTP	Deoxynucleotide triphosphate
DPY	Dumpy
DTC	Distal tip cell
EGF	Epidermal growth factor
ELC	Elongin C
EMB	Abnormal embryogenesis
EPH	Erythropoietin-producing human hepatocellular receptors
ERK	Extracellular-signal-regulated kinase
F1	First filial generation

FB	Fibrous bodies
FER	Fertilization defective
FLN	Filamin
GDP	Guanine diphosphate
GFP	Green fluorescent protein
GSK	Glycogen synthase kinase
GSKL	Glycogen synthase kinase -3 like
GSP	Glc-seven-like phosphatase
GTP	Guanosine triphosphate
GLD	Defective in germline development
GPCR	G-protein-coupled receptor
HEPES	4-(2-hydroxyethyl)-1-piperazineethanesulfonic acid
HORMA	<u>H</u> op1p <u>R</u> ev7p <u>M</u> ad2 protein containing domain
HTP	Hydroxytryptophan
IP3	Inositol triphosphate
IPTG	isopropyl β -D-1-thiogalactopyranoside
L1	Larval instar stage 1
L4	Larval instar stage 4
LAB	Long arm of bivalent
LB	Luria Bertani broth
LG	Linkage group associated with a particular chromosome
MAPK	Mitogen-activated protein kinase
MAS	Martin A. Srayko (lab designation for <i>C. elegans</i> strain)
MBK	Mini brain kinase
MEI	Defective meiosis
MEMI	Meiosis-to-mitosis
MEL	Maternal effect embryonic lethal

MEX	Muscle excess
MFP	MSP fiber protein
mRNA	Messenger ribonucleic acid
MSP	Major sperm protein
MTOC	Microtubule-organizing center
MO	Membranous organelles
MPAK	MSP polymerization-activating kinase
MPOP	MSP polymerization organizing protein
NGM	Nematode growth medium
OMA	Oocyte maturation defective
P0	Parental generation
PAM	Protospacer adjacent motif
PBS	Phosphate-buffered saline
PCR	Polymerase chain reaction
PEL	Paternal effect embryonic lethal
PIEZO	Piezo type mechanosensitive ion channel component
PLK	Polo-like kinase
PP1	Protein phosphatase 1
PP2A	Protein phosphatase 2 A
PTEN	Phosphatase and tensin homolog
RAS	Rat sarcoma virus
RCC	Regulator of chromosome condensation
RE	Restriction enzyme
REC	Recombination defective
RNA	Ribonucleic acid
RNAi	Ribonucleic acid interference
ROL	Roller

ROS	Reactive oxygen species
SC	Synaptonemal complex
SDS-PAGE	Sodium dodecyl sulfate polyacrylamide gel electrophoresis
SM	Sperm media
SMC	Structural maintenance of chromosome
SKP	Ski interacting protein
Sp	Spermatheca
Spe	Spermatogenesis defective
SH	Src Homology
TAF	TATA-binding protein associated factor
TBST	Tris buffered saline tween 20
TEA	Triethanolamine
TEMED	Tetramethylethylenediamine
TPXL	Targeting protein for xenopus Klp-2 like
TRACR	Trans-activating crispr RNA
TRP	Transient receptor potential
TRY	TRYpsin-like protease
UT	Uterus
VAB	Variable abnormal morphology
WT	Wild-type
ZYG	Zygote defective
ZP	Zona pellucida

1. Introduction

1.1 A brief history of our conception of sexual reproduction

One of the most fundamental questions regarding life itself is how organisms reproduce. The great Greek physician Hippocrates (460 – 370 BCE) believed that semen of men and factor of women mixed inside the uterus to form the embryo. Later, the great Greek philosopher Aristotle (384 – 322 BCE) gave more credit to men for forming an embryo. This male-centric view was dominant until William Harvey, in the seventeenth century, proposed his “ex ovo omnia” theory, or “everything from the egg” (Harvey and animals. 1981). Jan van Horne, Jan Swammerdam, Neils Stensen, Regner de Graaf and Francesco Redi were other notable scientists during this time who were also in favour of this female-centric view (Lopata 2009). This female-centric view of fertilization changed again when Antonii van Leeuwenhoek discovered spermatozoa (Leeuwenhoek 1677). In many animals, fertilization of the female gamete occurs within the organism, therefore, mammalian eggs were not implicated in procreation until these cells were first viewed under the microscope in the early nineteenth century, by Karl Ernst von Baer (Baer 1827). Other notable scientists during that time, namely, Matthias Jakob Schleiden and Theodor Schwann hypothesized that the sperm and egg are both cells (Schleiden 1838; Schwann 1839). The discovery of sperm and egg fostered the logical proposal that both sperm and egg could contribute to form an embryo. Finally in 1876, Oscar Hertwig made his ground-breaking discovery that the nuclei of sperm and egg fuse during fertilization of sea urchins (Hertwig 1876).

This was the first experimental evidence to prove that both sperm and egg are essential components of fertilization, providing the genetic basis of new life.

1.2 The fusion of the products of meiosis give rise to the zygote

In sexual reproduction, the male provides the haploid sperm (n), and the female provides the haploid oocyte (n). These two highly specialized gametes unite upon fertilization to form the diploid zygote ($2n$). Fertilization is a multi-step process and, in mammals, it can be divided into three major steps: sperm activation in the female reproductive tract, sperm-egg association, and egg activation.

1.2.1 Sperm activation

In humans, millions of sperm are ejaculated into the female reproductive tract during sexual intercourse. Inside the female reproductive tract, sperm undergo a maturation process to become competent to fertilize the egg. This final sperm maturation process in the female reproductive tract is known as capacitation. Capacitation is accompanied by many changes in the spermatozoa. These changes include the loss of cholesterol from the sperm plasma membrane, increased tyrosine phosphorylation within the sheath cells of the sperm tail, increased intracellular cyclic adenosine monophosphate (cAMP) and reactive oxygen species (ROS), and changes in the expression of different receptor proteins on the sperm plasma membrane (Aitken and Nixon 2013). Also, flagellar movement of sperm dramatically changes from a low amplitude symmetric beat to a short asymmetric beat. This transformation of the sperm

motility is known as hyperactivation that makes the sperm competent for fertilization (Trebichalská and Holubcová 2020). The underlying molecular mechanism of capacitation is not clearly understood; however, the role of the cation channel of sperm (CatSper) in Ca^{2+} signalling during hyperactivation of sperm is well established. CatSper is a sperm-specific, pH-sensitive and low voltage-dependent cation channel that is composed of four pore-forming subunits and five accessory subunits (Sun et al. 2017). In humans, the female hormone progesterone was shown to induce the hyperactivation of human sperm. Progesterone binds with the α/β hydroxylase domain containing protein 2 (ABHD2) on the sperm and then ABHD2 degrades 2-arachidonoylglycerol (2AG) on the sperm membrane (Miller et al. 2016). The degradation of AG2 leads to CatSper opening and the subsequent hyperactivation of sperm. This progesterone-mediated CatSper activation is not conserved among species, however, as experiments showed that progesterone is unable to hyperactivate mouse sperm (Lishko et al. 2011).

1.2.2 Sperm-oocyte interactions

Scientists have been trying to decipher the molecular mechanism of sperm-to-oocyte interactions over the last four decades (Alexandre 2001; Clift and Schuh 2013). Early studies have shown that the extracellular coat that surrounds the mammalian egg, the zona pellucida (ZP) contains a few glycoproteins, namely ZP1 to ZP3 in mice and ZP1 to ZP4 in humans, which are required for mammalian sperm-egg binding (Wassarman and Litscher 2008). ZP3 was initially proposed to be the primary receptor for sperm binding. However, it was later found that ZP3 alone is insufficient for sperm

binding (Rankin et al. 1998). Alternatively, it was predicted that all zona pellucida proteins were required to form the binding site of the sperm and cleavage of ZP2 after fertilization was also predicted to disrupt that proposed sperm binding site (Bleil et al. 1981; Dean 2004). This model was further solidified by the discovery of Ovastacin, a component of cortical granules that cleaves ZP2 after fertilization (Burkart et al. 2012). This study has shown that the sperm cannot bind to the 2-cell embryo isolated from wild type mice but can bind to the 2-cell embryo isolated from mice expressing non-cleavable ZP2. A decade ago, it was revealed that the majority of the zona pellucida glycoproteins ended with an attached Sialyl-LewisX tetrasaccharide (Wassarman and Litscher 2008). It was shown that an anti-Sialyl-LewisX antibody reduces the sperm-egg binding affinity *in vitro*. Although the sperm-egg interaction is not clearly understood, all studies to date suggest that the three-dimensional structure of the zona pellucida is important for initiating this process (Clark 2013).

1.2.3 Egg activation

In humans, the oocyte undergoes periodic changes in cytosolic Ca^{2+} concentration, commonly known as calcium oscillations, after the sperm fuses with the oocyte. The calcium oscillations lead to an egg activation process that is characterised by the release of the oocyte from the secondary arrest at metaphase II, selective degradation of maternal mRNAs, pronuclear development, and initiation of embryonic gene expression (Stricker 1999). This egg activation initiates the transition from the meiotic cell division program to the mitotic embryo. The polyspermy block is another important event that also occurs simultaneously during the fertilization. Attachment of the first

sperm to the oocyte membrane causes a rapid change in the membrane potential from negative to positive charge (Jaffe 1976). This huge change in the membrane potential prevents other sperm from attaching to the oocyte membrane. This process is known as the fast block to polyspermy. An alternative mechanism to the fast block to polyspermy proposes that after the first sperm binding, the remaining receptors in the oocyte are discharged from the egg membrane to the extracellular vesicles (Chalbi et al. 2014). Thus, no additional sperm can bind to the egg membrane once a single sperm enters the oocyte. Other than these events (Ca^{2+} wave and polyspermy block) it is not clear how the cell division program is specified in these cells.

In all sexually reproducing organisms, the oocyte is primarily arrested at the late prophase I and in mammals it takes several months to years to release from this arrest. In addition, it is also difficult to study this oocyte maturation process in a living organism. So, the molecular mechanism of the transition from unfertilized oocyte to developing zygote is largely unknown.

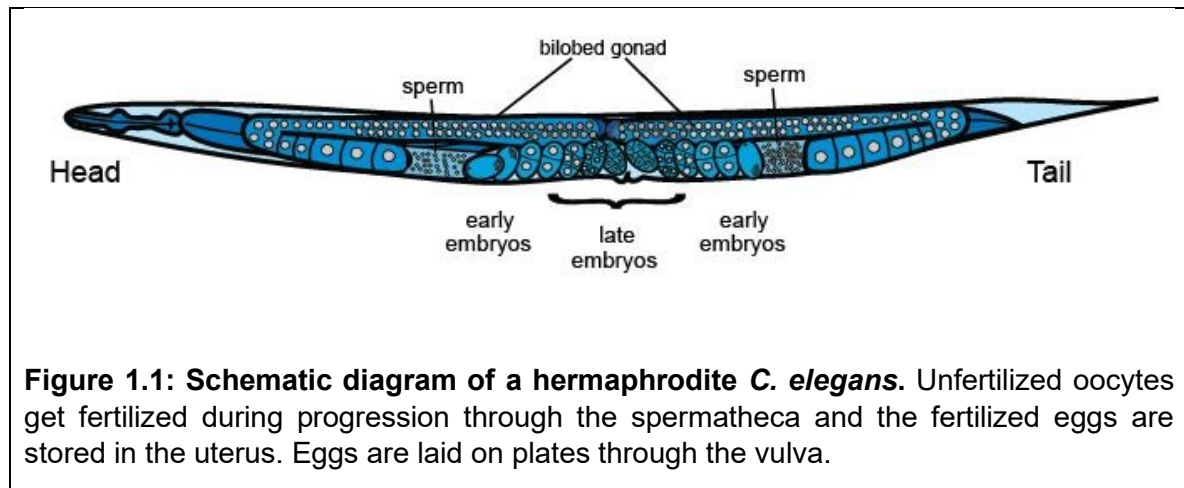
1.3 *C. elegans* – an excellent model to study fertilization *in vivo*

The challenges associated with studying complex cell and developmental processes *in vivo* became less daunting when Sydney Brenner introduced optically transparent *C. elegans* as a genetic model organism to the world in 1974 (Brenner 1974) (Figure 1.1). With respect to fertilization, *C. elegans* oocytes lack a zona pellucida and the sperm lack an acrosome, however, this system shares many features with mammalian counterparts, such as internal fertilization, sperm activation within the

reproductive tract, oocyte meiotic maturation, oocyte activation by sperm, mechanisms to prevent polyspermy, and degradation of selected maternal mRNAs (Marcello et al. 2013). Also, fertilization in *C. elegans* occurs within about one hour, and the gonad produces a fertilized embryo approximately every half hour, so the entire fertilization process can be viewed *in utero* through live-cell imaging. In addition, the worms are amenable to genetic manipulation and they have a relatively fast life cycle of 3 days. Furthermore, genome-wide loss-of-function approaches like RNAi-mediated interference and gene editing via CRISPR-Cas9 techniques allow the systematic examination of complex biological processes.

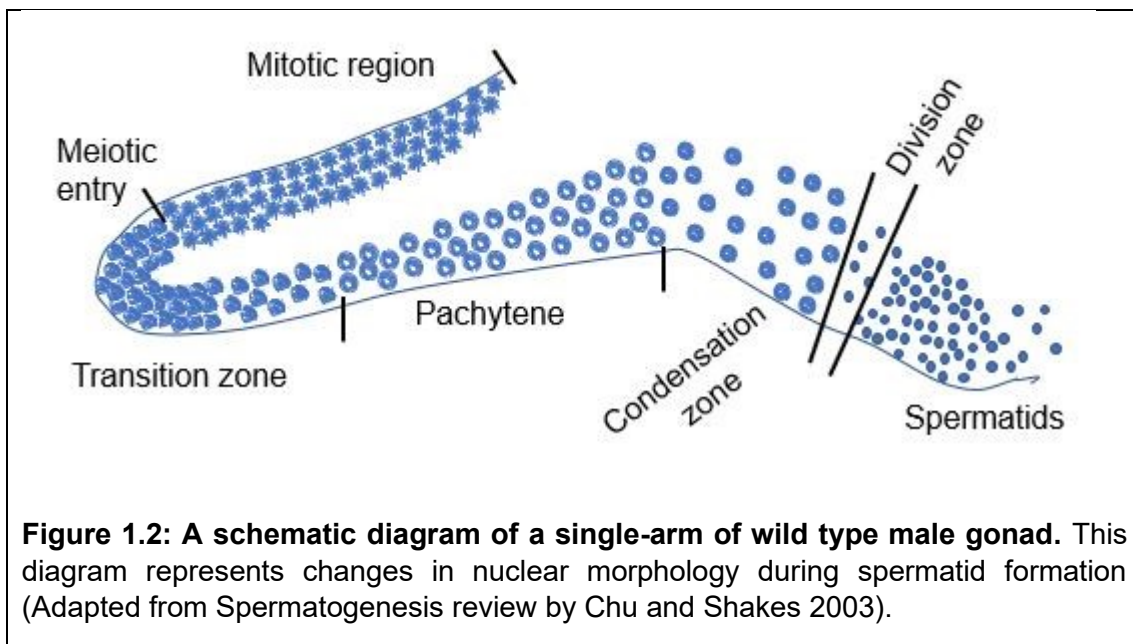
C. elegans has two sexual forms: male and hermaphrodite, which progress through four larval stages (L1 – L4) to become an adult. Worms can be maintained at 12°C to 25°C, whereby higher temperatures increase the developmental rate (Corsi et al. 2015). At 20°C, it takes approximately 72 hours for an adult worm to develop from the egg. Hermaphrodite and males have five pairs of autosomes, and sex in this model organism is determined by the X:A ratio; hermaphrodites have a pair of X chromosomes (XX) while males have only one X chromosome (X0) (Madl and Herman 1979; Zarkower 2006). Both males and hermaphrodites perform spermatogenesis during the L4 larval stage. After L4, hermaphrodite germ cells stop spermatogenesis and switch to oogenesis for the rest of their life, while males continue spermatogenesis. Hermaphrodites produce self-progeny using their own sperm; the vast majority of self-progeny are XX hermaphrodites, however a small fraction of males are also produced (0.1-0.2%) because of nondisjunction of the X chromosome (Hodgkin et al. 1979). If hermaphrodites mate with a male, the male sperm is preferentially used because the

larger male sperm gain an advantage by outcompeting smaller hermaphrodite sperm (LaMunyon and Ward 1998; Anderson et al. 2010). As a result of this highly efficient out-crossing system, successful matings are evident by the presence of 50% males in the progeny.



Males can be distinguished from the hermaphrodites by their flat fan-shaped tails. This distinct morphology is dependent on the activity of the transcription factor TRA-1, inactivation of which leads to male development (Hunter and Wood 1990). Hermaphrodites have two U-shaped gonads, consisting of germline nuclei that develop in the distal portion of the gonad and migrate towards the proximal region. During the L4 stage, nuclei in the proximal region mature into sperm and in the adult stage they develop into oocytes. The distal tip cell (DTC) plays an important role in controlling the production and maturation of germ cells (Kimble and White 1981; Cecchetelli and Cram 2017). The nuclei enter into the meiotic prophase stage upon reaching the transition zone and arrest briefly at the pachytene stage before proceeding to diplotene (Figure 1.2). During spermatogenesis, they exit from pachytene without any delay, but during

oogenesis they arrest for a second time in diakinesis. Activation of mitogen-activated protein kinase (MAPK) in both oocyte and sperm are important for the cells to exit from the pachytene arrest (Church et al. 1995). Sperms are stored inside a specialized sac in the proximal part of the gonad arm, known as the spermatheca. The mature oocytes travel through the spermatheca to get fertilized by the sperm and enter into the uterus. Young embryos complete the early stages of development within the uterus before they exit through the vulva.



Although *C. elegans* provides an excellent *in vivo* platform to study the entire fertilization process, it also presents some challenges for researchers. One of the major issues that makes it difficult to assess gene function in this system is that many genes exhibit functional redundancy. For example, a sperm specific protein, major sperm protein (MSP), is encoded by more than forty genes (Burke and Ward 1983; Klass et

al. 1984; Ward et al. 1988). That makes it difficult to genetically alter MSP to study its functions. Another potential drawback is that many metazoan genes are absent in *C. elegans* (Ruvkun and Hobert 1998). For example, Hedgehog signalling is required in vertebrates for the patterning of various organs but many genes in the Hedgehog signalling pathway are absent in *C. elegans* (Bürglin and Kuwabara 2006). Despite the lack of sequence conservation, however, there are many instances of functional conservation between distantly-related or seemingly unrelated proteins in *C. elegans* and other metazoans. For example, *tpxl-1* in *C. elegans* shares only limited homology with its vertebrate ortholog *tpx2* only in the N terminal region and it has been contested whether this protein is a bona fide TPX2 ortholog (Karsenti 2005). However, functional analyses indicated that this protein does perform functions in *C. elegans* that are similar to the vertebrate TPX2 counterpart, despite having only traces of similarity at the primary sequence level (Ozlu et al. 2005).

1.4 Spermatogenesis in *C. elegans*

1.4.1 Overview

Spermatogenesis may be defined as the process of making sperm from undifferentiated germ cells. In *C. elegans*, syncytial germ cells progress through the early stages of meiosis within the rachis, a central core of cytoplasm that bathes the germ-cell nuclei. As meiosis progresses, individual nuclei compartmentalize to form the primary spermatocyte cells. Primary spermatocytes become separated from the rachis to undergo two rounds of meiosis cell divisions. During meiosis I, homologous

chromosomes separate from each other and in meiosis II, sister chromatids separate from each other to form four haploid spermatids that bud off, leaving behind a central residual body. Cytoplasmic contents such as tubulin, actin, and ribosomes, all of which are not necessary for further physiological activities of sperm, are deposited into the residual body (Ward 1986; Machaca et al. 1996).

In all organisms, sperm cells undergo morphological changes during sperm activation, a process usually called spermiogenesis. In mammals, this morphological change is accompanied by sperm-specific transcription and translation (Freitas et al. 2016). In *C. elegans*, there is no detectable protein synthesis in mature spermatids because of the absence of ribosomes (Ward et al. 1983). Spermatids seem to possess all of the proteins required for motility and fertilization, and they employ a number of mechanisms to regulate the activity of these proteins. For example, the major sperm protein, MSP is the primary cytoskeletal subunit that is required for sperm motility. This protein can form dynamic polymers, but it is subjected to extensive regulation throughout spermatogenesis to control where and when this occurs. Fibrous bodies (FBs) and Membranous organelles (MOs) are two key components that help to properly assemble MSP in the spermatid and allow the spermatid to undergo morphological changes during sperm activation (Ward et al. 1981; Roberts et al. 1986). MOs form from the Golgi apparatus and FBs develop on the surface of MOs. This FB-MO complex can be visible during the late pachytene stage. On the other hand, MSP synthesis starts during mid pachytene stage and, towards the end of meiotic prophase it is sequestered inside the FBs. Assembly of MSP into FBs facilitates both FB growth and MSP sequestration. FB-MO complexes grow in size throughout the meiotic divisions, and

they are segregated into the budding spermatids during anaphase II. It was previously reported that when spermatids separate from the residual body, the membrane surrounding the FB retracts into the MO, and MSP contents depolymerize to disperse throughout the cytoplasm of the spermatid (Roberts et al. 1986; L'Hernault 2006). However, later observations revealed that some FBs are released from the MOs but they are not fully disassembled (Wu et al. 2012). This observation suggested that the disassembly of MSP from FBs and their distribution throughout the cytoplasm does not occur instantly when spermatids bud off from the residual body; rather, it is a gradual process that occurs during the sperm activation when MSP is polarized to form the pseudopod. Proper formation of the pseudopod is necessary for sperm motility. As *C. elegans* sperm has no actin like mammalian sperm, the sperm motility is entirely dependent on the dynamics of MSP in the pseudopod region.

1.4.2 Regulation of MSP distribution in the FB-MO complex

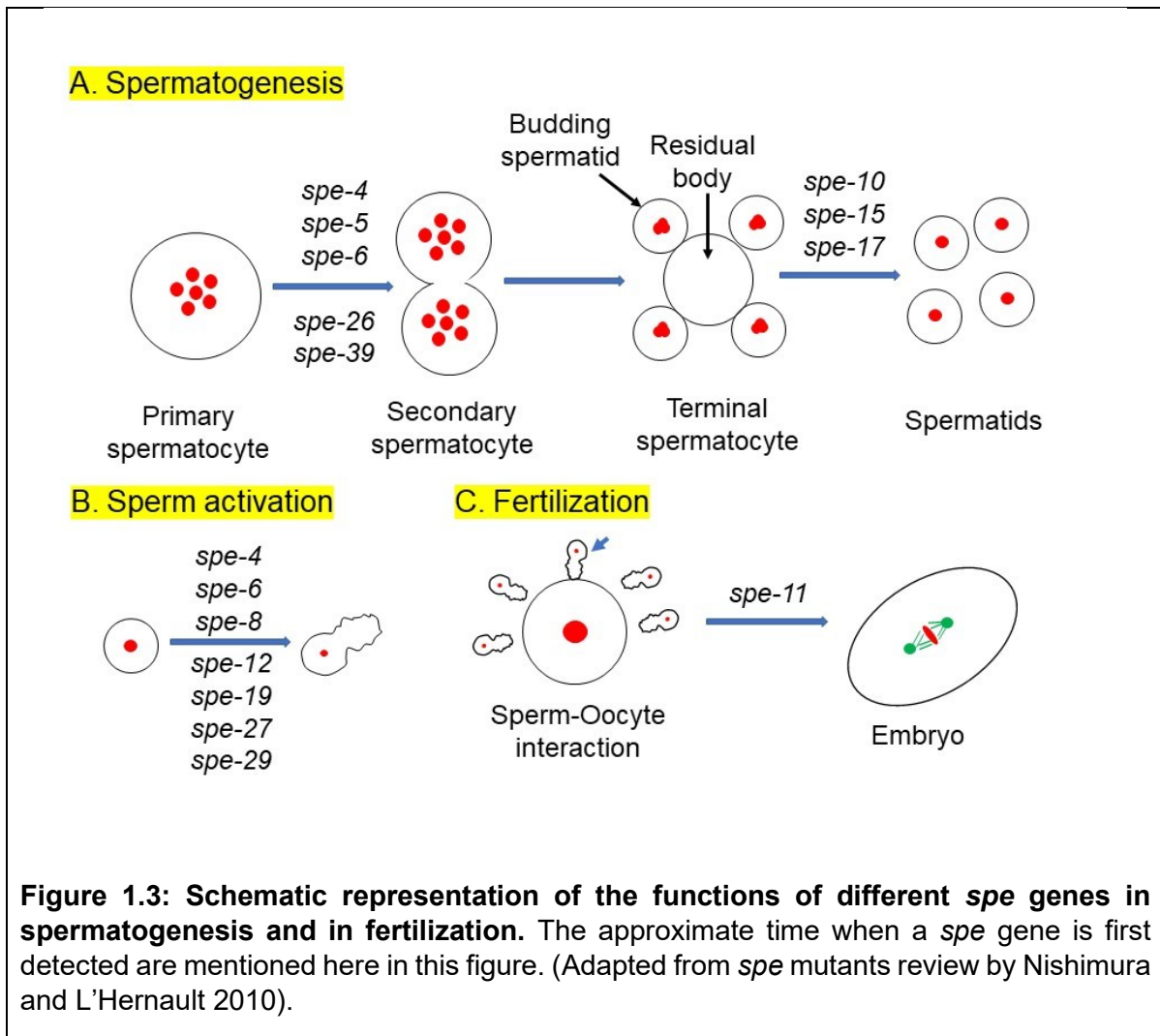
Previous work has identified many genes in *C. elegans* that are required for spermatogenesis, collectively referred to as the *spe* genes (Figure 1.3). Analysis of the phenotypes of some *spe* mutants suggested that regulation of MSP is key to many developmental events during the production of sperm (Nishimura and L'Hernault 2010). For example, proper assembly of MSP into FBs during meiosis prevents MSP from interfering with chromosome segregation (Price et al. 2021) and this sequestration of MSP is also necessary for the motility of the future spermatozoan after budding. The *spe-39* gene encodes a hydrophilic protein and has orthologs in many metazoans. In *spe-39* mutants, instead of proper MOs, many small MO-like vesicles form but the FBs

appear to be uncovered and free from the membrane envelope. In this case, the *spe-39* mutant spermatids do not separate from the residual body during budding (Zhu and L'Hernault 2003).

Premature disassociation of the FB-MO complexes in *spe-4* and *spe-10* mutants also result in similar defects. The *spe-4* gene encodes a sperm-specific intramembranous aspartyl protease, that is similar to members of the presenilin protein family (L'Hernault and Arduengo 1992). Presenilin is predicted to be involved in processing different membrane proteins, for example, Alzheimer's precursor protein in the human brain (Xia and Wolfe 2003). In *spe-4* mutants, spermatocytes complete chromosome segregation but are unable to initiate the budding process, presumably due to the misregulation of the cleavage of specific integral membrane proteins (Arduengo et al. 1998). The *spe-10* gene encodes a 4-pass transmembrane protein with a DHCC-CRD zinc-finger motif that is predicted to be palmitoyl transferase which localizes within FB-MO (Gleason et al. 2006). In *spe-10* mutants, FB-MO morphogenesis begins normally but during spermatid budding, FBs are left in the residual body that leads to the development of MSP-deficient immotile spermatids (Shakes and Ward 1989a; Gleason et al. 2006).

A casein I type serine threonine kinase, SPE-6 is also predicted to be required for proper formation of FBs. In *spe-6* null mutants, MSP fails to assemble into FBs and remains in the cytosol. As a consequence, the FB-MO complex never forms and spermatocytes arrest without completing meiotic divisions or undergoing cytokinesis (Varkey et al. 1993). This observation indicated that a regulatory phosphorylation may control the proper assembly of MSP into FBs but substrates of the SPE-6 kinase remain

unknown. Recently, an intrinsically disordered protein, SPE-18 was found to play an important role with SPE-6 to properly assemble MSP into FBs (Price et al. 2021). SPE-18 is expressed during the late pachytene stage and it localizes to pre-FBs that are closely associated with MOs. As the cell division cycle progresses, SPE-18 forms a distinct barbell or multi-point pattern with the growth of FBs. MSP is also expressed during the late pachytene stage and its levels increase with the subsequent meiotic divisions. Interestingly, in *spe-6* mutants, SPE-18 localizes to the pre-FB structure initially but these are unable to form the distinct barbell or multi-pointed pattern. As a result, MSP can not form the polymer, but instead remains scattered in the cytosol. This finding established that *spe-18* alone is sufficient to form pre-FB structures; however, *spe-6* is eventually required for proper assembly of MSP into FBs (Price et al. 2021).



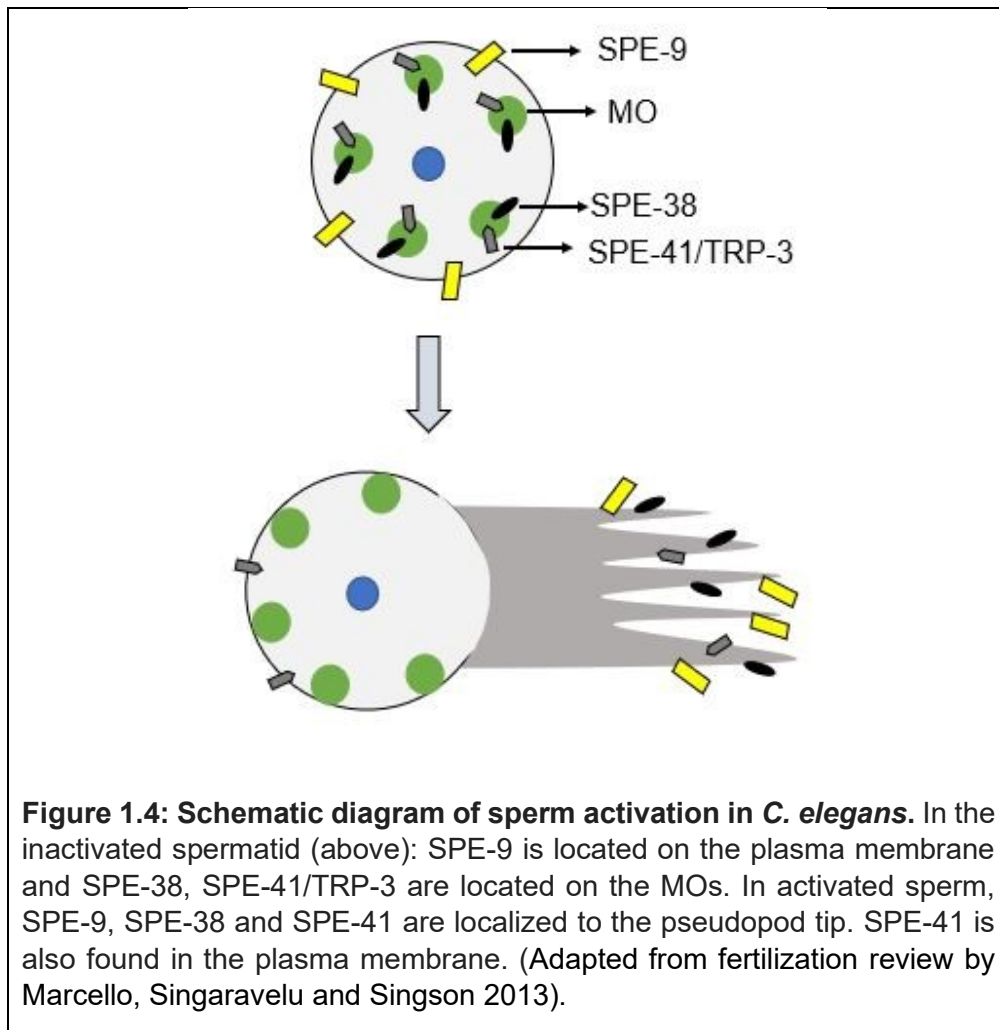
1.4.3 Post-meiotic sperm activation

Like other sexually reproducing animals, *C. elegans* sperm also progress through a series of post-meiotic events to activate their sperm. Hermaphrodite spermatids become active soon after they are formed, when they are pushed into the spermatheca during the first ovulation. Male sperm become active upon ejaculation, when they mix with the seminal fluid. Regardless of the type of sperm involved, two visible changes

occur during sperm activation (Figure 1.4) (Marcello et al. 2013). Firstly, MOs fuse with the plasma membrane to release their glycoproteins and transmembrane proteins. Secondly, MSP, along with the structural components originally sequestered inside the FBs, become asymmetrically distributed to one side of the cell body to form the pseudopod. Changes in the localization of some sperm proteins are also observed during this activation process. For example, the sperm membrane protein, SPE-9, is relocalized exclusively to the pseudopod region from the plasma membrane. In addition, two proteins, SPE-38 and SPE-41/TRP-3, are originally in the MOs within the spermatids. After sperm activation, SPE-38 relocalizes to the pseudopod, while SPE-41/TRP-3 distributes to both pseudopod and cell body.

Sperm activation in *C. elegans* does not start automatically at the end of the meiotic divisions. *In vitro* studies revealed that activation can be achieved by treating inactivated spermatids with a wide range of compounds; though, the molecular targets of those compounds are still unknown (Ellis and Stanfield 2014). For example, a protease mixture called Pronase, the weak base triethanolamine (TEA), calmodulin inhibitors, the ionophore monensin, the stilbene chloride channel inhibitor DIDS, wortmannin, as well as zinc (Nelson and Ward 1980; Ward et al. 1983; Shakes and Ward 1989a; Machaca et al. 1996; Bae et al. 2009; Liu et al. 2013). The media used for *in vitro* sperm activation studies usually contain a mixture of buffered salts that generally includes Na⁺ and K⁺ (Ward et al. 1983). An independent study of the sodium- and potassium-transporting ionophore, monensin, revealed that sperm activation is dependent on extracellular Na⁺ and K⁺ ions, but not on the concentration of extracellular Ca²⁺ (Nelson and Ward 1980). Increases in intracellular pH during

treatment with monensin or TEA was also observed; however, Pronase treatment did not increase the intracellular pH level (Stanfield and Villeneuve 2006). This result indicated that the intracellular rise in pH during sperm activation is not absolutely required.



1.4.4 Sex-specific sperm activation

Included amongst the *spe* genes identified in genetic screens for spermatogenesis defects were five genes in the *spe-8* pathway (*spe-8*, *spe-12*, *spe-19*, *spe-27* and *spe-29*) that cause hermaphrodite-specific sperm activation defects (Shakes and Ward 1989a; Minniti et al. 1996; Nance et al. 1999; Nance et al. 2000; Geldziler et al. 2005). In these mutants, hermaphrodites are self-sterile because their sperm are unable to become active. However, the hermaphrodite sperm can be activated *in vivo* after mating with either wild-type or mutant males from the *spe-8* class. Males from these mutants are fertile and their sperm can activate normally. The *spe-8* class of genes encode various proteins, as follows: *spe8* encodes an SH2 domain-containing non-receptor tyrosine kinase, *spe-27* encodes a hydrophilic protein, *spe-12* and *spe-29* encode transmembrane proteins. These studies suggested that both male and hermaphrodite sperm possess components that respond to a sex-specific activation signal.

Through another genetic screen, *swm-1* was identified as a mutation that affects the fertility of only male sperm (Stanfield and Villeneuve 2006). In this case, males are incapable of transferring sperm efficiently during mating as their sperm are activated precociously within the seminal vesicle. *swm-1* encodes an extracellular protease inhibitor that is present in both males and hermaphrodites. Later, a male-specific seminal fluid protease, TRY-5, was discovered as a target of SWM-1 (Smith and Stanfield 2011). *try-5* is expressed in the valve and vas deferens of the male gonad and is transferred to hermaphrodites during ejaculation. It was also shown that *try-5*

mutant hermaphrodites are fertile but males devoid of both *swm-1* and *try-5* are infertile.

Interestingly, *spe-6* and *spe-4* were both found to suppress the *spe-8* class genes (Muhlrad and Ward 2002; Gosney et al. 2008). Sperm activation in hermaphrodites and males involves the inhibition of SPE-6, which allows SPE-4 to become active to cleave transmembrane proteins such as FER-1, a multi-pass trans-membrane protein. Proteolytic processing during sperm activation produces different forms of SPE-4 that are required for proper fusion of MOs. In mutant *spe-4* spermatids, MOs are unable to fuse properly with the plasma membrane and, as a result, short pseudopods are formed (L'Hernault and Arduengo 1992). Also, *spe-4* mutant sperm are infertile, as proteins that are required for sperm-oocyte interactions remain within the unfused MOs (e.g., SPE-38).

1.4.5 Phosphorylation signalling during sperm activation in *C. elegans*

The biochemical basis of *C. elegans* sperm activation is not clearly understood; however, this biochemical process is well studied in another nematode, *Ascaris suum*. *Ascaris* is a parasitic nematode and much larger than *C. elegans* (>300 X), thus facilitating biochemical purifications of tissues and proteins. One other major difference between these two model organisms is that *Ascaris* is dioecious. However, during spermiogenesis, *Ascaris* displays similar process like MO fusion with the plasma membrane and polarized localization of MSP during pseudopod formation (Ma et al. 2012). In addition, larger sperm size and easier sperm isolation make it a suitable *in vitro* model for biochemical studies of amoeboid sperm motility.

The MSP-based sperm motility of *Ascaris* was reconstituted *in vitro* by adding ATP to a cell-free sperm extract. A columnar meshwork of MSP was observed at the leading edge of protrusions extending from sperm cell bodies, which indicated the importance of MSP polymerization in forward extension of the pseudopod (Italiano et al. 1996). Later, by adding *Yersinia enterocolitica* tyrosine phosphatase to cell-free sperm extracts, retraction of MSP polymer at the basal side of the sperm pseudopod was reconstituted *in vitro* (Miao et al. 2003). Together these data suggest that phosphorylation at the leading edge and dephosphorylation at the base of the pseudopod are required for the MSP dynamics.

Several biochemical studies have identified different key components that regulate the MSP dynamics in active sperm. To initiate MSP assembly, a 48-kDa MSP polymerization organizing protein (MPOP) is required. MPOP is predicted to be phosphorylated by a tyrosine kinase. At the leading edge, phosphorylated MPOP recruits a serine/threonine kinase MPAK (MSP polymerization-activating kinase) that phosphorylates MFP-2 (LeClaire et al. 2003; Yi et al. 2007). MFP-2 has been shown to act oppositely to MFP-1; phosphorylated MFP-2 stabilizes the MSP polymer, while MFP-1 activity leads to MSP destabilization (Buttery et al. 2003). An unknown kinase is implicated in phosphorylating MFP-3 at the base of the pseudopod to stabilize MSP filament and PP2a phosphatase involved in dephosphorylating phospho-MFP-3 to disassemble MSP fibres (Yi et al. 2009).

The biochemical studies using *C. elegans* MSP revealed that the formation of fiber-like structures was induced when the cell-free sperm extracts were incubated with the *Yersinia* tyrosine phosphatase YOP, followed by addition of ATP (Fraire-Zamora et al.

2011). This study also predicted two phosphorylation sites on MSP that could be involved in assembly and disassembly of the polymer. One of them was identified as a Protein Kinase C phosphorylation site (SaR) in amino acids 38-40; and the other one was a Casein Kinase II phosphorylation site (TnnD) in amino acids 85-88. As mentioned previously, casein-kinase I (SPE-6) is required for the proper assembly of MSP into the fibrous bodies. Thus, it is possible that SPE-6 could directly phosphorylate MSP for its assembly inside the FBs. Interestingly, GSP-3/4 was previously found to co-localize with MSP in the sperm, and was concentrated at the base of the pseudopod, thus, it could facilitate MSP disassembly (Wu et al. 2012). However, no direct evidence is available until now whether MSP undergoes phosphorylation/dephosphorylation in the active sperm. Recent discovery of *C. elegans* homologs of the *Ascaris* MFP1 and MFP2 and their co-localization with MSP in the pseudopod also raises the possibilities that those structural components of MSP can also be involved in phosphorylation/dephosphorylation during pseudopod treadmilling (Morrison et al. 2021).

1.5 Oocyte meiotic maturation in *C. elegans*

1.5.1 Oocyte growth and development

Like mammals, the RAS/ERK signalling pathway controls oogenesis in *C. elegans* (Verlhac et al. 1993; Church et al. 1995; Fan and Sun 2004; Lee et al. 2007; Fan et al. 2009). Mutations in the components of the RAS/ERK pathway cause meiotic arrest in mid-pachytene. Activation of ERK for ~18 hours is essential to progress through the

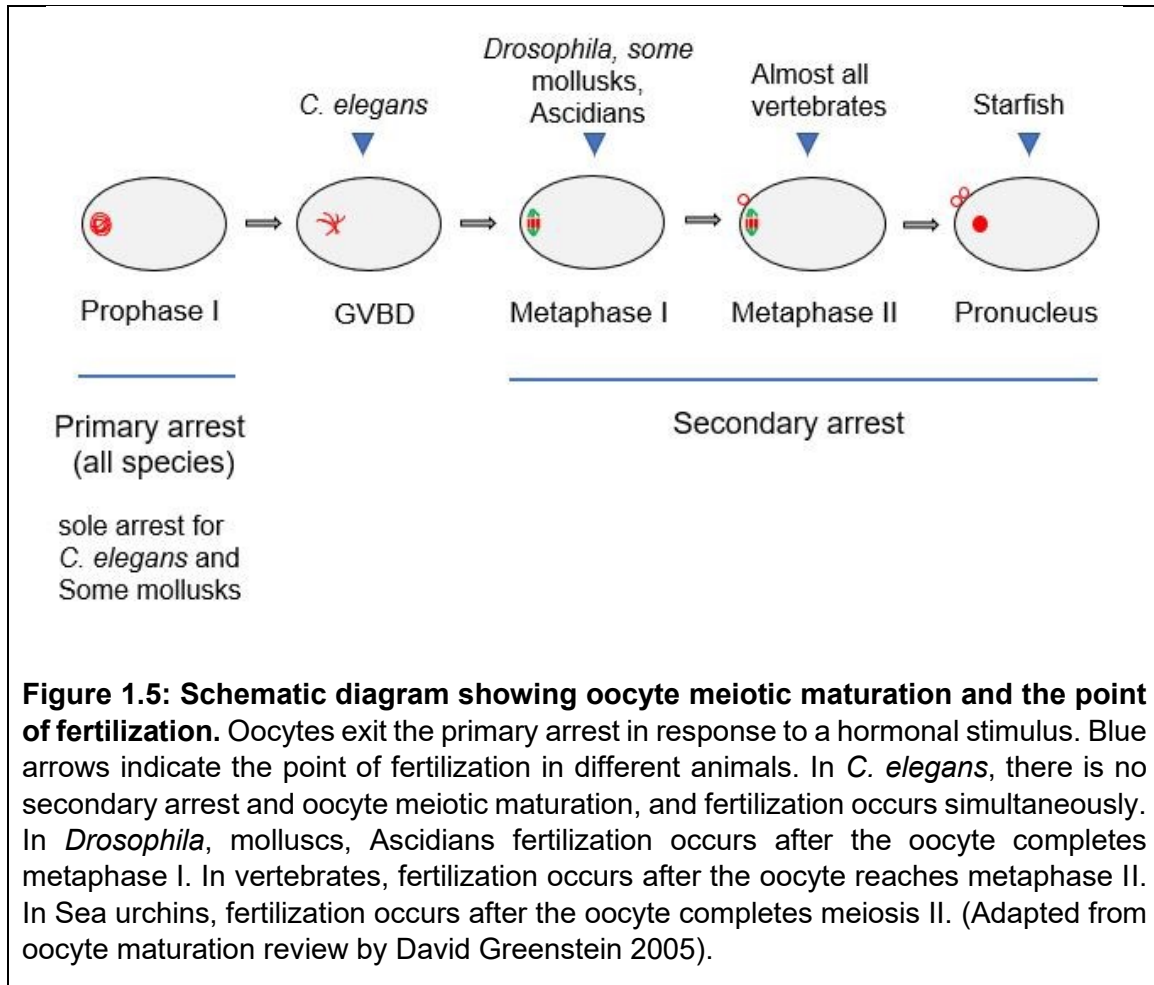
pachytene stage (Lee et al. 2007; Lopez et al. 2013). Reduction in ERK signalling during mid pachytene stage resulted in “pachytene progression” phenotype in which extension of mid pachytene caused a decrease in oocyte numbers. Intriguingly, gain-of-function mutations in ERK signalling resulted in an increase in low quality oocyte numbers. In both loss-function and gain-of-function backgrounds, the mutant animals are either sterile or produced progeny that died during early larval stages of development. Usually, the RAS/ERK pathway regulates cell numbers in developmental pathways, either by controlling proliferation or by apoptosis. It is recently shown that the RAS/ERK pathway does not regulate the oocyte numbers in *C. elegans* by proliferation or apoptosis; rather, RAS/ERK pathway regulates timely exit from the pachytene stage to regulate the oocyte numbers (Das et al.2020). ERK phosphorylates one of the chromosome axis components of Horma domain containing protein, HTP-1 to coordinate formation and maintenance of synaptonemal complex (SC) (Das et al. 2020).

As oocytes develop, several genes play a significant role in regulating the production and degradation of proteins. For example, a *C. elegans* homolog of the human Deleted Azoospermia gene, *daz-1*, encodes an RNA-binding protein that may regulate the translation of transcripts during female meiosis progression (Karashima et al. 2000). Two *Skp1*-related genes in *C. elegans* are predicted to interact with CUL-1 or CUL-6 to regulate ubiquitin-mediated protein degradation during progression through pachytene (Nayak et al. 2002). The maxi-KH/STAR domain RNA binding protein, GLD-1, is predicted to prevent the translation of proteins needed for oocyte growth. In this manner, the inhibitory effects of GLD-1 are highest during pachytene,

but decrease gradually in the growing oocyte to allow specific protein production (Jones et al. 1996; Jan et al. 1999; Lee and Schedl 2001). Oocytes that lack *gld-1* exit from meiosis immediately after the pachytene stage and re-enter mitosis, to form a germline tumor (Francis et al. 1995).

1.5.2 Oocyte meiotic maturation and MSP signalling

The oocytes of almost all sexually reproducing organisms primarily arrest during meiotic prophase to permit oocyte growth, differentiation and stockpiling of maternal components (Von Stetina and Orr-Weaver 2011; Huelgas-Morales and Greenstein 2018). Oocyte meiotic maturation may be defined as the transition between this prophase arrest and metaphase I. Exit from prophase is indicated by nuclear envelope breakdown, assembly of the meiotic spindle and rearrangement of the cortical cytoskeleton. This essential process prepares the oocyte for fertilization (Figure 1.5).



In many animals, meiotic maturation involves hormones such as luteinizing hormone (LH) in mammals or prostaglandins and ecdysone in *Drosophila* (Von Stetina and Orr-Weaver 2011). In a remarkable study, Miller et. al., (2001) showed that the cytoskeletal sperm protein, MSP, also induces oocyte meiotic maturation and gonadal sheath cell contraction. Gonadal sheath contraction is required to push the oocyte into the spermatheca for fertilization. In this study, the authors developed an *in vivo* assay in which MSP was injected into the uterus of *fog* (feminization of germline) mutant hermaphrodite worms that cannot make sperm. This resulted in a dramatic increase in oocyte maturation and sheath cell contraction. As a further test, anti-MSP antibody was

injected into the uterus of wild-type hermaphrodites, which resulted in a significant decrease in oocyte maturation. Further experiments revealed that MSP lacking a conserved 20 aa C-terminal domain can promote oocyte maturation but is unable to promote sheath cell contraction required for ovulation.

Several studies reported that MSP-dependent oocyte maturation is mediated by protein kinase A (PKA) signalling in the gonadal sheath cells (Govindan et al. 2006; Harris et al. 2006; Cheng et al. 2008; Jud et al. 2008; Govindan et al. 2009; Nadarajan et al. 2009; Kim et al. 2012). Conserved components of heterotrimeric G-protein pathways, like GSA-1 (the simulator G-protein $G_{\alpha s}$), ACY-4 (adenylate cyclase) and KIN-1 (the PKA catalytic subunit) are identified as key players in this process. MSP is released from the sperm by a vesicle budding mechanism. MSP binding with the sheath cells activates G_{α} GSA-1, which, in turn, activates adenylate cyclase to elevate the cAMP levels (Govindan et al. 2006; Govindan et al. 2009). Mosaic animals with *gsa-1*^{-/-} in the somatic gonad and *gsa-1*^{+/+} in the germline failed to produce mature oocytes, however, mosaic animals with *gsa-1*^{+/+} in somatic gonad and *gsa-1*^{-/-} in germline were capable of initiating oocyte meiotic maturation (Govindan et al. 2009). Therefore, the MSP-mediated oocyte meiotic maturation is dependent on the expression of $G_{\alpha s}$ within the gonadal sheath cells.

In addition to the stimulatory G-protein signalling, inhibitory G-protein signalling in the gonadal sheath cell is required to prevent meiotic maturation in the absence of sperm (Govindan et al. 2006; Govindan et al. 2009). For example, oocytes undergo meiotic maturation constitutively in females that are mutant in *goa-1*, the gene that encodes a $G_{\alpha o/i}$ subunit. This inhibitory signalling is also mediated by the gap junction,

Innexin, an invertebrate homolog of connexin. Mutations in the Innexin encoding *inx-14* and *inx-22* genes suppress the oocyte maturation failure of *gsa-1* mutants (Whitten and Miller 2007).

Because of the involvement of heterotrimeric G-proteins in the maturation process, it is assumed that a G-protein-coupled receptor should also be involved in this process. There are more than 1000 GPCRs present in *C. elegans* (Fredriksson and Schiöth 2005). To date, the only receptor implicated in oocyte maturation is the VAB Eph receptor, which is an MSP receptor that negatively regulates oocyte maturation. It was reported that *gsa-1* and *acy-4* regulate exclusion of VAB-1 Eph receptor trafficking through gap junction Innexin; during that transition recycling endosome VAB-1 Eph inhibits meiotic maturation (Cheng et al. 2008). Another study showed that VAB-1 inhibits oocyte maturation by negatively regulating the DAF/PTEN pathway (Brisbin et al. 2009).

1.5.3 Ovulation

Oocyte entry into the spermatheca is controlled by two spermathecal valves (Figure 1.6). The proximal oocyte secretes LIN-3/EGF that is predicted to activate IP3/DAG in the sheath cells, this IP3 stimulation triggers calcium release from the IP3 receptor cells (Clandinin et al. 1998). Then, the ovulated oocyte stays inside the spermatheca for 3-5 minutes to allow the sperm to fertilize the oocyte. A filamin protein FLN-1 senses the presence of the oocyte inside the spermatheca and, together with PLC-1/phospholipase C and gap junction proteins generate a directional wave of calcium that leads to the constriction of the spermatheca (Kovacevic and Cram 2013).

Opening of the spermathecal-uterine valve after constriction of the spermatheca allows the fertilized oocyte to move away from the spermatheca and enter the uterus. Recently, it was shown that the sole PIEZO-like mechanosensing protein in *C. elegans*, PEZO-1, regulates the spermathecal sheath cells and the distal valve opening during the ovulation process, possibly by replenishing cytosolic Ca^{2+} (Bai et al. 2020).

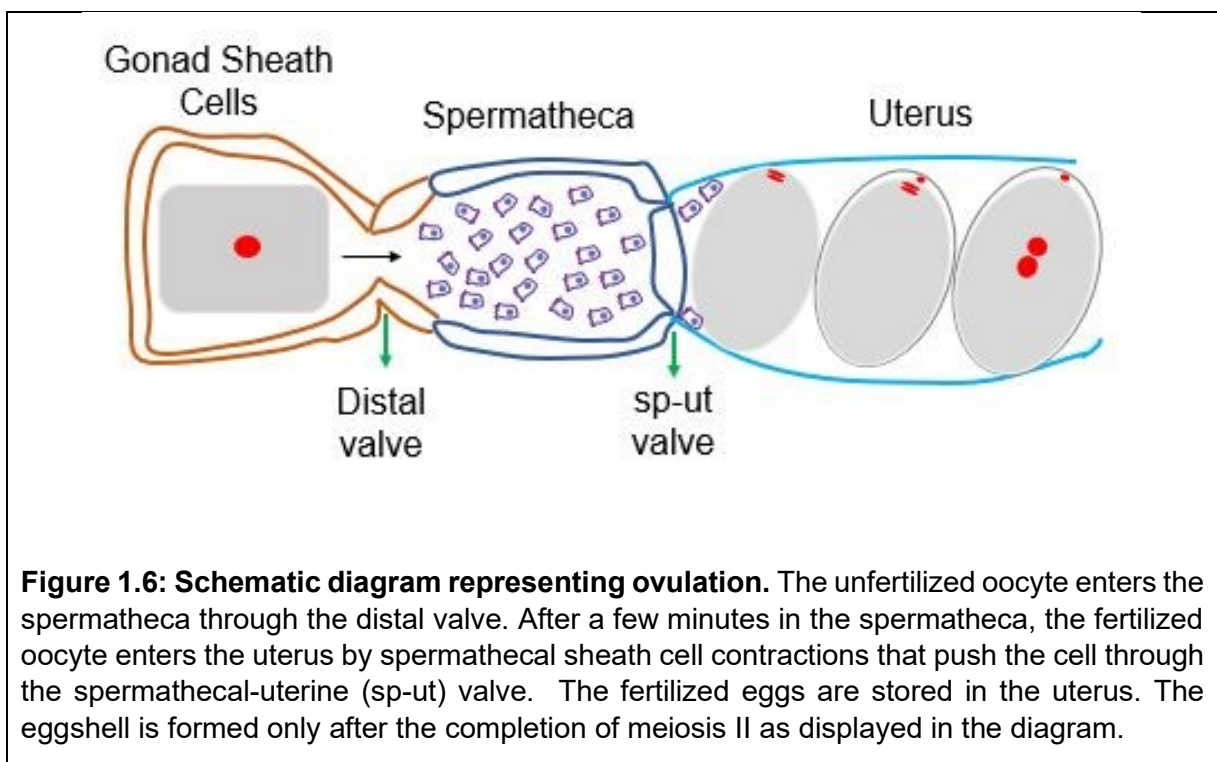


Figure 1.6: Schematic diagram representing ovulation. The unfertilized oocyte enters the spermatheca through the distal valve. After a few minutes in the spermatheca, the fertilized oocyte enters the uterus by spermathecal sheath cell contractions that push the cell through the spermathecal-uterine (sp-ut) valve. The fertilized eggs are stored in the uterus. The eggshell is formed only after the completion of meiosis II as displayed in the diagram.

1.6 Fertilization in *C. elegans*

The secondary arrest of the oocyte in many organisms coordinates the completion of the female meiotic program with fertilization. In most vertebrates, the secondary arrest occurs at metaphase of meiosis II; in insects, it occurs at metaphase of meiosis I; and in many marine invertebrates such as echinoderms, it occurs after the oocyte completes both meiotic divisions (Figure 1.4). In *C. elegans*, the process of ovulation and fertilization are developmentally coordinated, whereby fertilization typically occurs in the spermatheca a few minutes after ovulation. Previous observations of mutants that produce sperm that are incapable of fertilization, but still allow oocyte maturation, have revealed clues about the fate of mature oocytes that are not fertilized in a timely manner. For example, in *fer-1* mutants, the unfertilized mature oocyte progresses into anaphase I, but this process is aborted and the segregated chromatin is resorbed into the oocyte cytoplasm without forming a polar body. Then, the meiosis II program is skipped, and a nuclear envelope forms around the meiotic chromatin. These unfertilized cells lack other sperm components required for mitotic spindle assembly; however, they appear to cycle mitotically, exhibiting repeated DNA replication and nuclear envelope breakdown. Despite these aforementioned abnormal events, which only occur with very specific mutants, the process of fertilization is incredibly precise and efficient in wild-type *C. elegans*. In these cases, sperm entry initiates a series of events described below.

1.6.1 Female meiotic spindle assembly

Upon oocyte maturation (see above), the nuclear envelope breaks down and meiosis I spindle assembly initiates, usually before sperm entry, as the oocyte enters the spermatheca. One main distinction between female meiotic spindles and with male meiotic spindles or mitotic spindles, is that female spindles form without centrioles. During diplotene of the oocyte maturation process, centrioles are eliminated from the female germ cells (Mikeladze-Dvali et al. 2012). This elimination is likely regulated by cyclin-dependent kinase inhibitor-2 (*cki-2*), as multipolar mitotic spindles were observed in *cki-2* mutant embryos (Kim and Roy 2006). In the absence of centrioles, female meiotic spindle microtubules form a barrel-shape structure, and a specialized pathway is employed to nucleate and organize microtubules during this process (Müller-Reichert et al. 2010). In other systems, the guanine exchange factor RCC1 is responsible for generating a Ran-GTP concentration gradient around the meiotic chromatin. This gradient influences microtubule dynamics, such that microtubules near the chromatin are stabilized and microtubules growing away from chromatin remain dynamic (Bischoff and Ponstingl 1991). In *C. elegans*, the female meiotic spindle assembly does not require Ran-GTP. Rather, the microtubule-severing protein Katanin, a two-subunit complex encoded by *mei-1* and *mei-2*, are essential for proper meiotic spindle assembly (Srayko et al. 2000). In the absence of *mei-1*, very long and fewer microtubules are visible around the meiotic chromatin and they fail to organize into bipolar spindles (Srayko et al. 2006). This suggests that during acentrosomal female meiosis in *C. elegans*, katanin functions, in part, to convert long microtubules into shorter fragments, which become incorporated into the bipolar spindle. Though

severing occurs during metaphase but a recent analysis based on mathematical model for microtubule dynamics proposed that rearrangements of spindle during anaphase are dependent on changes in nucleation rather than cutting rates (Lantzsch et al. 2021).

Shortly after its formation the meiosis I spindle shortens over a period of several minutes and rotates toward the cortex of the embryo, at which time it becomes approximately 4.6 μm in length (Ellefson and McNally 2011). Recent analysis from *in utero* time-lapse imaging revealed a significant space between spindle poles and plasma membrane before the spindle rotation; further quantification suggests a better correlation between spindle rotation and spindle aspect ratio, than the correlation between spindle rotation and spindle length (Crowder et al. 2015). This rotation requires both the APC (anaphase-promoting complex) and cytoplasmic dynein (Yang et al. 2005; Ellefson and McNally 2009). Dynein heavy chain accumulates on meiotic spindle poles through an APC-dependent process before spindle rotation (Ellefson and McNally 2009). Further study revealed that the inhibition of cyclin B/CDK-1 was sufficient to induce dynein-dependent spindle rotation in APC-depleted embryos (Ellefson and McNally 2011). Later, p150 dynactin subunit, DNC-1 was identified as a target of CDK-1 (Crowder et al. 2015). Together, all these studies suggest that a dynein-dependent cortical pulling mechanism is responsible for *C. elegans* spindle rotation.

1.6.2 Chromosome segregation during female meiosis

Proper meiotic chromosome segregation first depends on proper chromosome pairing, which occurs during the extended prophase stage of meiosis. This process is characterized by the appearance of a proteinaceous synaptonemal complex (SC) between chromosomes, and corresponding DNA strand exchanges that allow for genetic recombination between homologous chromosomes. The process of chromosome segregation begins only after oocyte maturation and spindle assembly. A kinetochore-independent mechanism of chromosome segregation during female meiosis in *C. elegans* was previously proposed (Dumont et al. 2010). According to that study, microtubule polymerization between the segregating chromosomes could generate the pushing force to segregate them. Alternative to that model, a role for kinetochore proteins KNL-1 and KNL-3 in generating pulling forces during a pre-anaphase stage associated with spindle shortening was recently reported (Danlasky et al. 2020). Anaphase I occurs shortly after meiotic spindle rotation and the first polar body is extruded near the cortex. Metaphase II chromosomes appear in a pentagonal array and meiosis II spindles form within approximately 5 minutes after completion of anaphase I (McNally and McNally 2005). Sister-chromatid segregation occurs during anaphase II to release the second polar body. The centrosomal microtubules appear after the completion of female meiosis II. The centrosomal nuclear complex starts migrating towards the female pronuclei for fusion and rotation, with the centrosomes on opposite sides of the two fused nuclei, and aligned along the anterior-posterior axis of the one-cell embryo.

Timely establishment and removal of chromatid cohesion (SCC) is a key to successfully complete chromosome segregation during meiosis and mitosis in all sexually reproducing organisms. Two SMC proteins, Smc1 and Smc3, form the core cohesin complex and Scc1 kleisin topologically surrounds that core structure (Nasmyth and Haering 2009). In monocentric chromosome, such as flies, vertebrates and yeast, cohesion is removed from the arms of homologous chromosomes during anaphase I but remains at the centromeric regions until anaphase II (Watanabe and Nurse 1999; Clyne et al. 2003; Lee and Amon 2003). Shugosin protects cohesion at the centromere by recruiting protein phosphatase 2A (PP2A), which prevents Aurora B kinase-mediated phosphorylation of REC-8 to prevent it from separase-mediated degradation (Kitajima et al. 2006). In holocentric *C. elegans* chromosomes, REC-8 is lost from the short arm of the bivalent but it remains on the long arm. The aurora B kinase homolog, AIR-2, is located on the short arm during meiosis I and is predicted to phosphorylate REC-8 for proteolytic degradation by separase (Kaitna et al. 2002; Rogers et al. 2002). Unlike other systems, the Shugoshin homolog in *C. elegans*, SGO-1, does not seem to be involved in protecting sister chromatid cohesion in meiosis I (de Carvalho et al. 2008). Instead, worm-specific LAB-1 (long arm of the bivalent) protects REC-8 by targeting PP1 to antagonise AIR-2 phosphorylation (Tzur et al. 2012). Like cohesin, HORMA domain proteins are also associated with chromosomes to execute successful homolog pairing, cross-over formation and progress through the checkpoint (Rosenberg and Corbett 2015). It was previously shown SCC release during meiosis I was prevented by *C. elegans* HORMA domain protein homologs HTP-1 and HTP-2 (Martinez-Perez et al. 2008; Severson et al. 2009). Recently, it is shown that HTP-1

and HTP-2 act as antagonists of Haspin kinase, which promotes Aurora B recruitment (Ferrandiz et al. 2018).

1.6.3 Degradation of different proteins

Egg activation and the oocyte-to-embryo transition involves the degradation of different proteins at the different stages of meiosis (Bowerman and Kurz 2006; Robertson and Lin 2013). Three phosphatases EGG-3, EGG-4 and EGG-5 were identified to coordinate egg activation events (Maruyama et al. 2007; Stitzel and Seydoux 2007; Cheng et al. 2009; Parry et al. 2009). One of the main functions of EGG-3/4/5 is to regulate the DYRK family kinase, MBK-2 (mini-brain kinase-2). MBK-2 phosphorylates different substrates during the oocyte-to-embryo transition. Some known targets of MBK-2 are MEI-1, OMA-1, OMA-2, MEX-5 and MEX-6. The microtubule severing protein Katanin is required for female meiotic spindle assembly, but it needs to be degraded before mitosis, and MBK-2 mediated phosphorylation triggers this degradation process (Lu and Mains 2007; Johnson et al. 2009; Beard et al. 2016). In addition, the CCCH-type zinc-finger proteins, OMA-1 and OMA-2, act as translational repressors by sequestering the transcription factor TAF-4 (TATA-binding protein associated factor-4) to prevent precocious embryogenesis, and this process is regulated by MBK-2 mediated phosphorylation of OMA-1 and OMA-2 (Detwiler et al. 2001; Nishi and Lin 2005; Guven-Ozkan et al. 2008). The anterior-posterior polarity of the *C. elegans* embryo also establishes after fertilization, as marked by the localization of PAR proteins at the cortical region of the embryo. The posterior region is determined by the site through which sperm enters the oocyte (Goldstein and Hird 1996; O'Connell

et al. 2000). During polarization of the one-cell embryo, two cytoplasmic proteins MEX-5 and MEX-6 localize to the anterior pole of the embryo (Schubert et al. 2000; Cuenca et al. 2003). MBK-2-mediated phosphorylation is a prerequisite for MEX-5 and MEX-6 activation by polo-like kinases, PLK-1 and PLK-2, to properly establish the embryonic polarity (Nishi et al. 2008).

MBK-2 activity needs to be regulated precisely for a successful oocyte-to-embryo transition. EGG-4/5 binds to the activation loop of MBK-2 to form a complex structure, which is sequestered to the oocyte cortex by an interconnection between EGG-3 and the integral membrane protein, CHS-1 (Cheng et al. 2009). MBK-2 is released from this complex in two steps. During meiosis I, CDK-1 phosphorylates MBK-2 and then, EGG-3 is degraded by the ubiquitin ligase, APC (Cheng et al. 2009). This early regulation of MBK-2 by the EGG complex is dependent on cell-cycle progression rather than fertilization; but, without fertilization, embryogenesis eventually fails. During the oocyte-to-embryo transition, MBK-2 is uniformly distributed on the cortex of the oocyte, but then undergoes a dramatic rearrangement to form a punctate pattern on the cortex of the embryo after metaphase I and prior to the second meiotic division (McNally and McNally 2005). This indicates that the intracellular location of MBK-2 changes in coordination with sperm entry during the fertilization.

1.7 The MEMI pathway

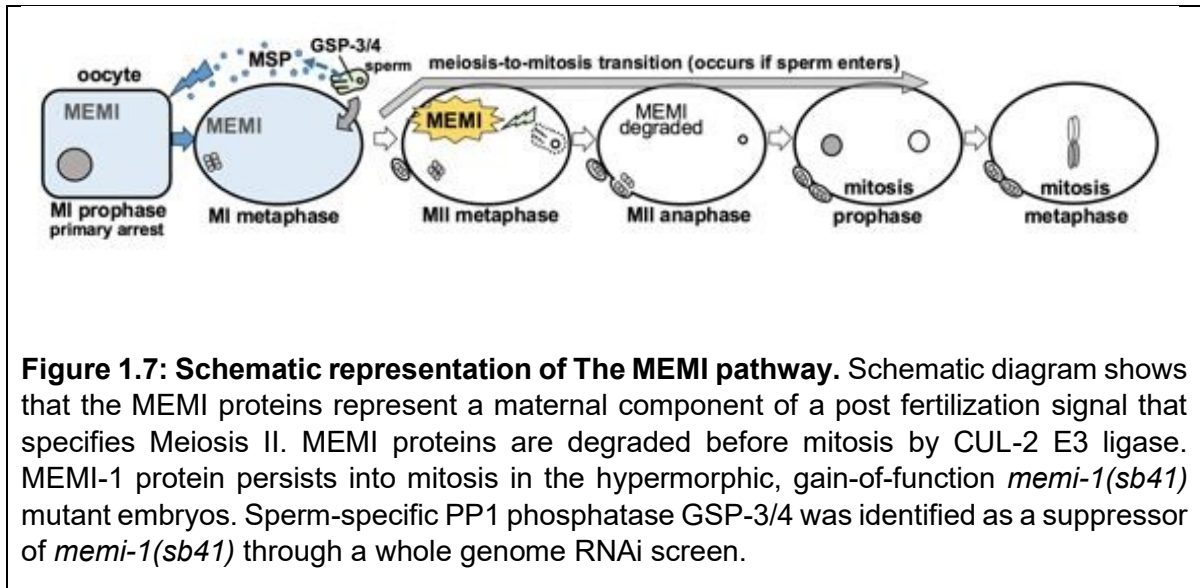
The Srayko lab studies the *memi* (meiosis to mitosis defective) genes, which encode maternal proteins that are required for female meiosis II (MII) (Ataeian et al.

2016). Three very similar paralogs *memi-1*, *memi-2*, and *memi-3* function redundantly, but loss of all three paralogs results in phenotypes that are similar to what happens when immobile, fertilization-defective sperm do not enter the mature oocyte (Ward and Carrel 1979; McNally and McNally 2005). Despite being fertilized, *memi-1/2/3(RNAi)* embryos abort anaphase I, skip meiosis II entirely, and then enter mitosis (Ataeian et al. 2016).

A gain-of-function, temperature-sensitive *memi-1(sb41)* mutation has a different effect. *memi-1(sb41)* was identified as a dominant temperature-sensitive maternal-effect-lethal (MEL) mutation in a genetic screen to identify redundant genes affecting embryonic development in *C. elegans* (Mitenko et al. 1997). At 15°C, *memi-1(sb41)* worms produce around 15% viable progeny, but at 25°C, no viable progeny are produced. The *memi-1(sb41)* embryos displayed several MII defects, including improper sister chromatid segregation and abnormal spindle microtubule rearrangement (2). These embryos enter MII but are unable to exit MII properly. MEMI proteins are degraded before mitosis, and this degradation is dependent on CUL-2 E3 ligase activity. The hypermorphic *sb41* mutation interferes with the degradation of MEMI-1, and its persistence in mitosis is likely responsible for the gain-of-function mitotic phenotype.

A loss or reduction of function in any gene required for MEMI activity could suppress the embryonic lethality characteristic of this mutation as the *sb41* mutation results in persistent or inappropriate MEMI activity into mitosis. A whole genome RNAi screen was done to identify the suppressors of *memi-1(sb41)*. Out of almost 16,000 genes tested, only sperm-specific PP1 phosphatase *gsp-3/4* was found as a

suppressor of *memi-1(sb41)*. *gsp-3* and *gsp-4* are 98% identical and RNAi targets both the genes. Previously it was reported that *gsp-3/4* are functionally redundant and they are required for sperm development and motility (Wu et al. 2012). The MEMI pathway is schematically described in the following figure:

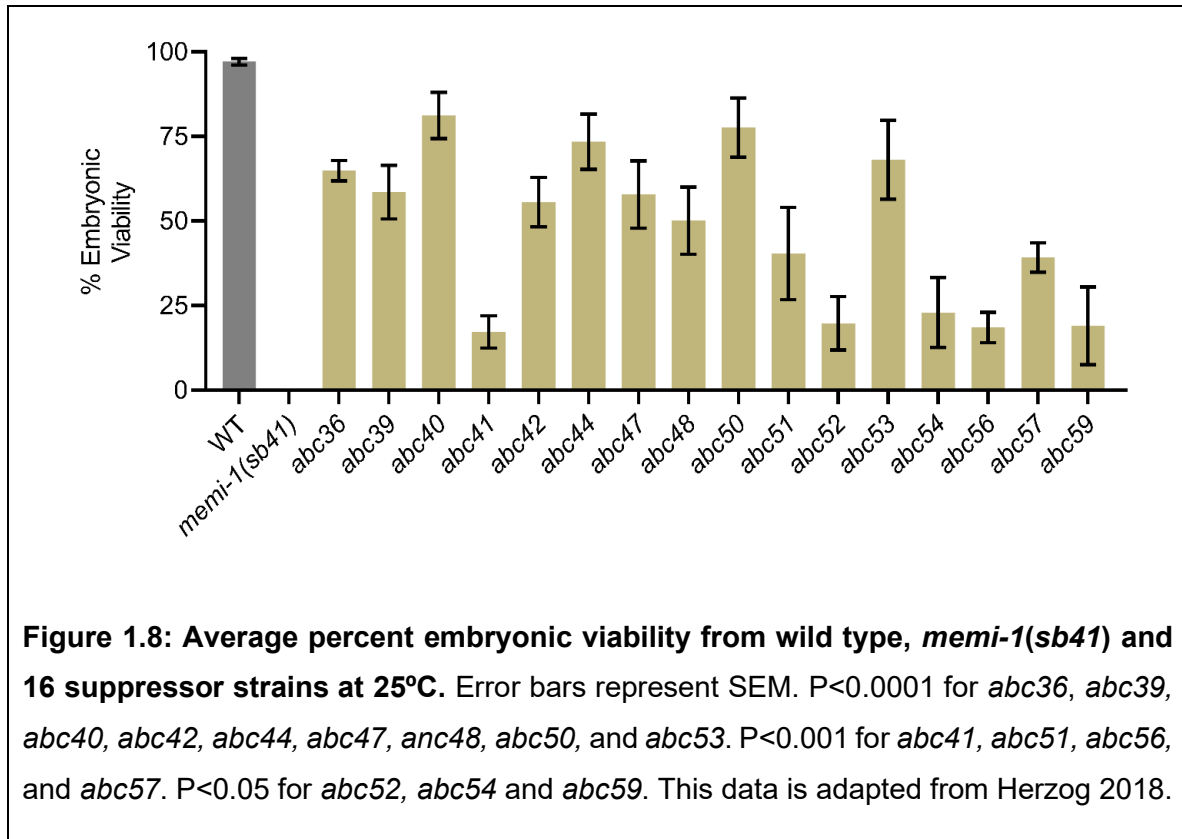


1.7.1 EMS screen to identify suppressors of *memi-1(sb41)*

Through whole-genome RNAi screening, sperm-specific PP1 phosphatases GSP-3 and GSP-4, were identified as suppressors of *memi-1(sb41)* (Ataeian et al. 2016). To identify additional suppressors of *memi-1(sb41)*, an EMS screen was performed. Out of 20,226 haploid genomes screened, 30 suppressors were identified for a hit rate of 1 in 675 genomes. This mutation rate is approximately 3X higher than the expected rate of 1/2000 for a single genetic locus using standard EMS mutagenesis protocols (Drake et al. 1998; Denver et al. 2004; Kutscher and Shaham 2014). As *memi-1(RNAi)* suppresses the *memi-1(sb41)* phenotype, it was expected that at least some

suppressors should be intragenic mutations. The high rate of suppressors could be because of the higher mutability of *memi-1(sb41)* or the creation of new suppressors capable of interfering with the function of *memi-1*. If we exclude the possibility of *memi-1(sb41)* being a mutational hotspot, the observed 3X higher mutagenesis rate suggests that there could be many distinct suppressor loci, including *memi-1(sb41)*. This hypothesis predicts that one out of three suppressors should be present within the *memi-1(sb41)* gene. Therefore, the EMS-generated suppressors were first sequenced to find intragenic suppressors and total 11 intragenic suppressors were found that suppressed the *memi-1(sb41)* (Caitlin Slomp, *pers. comm.*). The remaining suppressor strains were submitted for whole genome sequencing (WGS) to detect possible lesions responsible for extragenic suppression. Embryonic viability of each strain was used to calculate the percentage of suppression of *memi-1(sb41)* embryonic lethality by individual suppressor strains (Figure 1.8) (Herzog 2018).

Five suppressor strains contained a mutation in the *gsp-4* gene. *gsp-4* encodes a sperm-specific PP1 phosphatase subunit that was originally identified as a suppressor of *memi-1(sb41)* in a genome-wide RNAi-feeding screen. This validates the power of the EMS suppressor screen and further supports the placement of this PP1 phosphatase in the MEMI pathway. Four mutations were found within the gene, *R03D7.5*. *R03D7.5* encodes a glycogen synthase kinase 3 family member. Based on functional analysis *R03D7.5* was renamed *gskl-1* (GSK-3 kinase like-1). Candidate genes in the remaining seven suppressor strains were narrowed down based on mapping data and complementation analysis (Herzog, 2018).



1.8 The role of GSK-3 and PP1 phosphatases in fertilization

GSK-3 was originally characterized for its role in glycogen metabolism, but it became the interest of developmental biologists after its role in canonical Wnt signalling was discovered in *Drosophila*. In addition to the Wnt pathway, the role of GSK-3 in various physiological functions such as cell cycle, development, and apoptosis, is well established. GSK-3 is an evolutionarily conserved serine-threonine protein kinase. Mammalian GSK-3 enzymes have been split into two main groups, α and β , based on structural features. GSK-3 α and GSK-3 β (483 and 433 aa in humans) are 98% identical within their ATP binding domain, but there are important differences within the N- and

C- terminal domains (Woodgett 1990; Doble and Woodgett 2003). Although both isoforms perform similar functions, they are not completely redundant, as GSK-3 α alone cannot rescue the lethal phenotype of null GSK-3 β in mice. In addition, a testis-specific knock out mutation of GSK-3 α causes male infertility (Bhattacharjee et al. 2015; Bhattacharjee et al. 2018). Inhibition of catalytic activity of GSK-3 occurs due to phosphorylation on Ser21 (GSK-3 α) or Ser9 (GSK-3 β) (Cross et al. 1995).

Different metabolic enzymes, cytoskeletal proteins, and transcription factors have been identified as substrates of GSK-3 (Patel and Woodgett 2017). Known substrates of GSK-3 typically contain a sequence of S/T-X-X-X-S/T, in which the first S/T is the target residue of GSK-3 and the last S/T residue is the site of priming phosphorylation (ter Haar et al. 2001). This priming phosphorylation is not absolutely required, but it increases the activity of GSK-3 by 10 to 100 times (Thomas et al. 1999). Glycogen synthase (GS), the prototypical substrate for GSK-3, requires prephosphorylation at a serine or threonine residue just C terminal to the GSK-3 target, however, some GSK-3 substrates, such as β -catenin do not require prephosphorylation. Thus, different substrate level phosphorylation may be the key regulatory mechanism that allows GSK-3 to act on different pathways independently.

Both GSK-3 and PP1 genes were identified in the previous screens for suppressors of *memi-1(sb41)*. There are more than 400 genes that encode serine/threonine kinases in the human genome but only 40 genes encode serine/threonine phosphatase. Phospho Protein phosphatase (PPP) is the largest sub family of serine/threonine phosphatase consisting of seven enzymes. Out of these, Protein phosphatase 1 (PP1) is highly characterized. Four different catalytic subunits of PP1 are present in

mammals, they are PP1 α , PP1 β/δ , PP1 γ_1 and PP1 γ_2 ; out of these, PP1 α , PP1 β/δ , PP1 γ_1 are ubiquitously expressed in all cells while PP1 γ_2 is expressed only in testis (Shi 2009). PPP activities are often regulated by inhibitory proteins and regulatory proteins (Bollen et al. 2010). To regulate PP1 activity, many PP1 inhibitors, for example, inhibitor-2 and DARP bind to the Mn²⁺ ions in the active site of PP1 to block dephosphorylation (Kelker et al. 2009; Dancheck et al. 2011). Binding of these inhibitors or other regulatory proteins with PP1 occurs via a primary PP1 binding motif, some identified motifs are RVxF, SILK, MyPhoNE motifs (Wakula et al. 2003; Meiselbach et al. 2006; Hendrickx et al. 2009).

In mammals, GSK-3s engage in complex regulatory networks that involve PP1 and/or PP2A phosphatases, or their respective regulatory subunits to regulate sperm motility. For example, bovine PP2A and PP1 activity in immature sperm has been correlated with increased activity of GSK-3 (Vijayaraghavan et al. 1996). GSK-3 can also phosphorylate inhibitor 2, a PP1 regulatory subunit (Lin et al. 2003), and this phosphorylation enhances PP1 catalytic activity in the motile caudal sperm in mice (Goswami et al. 2018). In *C. elegans*, PP1 phosphatase is required for sperm meiosis and motility (Wu et al. 2012). The connection, if any, between these two different classes of enzymes in the context of embryonic development was unclear, and one of the main areas of investigation for this thesis.

1.9 Goal of the thesis

The goal of my research was to characterize suppressors of the maternal-effect lethal (MEL) phenotype of *memi-1(sb41)* and to decipher the molecular role they have

in the MEMI pathway by using a combination of genetics and molecular biology techniques.

1.10 Summary of the thesis

Previously, we found that RNAi knockdown of a sperm-specific PP1 phosphatase, GSP-3/4, suppressed *memi-1(sb41)*. Through EMS screening, we recovered alleles of *gsp-4* and identified additional genes in this pathway. One of the genes was *gskl-1*. *gskl-1* deletion homozygotes appear wild type, however, double-deletion analysis revealed functional redundancy with one other GSK-3 member, *gskl-2*. The *gskl-2(Δ); gskl-1(Δ)* worms exhibited embryonic lethality and lower brood sizes. The embryonic lethality was completely rescued by mating hermaphrodites to wild-type males. Furthermore, *gskl-2(Δ); gskl-1(Δ)* males produced a significant number of inviable embryos when mated to *fog-2* hermaphrodites. Together, this suggested that these genes might encode sperm-specific components that have roles in the early embryo.

Approximately 38% of *gskl-2(Δ); gskl-1(Δ)* fertilized embryos exhibited normal MI, but MII spindle assembly was delayed, and the second polar body failed to extrude. This result suggested that these GSK-3s have a role in the early embryo. We also tested the relationship between *gsp-3/4* and *gskl-1* and discovered a synthetic genetic interaction whereby *gsp-4(Δ); gskl-1(Δ)* mutants produce 30% dead embryos. Interestingly, the triple-deletion, *gskl-2(Δ) gsp-4(Δ); gskl-1(Δ)* produce 68% dead embryos, some of which skip MII, similar to *memi-1/2/3(RNAi)*. Therefore, *gskl-1* and *gsp-4* could participate in the MEMI pathway to specify MII after fertilization.

Because of the genetic interaction between *gskl-1* and *gsp-4* in the early embryo, and the fact that GSP-3/4 is required for normal sperm motility and sperm meiosis, we also tested whether the *gskl-1/gskl-2* have sperm functions. FLAG and Ollas tagged *gskl-1* and *gskl-2* were found only in male-specific *fem-3* mutants but absent in female-specific *fem-1* mutants by western blot. Immunostaining revealed strong expression of those tagged proteins in sperm. It was also found that the *gskl-2(Δ); gskl-1(Δ)* mutants exhibited reduced sperm motility *in vivo*, as well as altered sperm morphology and slow pseudopod formation *in vitro*. Consistent with these defects, pseudopod treadmilling rates were also reduced in the *gskl-2(Δ); gskl-1(Δ)* mutant. Frequent chromosome segregation defects and spermatid budding defects during sperm meiosis were also observed in *gskl-2(Δ); gskl-1(Δ)*.

This work suggests that the GSK-3s and PP1 phosphatases perform some similar functions with respect to sperm motility and meiosis, and they participate in post-fertilization functions involving MEMI.

2. Materials and methods

2.1 *Caenorhabditis elegans* nomenclature

The nomenclature for *C. elegans* was first described by Sydney Brenner (Brenner 1974). Later, many other eminent scientists, namely, Bob Horvitz, Jonathan Hodgkin, Don Riddle, Mark Edgley, and Tim Schedl have played an instrumental role in standardizing the guidelines for nomenclature and helped to make it an essential part of WormBase, which provides necessary information about nematode genomes, transcriptome, genetic location and probable interactions among different genes (Horvitz et al. 1979; Thompson et al. 2013). In WormBase, each gene has a Gene ID, sequence name and gene name. Each Gene ID uniquely refers to a specific locus in the genome. Each sequence name is derived from the plasmid, cosmid or YAC on which they reside (1998). For example, 'R03D7.5' indicates that this is the fifth gene on the R03D7 cosmid. Gene names consist of an italicized three- or four-letter name that usually refers to either gene function or mutant phenotype, followed by a hyphen and an Arabic number. For example, *mei-1* is involved in the meiosis-to-mitosis transition of oocyte, and *dpy-10* refers to one of many genes that cause a Dumpy phenotype when mutated. Phenotypes can be described in a capitalized word (*i.e.*, Dumpy) or by a three-letter abbreviation (*i.e.*, Dpy). A specific allele of the gene is named by using a unique laboratory code of one to three italicized letters followed by an Arabic number. For example, 'abc' refers to the allele discovered in the Srayko laboratory in Alberta, Canada. Each *C. elegans* laboratory is assigned a code for naming strains, *i.e.*, the Srayko laboratory strain designation is MAS. Non-italicized

capitals letters are used to denote protein product of a specific gene, *i.e.*, GSP-4 is the protein product of the *gsp-4* gene. A gene condition caused by RNAi-mediated interference (RNAi) is indicated with parentheses after the gene name. For example, *gska-3(RNAi)* denotes double stranded RNAi-mediated interference of *gska-3*, thus, this notation is used similarly to mutant alleles of genes.

2.2 Strains and Maintenance

2.2.1 Maintenance

All worms were maintained following standard protocol (Brenner 1974). Worms were grown on NGM agar plates that consists of 3 gm NaCl, 2.5 gm Peptone, 17 gm Agar, 975 ml dH₂O, autoclave and cooled to 55°C. Further, 1ml of 1M CaCl₂, 1 ml 1M of MgSO₄, 25 ml of 1 M Potassium Phosphate pH 6.0, 1ml of 5 mg/ml cholesterol in Ethanol were added. The plates were left overnight at room temperature to solidify and then seeded with an auxotrophic *E. coli* strain OP50. Unless otherwise state, all strains were maintained at 20°C. In general, temperature-sensitive strains were maintained at 15°C, and shifted to the restrictive temperature of 25°C for phenotypic characterization.

2.2.2 Mating Strategies

C. elegans has two sexual forms: male and hermaphrodite, which progress through four larval stages (L1 – L4) to become adult (Hodgkin 1987; Zarkower 2006). Both

males and hermaphrodites perform spermatogenesis during the L4 larval stage. After L4, hermaphrodite germ cells stop spermatogenesis and switch to oogenesis for the rest of their life, while males continue spermatogenesis. The oocytes progress through the spermathecae to be fertilized by sperm and then the fertilized eggs get released into the environment after spending a variable amount of time developing within the uterus. Once the hermaphrodite's sperm is depleted, unfertilized oocytes are expelled to the environment. Hermaphrodites typically produce less than 0.2% male progeny spontaneously, which can be used for mating, however the frequency of males can be increased by incubating L4-stage hermaphrodites at 30°C for four hours and then down-shifting the temperature back to physiological norms for egg-laying (Zevian and Yanowitz 2014). This heat shock increases the frequency of nondisjunction of X chromosomes during meiosis, which produces XO zygotes that develop as male. For mating, 20 L4 and young adult males were plated with 5 L4 hermaphrodites in mating plates for 20 hours. The hermaphrodites were then separated from the mating plates and were placed in individual plates. Successfully mated hermaphrodites produced almost 50% males as outcrossed progeny.

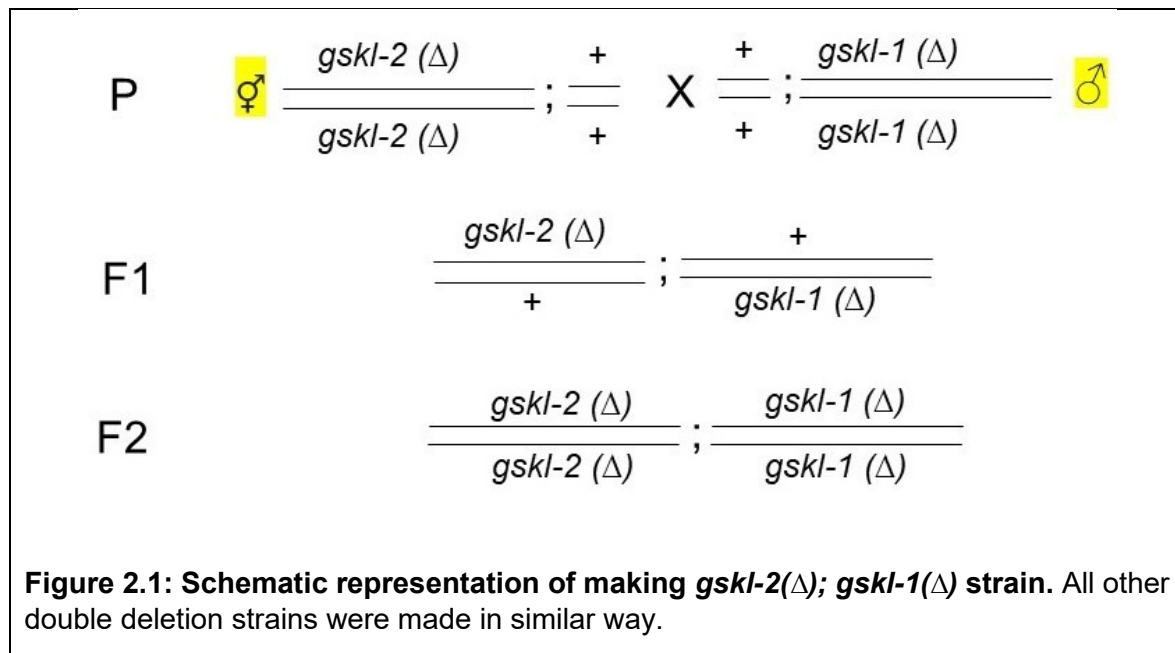
In order to facilitate male production without the heat-shock method mentioned above, I used the *him-8(e1489)* mutant strain, which allows hermaphrodites to produce 35% male by increasing non-disjunction of the X chromosome (Hodgkin et al. 1979; Phillips et al. 2005). The *swm-1(me87) him-5(e1490)* mutant strain was used to observe active sperm (Stanfield and Villeneuve 2006). This *swm-1(me87) him-5(e1490)* males does not mate easily to hermaphrodites. So, I set up several mating plates with five L4 *swm-1(me87) him-5(e1490)* males with two L4 hermaphrodites.

2.2.3 Making of Strains

All strains used in this thesis are listed in Table 2.1.

Table2.1: List of Strains		
Strain name	Genotype	Resource
N2	<i>wild type</i>	CGC
MAS305	<i>gskl-1(abc41)</i>	This study
MAS306	<i>gskl-1(abc57)</i>	This study
MAS318	<i>gskl-1(abc57); dpy-10</i>	This study
MAS319	<i>gskl-1(abc41); dpy-10</i>	This study
MAS320	<i>gskl-1(abc57); mCherry</i>	This study
MAS329	<i>gskl-1(abc51)</i>	This study
MAS330	<i>gfp::gsp-4; mCherry</i>	This study
MAS331	<i>gskl-1(abc41); mCherry</i>	This study
MAS332	<i>gskl-1(abc51); mCherry</i>	This study
MAS333	<i>gskl-1(abc59)</i>	This study
MAS334	<i>gskl-1(abc57); memi-1(sb41)</i>	This study
CB4108	<i>fog-2(q71)</i>	CGC
FX04146	<i>R03D7.5(tm4146)</i>	NBRP
FX01237	<i>gsk-3(tm1237)</i>	NBRP
RB1034	<i>gska-3(ok970)</i>	CGC
FX02789	<i>Y106G6E.1(tm2789)</i>	NBRP
FX05959	<i>C44H4.6(tm5959)</i>	NBRP
FX04021	<i>F21F3.2(tm4021)</i>	NBRP
FX04165	<i>Y106G6D.4(tm4165)</i>	NBRP
FX05415	<i>gsp-4(tm5415)</i>	NBRP
CA151	<i>him-8(me4)</i>	CGC
MAS335	<i>gska-3(ok970); R03D7.5(tm4146)</i>	This study
MAS336	<i>gsp-4(tm5415); R03D7.5(tm4146)</i>	This study
MAS337	<i>R03D7.5(tm4146); Y106G6D.4(tm4165)</i>	This study
MAS338	<i>R03D7.5(tm4146); C44H4.6(tm5959)</i>	This study
MAS339	<i>R03D7.5(tm4146); gsk-3(tm1237)</i>	This study
MAS340	<i>R03D7.5(tm4146); F21F3.2(tm4021)</i>	This study
MAS352	<i>R03D7.5(tm4146); Y106G6E.1(tm2789)</i>	This study
MAS343	<i>him-8(me4) itls37[pie-1::mCherry-HIS58]; ruls57[pie-1::GFP-tbb-2]</i>	This study
MAS344	<i>gska-3(ok970); R03D7.5(tm4146); him-8(me4) itls37[pie-1::mCherry-HIS58]; ruls57[pie-1::GFP-tbb-2]</i>	This study
AV285	<i>swm-1(me87) him-5(e1490)</i>	CGC
MAS356	<i>gska-3(ok970); R03D7.5(tm4146); swm-1(me87) him-5(e1490)</i>	This study
MAS367	<i>3xFLAG::R03D7.5</i>	This study
MAS372	<i>Ollas::gska-3</i>	This study
MAS373	<i>Ollas::gska-3; him-8(me4)</i>	This study
MAS374	<i>3xFLAG::R03D7.5; him-8(me4)</i>	This study
MAS375	<i>Ollas::gska-3; swm-1(me87) him-5(e1490)</i>	This study
MAS376	<i>3xFLAG::R03D7.5; swm-1(me87) him-5(e1490)</i>	This study
JK816	<i>fem-3(q20)</i>	CGC
BA17	<i>fem-1(hc17)</i>	CGC
MAS383	<i>Ollas::gska-3; fem-1(hc17)</i>	This study
MAS384	<i>3xFLAG::R03D7.5; fem-1(hc17)</i>	This study
MAS387	<i>3xFLAG::R03D7.5; fem-3(q20)</i>	This study
MAS390	<i>Ollas::gska-3; fem-3(q20)</i>	This study

To characterize the function of *gskl-1*, a deletion allele *gskl-1(Δ)* was used to make pairwise double-deletion combinations with other members of the *gsk-3* family. *gskl-1(Δ)* males were crossed to each deletion allele strain to get F1 trans heterozygotes. The probability of getting a double homozygote from F1 trans heterozygous was 1/16 if the two genes concerned are located on different chromosomes. So, in the F2 generation, 36 worms were screened by PCR to detect worms homozygous for *gskl-1(Δ)* and the other deletion allele.



To visualize chromatin and tubulin during *in vivo* imaging, I made a *him-8(me4)* strain that expressed *mCherry::histone* and *GFP::tubulin*. The tubulin-GFP and histone-mCherry markers were made by particle bombardment and we had previously determined that mCherry is linked with LG IV (Ataeian et al. 2016). *him-8(me4)* males were mated to *mCherry::histone* and *GFP::tubulin* expressing hermaphrodites to get trans heterozygotes *him-8(me4) +/ + mCherry; GFP::tubulin/ +*. Because *him-8* and

mCherry are on the same chromosome (IV), I screened 115 *him-8(me4); GFP::tubulin* hermaphrodites in the F2 generation to identify 1 *mCherry* heterozygous recombinant. I picked 16 progeny from that worm to identify the *him-8(me4) mCherry::histone; GFP::tubulin* homozygous strain. I used this strain to mate with *gskl-2(Δ); gskl-1(Δ)* to get the *gskl-2(Δ); gskl-1(Δ); him-8(me4) mCherry::histone; GFP::tubulin* strain.

gskl-2(Δ); gskl-1(Δ); him-8(me4) mCherry::histone; GFP::tubulin males were mated to a *gsp-4(Δ); gskl-1(Δ)* strain to get a trans heterozygote *gskl-2(Δ) +/- + gsp-4(Δ); gskl-1(Δ); him-8(me4) mCherry::histone/ +; GFP::tubulin / +*. In next generation, I first picked up 60 homozygous worms that expressed both *mCherry::histone* and *GFP::tubulin* and then did PCR to confirm the genotype of *gskl-2(Δ)* and *gsp-4(Δ)*. From the *gskl-2(Δ) +/- + gskl-2(Δ) gsp-4(Δ)* worm, I picked 32 *GFP::tubulin* and *mCherry::histone* positive progeny and then used PCR to identify *gskl-2(Δ) gsp-4(Δ); gskl-1(Δ)* homozygous worms. Subsequent screening for *mCherry::histone* and *GFP::tubulin* fluorescence in the progeny confirmed the strain *gskl-2(Δ) gsp-4(Δ); gskl-1(Δ); mcherry::histone; GFP::tubulin*. For example, it would be unlikely to recover 16/16 mCherry progeny from an mCherry-positive hermaphrodite unless that parent was homozygous (99% confidence).

Using the CRISPR-Cas9 technique (described below), I created 3xFLAG-tagged *gskl-1* and Ollas-tagged *gskl-2*. I used males from those strains to mate with feminized *fem-1(hc17)* and masculinized *fem-3(q20)* mutants. Both of these mutations are temperature sensitive and self-fertilize at the permissive temperature of 15°C. Fifty progeny of the F1 trans heterozygous worms were allowed to lay eggs at 15°C for 36 hours. After 36 hours, the worms were transferred to 25°C on fresh plates. As *fem-*

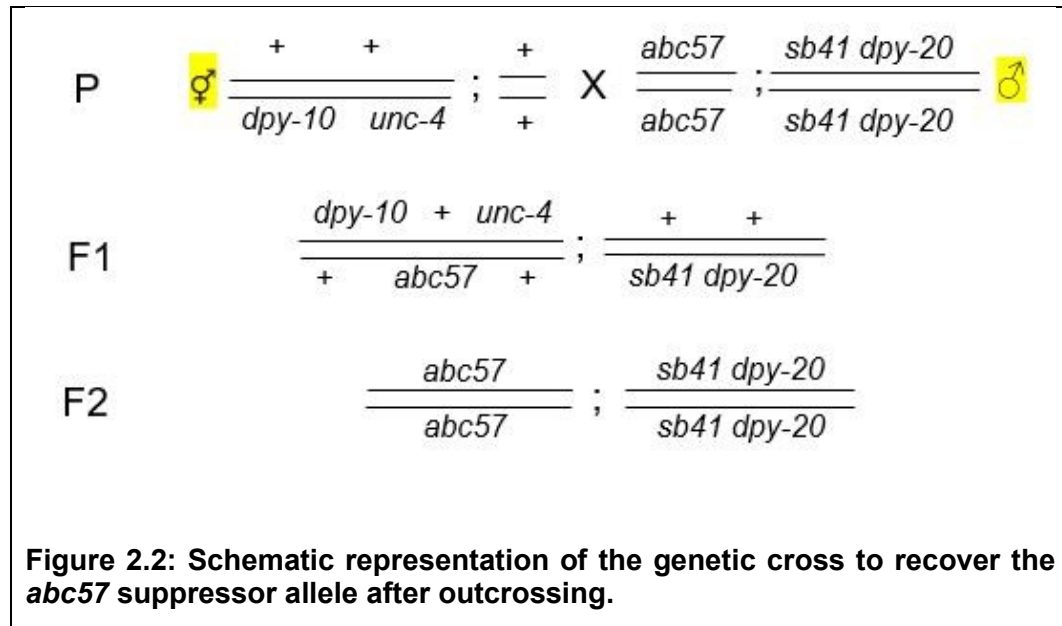
1(hc17) and *fem-3(q20)* become sterile at 25°C, I identified *fem-1(hc17)* and *fem-3(q20)* homozygotes on the basis of the respective phenotype and then *3xFLAG::gskl-1* and *Ollas::gskl-2* were identified by PCR. In this way, I made *3xFLAG::gskl-1; fem-1(hc17)*, *3X-FLAG::gskl-1; fem-3(q20)* and *Ollas::gskl-2; fem-1(hc17)* and *Ollas::gskl-2; fem-3(q20)* strains.

In order to make *gskl-2(Δ); gskl-1(Δ); swm-1(me87) him-5(e1490)* males from *swm-1(me87) him-5(e1490)* were mated to *gskl-2(Δ); gskl-1(Δ)* hermaphrodites to get trans heterozygotes in F1 generation. Based on *him-5(e1490)* phenotype, 40 *him-5(e1490)* worms were picked up in F2 generation to find out *gskl-2(Δ); gskl-1(Δ)/ +* worms. In next generation, homozygous *gskl-2(Δ); gskl-1(Δ); swm-1(me87) him-5(e1490)* were confirmed by PCR and *swm-1(me66)* was confirmed by sequencing.

2.2.4 Recovering *gskl-1* suppressor alleles after outcrossing

In an EMS-based screen for suppressors of *memi-1(sb41)*, we identified four alleles of *gskl-1*: *abc41*, *abc51*, *abc57* and *abc59* (Herzog 2018). As the EMS treatment causes several mutations, it was therefore necessary to backcross those suppressor strains to the wild-type in order to reduce background mutations. I used a strain with two markers that flank *gskl-1*, *dpy-10* and *unc-4* on chromosome II, to recover *abc57* and *abc41* suppressor alleles after backcrossing. At first, *abc57; memi-1(sb41) dpy-20* hermaphrodites were mated to heterozygous *dpy-10 unc-4* males. In the F1 generation, 50% of the progeny were *trans* heterozygous *+ abc57 + / dpy-10 + unc-4; memi-1(sb41) dpy-20 / + +*. In the F2 generation, 32 worms were picked from

the *trans* heterozygous mother to recover *abc57; memi-1(sb41) dpy-20* (Figure 2.2). Using a similar approach, I recovered *abc41; memi-1(sb41) dpy-20*.



2.2.5 Freezing Strains

Five L4 stage hermaphrodites were placed on fresh agar plates seeded with OP50 and allowed to lay eggs. Within two generations, the plates are depleted with OP50 and crowded with L1 or L2 larvae. In the absence of food, L1 or L2 enters the “dauer” stage. Then, the worms were serially washed off from those plates to make a concentrated stock in 1 ml. The concentrated stock was then divided amongst five 1.5 ml cryo tubes (Corning) and an equal volume of freezing solution was added. Those tubes were then placed in the -80°C freezer within a well-insulated styrofoam box to facilitate slow cooling. One tube was thawed after two days to confirm survival after freezing. After the confirmation, two tubes were kept at -80°C and two tubes were

placed in a liquid Nitrogen tank. The location of the strain was then recorded, *i.e.*, the MAS344 strain is located at Box number 14, position 1 and 2, and this information was entered into the Srayko lab worm database. Frozen strains can be thawed at room temperature on warm plates for future experiments.

2.3 PCR and Sequencing

PCR and sequencing were frequently used to determine the genotype of worms. Sequencing of a candidate gene was made by following the steps as mentioned below:

2.3.1 Worm Lysis

To prepare the DNA, 2 to 4 gravid hermaphrodites were transferred into 6 μ l of worm lysis buffer (50 mM KCl, 10 mM Tris pH 8.3, 2.5 mM MgCl₂, 0.45% NP-40, 0.45% Tween 20, 0.01% Gelatin) with a final concentration of 1 mg/ml proteinase K. The mixture was then heated at 65°C for an hour followed by another 15 minutes at 95°C. This sample was used as the template for PCR reaction.

2.3.2 PCR reaction

In general, a master mix was made for all control and experimental PCR samples. For each PCR sample, 0.25 μ l Taq DNA polymerase (NEB), 5 μ l 10X buffer, 0.25 μ l of 10 mM of each dNTPs, 1 μ l Forward and 1 μ l Reverse primer of 10 mM were added in the master mix. The final volume was adjusted to 25 μ l by adding dH₂O. For the

amplification of *gskl-2*, 0.5 μ l Taq DNA polymerase was used for each sample because the product size for the wild type was 3300 bp.

A Biorad thermocycler was used for performing PCR reactions. During the PCR reaction DNA samples were made to undergo denaturation phase, annealing phase, and extension phase and this cycle was repeated for 35 times. Denaturation of the sample was done for 30 seconds at 95°C. For annealing of primers as observed in most cases, an annealing temperature of 56°C was maintained and the duration of the annealing process was set for 30 seconds. In general, the extension time was set for 1 minute per 1000 bp PCR product, and the temperature was 72°C. Primers annealing temperatures used in this thesis are provided in Table 2.

For some experiments, a high fidelity PCR reaction was performed by using Roche high fidelity Taq polymerase (Roche, 11732641001). In this case, reaction mixture 1 containing dNTPs, forward primer, reverse primer and 25 ng DNA and reaction mixture 2 containing 5 μ l 10X buffer, 0.75 μ l Roche high fidelity Taq polymerase were prepared separately on ice at first. Then, both mixtures were mixed up together to make the final reaction volume 50 μ l. The PCR reaction was set up in a thermocycler as mentioned above with an additional 10 minute extension phase at 72°C after completion of the final PCR cycle.

2.3.3 Preparation of sequencing sample

The size of the PCR product was first confirmed by gel electrophoresis. A gel having 1% agarose with 2.5 μ l of 0.5 μ g/ml Ethidium Bromide per 100 ml of agarose

was commonly used to identify PCR products. For DNA sequencing, if the right size band was detected, the PCR product was purified by Qiagen PCR purification kit. The concentration of purified DNA was determined by a spectrophotometer. A total volume of 10 μ l, containing 22.5 ng/ μ l of purified DNA and 1 μ l of sequencing primer of 2.5 mM was submitted to Molecular Biology Service Unit (MBSU) at University of Alberta for sequencing.

2.4 RNAi by feeding

RNA-mediated gene interference (RNAi) was used to reduce the function of some genes. Usually, RNAi in *C. elegans* is achieved either by feeding worms bacteria that express the dsRNA, or by injecting dsRNA directly into the worm. For my experiments, I used RNAi by feeding according to a standard protocol (Kamath and Ahringer 2003). Freshly prepared NGM plates with 0.1 mM IPTG (isopropyl β -D-1-thiogalactopyranoside) and 25 μ g/ml Carbenicillin were used for bacterial seeding. The RNAi vector L4440 consists of a T7 promoter on each side of the MCS. These plasmids are used to transform an RNase III-deficient *E. coli* strain (HT115) that carries IPTG-inducible T7 polymerase. The transformed HT115 strains were grown overnight at 37°C in LB broth (1.0 mg/ml Bacto-tryptone, 0.5 mg/ml Bacto-yeast extract, 0.5 mg/ml NaCl) with 50 μ g/ml ampicillin. The RNAi plates were seeded with this RNAi bacterial culture and left overnight at room temperature, to allow induction of the dsRNA. The next day, L4 larval stage worms were transferred into those plates. Those worms were transferred into fresh RNAi plates after 24 hours. For all RNAi experiments, the L4440

empty vector was used as a negative control and *mel-26(RNAi)* was used as positive control to make sure that RNAi plates were working. *mel-26* encodes a CUL-3 substrate-specific adaptor that is required to degrade katanin subunit MEI-1 and loss of *mel-26* results in maternal-effect embryonic lethality (Dow and Mains 1998).

2.5 Embryonic viability assays

Scoring the viability of eggs on a plate is a common first step to determine if a gene has an essential function during any stage of embryogenesis. I used RNAi or deletion alleles of those genes. I calculated embryonic viability to see if that deletion or RNAi mediated knocking down caused any significant difference with the respective control group. Worms of respective control and experimental groups were maintained in freshly prepared NGM plates at permissive temperature before the experiment. Single L4 hermaphrodites were transferred to a fresh plate and allowed to lay eggs on individual NGM agar plates with fresh *Escherichia coli* OP50 at the indicated temperature. This was followed by the transfer to fresh plates every 24 hours until the worms stopped laying eggs. Eggs that were not hatched after 48 hours at 20°C or 36 hours at 25°C were scored as dead. Embryonic viability refers to the number of hatched larvae divided by the total progeny. Unfertilized oocytes are distinguishable from eggs and were not included in the total progeny when determining embryonic viability.

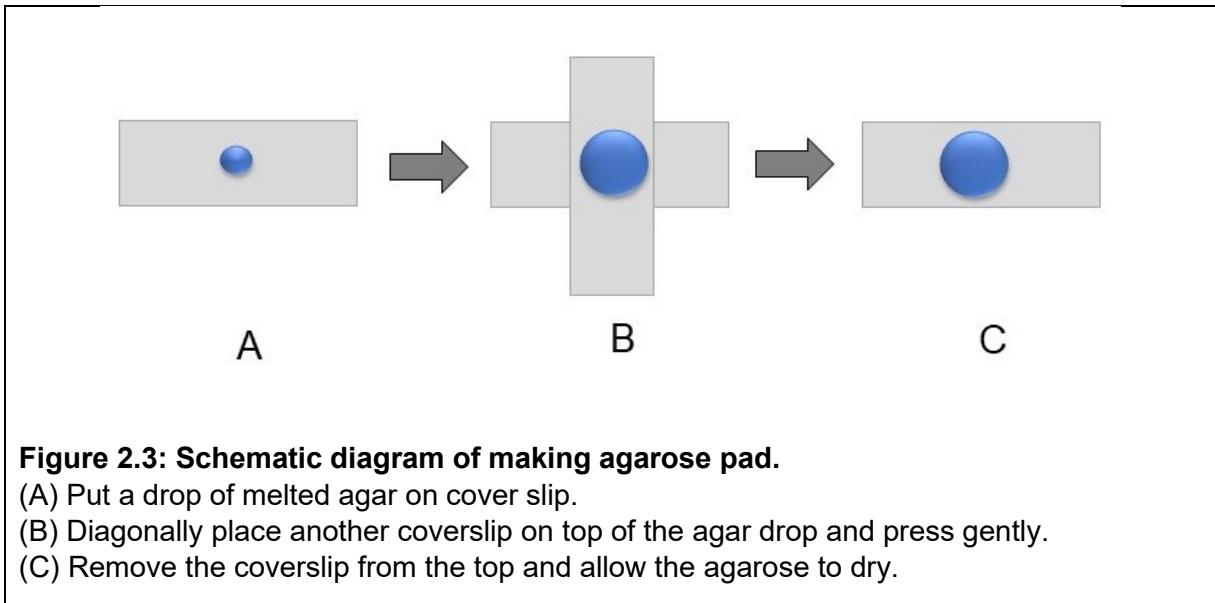
Embryonic viability was also calculated to determine the suppression of *memi-1(sb41)*. For this purpose, L4 hermaphrodites from the suppressor strain were transferred from permissive temperature 15°C to restrictive temperature 25°C.

2.6 Testing paternal-effect embryonic lethality

Paternal-effect embryonic lethality was determined by three different methods. For each experiment, twenty males of a given genotype were mated to five hermaphrodites of indicated genotype at 20°C, as described below. Firstly, I used *him-8(e1489)* males to mate to *gskl-2(Δ); gskl-1(Δ)* hermaphrodites and scored embryonic viability of the outcrossed progeny. Successful mating was determined by the presence of approximately 50% male progeny amongst survivors. Secondly, I used *fog-2(q71)* females, which can only produce progeny after mating with males (Schedl and Kimble 1988). Males of *gskl-2(Δ); gskl-1(Δ)* were mated to *fog-2(q71)* females, followed by scoring embryonic viability. Lastly, *gskl-2(Δ); gskl-1(Δ)* males were used to mate with *gskl-2(Δ); gskl-1(Δ)* hermaphrodites to observe whether both *gskl-2(Δ)/+; gskl-1(Δ)* and *gskl-2(Δ); gskl-1(Δ)* progeny were viable in a 1:1 ratio. The genotypes of 42 outcrossed worms were confirmed through PCR for both *gskl-1* and *gskl-2*.

2.7. Preparation of agarose pads for *C. elegans* microinjection

Worms were mounted on an agarose pad before imaging and microinjection. An agarose solution (2.1% in 1X PBS) was melted in the microwave and then a small drop was placed on a 22X60 mm coverslip. Perpendicular with the first slide, another 22X60 mm coverslip was placed on top of that melted agar very quickly. After the agarose solidified, one cover slip was gently slid away from the other, leaving the agarose stuck to one slide. Agarose pads were allowed to dry completely and stored at room temperature.



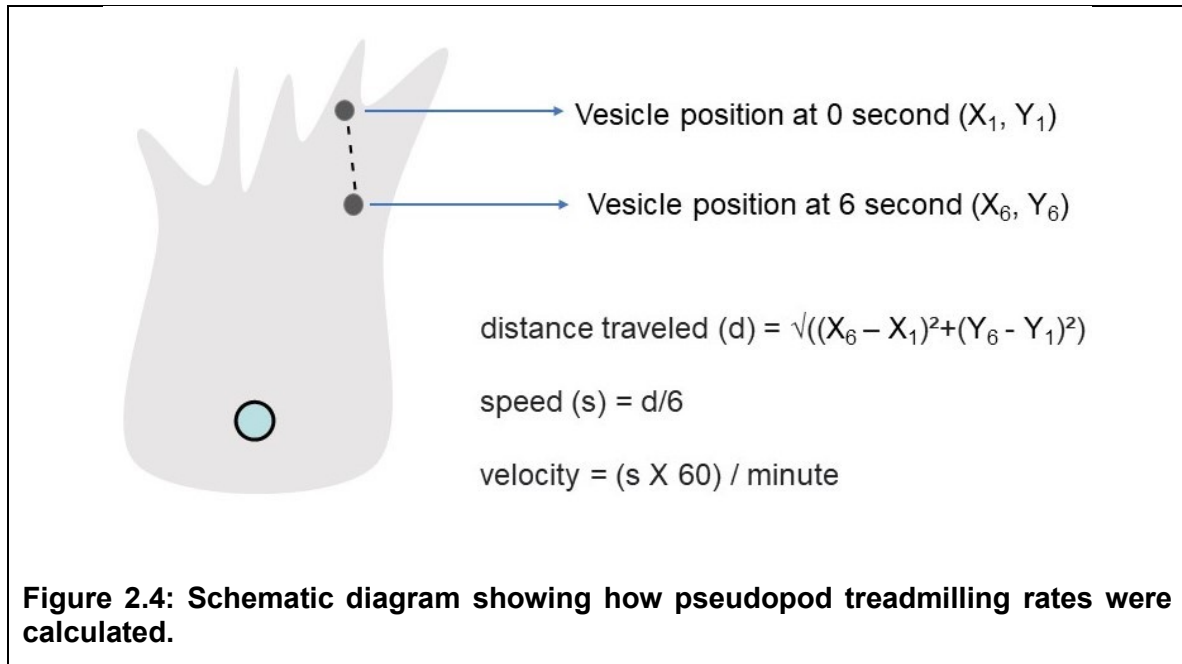
2.8. Sperm migration assay

In order to assess the efficiency of male sperm migration towards the hermaphrodite spermatheca after copulation, *gskl-2*(Δ); *gskl-1*(Δ) and wild-type male worms expressing mCherry histone were used as experimental and controls, respectively. In this assay, 35-40 males of each group were mated to five L4 larval stages wild-type hermaphrodites at 20°C for 24 hr. After that, hermaphrodites were picked off from the mating plates and kept on fresh plates for an hour in the absence of any male. Then, hermaphrodites were anesthetized with 200 μ m levamisole in M9 buffer (3.0 g KH₂PO₄, 6.0 g Na₂HPO₄, 0.5 g NaCl, 1.0 g NH₄Cl in H₂O to make final volume 1 litre) and mounted onto a freshly made 2% agarose gel pad. Fluorescent images were taken for each worm (a Z-stack of 14 planes, spaced 1.5 μ m apart). The

fluorescent image stacks were projected as a maximum before merging with DIC in Adobe photoshop.

2.9 Pseudopod treadmilling rate analysis

swm-1(me66) him-5(e1490) and *gskl-2(Δ); gskl-1(Δ); swm-1(me66) him-5(e1490)* male worms were used as control and experimental respectively to measure pseudopod treadmilling rates. L4 larval stage males of respective genotypes were separated from hermaphrodites and kept in a fresh plate at 20°C overnight. On the next day, males were cut, approximately 2/3 distance from the head, in 50 μL SM buffer (defined) on a polylysine-coated 22X60 coverslip to release the activated sperm. Pseudopod treadmilling was captured by time-lapse recordings with a 1 sec interval using a 60X oil (NA 1.42) objective on an Olympus DIC IX-81 microscope with a Hamamatsu Orca R2 camera controlled by MetaMorph software. Vesicles within the pseudopod were tracked for 6 seconds to determine treadmilling rates.



2.10 *In vitro* sperm activation

L4 virgin *him-8* and *gskl-2*(Δ); *gskl-1*(Δ) males were transferred to fresh NGM plates for 18 hours at 20°C to prevent spermatid activation. Two males were dissected in an activation solution that contained 200 $\mu\text{g}/\text{mL}$ Pronase in SM buffer with 1 mg/mL BSA. Vaseline was used to surround the buffer and then an 18X18 mm coverslip was placed on top to make a hollow chamber to prevent evaporation. Times lapse DIC images were captured at 20 second intervals using a 60X oil (NA 1.42) objective on an Olympus IX-81 microscope.

2.11 Live imaging of male meiosis

Male worms expressing mCherry-histone and GFP-tubulin were dissected in 3.5 μ L sperm media (SM) buffer that contained 50 mM HEPES (pH 7), 50 mM NaCl, 25 mM KCl, 1 mM MgSO₄, 5 mM CaCl₂, and 1 mg/ml BSA. An 18X18 mm coverslip was placed on top and gentle pressure was applied to release spermatocytes from the gonad. The coverslip was sealed with a thin ring of Dow Corning high vacuum grease to prevent evaporation. Time-lapse images were captured with a Hamamatsu Orca R2 camera on an inverted Olympus IX81 microscope with a Yokogawa CSU-10 spinning disc confocal head modified with a condenser lens in the optical path (Quorum Technologies). Z stacks of 3 planes with 1.2 μ m apart, were captured at 15 second-interval using a 60X oil (NA 1.42) objective lens controlled by MetaMorph software. Image files were analyzed using MetaMorph software. A maximum projection of these three planes was used to make the figures. TIFF Raw images were converted to 8 bit RGB planes for each colour and these were merged in adobe photoshop to make the figures.

2.12 CRISPR-Cas9 mediated gene editing

The Type II CRISPR/Cas9 bacterial immune system has been exploited to precisely edit genomic DNA (Doudna and Charpentier 2014). The function of the Cas9 nuclease depends on two sequences on the target DNA: a protospacer adjacent motif (PAM) and a 20 bp region which is complementary to CRISPR RNA (crRNA) sequence. This crRNA guides Cas9 to identify the PAM site and a *trans* activating RNA binds to

both crRNA and Cas9 to form the ribonucleoprotein (RNP) complex. At the initial step, this RNP complex introduces a double-stranded break (DSB) in the target DNA (Jiang and Marraffini 2015). Following this, the DSB is repaired by the endogenous homology directed repair system by using an already provided DNA template which contains the desired edit (Jasin and Haber 2016). In *C. elegans*, a *dpy-10* co-CRISPR strategy is adopted to identify successfully injected hermaphrodites. A point mutation in *dpy-10* causes a dominant Roller phenotype, such that heterozygous F1 progeny of successfully injected hermaphrodites can be identified (Arribere et al. 2014; Paix et al. 2014). This co-CRISPR strategy increases the chances of getting desired edits in the target gene (Paix et al. 2015).

There are mainly eight steps to successfully edit a target gene by CRISPR-Cas9:

- i. Identify PAM sites
- ii. Design crRNA
- iii. Design tracrRNA
- iv. Perform *in vitro* Cas9 digestion assay
- v. Prepare repair templates
- vi. Make injection cocktails
- vii. Inject worms
- viii. Screen for jackpot broods using Co-transformation marker (Rol/Dpy)
- ix. Screen using PCR to isolate a homozygous strain

2.12.1 Identifying PAM sites

The first step in CRISPR-Cas9 mediated gene editing technique is to identify a PAM site in the target gene which is recognised by the Cas9 enzyme. NGG is the canonical PAM site for *Streptococcus pyogenes* cas9, which was used for all of my experiments (Cas9 enzyme; IDT 1081059, derived from *S. pyogenes*). The distance of the PAM site from the point of editing was kept between 10-30 nucleotides, as the efficiency of editing is inversely proportional to this distance (Paix et al. 2015). I used <http://crispr.mit.edu/> to check the off target sites of the selected PAM site.

2.12.2 Designing crRNA

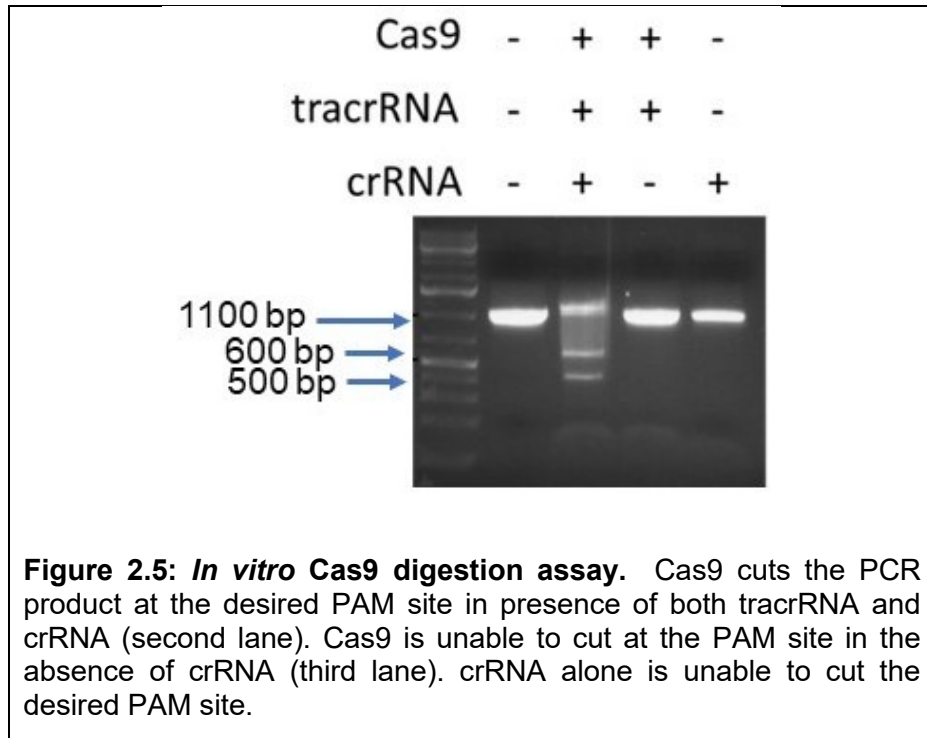
The crRNA refers to a region of homology 20 nt immediately upstream of the PAM site, excluding the PAM site. This guide RNA segment is followed by a universal sequence that is necessary for cutting the double-stranded DNA target. Therefore, the sequence of the crRNA will be 20 nt, specific to the target gene, followed by a universal sequence, GUUUUAGAGCUAUGCUGUUUUG. crRNAs (10 nmol) were ordered from IDT and 16.7 µl TE buffer (pH 7.6) was added to make a 0.6 mM crRNA stock. From the stock solution, 1 µl aliquots were made and stored at -80°C. For the *dpy-10* crRNA, 0.2 µl aliquots were frozen.

2.12.3 CRISPR tracrRNA

tracrRNA is a 74 nt universal sequence required for Cas9 function. I ordered 20 nmol tracrRNA from IDT and added 117.6 μ l TE buffer (pH7.6) to make a 0.17 mM stock solution. Aliquots (5 μ l) were made from the stock solution and stored at -80°C. In addition, I also made another 0.01 mM stock solution of tracrRNA to use in *in vitro* cas9 digestion assays.

2.12.4 *In vitro* Cas9 digestion assay

I conducted an *in vitro* Cas9 digestion assay to make sure that crRNA was able to guide Cas9 enzyme to the PAM site to precisely cut the DNA. I designed primers to amplify the target gene, with the expected cut site at 2/3 total PCR fragment length. If cas9 cuts the DNA, I expect to observe two separate bands on an agarose gel. At first, 2 μ l 10x buffer, 0.5 μ l Cas9 (IDT), 1 μ l tracrRNA (10 μ M) and 1 μ l crRNA (10 μ M) was mixed on ice and then incubated at 25°C for 10 minutes. Next, 1 pmol DNA was added and the final volume was adjusted to 20 μ l by adding nuclease free water. The reaction mixture was kept at 37°C for 1 hour. After incubation, the sample was run on an agarose gel with ethidium bromide to see if the target DNA was cut or not (Figure 2.5).



2.12.5 Preparing Repair Templates

There are three different approaches I have taken to tag my target genes. They are

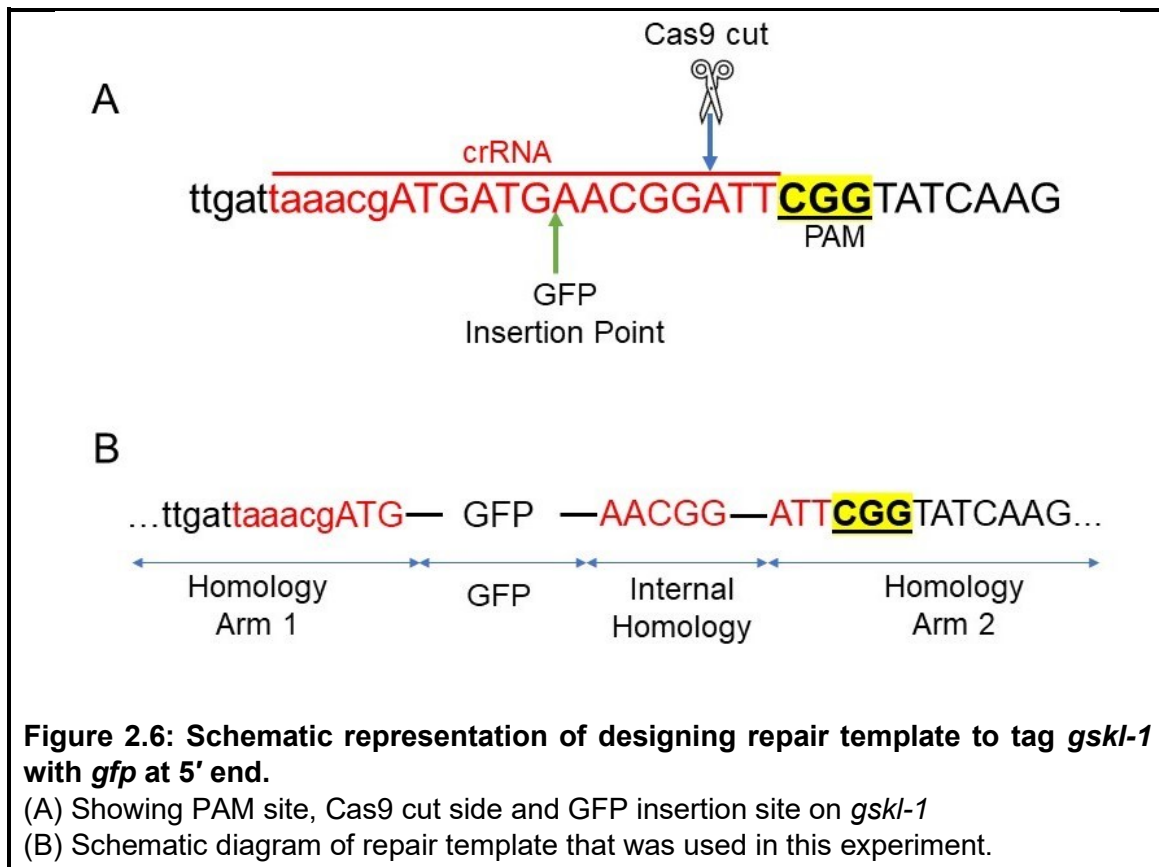
- i) Tagged with GFP
- ii) Tagged with small tags *i.e.*, 3xFLAG, Ollas
- iii) Creation of point mutation.

In each case, different strategies to design the repair template were used as described below:

2.12.5.1 Preparing GFP repair template

I tagged *gskl-1* with GFP in its 5' end. I used pcM1.53 plasmid DNA as my PCR template to generate a PCR fragment with the GFP gene flanked by *gskl-1*. Plasmid DNA was isolated with a CTAB precipitation following standard protocol. Briefly, 50 ml DH5 α culture with the plasmid was grown overnight. The culture was centrifuged to collect the pellet, which was resuspended in 1.25 ml of GTE (50 mM Glucose, 25 mM Tris pH 8.0, 10 mM EDTA). Then, 2 ml of 0.2 M NaOH with 1% SDS was added, gently mixed, and incubated at room temperature for 5 minutes. Further, 1.85 ml of KAc (3 M potassium acetate, 2M acetic acid) was added. After keeping that tube in an ice bath for 5 minutes, it was centrifuged at 12,000 g at 4°C for 10 minutes. The supernatant was discarded and 4 ml NH₄Ac/EDTA (1 M ammonium acetate, 10 mM EDTA) was added to the pellet. Cold 95% ethanol (10 ml) was added and the solution was centrifuged at 12,000 g at 4°C for 5 minutes. The pellet was collected and washed with 5 ml of 70% ethanol and was allowed to air dry at room temperature. The pellet was then resuspended in 500 μ l of TE pH 7.5 and the DNA concentration was measured using a spectrophotometer. This purified DNA was then used as a PCR template to amplify GFP. I designed two primers to amplify GFP that included 35 bp homology arms from *gskl-1* and I used high-fidelity Taq polymerase (Roche) to avoid replication errors during PCR. The PCR product was separated on a 1% agarose gel to extract the appropriate size band by using a gel extraction kit (Qiagen). This purified product was then used as a template for the second round of high-fidelity nested PCR. This time, the flanking region of *gskl-1* on the first primer set was used as a nested primer. I aimed to set up eight reactions in the second round of high-fidelity PCR and combined

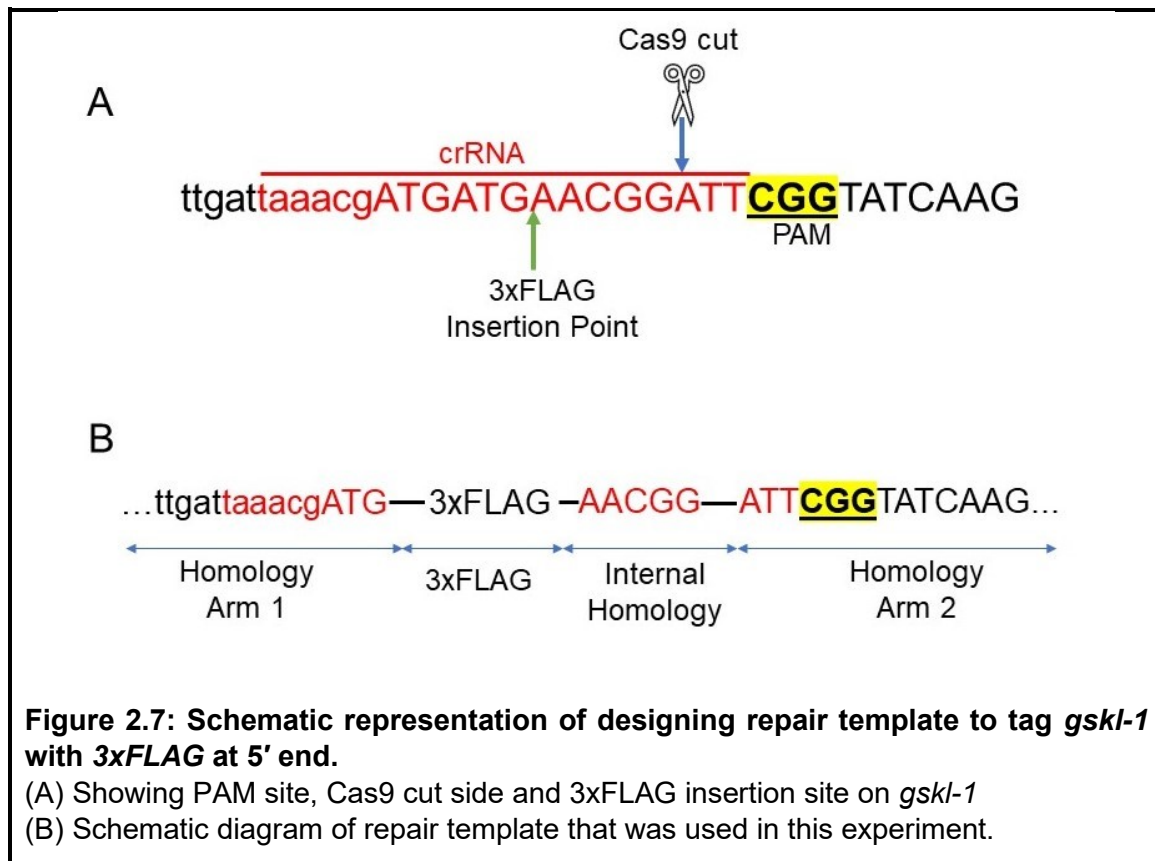
all PCR products together in the end. I analyzed the sample (1 ul) in 1% agarose gel to confirm the product size. In the final step, I used the Qiagen minelute kit to isolate the PCR product. I used 20 µl HPLC grade water to elute the DNA. The concentration of that purified DNA was 475 ng/µl which was used as a repair template. The detail of this process is schematically represented in the following diagram.



2.12.5.2 Preparing repair templates for small tags

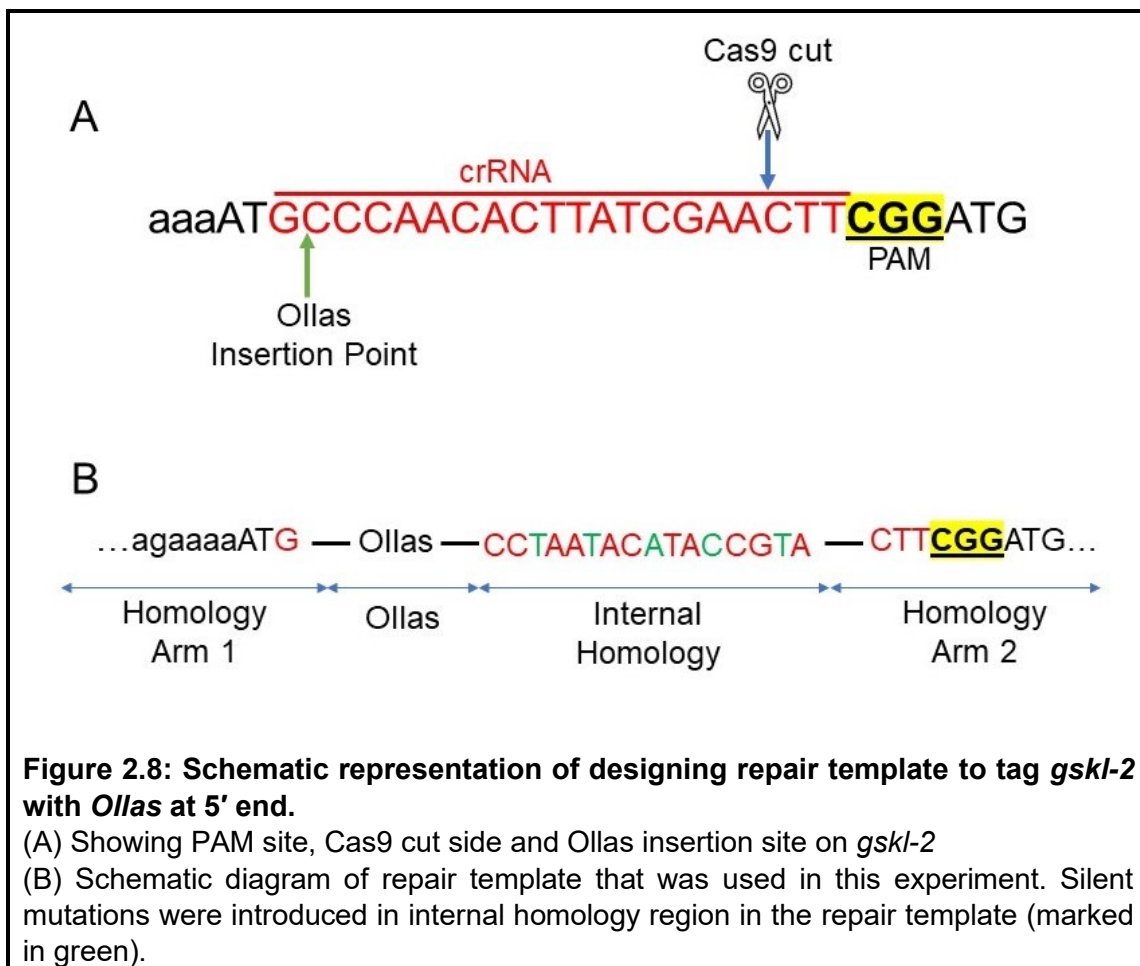
I used 3xFLAG to tag *gskl-1* at its 5' end. In this case, the small tag sequence was flanked by a 50 bp homology arm on each side. The repair template sequence was

initiated with Homology Arm 1 followed by the small tag sequence and then the internal homology region and Homology arm 2. As the 3xFlag sequence disrupted the crRNA sequence in the repair template no silent mutation was introduced in the repair template to protect it from Cas9 nuclease activity. This repair template was ordered from IDT (4 nmol Oligomer).



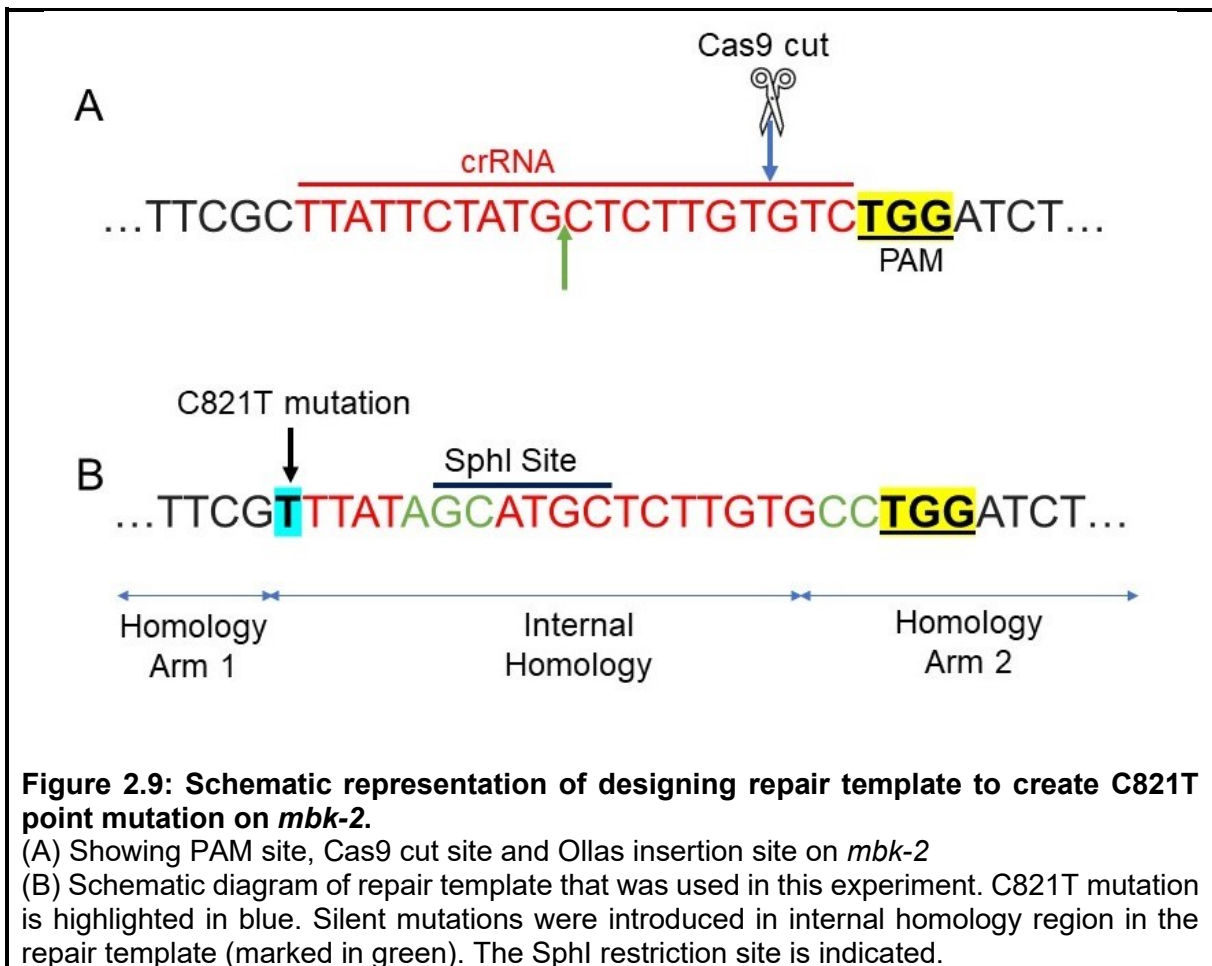
I used Ollas to tag *gskl-2* at its 5' end. The Ollas (*E. coli* OmpF Linker and mouse Langerin fusion Sequence) tag is approximately 100 times more sensitive to detect by monoclonal antibodies than other available tags (Park et al. 2008). The repair template sequence was initiated with Homology Arm 1 followed by the Ollas sequence, internal

homology regions with silent mutation and then Homology arm 2. In this case, the Ollas sequence was flanked by a 50 bp homology arm on each side. As crRNA sequence was not disrupted by Ollas insertion in the repair template, to prevent cutting by Cas9 nuclease, some silent mutations were introduced. This repair template was directly ordered from IDT (4 nmol Oligomer). This detailed process is schematically presented in the following figure:



2.12.5.3 Preparing repair templates for creating point mutations

We found *abc56* as a suppressor of *memi-1(sb41)* in a previous EMS screen. One candidate gene, *mbk-2*, was revealed by genome sequencing. I recreated the putative suppressor point mutation in *mbk-2* to verify that the mutation is responsible for suppressing *memi-1(sb41)*. In this case, 50 bp upstream and 50 bp downstream from the cas9 cutting side was used for homology arms. Some silent mutations were introduced in the repair template to prevent it from being cut by Cas9 nuclease. A SphI restriction endonuclease recognition site was also introduced in the repair template to identify the insertion. Details of this design are explained in the following Figure:



2.12.6 Making injecting cocktails

The injection mixture was prepared on ice. A 20 μ L injection mixture contained 5 μ L of 10 μ g/ μ L Cas9 (Alt-R® *S.p.* Cas9 Nuclease V3 from Integrated DNA technologies), freshly prepared 1 μ L 1M KCl (Invitrogen), freshly prepared 0.75 μ L 200mM HEPES (pH 7.4 from Invitrogen), 5 μ L 0.17 mM tracrRNA (Alt-R® CRISPR-Cas9 tracrRNA, 5 nmol from IDT), 0.4 μ L 0.6 mM *dpy-10* crRNA (Alt-R® CRISPR-Cas9 crRNA, 2 nmol from IDT), 1 μ L 0.6 mM targeted gene crRNA (Alt-R® CRISPR-Cas9 crRNA, 2 nmol from IDT), 0.55 μ L 16 μ M *dpy-10* ssODN (IDT), 10 pmolar ssODN repair (IDT), and nuclease free water (Invitrogen) to a final volume of 20 μ L. This cocktail was then centrifuged at 12000 g for 2 minutes and after that distributed in six small aliquots and stored in -20°C. Before injection, one small aliquot was incubated at 37°C for 20 minutes and immediately loaded into the injection needle.

2.12.7 Injecting worms

Worms were grown up at the 15°C incubator before injection. Around 1000 L4 larvae were picked up and kept in several plates at 15°C for 16 to 18 hrs before injection. The injection mixture was loaded in an injection needle at least 15 minutes before the start of injection. The tip of the needle was opened carefully to allow the injection mixture to flow smoothly. A small drop of halocarbon oil was placed on a dry 1.2% agarose pad and L4 larval or young adult worms were placed in the oil. Once the worms stopped moving, the slide was transferred to the microscope stage. I used a 20X objective lens to visualize worms during injection and usually injected both gonad

arms. After successful injection, worms were recovered from the injection pad and placed in a fresh NGM plate. In every 5 to 10 minutes 5 μ l of M9 buffer was added to the plate until the rescued worms started to crawl around freely. Within approximately 45 minutes, injected survivors were transferred to a fresh plate. In every subsequent 15 minutes M9 buffer was added to that new plate. After an hour, all injected worms were carefully transferred to another new plate to completely remove adhered oil from the body of worms. Finally, all successfully recovered worms (P0) were transferred to individual plates and were kept at 25°C to allow them to lay eggs over the next 48 hrs.

2.12.8 Screening injected worms

The percentage of Dumpy and Roller worms among the progeny of P0 worms were scored. Typically, three plates with the highest percentage of Roller and/or Dpy worms (“jackpot” broods) were considered for further screening.

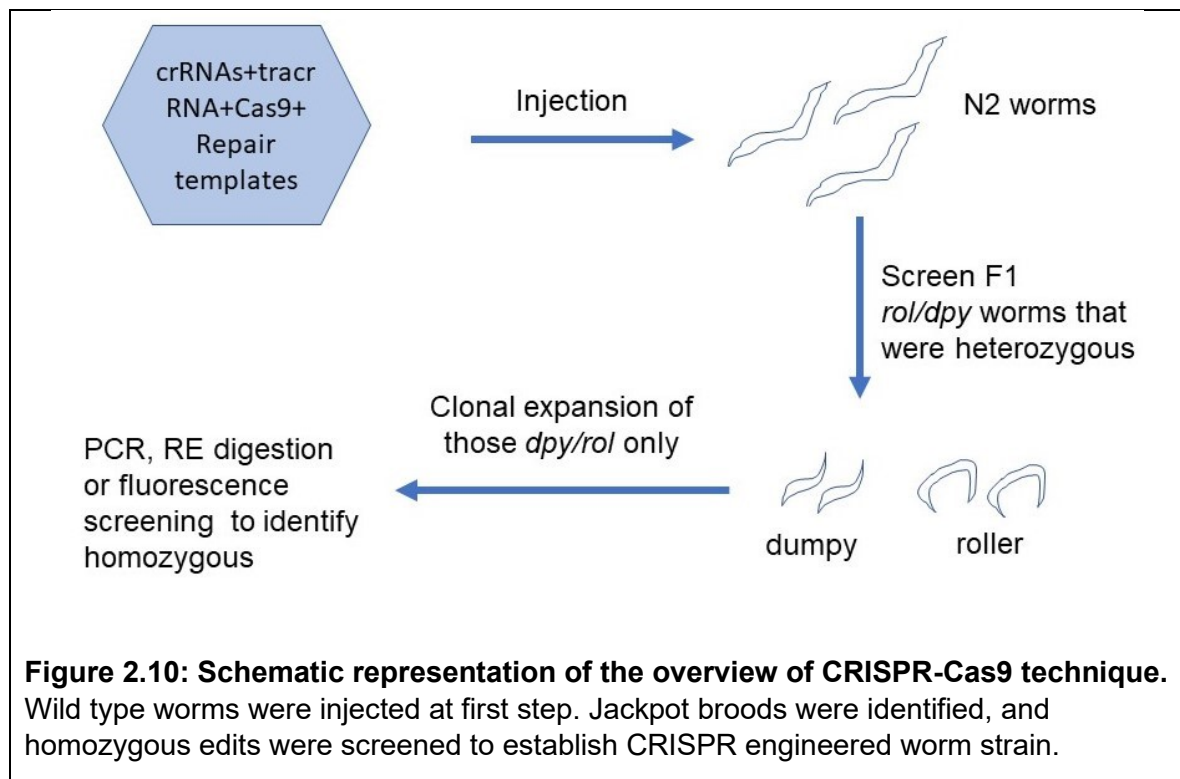
2.12.9 Screening for edits

From the jackpot broods, all F1 Roller worms were picked in cohorts of 2 worms per plate to allow them to lay eggs. The F1 Roller progeny were screened either by PCR or by fluorescence to detect the desired edits. The PCR product was analysed by either size shift on 2% agarose gel to detect insertions of small tags, or by restriction digestion to detect insertions of restriction endonuclease site-modifying point mutations. GFP insertions were detected by fluorescence signals under the microscope. From the F1 pools which gave positive results, 40 F2 Dpy/Rol

hermaphrodites were separated and kept on individual plates. After the F2 laid eggs, genotyping was done using standard lysis and PCR protocols. Primers were designed at least 250 bp upstream and downstream of the insertion site to detect the homozygous edit.

2.12.10 Isolating homozygous worm strains

Based on the screening results, I selected 4 worms from each predicted homozygous worm-containing plate, and isolated the worms on individual plates for 48 hours. After egg laying, single-worm PCR was done on the mother, and the DNA sample was sent for sequencing. Following this, based on the sequencing result, homozygous worms were given a strain name and an allele name, following standard protocols.



2.13. Immunostaining

Immunostaining was performed based on the “Freeze-Crack” method (Duerr 2013). L4 males of respective genotypes were harvested overnight at 20°C in the absence of hermaphrodites to observe inactive spermatids or active spermatozoa. The next day, 20-25 males were dissected in 5 µL SM media on a polylysine-coated slide with an 18X18 mm coverslip placed on top. Gentle pressure was applied to release the spermatids from gonads. To observe embryos, approximately 35 young adult hermaphrodites were picked into 5 µL of egg buffer (25 ml 25mM HEPES pH 7.3, 59 ml 118 mM NaCl, 24 ml 48mM KCl, 2 ml 2mM CaCl₂, 2 ml 2mM MgCl₂, volume adjust to 1 litre with ddH₂O) on a polylysine-coated slide and gentle pressure was applied to squeeze the embryos out of the worms. Slides were immediately frozen in liquid nitrogen. After freeze-cracking by removal of the coverslip, slides were fixed in methanol for 15 minutes at -20°C. After washing in phosphate-buffered-saline (PBS) for 20 minutes, slides were incubated with 25% goat serum for one hour followed by washing in PBS for 10 minutes. The slides were then incubated in primary antibody solution (5% goat serum, 0.01% Triton-X100 and 1 µg/µL primary antibodies) for one hour at room temperature. 3x-FLAG was detected by mouse anti-FLAG antibody (F1804, Sigma Aldrich) at 1/500 dilution, Ollas was detected by rat anti-Ollas antibody (NBP1-06713, Novus Biologicals) at 1/250 dilution, membranous organelles (MO) were observed by AlexaFluor 488-conjugated wheat-germ agglutinin at 1/1000 dilution, MSP was visualised by mouse anti-MSP 4A5 antibody at 1/500 dilution (Developmental Studies Hybridoma Bank) and rabbit anti-GSP-3/4 antibodies were used at 1/1000 dilution. Slides were washed in PBS for 3X10 minutes before they were incubated in a

secondary antibody solution (5% goat serum, 0.01% Triton-X100 and 1ug/ μ L secondary antibodies) for an hour at room temperature. Alexa488 goat anti-mouse, Alexa546 goat anti-mouse, or Alexa488 goat anti-rat secondary antibodies were used. Slides were washed in PBS for 3X10 minutes and mounted in media that contained DAPI (F6057- Fluoroshield with DAPI). Images were captured using a 60X oil (NA 1.42) objective with an Olympus IX81 spinning disc confocal inverted microscope.

2.13.1 Troubleshooting Secondary antibody for false positive staining

Initially, I used Thermo Fisher goat anti-rat Alexa Fluor 546 secondary antibodies to detect Ollas, but the secondary antibody itself gave a fluorescence signal (Figure 2.11).

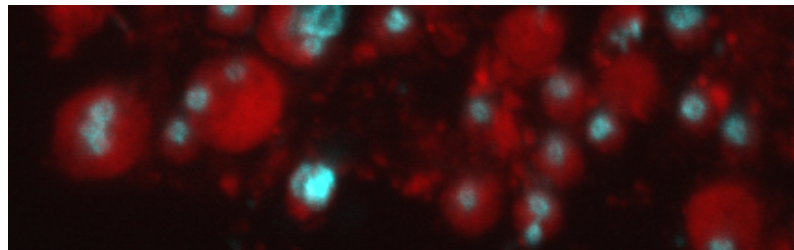


Figure 2.11: False Positive signal from goat anti-rat antibody. Male worms were stained only with Alexa546 Thermo Fisher goat anti-rat antibody and DAPI after dissection. This secondary antibody gave a fluorescence signal in the absence of primary antibody.

In an attempt to clean up this antibody, wild-type worms were serially washed off with an M9 buffer from plates to collect worms and a concentrated stock of 1 ml was prepared. Those worms were completely disrupted by using a sonicator. The sample

was then centrifuged to collect the 100 μ l pellet. Next, 400 μ l chilled acetone (placed in -20°C for an hour before use) was added to incubate it for one hour at -20°C . After the incubation, the sample was centrifuged at 13000 x *g* for 10 minutes. Supernatant was decanted carefully to collect the pellet for future use. 1 μ g of pellet was added into 100 μ l of that secondary antibody and incubated for an hour at room temperature. After 10 minutes it was centrifuged at 13000 x *g* to collect the supernatant. Unfortunately, it did not clean up and gave a bright fluorescence signal on its own. Therefore, I obtained a goat anti-rat 488 secondary antibody from Dr. Shelagh Campbell (University of Alberta) which did not give any signal on its own (Figure 2.12). I used this secondary for all immunostaining experiments involving the Ollas tag.

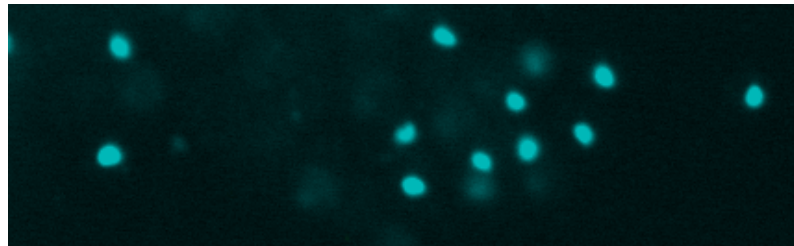


Figure 2.12: Testing Alexa 488 goat anti-rat antibody.

Male worms were stained only with Alexa 488 goat anti-rat antibody (gift from Dr. S. Campbell lab) and DAPI after dissection. No fluorescence signal from this Alexa 488 Goat anti Rat was detected.

2.14 Western Blotting

Western blotting was performed on whole worm lysates using the following procedure (Gusnowski and Srayko 2011):

2.14.1 Preparation of sample

Worms containing *fem-1(hc17)* and *fem-3(q20)* mutants were grown at 15°C. When they reached the L4 stages, 8 L4 hermaphrodites were placed in one plate together. Five such plates were transferred to 25°C to allow the worms to lay eggs over the next 48 hrs, after which, the mothers were removed from the plates. Approximately 36 hrs after removal of mothers, the progeny worms were serially washed off from the plates with M9 buffer and pelleted at 1000 g for 2 min. The pellet was then washed one more time with fresh M9 buffer, spun, and resuspended in a final volume of 50 µl M9. An equal volume of 2X Laemmli buffer (Sigma-Aldrich) was added, and the sample was boiled for 5 minutes at 95°C. This sample was either loaded onto a 10% SDS-PAGE stacking gel or stored at -20°C. Frozen samples were heated at 95°C for five minutes just before loading the stacking gel.

2.14.2 Western Blot

Proteins were separated by SDS-PAGE using a stacking gel (3.75 Acrylamide/Bis, 130 mM Tris pH 6.8, 1% SDS, 1% ammonium persulfate and 0.1% TEMED) and a 10% resolving gel (10% Acrylamide-Bis, 390 mM Tris pH 8.8, 1% SDS, 1.5% Ammonium persulfate and 0.04% TEMED). Gels were placed in a running buffer (25 mM Tris, 192 mM glycine, 0.1% SDS, pH 8.3) at 90 V for one hour at room temperature. A prestained protein marker (26616, Thermo Fisher) was used to estimate the relative mass of the proteins. After the run was completed, proteins were transferred from the gel to a nitrocellulose membrane (Hybond-N, GE Healthcare) at 100 V for 2 hr. The membrane

was blocked in 5% skim milk in TBST for 1 hr (20 mM Tris-HCl, pH 7.4, 500 mM NaCl, and 0.05% Tween 20).

2.14.3 Standardization of antibodies

The Ollas tag was detected by rat anti-Ollas antibody (NBP1-06713, Novus Biologicals) at 1/250 dilution, mouse anti-tubulin (DM1A, Sigma) at 1:500 dilution and mouse anti-MSP 4A5 antibody (Developmental Studies Hybridoma Bank) at 1/1000 dilution. All antibodies were diluted in TBST + 4% skim milk and incubated for 1 hr at RT. HRP-bound Goat anti-rat and goat anti-mouse secondary antibodies (Bio-Rad) were used at 1:5000 in TBST + 4% skim milk and incubated with the membrane for 1 hr at RT. The secondary antibodies were detected via SuperSignal West Pico ECL (Thermo Fisher Scientific) and imaged on the ChemiDoc MP Imaging system (BioRad).

To detect FLAG, I used anti-Flag HRP conjugate antibodies at a 1/1000 dilution (2044-S, Cell Signaling Technology) as previously reported (Paix et al. 2017). I was unable to detect the expected 41 kd band for my target protein 3xFLAG::GSKL-1 at 1/1000, 1/500 dilution or 1/125 dilution. Similar problems with this antibody were reported by other researchers in the worm community, therefore, I tried mouse anti-FLAG antibodies (F1804, Sigma Aldrich). First, I tested the specificity of this antibody using a FLAG::GSP-4 positive control worm (gift from Dr. Diana Chu, San Francisco State University) in 1:50 and 1:500 dilution. The samples were separated via SDS-PAGE and blotted, as described above, and then each lane of protein sample was stripped off to probe with different concentrations of mouse anti-FLAG antibody (F1804,

Sigma Aldrich). The right size band was detected in both 1:50 and 1:500 concentrations (Figure 2.13). So, I decided to use mouse anti-FLAG antibodies (F1804, Sigma Aldrich) at 1:500 dilution for my further experiments.



Figure 2.13: Testing F1804 FLAG antibody. FLAG was detected by F1804 (Sigma Aldrich) antibody in both 1:50 and 1:500 dilution. 3xFLAG::GSP-4 worm lysates were used as positive controls.

After determining the appropriate antibody concentration to detect GSKL^{FLAG}, I encountered a problem detecting the FLAG signal when used in combination with other probes to detect different proteins. In this case, I probed for loading controls α -tubulin and MSP, in addition to 3xFLAG::GSKL-1. I used three different anti mouse primary antibodies to detect these three different proteins. All of them were verified individually previously, but only α -tubulin and MSP signals were detected in the blot that was probed for all three antigens. I used a mild stripping buffer (15 gm glycine, 1 gm SDS, 10 ml Tween 20, volume adjusted to 1 ml by dH₂O, pH 2) to remove primary and secondary antibodies from the membrane by following standard protocols. Briefly, I kept the membrane in a stripping buffer at room temperature for a total of 15 minutes and in every 5 minutes I kept changing the buffer. Then the membrane was washed in

1X PBS for 10 minutes followed by washing in TBST buffer for 5 minutes, which was repeated for one more time. The membrane was then blocked in a blocking solution and re-probed with only the FLAG antibody. Then, I was able to detect the FLAG signal. To avoid this problem, I probed the membrane with anti-FLAG antibody first, and then used the same membrane to re-probe for anti- α -tubulin and anti-MSP antibodies.

2.14.4 Visualizing proteins after Western blotting

The HRP conjugate secondary antibodies were detected via SuperSignal West Pico Chemiluminescent substrate (Thermo Fisher Scientific). This product comes with two different solutions, namely, stable peroxide solution and Luminol solution. Just before imaging, both solutions were mixed in equal volumes to make the working solution. The membrane was incubated with this working solution for 2 minutes. After removing the working solution from the membrane, images were acquired on the ChemiDoc MP Imaging system (BioRad).

2.15 *In utero* confocal imaging

For *in utero* imaging, worms were picked into 7 μ l of egg buffer containing 5 mM tetramisole hydrochloride. This was done to immobilize the worms prior to imaging. Once the worms stopped moving (typically 10 minutes), the cover slip was inverted onto a 2% agarose pad. Fluorescent images of 3 planes, spaced 1.5 μ m apart, were taken in 30 second intervals using a 60X oil (NA 1.42) objective lens with an Olympus IX81 spinning disc confocal inverted microscope. A maximum projection of these three

planes was used to make the figures. TIFF Raw images were converted to 8 bit RGB planes for each colour and these were merged in adobe photoshop to make the figures.

2.16 Statistical analysis

Student's T-tests were performed assuming that the two populations exhibited unequal variance (Welch's correction). Graphs were plotted using GraphPad software (USA).

3. Identification of suppressors of embryonic lethality of *memi-1(sb41)*

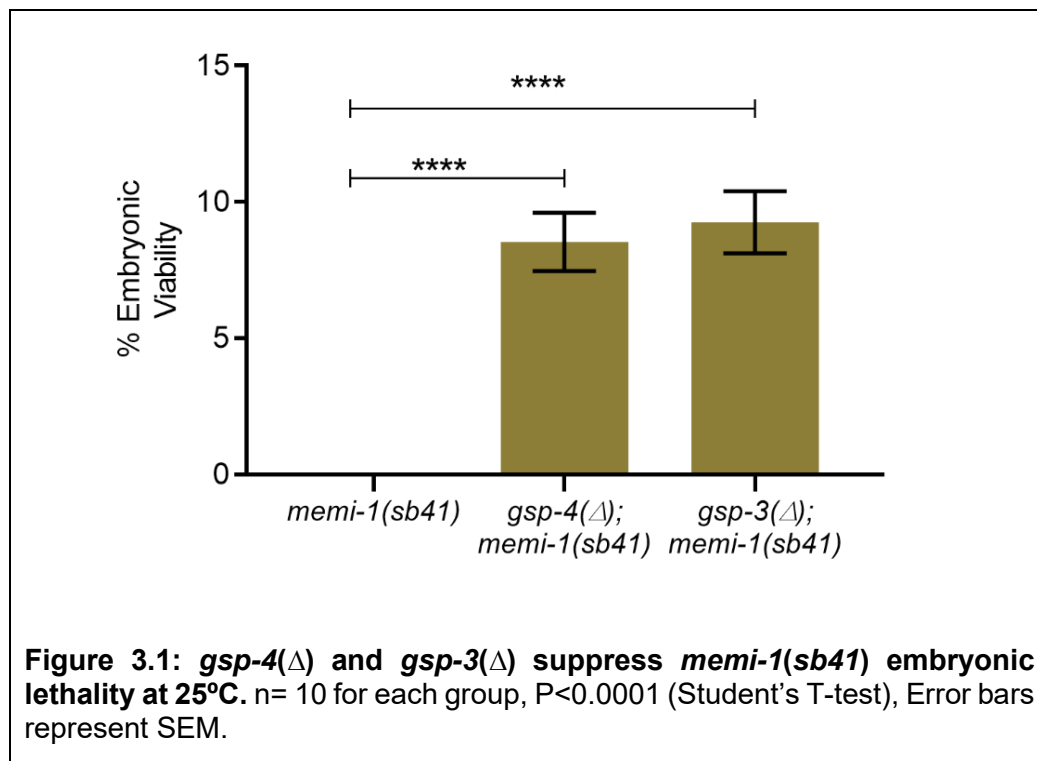
3.1 Identification of suppressor loci

The *memi-1(sb41)* mutation has proven to be useful for genetic screens that identify components of the post-fertilization signal for regulating female meiosis II. An EMS screening was done to identify suppressors of *mem-1(sb41)*. The details of this EMS screening are described in chapter 1.7.1 (page 35). Briefly, through this genetic screening, 31 suppressors of *memi-1(sb41)* were found. 11 of the 31 suppressors were second-site alterations within the *memi-1* gene (intragenic suppressors) (Catilin Slomp, *pers. comm.*). Any extragenic suppressor strains that contained alleles of the same gene and belonged to a common complementation group were noted as suppressor candidates (Herzog 2018). Only two genes, *gsp-4* and *gskl-1*, were identified as candidate suppressors of *memi-1(sb41)* based on these criteria.

3.2 *gsp-3* and *gsp-4* suppress *memi-1(sb41)* embryonic lethality

The EMS screen recovered 5 alleles of *gsp-4*: *abc39*, *abc40*, *abc44*, *abc47* and *abc48*. Out of these suppressors, *abc39*, resulted in a G89E substitution, *abc40* resulted in G221R, *abc44* resulted in H64Y, *abc47* resulted in L50H and C107Y, and *abc48* resulted in a G61E substitution. All of these missense mutations occurred in conserved regions that were identical among PP1 phosphatases of different organisms. To further validate that loss of *gsp-4* is responsible for suppression, a deletion allele of *gsp-4(tm5415)* was used. The *gsp-4(tm5415); memi-1(sb41)*

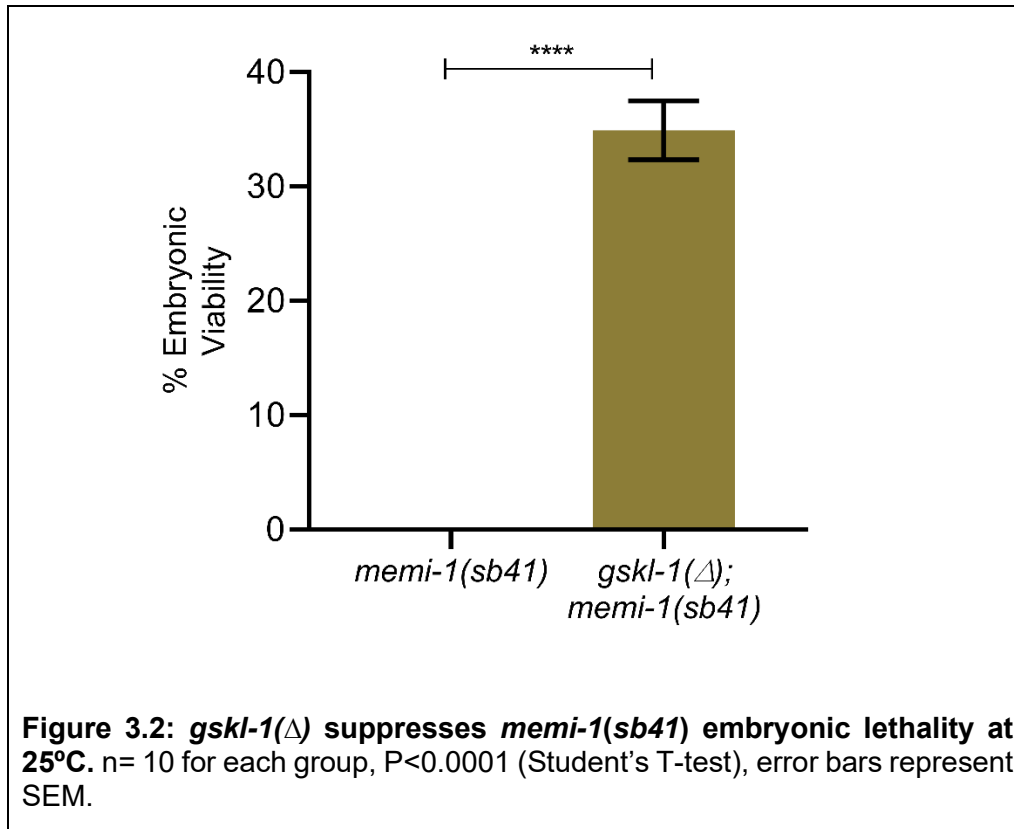
suppressed the embryonic lethality *memi-1(sb41)* to 9% survival compared to 0% of *memi-1(sb41)* at 25°C (Figure 3.3, P<0.0001). *gsp-4* is functionally redundant with *gsp-3*, however, *gsp-3* was not recovered as a suppressor in this EMS screen. This raised the possibility that, although *gsp-3* and *gsp-4* are functionally redundant for sperm functions, they may not be redundant with respect to the MEMI pathway. Therefore, in order to directly test whether *gsp-3* alone can suppress *memi-1(sb41)*, I obtained a deletion allele and made a double mutant. *gsp-3(tm1647); memi-1(sb41)* produced 9% viable progeny compared to 0% of *memi-1(sb41)* at 25°C (Figure 3.1, P<0.0001). This data confirmed that loss of *gsp-3* or *gsp-4* is sufficient to suppress *memi-1(sb41)*. Original experiments were conducted using RNAi, hence, *gsp-3/4(RNAi)* likely suppresses by lowering the activity of both of these highly similar genes (Ataeian et al. 2016).



3.3 *gskl-1* suppresses *memi-1(sb41)* embryonic lethality

Four suppressor mutations were found in the *gskl-1* gene. *abc57* represents a 5-bp deletion that is expected to produce a truncated protein (60 aa); *abc41* and *abc59* are missense mutations resulting in T210I and G240R substitutions, respectively; and, *abc51* contains a G to A mutation in the splice site acceptor region of intron six (details of these mutants are discussed in next chapter). *gskl-1* belongs to the glycogen synthase kinases-3 (GSK-3) family (Manning 2005). Transcripts of *gskl-1* are most abundant in L4 male larvae, suggesting that the primary function for *gskl-1* might be related to the male germline, which initiates spermatogenesis at this stage (Marcello et al. 2013). Although four mutations were identified in *gskl-1* within four different suppressor strains, independent verification that loss of *gskl-1* function alone can suppress *memi-1(sb41)* was necessary. In order to test this, I obtained a deletion mutation of this gene *gskl-1(tm4146)* and made a double-mutant strain with *memi-1(sb41)*. In this double mutant, embryonic viability increased from 0% in control *memi-1(sb41)* to 34.9% in the *gskl-1(Δ); memi-1(sb41)* double-mutant hermaphrodites at 25°C (Figure 3.2, P<0.0001). This indicated two important results, that the suppressor gene involved was indeed *gskl-1*, and that the suppression was due to a loss of function for this gene.

The *gskl-1* gene was not previously characterized and was not attributed to any specific function in *C. elegans*. I decided to further characterize this gene and this work is presented in Chapter 4 of this thesis.



3.4 Towards the identification of extragenic suppressors of *memi-1(sb41)*

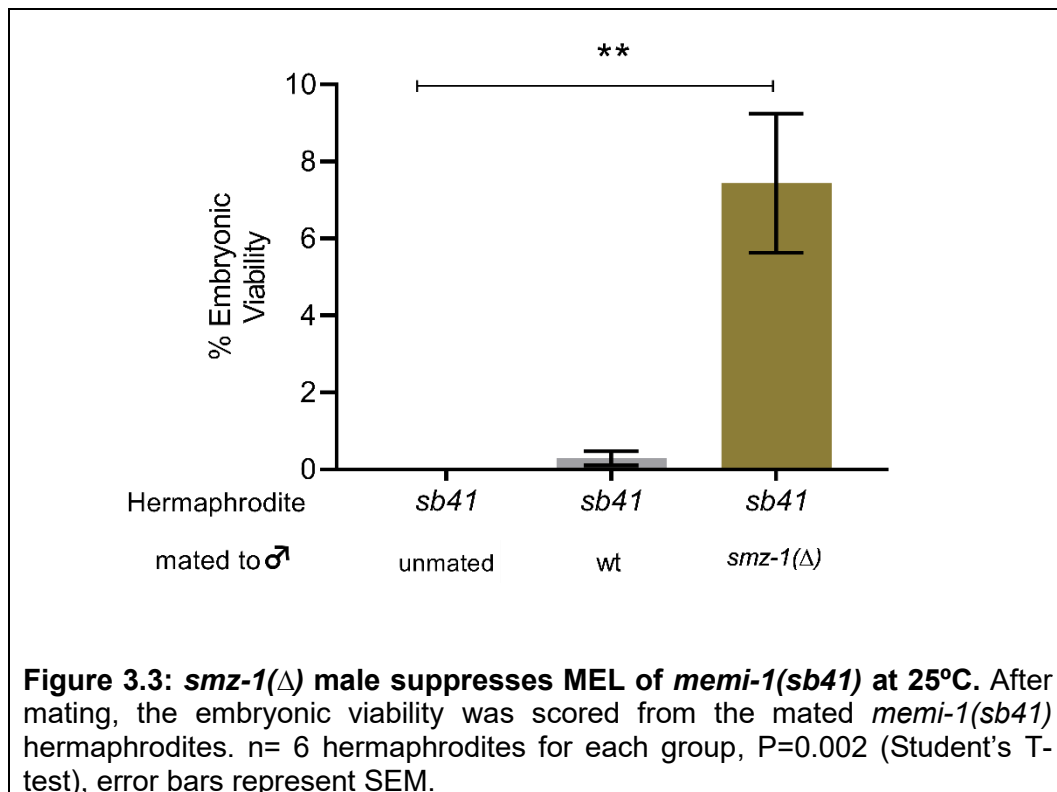
At the start of this project, some candidate *memi-1(sb41)* suppressor genes were identified based on genetic mapping, complementation analyses and RNAi (Herzog 2018). Considering the mapping data of the suppressor strains, the mutations on chromosomes that were unlinked to suppression were eliminated, and those that showed linkage were identified and isolated. Three genes on two different suppressor strains, *smz-1*, *frm-8*, *mbk-2* were selected as candidates based on these criteria. Out of the remaining suppressors, *abc36*, *abc52* and *abc54* were linked to LGX, LGIII and LGII respectively. There were only 4 possible mutations present in *abc36* on LGX.

abc50 has 12 mutations on LGIII and *abc54* has 25 mutations on LGII, many of these genes' functions were already known. Based on the functional data and transcriptome analysis available (reference), I narrowed down the number of candidate genes. Finally, 4 genes were pursued as part of this thesis, *smz-1*, *frm-8*, *mbk-2* and *ceh-18*.

3.4.1 *smz-1* suppresses *memi-1(sb41)* embryonic lethality

In the *abc53* suppressor strain, seven genes were found on LGIV, consistent with genetic mapping data (Table 3.2). Out of these, only *smz-1* (sperm meiosis PDZ domain-containing proteins) was previously characterized. Within the *abc53* strain, *smz-1* contains a missense mutation to produce I133N amino acid alteration. *smz-1* has a highly similar paralogue *smz-2*, and knockdown of either *smz-1(RNAi)* or *smz-2(RNAi)* individually caused chromosome segregation defects during spermatogenesis (Chu et al. 2006). Preliminary characterization of *smz-1(Δ)* indicated that it was superficially wild-type, with respect to embryonic viability. As *smz-1* is involved in sperm function like another suppressor, *gsp-4*, it was hypothesized that *smz-1* could be the suppressor in this suppressor strain (Herzog, 2018). If this hypothesis is correct, it is expected that *smz-1(RNAi)* should suppress the embryonic lethality of *memi-1(sb41)*. Indeed, *smz-1(RNAi)* suppressed *memi-1(sb41)* embryonic lethality, albeit weakly (J. Chum, *pers. comm.*). To further test the molecular basis of suppression, a deletion allele of *smz-1(Δ)* was used. I crossed *smz-1(Δ)* males to *memi-1(sb41)* hermaphrodites at 25°C and found that *smz-1(Δ)* males suppressed *memi-1(sb41)* (Figure 3.4, P=0.002).

The observed suppression rate by *smz-1*(Δ) males was much lower in comparison to the original suppressor strain (7% vs. 73%). However, this experiment relied on male mating, thus, to test the suppression by *smz-1*(Δ) in a hermaphrodite self-cross, an *smz-1*(Δ); *memi-1*(*sb41*) double mutant strain would need to be constructed in the future. Both genes are on chromosome IV, thus recombinants need to be identified to make the double mutant. Alternatively, CRISPR-Cas9 method can be used to recreate the *abc53* point mutation to further validate *smz-1* as a suppressor of *memi-1*(*sb41*).

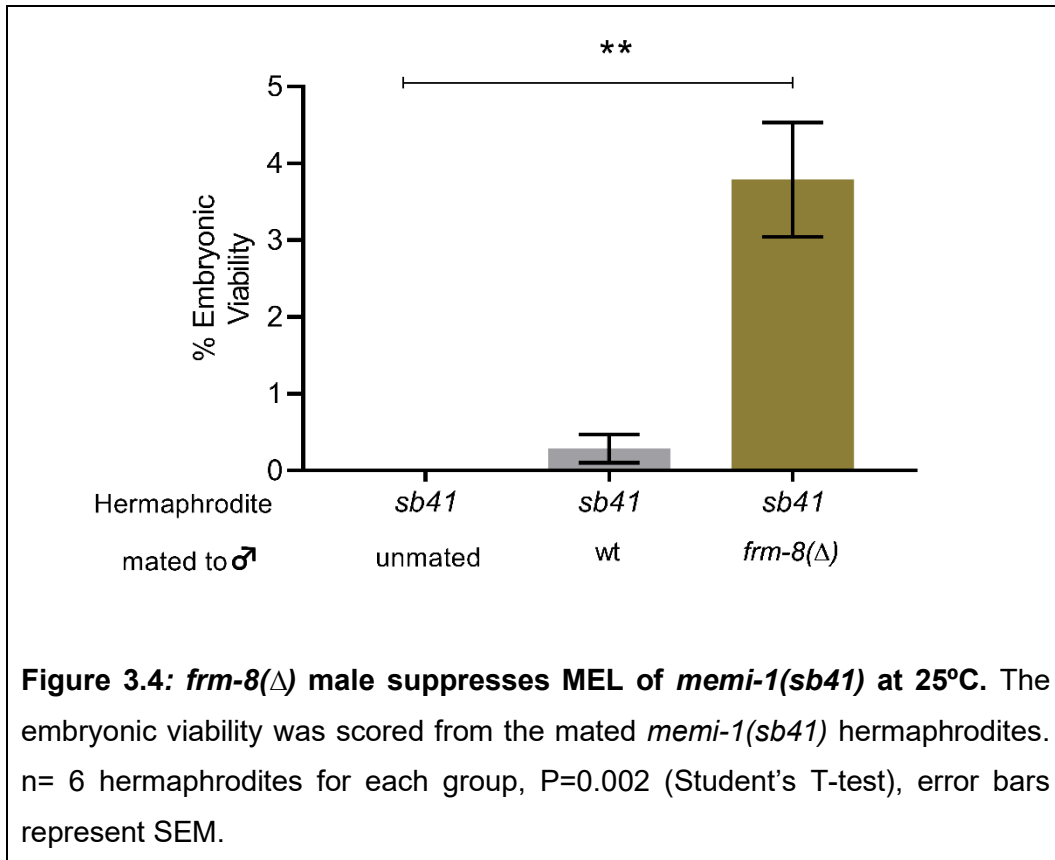


3.4.2 *frm-8* is identified as a suppressor of *memi-1*(*sb41*) embryonic lethality

In the *abc50* suppressor strain, seven candidate genes were identified on LGIII consistent with genetic mapping data (Herzog 2018). Out of which, *frm-8* was selected

as a candidate gene. *frm-8* is an ortholog of human *FERM and PDZ domain-containing protein 1 (FRMPD1)* and *FRMPD4* genes and the *abc50* strain contains a missense mutation within the *frm-8* gene that resulted in I643N substitution. In humans, FRMPD1 helps to stabilize membrane-bound G protein signalling modulator 1, and FRMPD4 binds with phosphatidylinositol 4,5-bisphosphate to maintain excitatory synaptic transmission (An et al. 2008). Also, SNP analyses indicated that FRMPD4 in humans is associated with several X-linked diseases (Urio et al. 2020; Wang et al. 2020). The role of *frm-8* in *C. elegans* has not been characterized yet. In order to test whether loss of *frm-8* can suppress *memi-1(sb41)*, I obtained a deletion allele of *frm-8(ok1769)*. I crossed *frm-8(Δ)* males to *memi-1(sb41)* hermaphrodites at 25°C and found that *frm-8(Δ)* males suppressed *memi-1(sb41)* (Figure 3.4, P=0.002).

The observed suppression rate by *frm-8(Δ)* male is much lower in comparison to the original suppressor strain (6% vs 76%). However, this experiment relied on male mating, thus, to test the suppression by *frm-8(Δ)* in a hermaphrodite self-cross, *frm-8(Δ); memi-1(sb41)* double mutant strain would need to be constructed in the future. Alternatively, CRISPR-Cas9 method can be used to recreate the *abc50* point mutation to further validate *frm-8* as a suppressor of *memi-1(sb41)*.



3.4.3 *mbk-2* is identified as a suppressor of *memi-1(sb41)* embryonic lethality

In the *abc56* suppressor strain, seven candidate genes were identified on LGIV, consistent with genetic mapping data (Herzog 2018). Among these, the gene *mbk-2* (Mini Brain Kinase), encodes a DYRK (dual-specificity tyrosine-regulated kinase), stands out as a potential suppressor because it has been implicated in a variety of processes important to the oocyte-to-embryo transition. This *abc56* mutation changed an evolutionarily-conserved alanine residue at 274th position to valine in the MBK-2 (Figure 3.5). In unfertilized oocytes, MBK-2 is distributed throughout the cortex, but after completion of anaphase I and before the formation of the meiotic II spindle, the

distribution of MBK-2 is changed to a punctate pattern in the fertilized embryo (McNally and McNally 2005). The CCCH-type zinc finger protein OMA-1 prevents premature activation of oocytes, and during MI, this OMA-1 protein is normally degraded by CUL-2 based E3 ubiquitin ligase. This timely degradation of OMA-1 is required for proper oocyte to embryo transition. MBK-2 phosphorylates OMA-1 to facilitate its degradation (Shirayama et al. 2006; Guven-Ozkan et al. 2010). Two other proteins, MEI-1 and MEI-2, also play a crucial role during the oocyte-to-embryo transition. As a part of the katanin microtubule-severing complex, they are required to form the female meiosis spindle and must be degraded quickly to form a mitotic spindle successfully. Together with CUL-3-based E3 ubiquitin ligase, MBK-2 is also involved in the degradation of MEI-1 (Johnson et al. 2009; Beard et al. 2016). Interestingly, a substrate-specific adaptor of the CUL-2 E3 ligase pathway, ZYG-11, is required to timely degrade MEMI during MII to mitosis transition (Ataeian et al. 2016). As MBK-2 is involved in the degradation of proteins during oocyte to embryo transition, we hypothesized that the suppression of *memi-1(sb41)* is due to the mutation in *mbk-2*. As *mbk-2* deletion caused embryonic lethality, it could not be used to verify the suppression. Hence, the CRISPR-Cas9 method was used to recreate *mbk-2::abc56* point mutation. It was found that *mbk2::(abc56) memi-1(sb41)* produced 26.33% viable embryos at 25°C (Figure 3.6). This data confirms *mbk-2(abc56)* as a suppressor of *memi-1(sb41)* embryonic lethality.

<i>Drosophila</i>	SLNLTRKFAQQQLCTALLFLSTPELNI IHCDLKPENILL CNPKRSAIKIVDFGSSCQLGQR 322
Human	SVQLVRKFAQSILQSLDALH--KNKI IHCDLKPENILLKHHGRSSTKVIDFGSSCFEYQK 365
<i>C.elegans</i>	SLMLVRKFAYSMLLCLDLLQ--KNRLIHC DLKPENVLLKQQGRSGIKVIDFGSSCFDDQR 617
	*: *.**** .: .* * : .:*****:** : **. *:***** *:

Figure 3.5: *abc56* causes a missense mutation (A274V) in an evolutionary conserved Alanine residue in MBK-2.

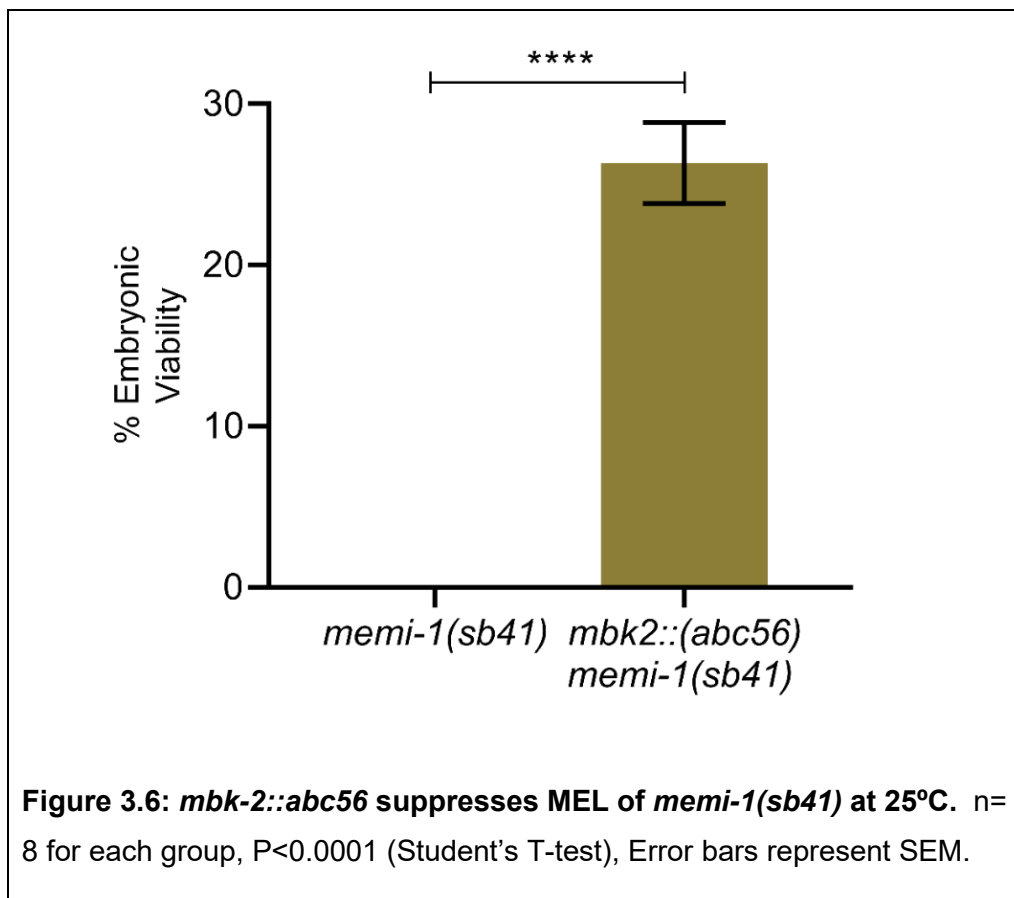


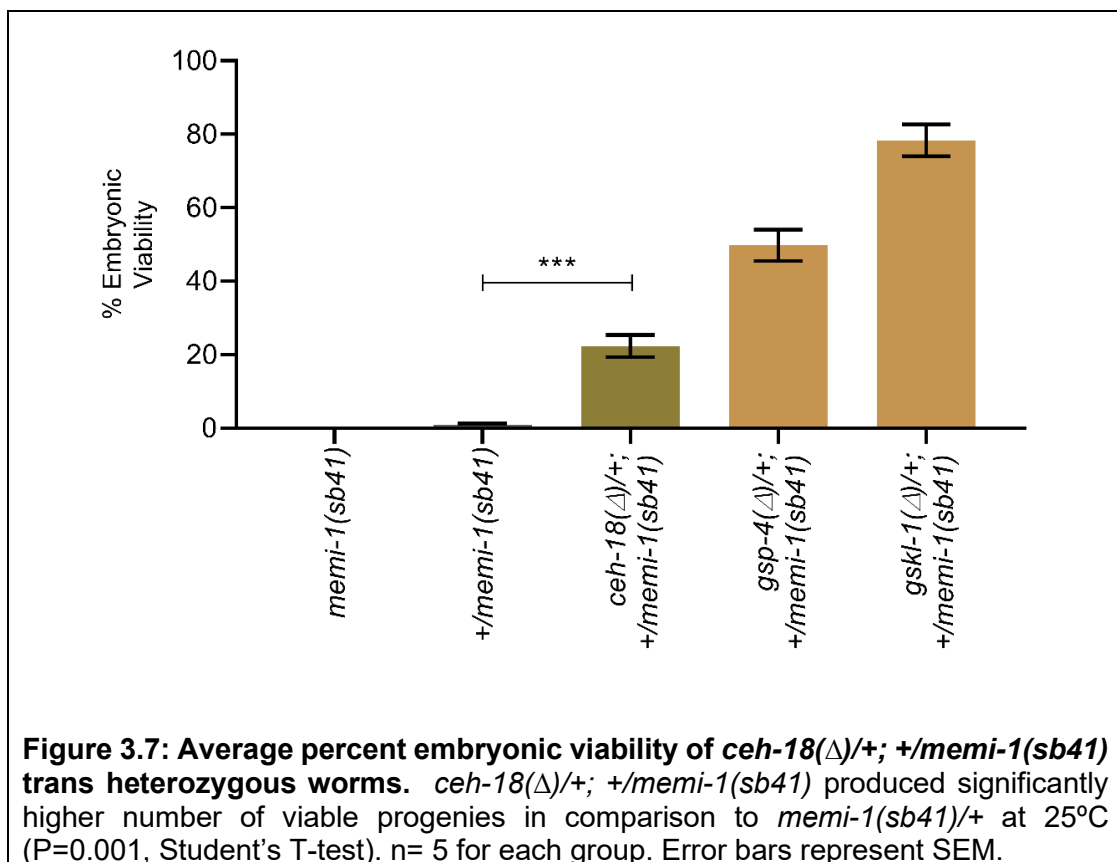
Figure 3.6: *mbk-2::abc56* suppresses MEL of *memi-1(sb41)* at 25°C. n= 8 for each group, P<0.0001 (Student's T-test), Error bars represent SEM.

3.4.5 Testing candidate genes to identify the suppressor mutation *abc36*

Previous work established that *abc36* suppression was linked to the X chromosome. In the *abc36* suppressor strain, four mutations were revealed by WGS predicted to disrupt four different genes on the X chromosome. Those genes are *F39C12.1*, *D1025.1*, *C15H9.3* and *K09C4.5*. *F39C12.1* is a very large gene with a transcript length of 15444 nucleotides, and it is an ortholog of the human gene *mios*, a meiosis regulator for oocyte development. In *Drosophila*, oocytes lacking *mios*, enter the meiotic cycle but mostly result in polyploids (Wei et al. 2014). The functions of the remaining three candidate genes, *D1025.1*, *C15H9.3* and *K09C4.5*, are not known in *C. elegans*.

In addition to the four genes mentioned above, a mutation in the intron region of *ceh-18* was also present in the *abc36* suppressor. The mutation in the intron region of *ceh-18* did not affect the splice acceptor or donor sequence raising the question of whether or not this mutation is to be responsible for any change in *ceh-18* function. However, information available on *ceh-18* function makes this gene a good candidate for involvement in the *memi* pathway. *ceh-18* is expressed in gonadal sheath cells and a loss of function *ceh-18(mg57)* mutant oocytes exhibit failure in arrest in diakinesis of female meiosis and undergo multiple rounds of DNA replication without cytokinesis (Rose et al. 1997). This suggests that *ceh-18* may be involved in sheath cell signalling that causes oocytes to maintain diakinesis arrest. It is well established that sperm sends an MSP-based signal to activate the oocyte from the arrest (Miller et al. 2001). After the fertilization, the sperm sends another signal that activates the MEMI pathway

to allow the oocyte to complete MII (Ataeian et al. 2016). As *ceh-18* is involved in the signalling pathway to control oocyte arrest, I sought to determine if *ceh-18*(Δ) suppressed the MEL of *memi-1*(*sb41*). I found *ceh-18*(Δ)/+; +/*memi-1*(*sb41*) worms exhibit around 30% embryonic viability at 25°C, which is significantly higher than *memi-1*(*sb41*)/+ (Figure 3.7, P=0.002). Two other suppressors, *gsp-4* and *gskl-1* also showed a similar trend that in the trans-heterozygous condition they produced significantly higher number of viable progenies. However, *ceh18*(Δ); *memi-1*(*sb41*) worms were extremely sick, and it was not possible to maintain that strain at the permissive temperature of 15°C. To confirm if the loss of *ceh-18* suppresses the embryonic lethality of *memi-1*(*sb41*), the CRISPR-Cas9 method can be used to recreate the point mutation.

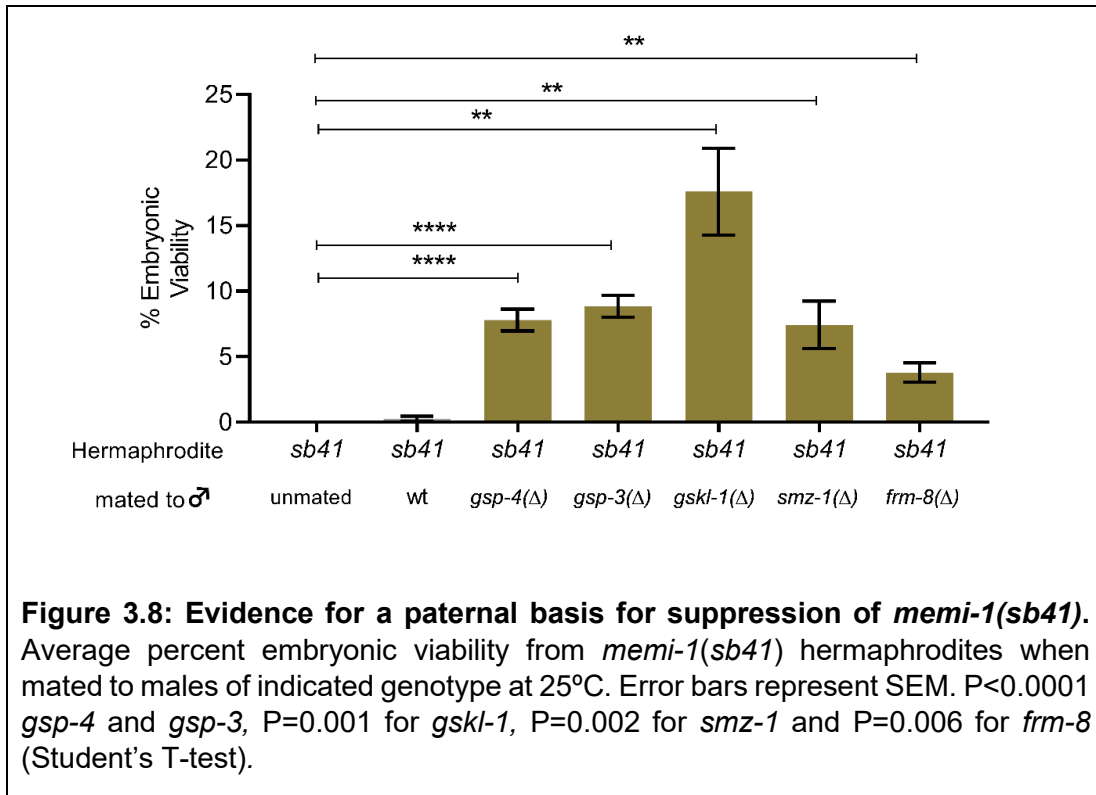


3.5 Uncharacterized suppressors

Three suppressor mutations *abc42*, *abc52* and *abc54*, remain unknown. However, the total number of possible mutations can be restricted by incorporating the mapping data. *abc42* has 17 candidate suppressor genes; 14 are on LG II, and 3 are on LG IV. *abc52* and *abc54* have 5 and 6 candidate suppressors on LGIII and LGII respectively. *abc36* has 4 candidates on LG X and, based on the data presented above (Figure 3.9), *ceh-18* could be the most promising candidate in this suppressor strain.

3.6 Evidence for a paternal basis for suppression of *memi-1(sb41)*

It was previously shown that *gsp-3/4(RNAi)* treated males suppressed *memi-1(sb41)* when mated to *memi-1(sb41)* hermaphrodites that were cultured in normal media; however, *gsp-3/4(RNAi)* treated hermaphrodites showed no suppression when mated to wild type males (Ataeian et al. 2016). This was probably because the larger wild type male sperms outcompeted smaller hermaphrodites sperm to fertilize the oocyte (LaMunyon and Ward 1998). Regardless of the mechanism, this result indicated that a similar approach could be used to help reveal whether or not any of the unknown suppressor mutations might be acting via the sperm after fertilization. Therefore, I isolated males for various deletion-mutants, representing the following genes: *gsp-4(Δ)*, *gsp-3(Δ)*, *gskl-1(Δ)*, *smz-1(Δ)*, *frm-8(Δ)*. In this way, males were mated to *memi-1(sb41)* hermaphrodites to see if they could suppress *memi-1(sb41)* lethality. All the tested deletion males showed significant suppression (Figure 3.8).



3.7 Summary

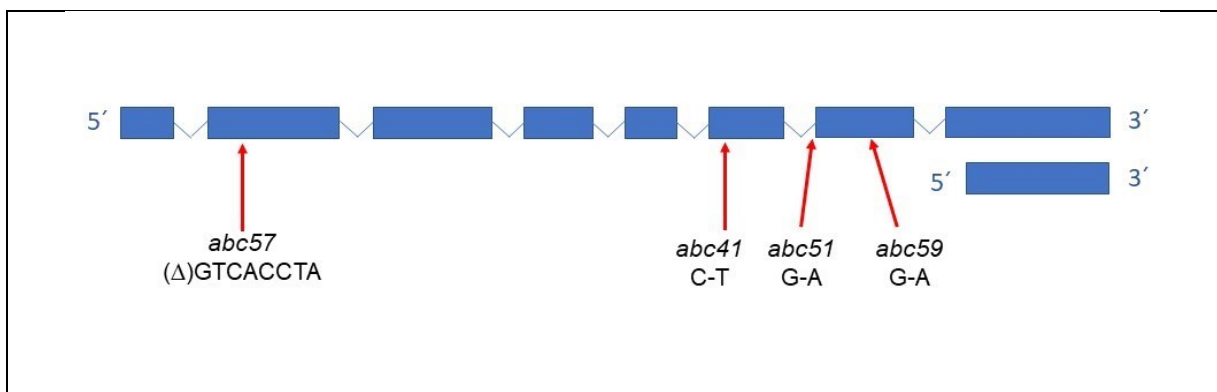
In summary, we identified five genetic suppressors of maternal-effect lethality of *memi-1(sb41)*. Molecular lesions responsible for suppressing five suppressor candidates were identified via WGS and single nucleotide polymorphism and verified either through deletion allele or recreating suppressor mutation by CRISPR-Cas9. We also identified thirteen intragenic suppressors of *memi-1(sb41)* which might be useful to understand the MEMI-1 functional motif in the future. We were unable to confirm which genes are responsible for suppression in four suppressor strains but, based on WGS and mapping data, most of the potential candidate genes are uncharacterized.

Characterization of these genes will significantly contribute to our understanding of how these genes are involved in the MEMI pathway.

4. Functional characterization of *gskl-1*

4.1 Genetic analysis of *gskl-1* suppressor alleles

As part of the EMS screen to identify suppressors of *memi-1(sb41)*, four independent suppressor strains contained mutations within the *gskl-1* gene were found (Figure 4.1). *abc57* resulted in a small deletion of GTCACCTA nucleotides in exon two which created a premature stop codon that is expected to produce a truncated protein of 60 aa (Figure 4.1). *abc41* contains a C673T missense mutation resulting in T210I change (Figure 4.1 and 4.2). *abc59* contains G762A missense mutations resulting in a G240R change (Figure 4.1 and 4.2). This Glycine in 240th position is conserved in all GSK-3 present in other organisms (Figure 4.3). *abc51* contains a G-A mutation in the splice site acceptor region of intron six, which is expected to reduce or eliminate splicing, based on the consensus site (Figure 4.1). For example, the consensus splice acceptor is UCCAG (Blumenthal T 1997) and *abc51* alters a nucleotide G-A to change the splice acceptor site to UCCAA. The position of these mutations and their effects on protein are summarized below:



aacattaaaaaatttcgattagaaatctctctgaaatcaattgattaaacgATGATGAAC	60
GGATTCCGGTATCAAGAATAATGGCGAATTTTATTCCGGTTAGCTTACAATTTGGAGgtttg	120
gaagcttatagaggttcataaaaccacaaaaaaagcaatttcagCGCACAAGCTATGTGG	180
AAGTGGGAGATTTTCAAACGTTTATTGTGGTCAAATGATATCTCCAATTGAAAAAGAGGT	240
CGCCGTGAAAAATGTGTGGTCTGATACGGAAACAC ^{abc57} GTCACCTAGCAACTAGTGAATATCC	300
GGAAATTCAAATTTTATCGAAACTTTTTCATCCGGCCATTTTGAATCTTTTGTATTTT	360
CTCGAGAAATGCGAATGACAAGgttttgaaattagagaaaaattagaaatctcaaaaa	420
ttggatattgttttagGTAATAAACTGCCTTGTCTGGACTATTTACCACAGGACCTGGCA	480
AGATTAAGAGATCAAGGTGTGAAATTCGATGTCCTCGACGCAAAGCTCTACACTTTTCAA	540
TTATTCTGTGCAATCAGTCACTTAACTTCAAAAAACATTGTTTCATATGGATATAAAGCCT	600
CAAAATGTTGTTCATGGATCGCATGgttcgacgagatttaatttagaattaggaaaaaaa	660
ttaggaattttcagGCGGGACGTTTGAAACTGGCAGATTTTCGAAATGCGAGACGACTTG	720
AGACAAATGAGAAGACAGGAAGTGCCTATCAGgtgacaaactactcaattaatcactatt	780
ttcctgataaatcacacataataatcttaatctatttaaagGTCACAAGATTCTATC	840
GACCGCCGAACTTCTTTTGGATGCGAAAAATTCACCGCTCTATCGgtaaaattaaaa	900
attgtgtttcaaaaattatttaaatgtatatttctcagATATTTGGTCAGCAAC ^{abc41} TTGTGT	960
GGCGTTTGAACTTTTCGCTAATCGAGTCTTTTTTAAAGGAAAGGACACTAAAGATCAGgt	1020
agttacagtcaaaaactggaaaacatggttaatttagctaatttccag ^{abc51} ATTGTGTTGATAA	1080
CTGGAGTTTTC ^{abc59} GGATATCCTACAGACGATGATATTTAAAGCATTGGAGTAAAAAGGCCTA	1140
GAGTTGCAAGAAAAGATGCGAGAGGAATAGAAACGgtaaaaattaaagaaaaaaccaata	1200
aaactaaaaagaagcgaacaaagcacacttgtccacgagaagtacacacgcgcgcgcg	1260
caatgtcgcgctccactgaaaacaaattggcgccagtttcaaattattttaaattcaaat	1320
aaaatttaatttcagTTCACCAGCAAGATGCTCGACTCGGAAATCTACGATTTTCATGAAA	1380
GCAACACTGAAATCGATCCGAAAAAGAGAAAATCCCGGATTGACGTGCTGAAATGCC	1440
CTTTTCGATATTCTACGATCGAGTCCACCGAAGAAGCGATCAAACGGAGTTGAGATGCCA	1500
AATCTCGGAGTTATACGGAAATGCATCACAAAAGGGAGCCGAAACGGAAGTGGTGGCA	1560
GATATTCAGACAACACTGAAAAGGCTGAAAAGGAGTCCGGATTGACGAATGAAGAATTGGAG	1620
GATTAGagaacttttcgagaagtctaccgtttagttttcgaaatagtaatttatttagt	1680
gacgtttataaaggtttacatgatt	1705

Figure 4.1: *gskl-1* sequence with the suppressor mutations.

A schematic representation of the exon and intron of *gskl-1* with suppressor mutations site. *gskl-1* has two isoforms as represented in the picture and blue boxes represent the exon. The sequence of *gskl-1* in which exons are in capital letters. Suppressor mutations are highlighted in yellow colour. *abc57* resulted in GTCACCTA deletion, *abc41* resulted in a C-T missense mutation, *abc51* resulted a G to A mutation in splice acceptor region and *abc59* resulted in a G to A missense mutation.

```

MMNGFGIKNN GEFYSVSLQF GAHKLCGSGR FSNVYCGQMI SPIEKEVAVK
NVWSDTETRHLATSEYPEIQ ILSKLFHPAISNLLYFYSRN ANDKVINCLV
LDYLPQDLARLRDQGVKFDV LDAKLYTFQL FCAISHLTSK NIVHMDIKPQ
NVVMDRMAGRLKLADFGNAR RLETNEKTGS AYQVTRFYRP PELLFGCEKF
TASIDIWSATCVAFELFANR VLFKKGDKTKD QIVLITGVFG YPTDDDIKSI
GVKRPRVARKDARGIETFTS KMLDSEIYDF MKATLKIDPK KRKSAIDVLK
MPLFDILRSS PPKKRSNGVE MPNLASYTEM HHKREPETEV VADIQTTEKA
EKESDSTNEE LED

```

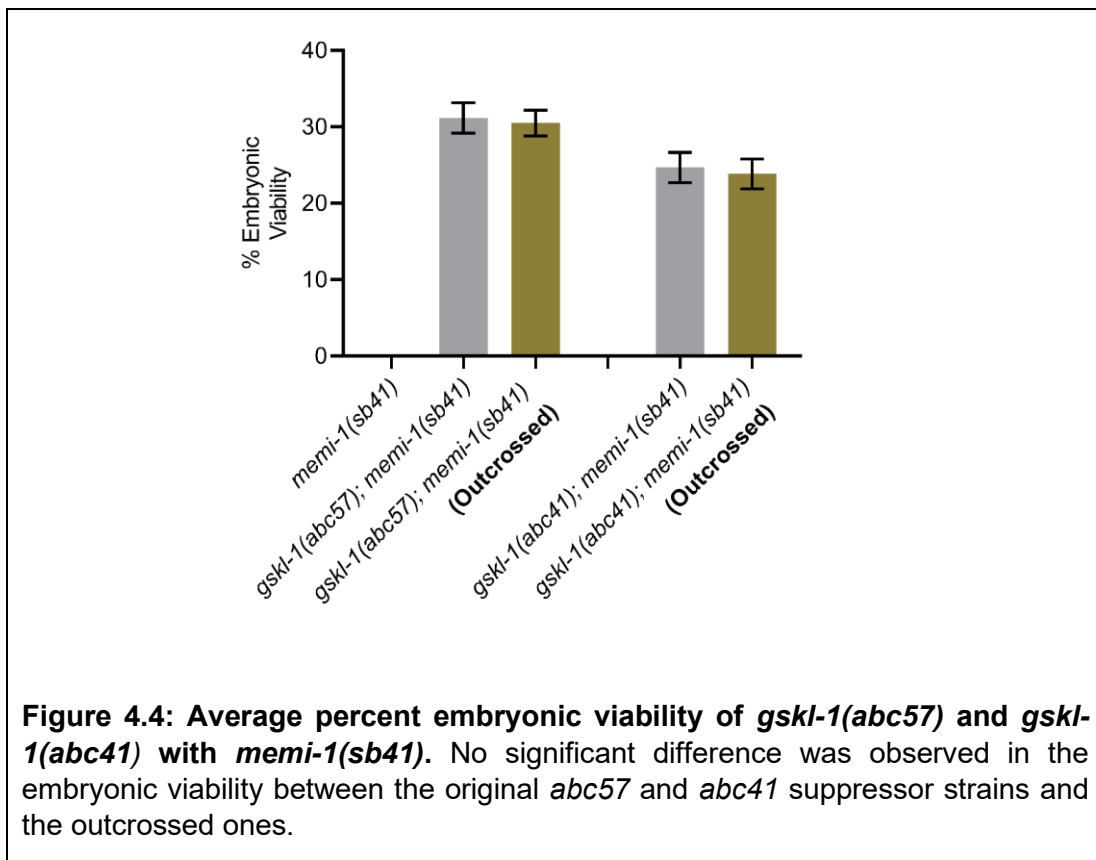
Figure 4.2: Amino acid sequence of GSKL-1. *gskl-1* produces a 363 amino acid protein. The kinase domain (20-304 amino acid) is highlighted in yellow. *abc41* is a T210I missense mutation and *abc59* is a G240R missense mutation. These two amino acids are highlighted in blue.

<i>gskl-1</i>	KFTASIDIWSATCVAFELFANRVLFKKGDKDKDQIVLITGVFGYPTDDDIKSIGVKRP---	255
Yeast	DYTHAIDIWSTGCVMAELMLGHPLFPGESGIDQLVEIILGTPSREQIKTMNPNYMEHR	268
GSK38	DYTSSIDVNSAGCVLAELLLGQPIFPGDSGVDQLVEIIVLGTPTREQIREMNPNYTEFK	292
Shaggy	NYTTKIDVNSAGCVLAELLLGQPIFPGDSGVDQLVEIIVLGTPTREQIREMNPNYTEFK	290
	..* **:** ** ** : : * *.. **:* : : * * : : * : : :	

Figure 4.3: *abc59* resulted to a change in evolutionary conserved region of GSK-3. Glycine in the 240th position in GSK-3 is evolutionary conserved and *abc59* resulted in a G240R change.

Due to treatment of EMS, it is important to remember that the four suppressor strains have several mutations at different loci (Anderson 1995). It was therefore necessary to backcross those suppressor strains to wild-type to reduce background

mutations. I used a strain with two markers that flank *gskl-1*, *dpy-10* and *unc-4* on chromosome II, to recover *abc57* and *abc41* suppressor alleles after backcrossing. At first, *abc57; memi-1(sb41) dpy-20* hermaphrodites were mated to heterozygous *dpy-10 unc-4* males. In the F1 generation, 50% of the progeny were *trans* heterozygous + *abc57 + / dpy-10 + unc-4; memi-1(sb41) dpy-20 / + +*. In the F2 generation, 32 worms were picked from the *trans* heterozygous mother to recover *abc57; memi-1(sb41) dpy-20*. Using a similar approach, I recovered *abc41; memi-1(sb41) dpy-20*. Then, I scored embryonic viability of the new *abc57; memi-1(sb41) dpy-20* and *abc41; memi-1(sb41) dpy-20* worms at 25°C. I found that the outcrossed *abc57* and *abc41* worms exhibited no significant differences in embryonic viability, in comparison to the original *abc57* and *abc41* worms respectively (Figure 4.4).



4.2 *gskl-1* mutants are superficially wild-type

Until now, there was no report available for the function of *gskl-1* in *C. elegans*. To determine whether any of the mutations in *gskl-1* result in any obvious phenotypes, they were each separated from the original *memi-1(sb41)* mutation. Briefly, the original strain was crossed to the WT male and F2 generation progeny from the F1 trans heterozygous were screened for *memi-1(sb41)* and the suppressor allele. After *memi-1(sb41)* was removed, the presence of each mutation in the four strains was confirmed by DNA sequencing. To test whether these mutants have any effect on fertility, individual N2 (wild type), *abc41*, *abc51*, *abc57* and *abc59* hermaphrodites were transferred daily to nematode growth medium (NGM) agar plates containing *Escherichia coli* strain OP50, for approximately 48 hours after the larvae reached the 4th larval stage at 20°C. The number of viable progeny and dead embryos were counted daily. All four mutants displayed a small but significant decrease in brood sizes and embryonic viability (Figure 4.5 and Figure 4.6).

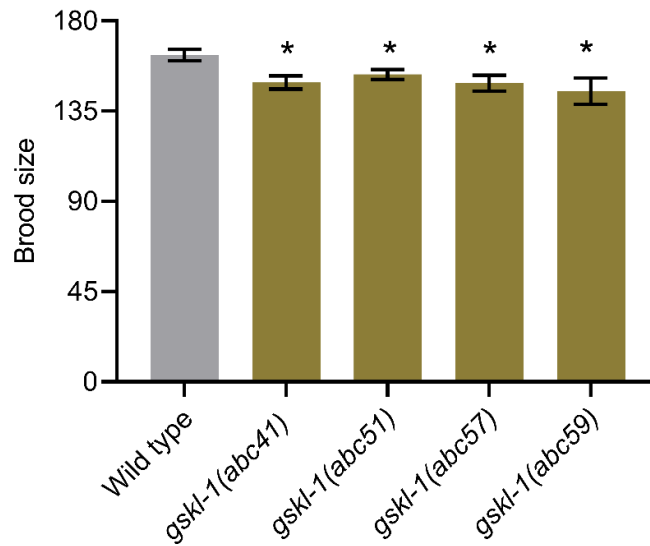


Figure 4.5: Average brood size from wild type, *gskl-1(abc41)*, *gskl-1(abc51)*, *gskl-1(abc57)* and *gskl-1(abc59)* at 20°C. P=0.01 for *gskl-1(abc41)* and *gskl-1(abc57)*, P=0.02 for *gskl-1(abc51)*, P=0.04 for *gskl-1(abc59)* (Student's T-test). n=10 for each group, error bars represent SEM.

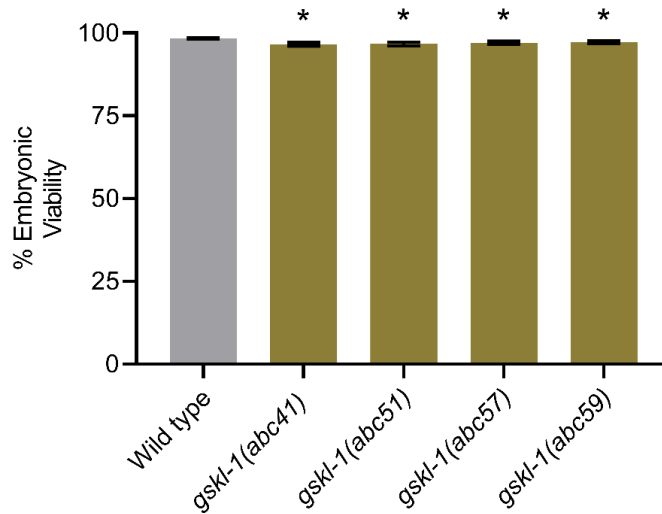


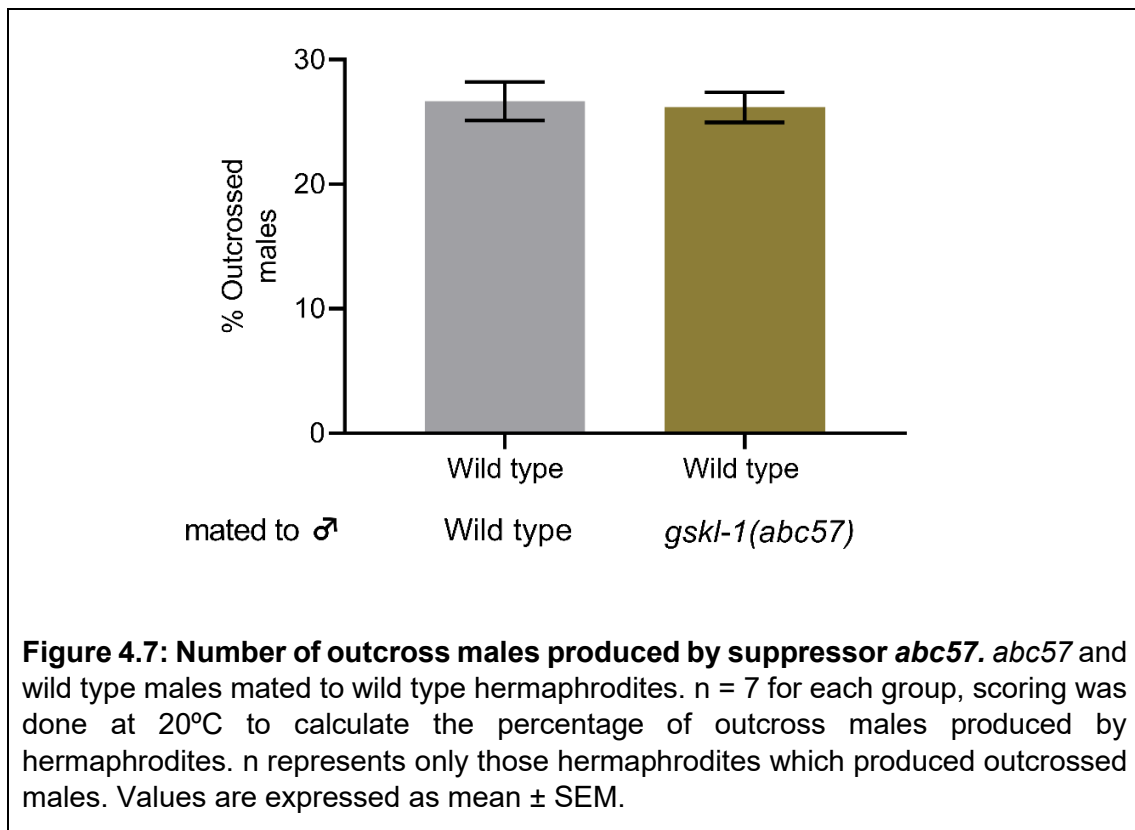
Figure 4.6: Embryonic viability from wild type, *gskl-1(abc41)*, *gskl-1(abc51)*, *gskl-1(abc57)* and *gskl-1(abc59)* at 20°C. P=0.02 for *gskl-1(abc41)* and *gskl-1(abc51)*, P=0.03 for *gskl-1(abc57)* and *gskl-1(abc59)* (Student's T-test). n=10 for each group, error bars represent SEM.

4.3 *gskl-1* mutant males are fertile

In *C. elegans* hermaphrodites, the sperm are the limiting factor for producing progeny, with each spermatheca carrying a maximum of about 150 sperm. Wild-type worms normally continue to produce unfertilized oocytes once they run out of sperm, and the oocytes are distinguishable from fertilized eggs on the agar surface. When scoring embryonic lethality, the hermaphrodite is transferred each day to a fresh plate, and the total progeny deposited on each plate is referred to as a separate “brood”. Thus, unfertilized oocytes are normally not observed in the first brood. While scoring the *gskl-1* mutants for embryonic lethality, I observed a few unfertilized oocytes in the first brood, suggesting that sperm was already being depleted. However, in the second brood, the hermaphrodites also laid eggs along with some unfertilized oocytes. The presence of eggs in the second brood indicated that they were not running out of sperm, rather, that some mutant sperm were unable to fertilize the oocyte, which was eventually deposited. Alternatively, the unfertilized oocytes on the plate could have represented fertilized eggs that were unable to synthesize an egg shell.

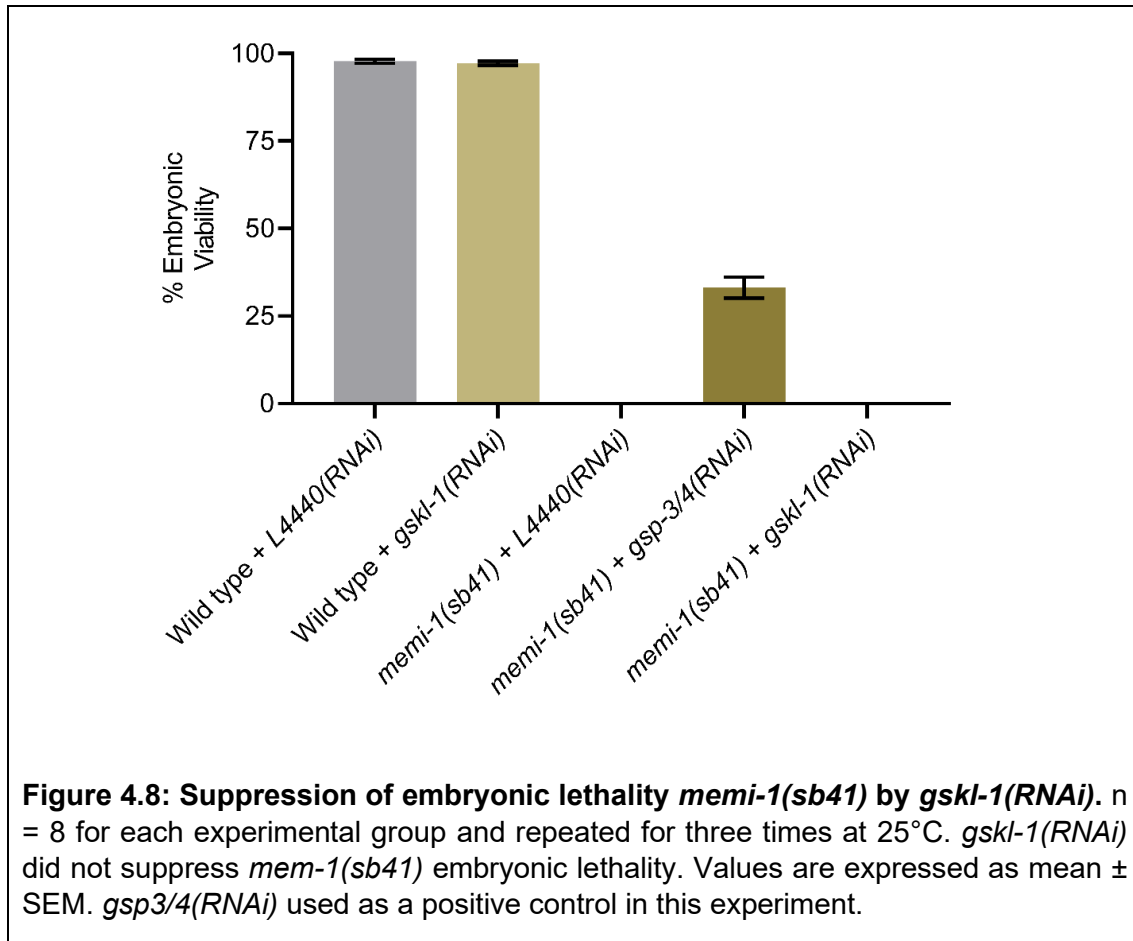
When males copulate with hermaphrodites, the male sperm efficiently outcompetes the hermaphrodite sperm for fertilization, such that a large group of progeny are usually exclusively outcross, until the male sperm is depleted. In order to test whether the *gskl-1* male mutants have the capability of producing progeny and whether or not they can compete with the hermaphrodite, I used *abc57* and *abc41* males to mate with wild-type hermaphrodites. I found no significant difference in the number of outcross males produced by *abc57* males, in comparison to wild-type controls (Figure

4.7). The *abc41* males appeared to not mate, as outcross progeny were not detected. There could be many possibilities for why *abc41* males did not lead to outcross progeny. Firstly, the point mutation may affect male sperm motility or spermatogenesis, which ultimately results in infertile sperm upon mating. The mutation could also affect some other aspect important for mating, such as the ability of males to detect hermaphrodites. Secondly, this mutation was identified through EMS mutagenesis, so, the strain could have another mutation that affects the mating process. Thirdly, this may be a spurious result, as sometimes wild-type worms treated similarly do not mate.



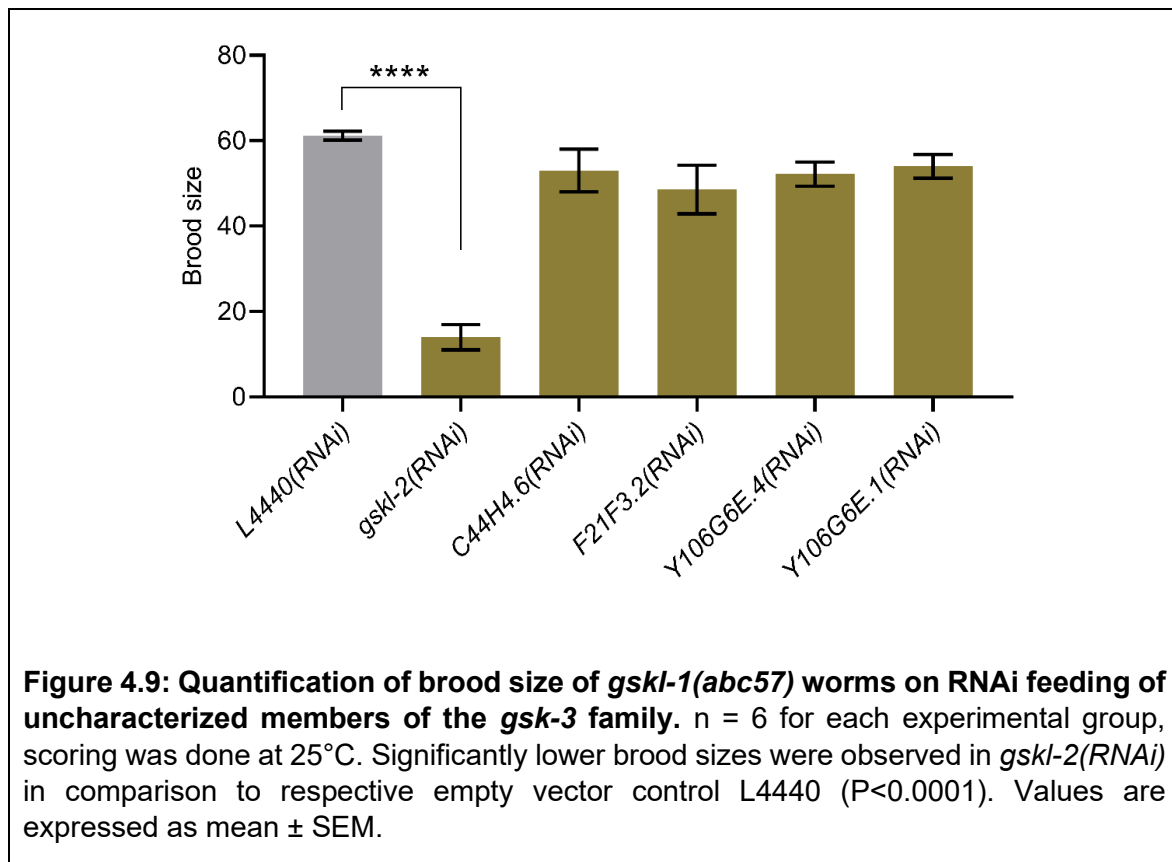
4.4 An RNAi-based approach to assess the function of *gskl-1*

Although four mutations were identified in *gskl-1* within four different suppressor strains, an independent verification that *gskl-1* is a suppressor of *memi-1(sb41)* was still necessary. One way to verify this was to use RNAi to determine if loss of function of *gskl-1* also suppressed *memi-1(sb41)*. *gskl-1(RNAi)* was performed by feeding *memi-1(sb41)* worms *E. coli* expressing dsRNA for *gskl-1*. I did not observe any evidence for suppression of *memi-1(sb41)* (Figure 4.8). There are at least two explanations for why *gskl-1(RNAi)* did not suppress *memi-1(sb41)*. First, the suppressors may not be simple loss-of-function mutations; however, this possibility is unlikely as the *gskl-1(Δ)* suppressed *memi-1(sb41)* (Data is shown in Chapter 3, Figure 3.2). Secondly, RNAi may not be effective for this gene. One disadvantage of RNAi-based techniques is that the efficacy varies between different genes and different target tissues, and it is difficult to verify that protein function has been reduced or eliminated.



When using *gskl-1(RNAi)* to test for suppression of *memi-1(sb41)* it was challenging to determine whether the *gskl-1(RNAi)* worked successfully or not, since *gskl-1(RNAi)* on its own displayed no phenotype, and the *gskl-1* mutants are superficially wild-type. It is possible that *gskl-1* is functionally redundant with one or more of the other putative GSK-3 genes, which may be why *gskl-1(RNAi)* or mutants do not result in any obvious phenotype. Previously, it was reported that, apart from *gskl-1*, there are likely six more genes that encode GSK-3 enzymes in *C. elegans*, *Y18D10A.5* (*gsk-3*), *R03D7.5* (*gskl-1*), *C36B1.10* (*gskl-2*), *Y106G6D.4*, *C44H4.6*, *Y10G6GE.1*, and *F21F3.2* (Manning 2005). Of these, only *Y18D10A.5* (*gsk-3*) is an

essential gene, as it is required for proper endoderm specification and mitotic spindle orientation in the embryonic precursor cell, EMS (Schlesinger et al. 1999). To test if *gskl-1* is functionally redundant with any one of the remaining five uncharacterized genes, I performed RNAi on those genes using two different *gskl-1* strains containing either *abc57* or *abc41* mutations. Significantly lower brood sizes were observed in *abc57* and *abc41* worms with *gskl-2(RNAi)* in comparison to the control, which indicated that *gskl-1* could share some redundant functions with *gskl-2*, related to fecundity (Figure 4.9 and 4.10).



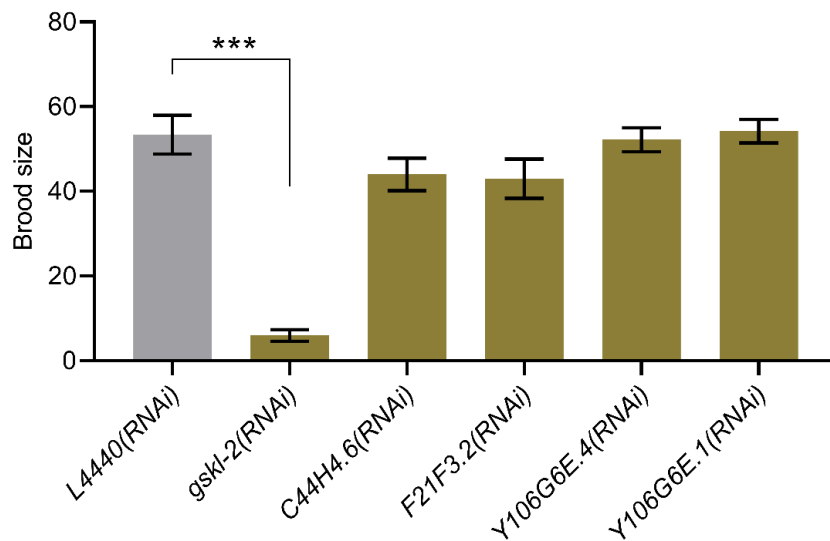
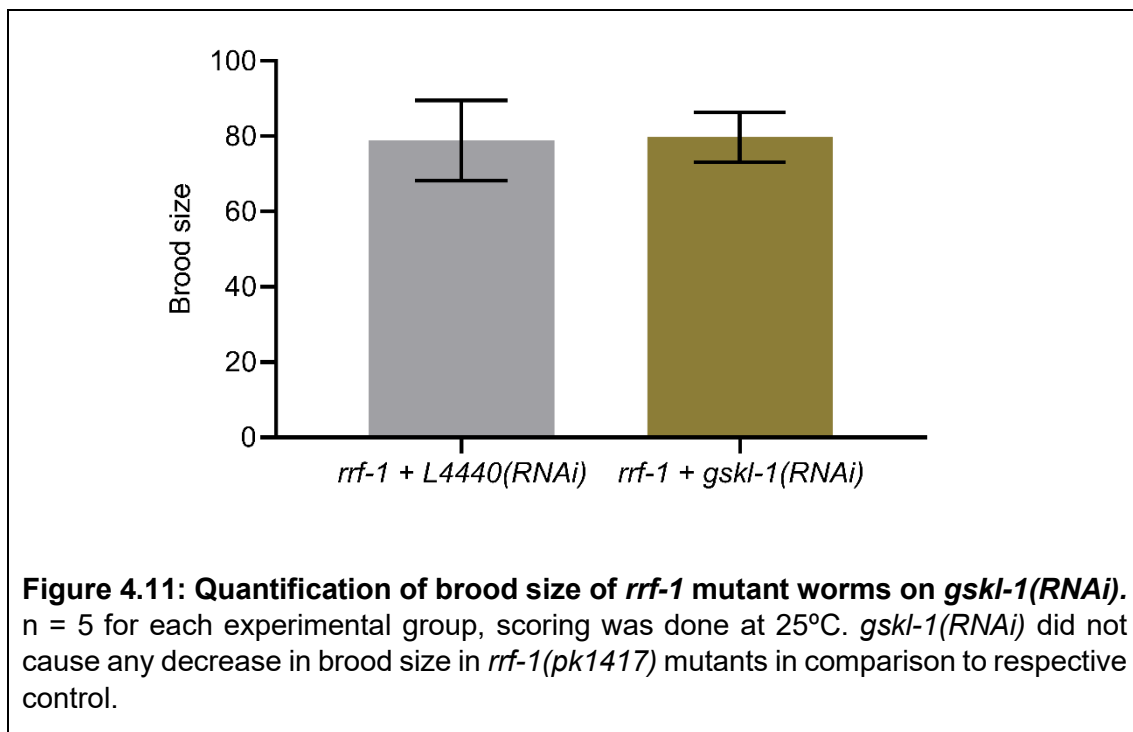


Figure 4.10: Quantification of brood size of *gskl-1(abc41)* worms on RNAi of uncharacterized members of *gsk-3* family. n = 6 for each experimental group, scoring was done at 25°C. Significantly lower brood size was observed in *gskl-2(RNAi)* in comparison to respective control (P=0.0002). Values are expressed as mean ± SEM.

4.5 Using *rrf-1* mutant background to test *gskl-1(RNAi)*

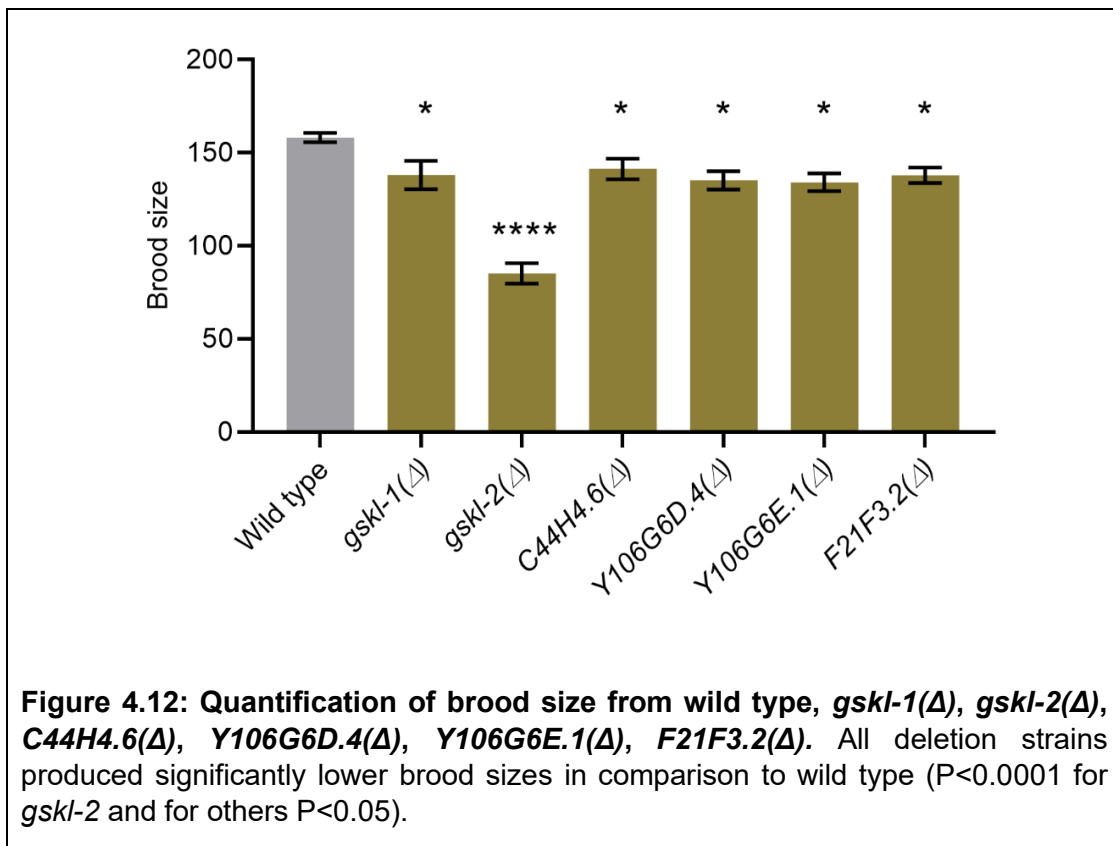
It has been previously shown that some genes in *C. elegans* are refractive to RNAi-based approaches (Sijen et al. 2001), thus it was possible that *gskl-1(RNAi)* was inefficient or ineffective. During RNAi, an RNase III family endoribonuclease Dicer cleaved the dsRNA into short-interfering RNAs (siRNAs) which are then loaded into the RNA-induced silencing complex (RISC). The RISC then guides the dsRNA to bind with the target mRNA and facilitates its degradation (Maine 2008; Fischer 2010). Only a few molecules of dsRNA are required to degrade a large pool of mRNA because RNA-dependent RNA polymerases (RdRPs) synthesize more dsRNA by using siRNAs as primers (Grishok 2005; Fischer et al. 2008). In *C. elegans*, RRF-1 is identified as one of the four RdRP homologs that is required for RNAi responses in somatic cells

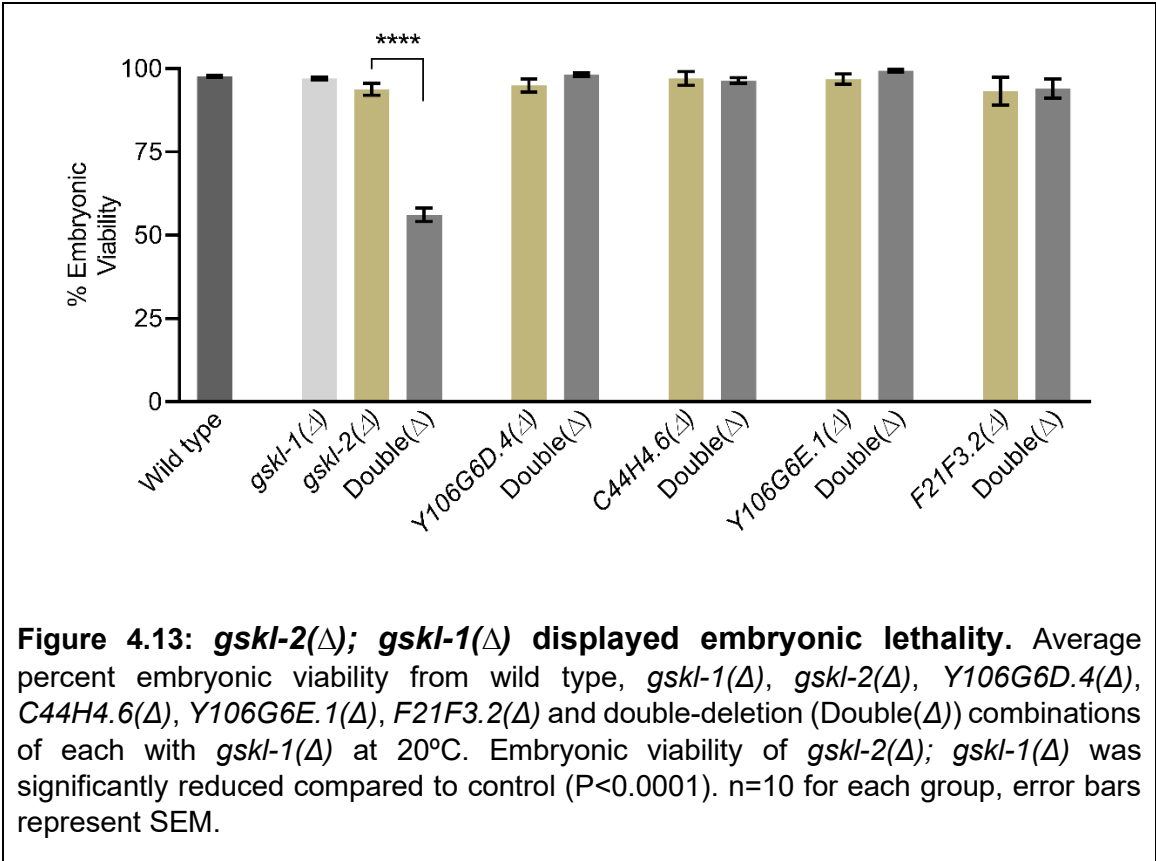
but is dispensable for germline RNAi which use EGO-1 RdRP (Smardon et al. 2000; Sijen et al. 2001). Thus, *rrf-1* deletion mutants are used to mediate RNAi of germline specific genes (Kumsta and Hansen 2012). As an initial approach, I used a deletion allele *rrf-1(pk1417)*. I fed *gskl-1* dsRNA-expressing bacteria to *rrf-1(pk1417)* mutant worms. I found no significant difference in the embryonic viability or number of unfertilized oocytes in comparison to the control. However, I observed that *rrf-1(pk1417)* worms on their own produced highly variable dead eggs. So, I used a different strain that had the same *rrf-1(pk1417)* deletion allele, but was outcrossed four times to clean the background. *gskl-1(RNAi)* neither reduced the brood size nor caused any visible phenotypes on *rrf-1(pk1417)* mutants (Figure 4.11). These experiments demonstrated that *gskl-1(RNAi)* was likely ineffective, and not improved by using the *rrf-1* mutation.



4.6. *gskl-1* is functionally redundant with *gskl-2*

To further test the hypothesis that *gskl-1* is functionally redundant, deletion mutant strains were obtained for the five uncharacterized non-essential GSK-3 members. As with *gskl-1*, all of the single-deletion strains appeared healthy, with worms producing viable progeny at levels comparable to wild type; however, brood sizes of all deletion strains were significantly lower in comparison to wild type (Figure 4.12). Next, I made double-deletion strains to test for synthetic phenotypes. From the five double-deletion strains, only *gskl-2(ok970); gskl-1(tm4146)*, hereafter referred to as *gskl-2(Δ); gskl-1(Δ)*, resulted in observable phenotypes (56% embryonic viability; $P < 0.0001$ and reduced brood size; $P < 0.0001$); suggesting that these two genes have at least some overlapping essential function(s) affecting embryogenesis (Figure 4.13 and Table 4.1).

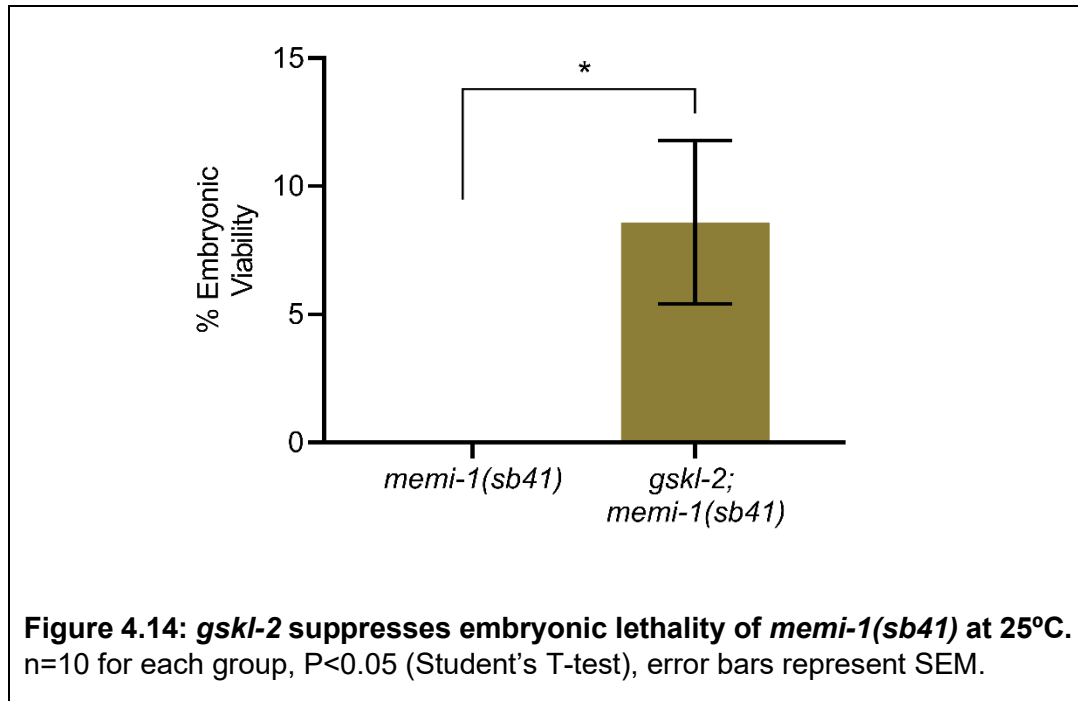




Genotype	Larvae	Dead Eggs	Brood Size
Wild type	181	3	184
<i>gskl-1</i> (Δ)	133	5	138
<i>gskl-2</i> (Δ)	86	6	92
<i>gskl-2</i> (Δ); <i>gskl-1</i> (Δ)	23	19	42
<i>Y106G6D.4</i> (Δ)	129	6	135
<i>gskl-1</i> (Δ); <i>Y106G6D.4</i> (Δ)	120	7	127
<i>C44H4.6</i> (Δ)	137	4	141
<i>gskl-1</i> (Δ); <i>C44H4.6</i> (Δ)	128	5	133
<i>Y106G6E.1</i> (Δ)	132	2	134
<i>gskl-1</i> (Δ); <i>Y106G6E.1</i> (Δ)	124	2	126
<i>F21F3.2</i> (Δ)	129	8	137
<i>gskl-1</i> (Δ); <i>F21F3.2</i> (Δ)	121	6	129

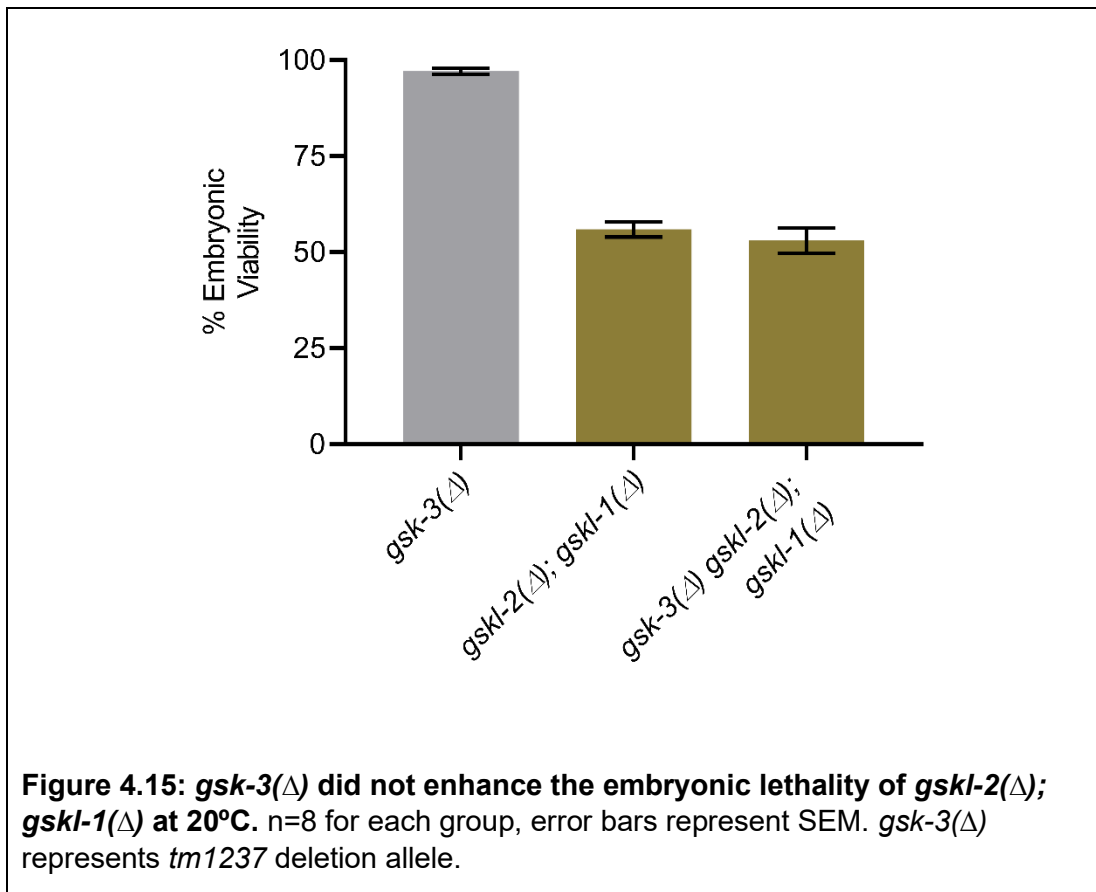
Table 4.1: Average brood size of different double-deletion combinations. Average brood size from wild type, *gskl-1*(Δ), *gskl-2*(Δ), *Y106G6D.4*(Δ), *C44H4.6*(Δ), *Y106G6E.1*(Δ), *F21F3.2*(Δ) and double-deletion (Double(Δ)) combinations of each with *gskl-1*(Δ) at 20°C.

The above results indicated that *gskl-1* and *gskl-2* were redundant for at least some essential functions. It is possible that the overlapping functions between these genes could also involve the *memi* pathway, therefore, loss of *gskl-2* might also suppress *memi-1*(*sb41*). However, *gskl-2* was not recovered as a suppressor of *memi-1*(*sb41*) in the EMS screen. So, I tested if *gskl-2*(Δ) suppressed *memi-1*(*sb41*). I found that *gskl-2*(Δ); *memi-1*(*sb41*) double mutants showed weak, albeit significant, suppression (9% viability at 25°C; P<0.05; Figure 4.14).



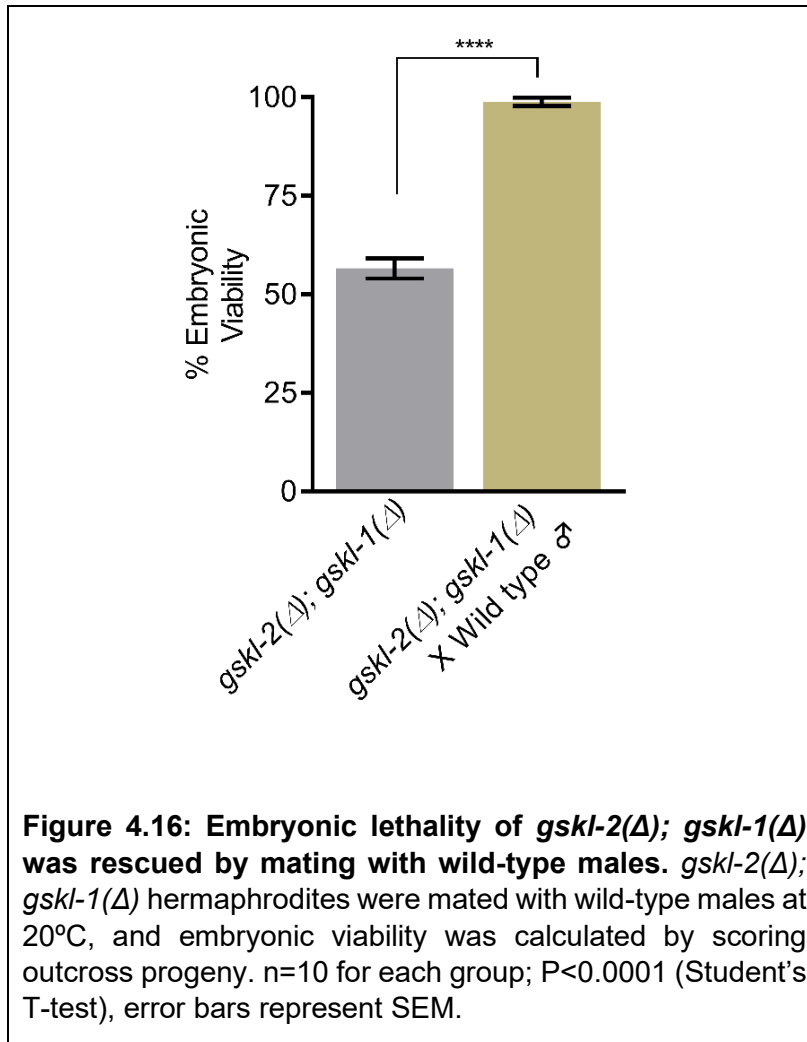
As mentioned above, one of the GSK-3 homologues, *gsk-3*, has been reported as essential and required for early embryonic development. In the course identifying reagents to test for redundancy with *gskl-1*, I discovered three deletion strains available for *gsk-3*. Two alleles, *gsk-3(tm2223)* and *gsk-3(nr2047)* are strong loss-of-function alleles that result in complete embryonic lethality, so it was not possible to test for functional redundancy in *gskl-1 gsk-3* double homozygotes. Surprisingly, homozygous worms for another allele, *gsk-3(tm1237)*, exhibited no obvious phenotypes. *gsk-3(tm1237)* 350 bp deletion removes part of the 2nd intron that might affect the splicing. This suggests that, either the “strong” *gsk-3* alleles contain other mutations responsible for the phenotype, or that *gsk-3(tm1237)* displays molecular evidence of a deletion, but that the gene function is somehow still intact. In the event that *gsk-3(tm1237)* represents the true loss-of-function phenotype for the gene, I used it to test for functional redundancy with *gskl-1*. Although the *gsk-3(tm1237)* produced no synthetic

lethality in the *gsk-3(tm1237); gskl-1(Δ)* double-deletion strain, I tested this mutation in combination with the other two interacting genes by making a triple mutant *gsk-3(tm1237) gskl-2(Δ); gskl-1(Δ)*. The *gsk-3(tm1237)* deletion did not enhance the phenotype of *gskl-2(Δ); gskl-1(Δ)*, indicating that, even if *gsk-3(tm1237)* did represent the true loss-of-function phenotype for *gsk-3*, this mutation did not reveal any functional redundancy with *gskl-1* (Figure 4.15).



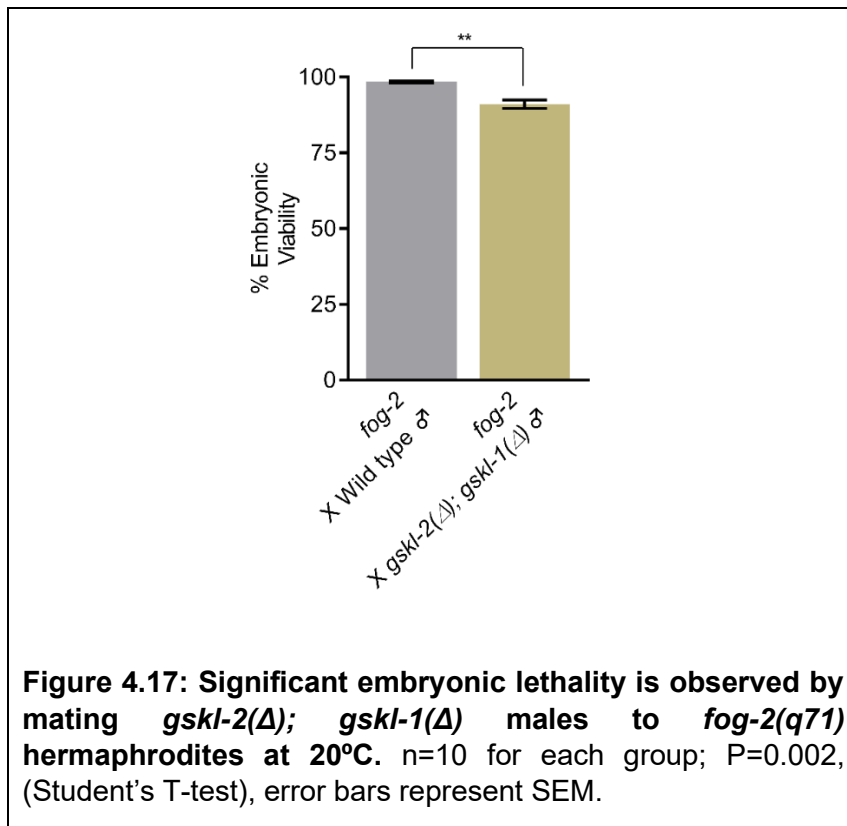
4.7 *gskl-1 gskl-2* mutants exhibit paternal-effect embryonic lethality

Some phenotypes associated with loss of *gskl-1* and *gskl-2*, for example, lower brood sizes or increased production of unfertilized oocytes, suggested that these genes could be involved in sperm functions. In addition, genome-wide transcriptional profiling indicates that transcripts for both genes are enriched in L4 males, which coincides with spermatogenesis (Reinke et al. 2000; Reinke et al. 2004). Therefore, to characterize the genetic basis for the phenotypes, *gskl-2*(Δ); *gskl-1*(Δ) hermaphrodites were mated to wild-type males and embryonic viability was determined. Embryonic lethality was completely rescued by wild-type males ($P < 0.0001$), consistent with either zygotic or paternal rescue (Figure 4.16).



If the GSK-3 double mutant were paternally rescued, then one would also expect all sperm from a heterozygous male to rescue a homozygous mutant hermaphrodite; in other words, the phenotype would be dependent on the genotype of the male parent and not the zygote or individual sperm haplotype. Therefore, I genotyped individual progeny after mating *gskl-2(Δ)/+; gskl-1(Δ)* males to *gskl-2(Δ); gskl-1(Δ)* hermaphrodites. Upon outcrossing, I observed a 1:1 ratio of the *gskl-2(+)* and (Δ) alleles in surviving progeny, indicating that homozygous mutant progeny were rescued by the presence of a “+” allele in the male parent.

To further test the idea that the embryonic lethality was due to defective sperm, *gskl-2*(Δ); *gskl-1*(Δ) males were mated to *fog-2*(*q71*) feminized hermaphrodites, which can only produce progeny if fertilized by males. Surprisingly, I observed 91% embryonic viability, compared to the 56% viability in *gskl-2*(Δ); *gskl-1*(Δ) hermaphrodite progeny (Figure 4.17; P=0.002 and Table 4.2).

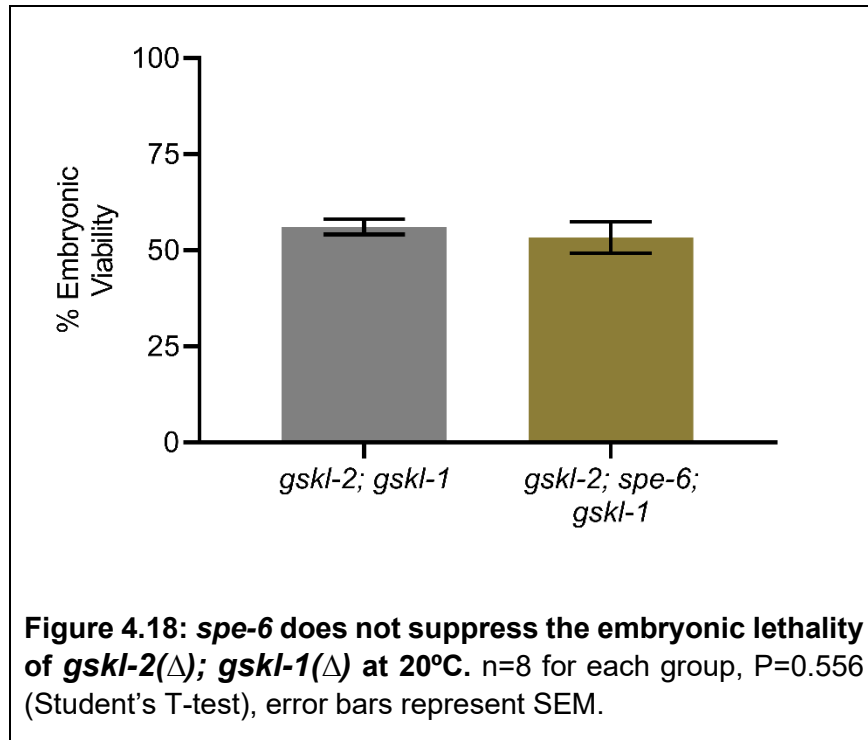


mated to ♂	Average brood Size 1		Average brood size 2		Average brood Size 3	
	Totale laid	% Dead Eggs	Totale laid	% Dead Eggs	Totale laid	% Dead Eggs
Wild type	134	0	185	0.68	112	0.98
<i>gskl-2</i> ; <i>gskl-1</i>	120	4	106	7	11	41

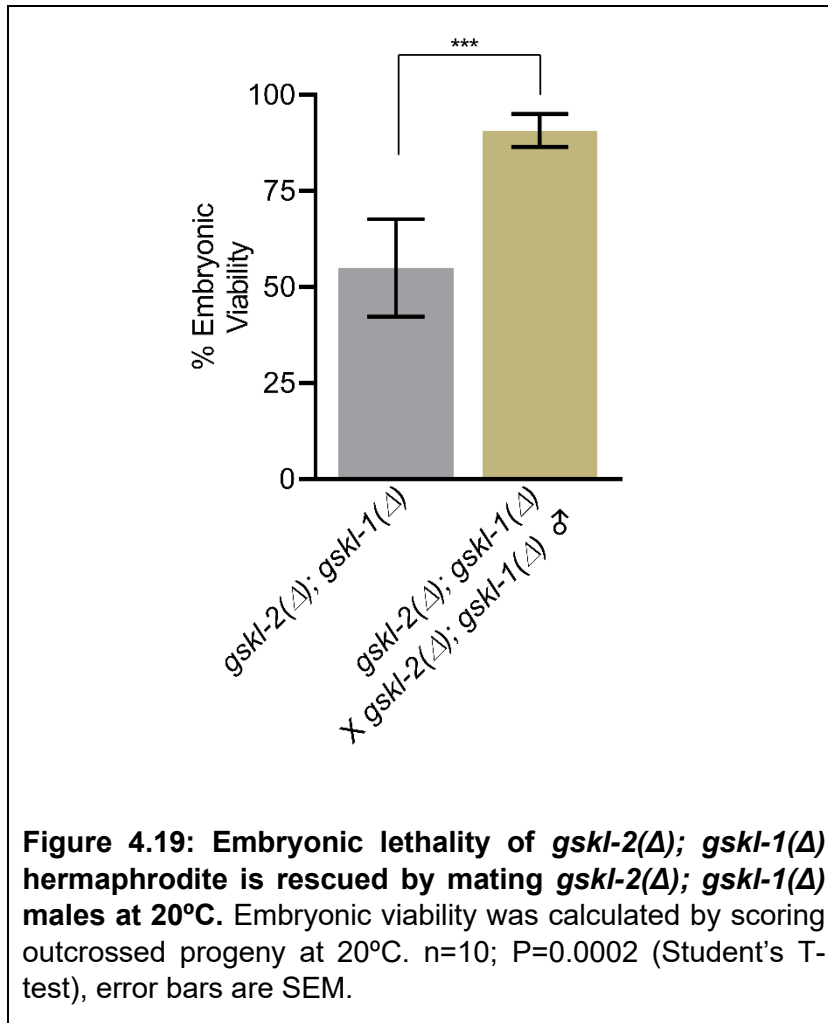
Table 4.2: Average brood size and percentage of dead eggs of *fog-2* hermaphrodites during en masse mating at 20°C.

4.8 *gskl-1* and *gskl-2* are not part of the *spe-8* pathway

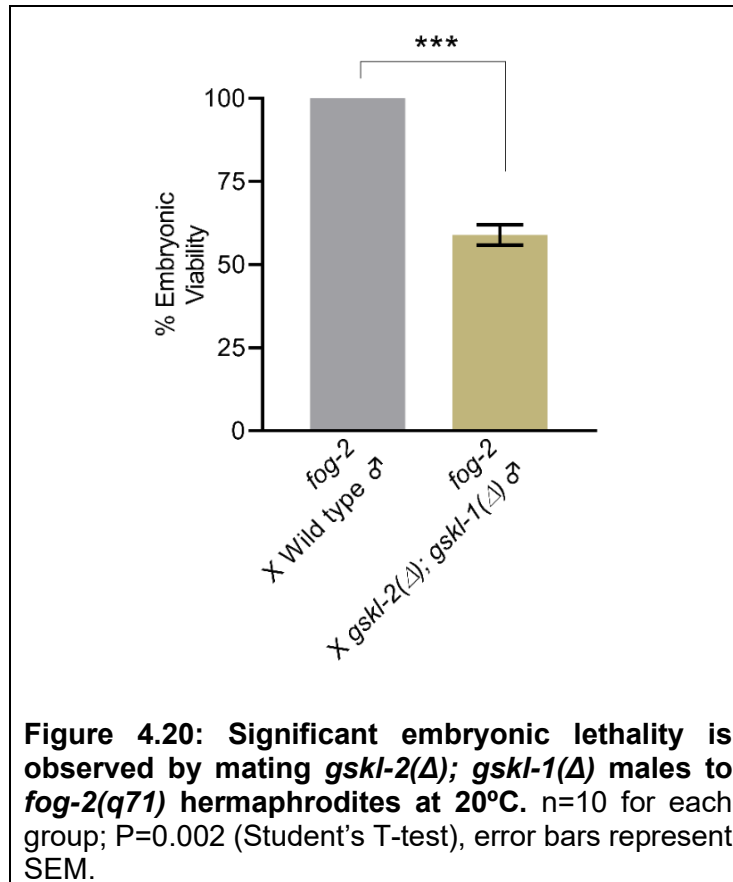
The fact that *gskl-2*(Δ); *gskl-1*(Δ) males did not confer embryonic lethality to *fog-2* mothers was unexpected. However, this could be explained if hermaphrodite sperm were more sensitive to the loss of *gskl-1* and *gskl-2* function than male sperm. For example, mutations in genes in the *spe-8* pathway (*spe-8*, *spe-12*, *spe-27*, or *spe-29*) result in hermaphrodite-specific spermiogenesis defects (Shakes and Ward 1989a; Minniti et al. 1996; Nance et al. 1999; Nance et al. 2000). In these cases, mutant hermaphrodites are self-sterile because their spermatids fail to activate. It has been suggested that the SPE-8 pathway negatively regulates the casein kinase SPE-6, because a loss-of-function allele *spe-6(hc163)* which suppresses all known mutations within the *spe-8* pathway (Muhlrad and Ward 2002). Therefore, in order to test whether *gskl-1* and *gskl-2* might be a part of the *spe-8* pathway, I constructed a *gskl-2*(Δ); *spe-6(hc163)*; *gskl-1*(Δ) triple mutant. However, *spe-6(hc163)* did not suppress *gskl-2*(Δ); *gskl-1*(Δ) embryonic lethality in unmated hermaphrodites (Figure 4.18), indicating that these two GSK-3 genes are likely not part of the *spe-8* pathway.



An alternative idea to explain the incomplete penetrance (91% vs., 56% embryonic viability) is that individual sperm could exhibit a range of phenotypic severity, such that some sperm could be approximately wild type and others could be severely affected. In this way, sperm selection might be more intense for male-derived sperm because they must first crawl from vulva to spermatheca to reach an oocyte, whereas hermaphrodite sperm are pre-stored within the spermatheca. If the fittest outcross sperm are selected for fertilization, then *gskl-2*(Δ); *gskl-1*(Δ) male mating should also partially rescue *gskl-2*(Δ); *gskl-1*(Δ) hermaphrodites. In this case, we observed that mated *gskl-2*(Δ); *gskl-1*(Δ) exhibited 88% viability, as compared to 56% in non-mated controls (Figure 4.19, P=0.0002). Therefore, the increase in viability we observed upon mating males to *fog-2* hermaphrodites was not due to a maternal wild-type allele, but likely due to selection for healthier mutant male sperm.



To further test the hypothesis that the incomplete penetrance (91% vs. 56% embryonic viability) was due to pre-fertilization competition among male sperm, single young adult males were mated to *fog-2* hermaphrodites and then males were transferred in every 8 hours to mate with new hermaphrodites. In this way, smaller number of male sperm should decrease pre-fertilization competition and thus should increase the number of inviable embryos. In this case, *fog-2* hermaphrodites mated to single *gskl-2(Δ); gskl-1(Δ)* male displayed 59% embryonic viability, as compared to 100% in wild-type male mated control (Figure 4.20, P=0.0002; Table 4.3).



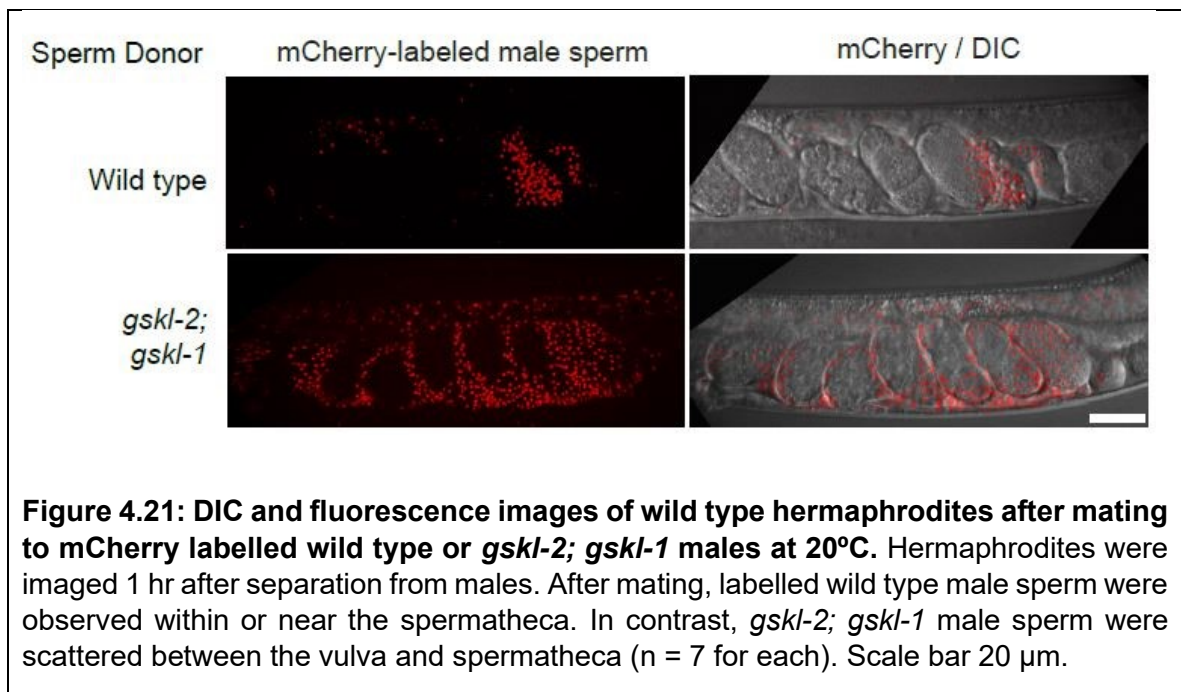
mated to ♂	Average brood size 1		Average brood size 2	
	Total laid	% Dead eggs	Total laid	% Dead eggs
Wild type	127	0	122	0
<i>gskl-2; gskl-1</i>	119	42	109	39

Table 4.3: Average brood size and percentage of dead eggs of *fog-2* hermaphrodites during single male mating at 20°C.

Together, these data suggest that *gskl-1* and *gskl-2* are functionally redundant and exhibit incompletely-penetrant paternal-effect embryonic lethality. My data also suggest that male-mating imposes a strict selection that can contribute to variable penetrance of embryonic phenotypes.

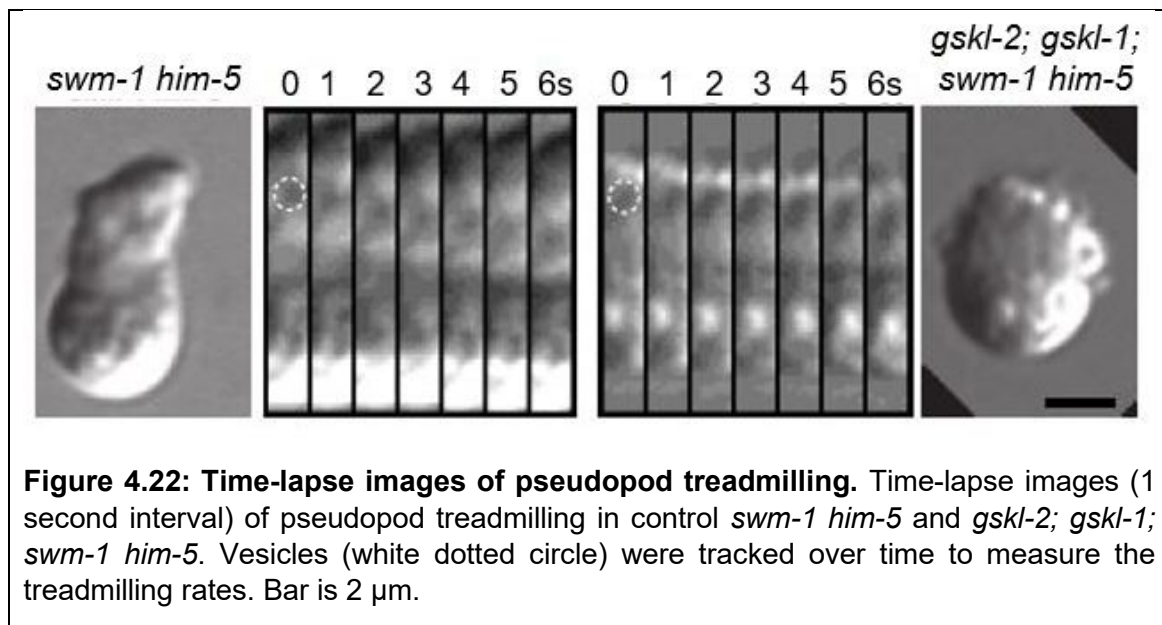
4.9 *gskl-1* and *gskl-2* are required for efficient sperm migration

Considering the results above, we hypothesized that the selection for healthier sperm after copulation was likely based on differences in sperm motility or guidance. Therefore, we tracked the location of male sperm in mated hermaphrodites, using male worms that express mCherry-histone to label chromatin. After mating to unlabelled wild-type hermaphrodites for 24 hr, fluorescent punctae representing wild-type male sperm were detected only in the spermathecae, adjacent to the uterus (Figure 4.21). In contrast, in all hermaphrodites mated to *gskl-2*(Δ); *gskl-1*(Δ) males, fluorescent punctae were scattered between the vulva and the spermatheca (Figure 4.21). This suggested that *gskl-2*(Δ); *gskl-1*(Δ) sperm can be transferred from male to hermaphrodite during mating, but many sperm are inefficient in migrating to the spermatheca.



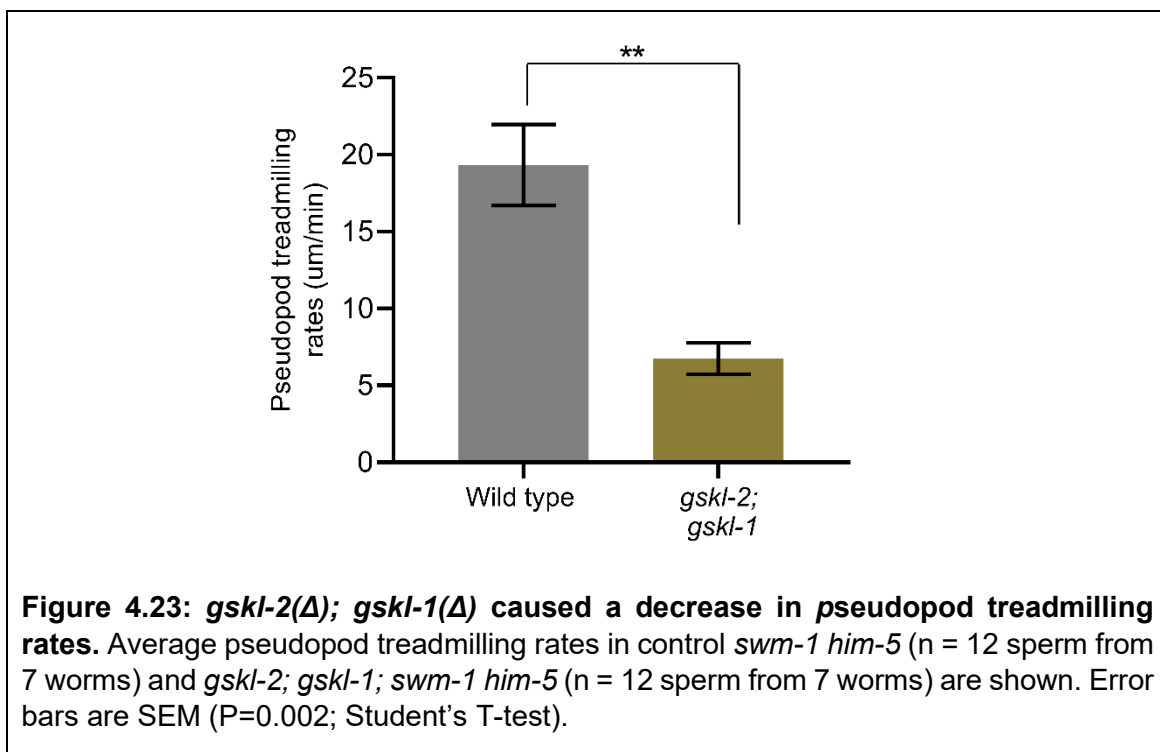
4.10 *gskl-1* and *gskl-2* are required for pseudopod formation and treadmilling

We next sought to determine whether *gskl-1* and *gskl-2* play a direct role in sperm motility. In *C. elegans*, activated sperm move by treadmilling of the cytoskeletal polymer MSP from the pseudopod tip toward the cell body (Nelson et al. 1982). Treadmilling rates, which directly correlate with sperm movement rates, can be observed indirectly by tracking vesicles within the cytoplasm (Figure 4.22) (Nelson et al. 1982; Wu et al. 2012).



In order to observe the pseudopod treadmilling rates, we used the mutant *swm-1(me66)*. *swm-1* is a negative regulator of spermiogenesis that normally inhibits male sperm activation until after transfer to the hermaphrodite; *swm-1* mutant spermatids are constitutively activated to crawl (Stanfield and Villeneuve 2006). Our analysis

showed that *swm-1(me66) him-5(e1490)* male sperm pseudopod treadmilling rates were $19.60 \pm 2.4 \mu\text{m}/\text{min}$ which is similar to previously reported data (Nelson et al. 1982; Shakes et al. 2009). In *gskl-2(\Delta); gskl-1(\Delta); swm-1(me66) him-5(e1490)*, male sperm pseudopod treadmilling rates were $8.8 \pm 2.5 \mu\text{m}/\text{min}$, which is significantly slower than the control ($P=0.002$; Figure 4.23).



To visualize the process of pseudopod development upon activation, sperm were treated with Pronase, which allows synchronous activation of male sperm *in vitro*. Quantification of the data showed that 100% of *him-8* (WT) male sperm activated within 12 minutes, as shown by the appearance of proper pseudopods (Figure 4.24). During activation, the control male sperm formed spikes or spicule-like structures, which

eventually developed into a pseudopod (Figure 4.25). In contrast, only three percent of *gskl-2*(Δ); *gskl-1*(Δ); *him-8* sperm activated within 10 minutes, and only 20% activated within 30 minutes (Figure 4.24). The inactivated sperm did not form any obvious spikes or protrusions (Figure 4.25). This data indicated that *gskl-1* and *gskl-2* are involved in sperm pseudopod formation and function.

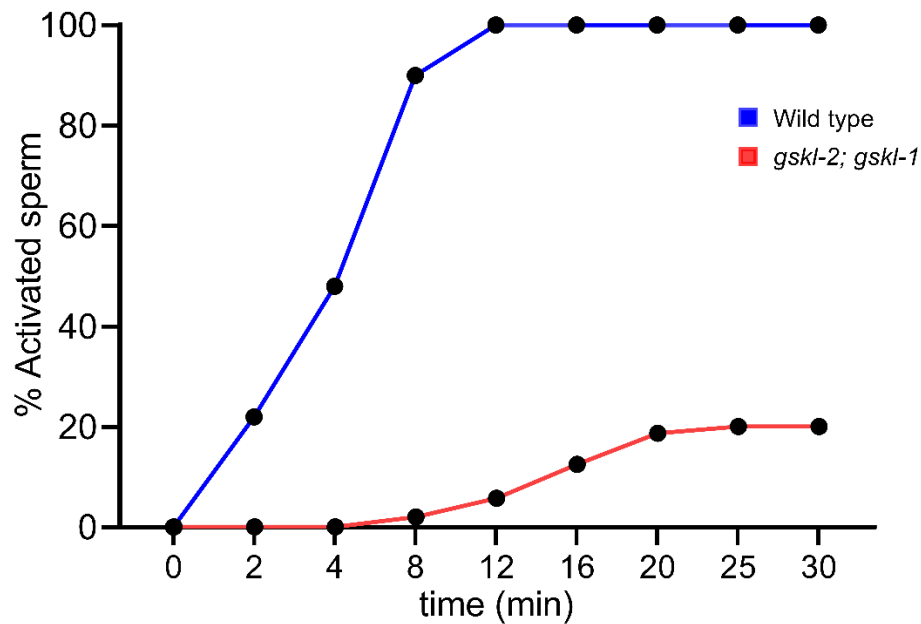
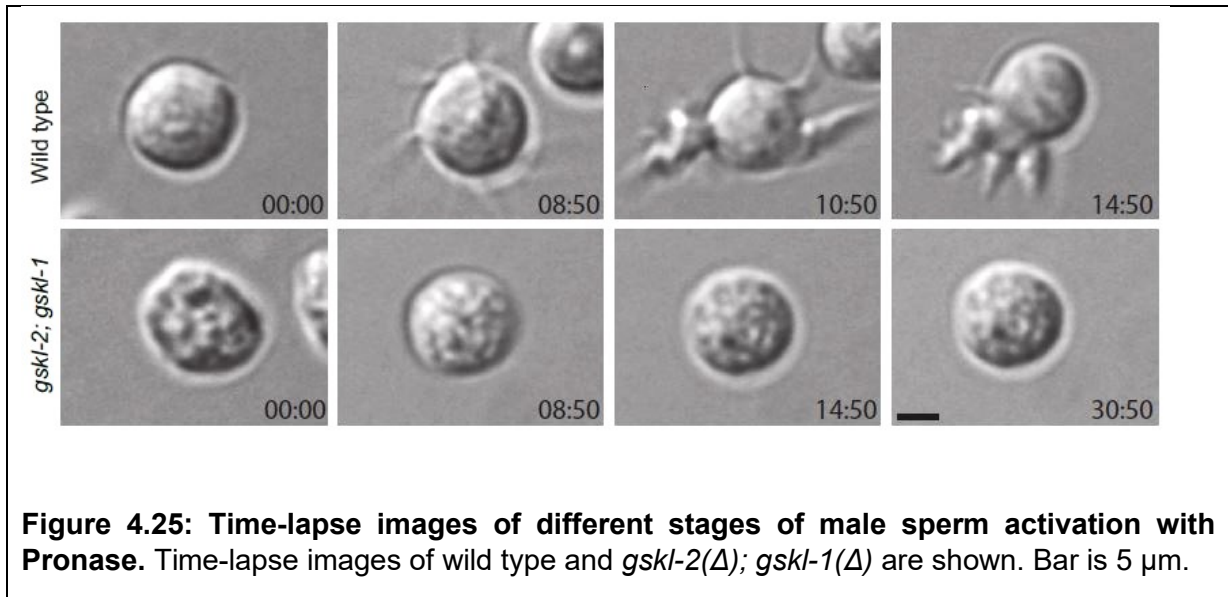


Figure 4.24: *gskl-2*(Δ); *gskl-1*(Δ) caused a delay in sperm activation. *In vitro* sperm activation with Pronase revealed that 100% wild type male sperm were fully activated within 12 minutes of treatment with Pronase (n=97) but only 2% of *gskl-2; gskl-1* male sperm were activated within 12 minutes and within 30 minutes only 20% sperm were activated (n=103).



4.11 Tagging *gskl-1* and *gskl-2* by CRISPR-cas9

In order to determine the location of the GSKL-1 protein, I used CRISPR-Cas9 methods to tag *gskl-1* with GFP. The predicted gene structure for *gskl-1* suggested that two isoforms are possible via alternative splicing. The short form does not contain the kinase domain, and likely does not encode a functional GSK-3 kinase. Although this short form could represent a regulatory component for the enzyme, I decided to tag the N-terminal portion of the long isoform, as this would allow tracking of this isoform specifically as the suppressors of *memi-1(sb41)* were located on the long isoform. To help identify successful CRISPR editing, the co-transformation mutant marker *dpy-10(cn64)* is co-injected. The presence of many F1 Dumpys or Rollers (this mutation exhibits variably dominant Rol and recessive Dpy phenotypes) indicates successful transformation. In total, 90 worms were injected, of which 70% segregated

Rollers or Dumpys in next generation (Table 4.4). As the target gene *gskl-1* and the co-crispr marker *dpy-10*, are both located on chromosome II, I performed fluorescence screening of all *Rol* and *Dpy* worms for the GFP edit. I found that out of the total 495 *Rol/Dpy* worms that were screened, 24 *Rol/Dpy* worms expressed GFP in the spermatheca region. However, all of those worms were sterile.

Experimental Set	Number of total injected worms	Number of worms yielding F1 <i>Rol/Dpy</i>	Percentage of <i>Rol/Dpy</i> in Jackpot broods
I	12	4	10 and 2 %
II	10	4	12 and 5 %
III	20	14	35 and 19 %
IV	20	18	31 and 63 %
V	28	23	37 and 40 %

Table 4.4: Summary of CRISPR injections to tag *gskl-1* with *gfp* at the 5' end.

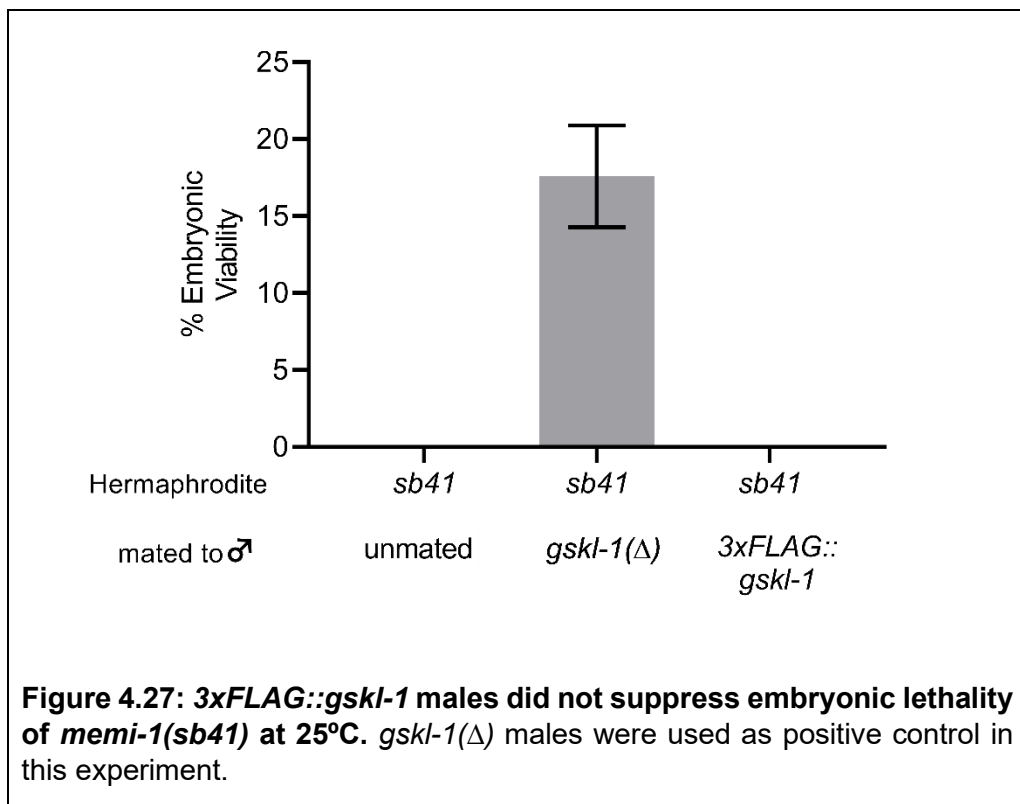
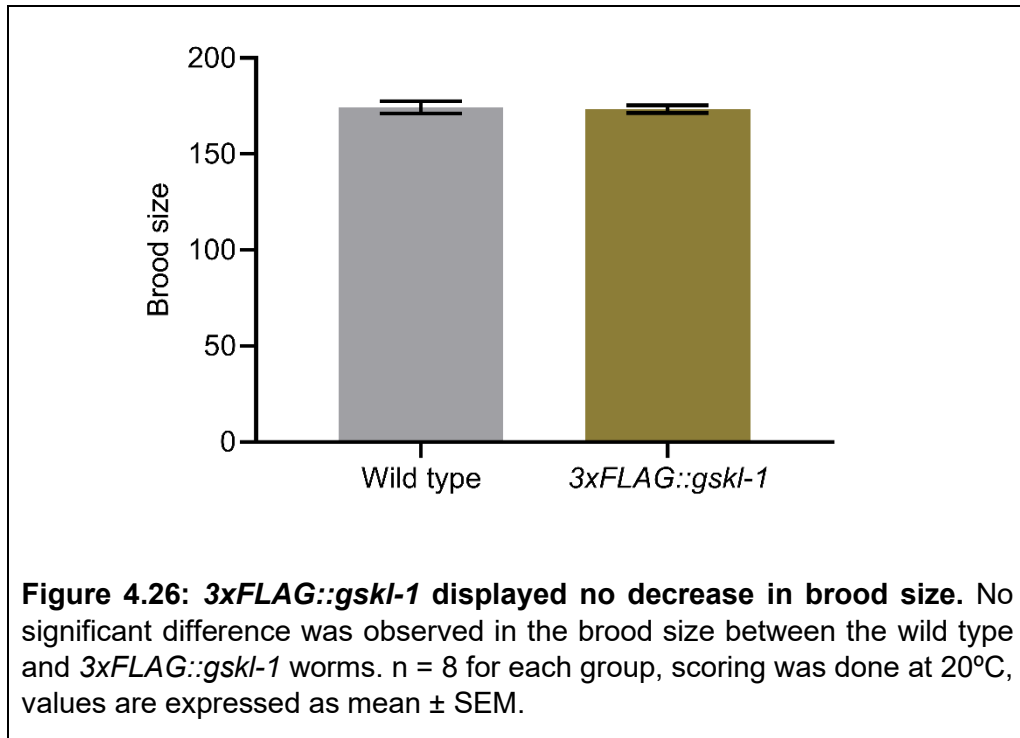
I next tried to tag *gskl-1* with 3xFLAG at 5' end. I injected a total of 57 worms, out of which 67 % worms segregated *Rol/Dpy* in the F1 generation. I screened all *Rol/Dpy* worms from jackpot broods using PCR to identify plates that had the 3xFLAG insertion. The frequency of edits were found to be highest amongst three broods that segregated the highest percentage of rollers (Table 4.5). Worms homozygous for the FLAG tag in the subsequent generation were identified by PCR, and the FLAG sequence, reading

frame, and flanking DNA was verified by DNA sequencing (MBSU, University of Alberta).

Experimental Set	Number of total injected worms	Number of worms yielding F1 Rol/Dpy	Percentage of Rol/Dpy in Jackpot broods
I	12	4	4 and 9 %
II	10	4	5 and 12 %
III	20	16	35 and 40 %
IV	15	14	50 and 61 %

Table 4.5: Summary of CRISPR injections to tag *gskl-1* with 3xFLAG at the 5' end.

Homozygous 3xFLAG-tagged *gskl-1* worms appeared healthy and did not show any embryonic lethality (Figure 4.26). However, because the suppressor mutations also did not exhibit obvious phenotypes on their own, it was important to assess whether this 3xFLAG tag disrupted the function of the *GSKL-1* gene. If the disruption indeed happened, then 3xFLAG tagged *GSKL-1* males should be able to suppress the lethality of *memi-1(sb41)* similarly to the extent that the *gskl-1* deletion male suppressed the lethality of *memi-1(sb41)*. I found that *3xFLAG::gskl-1* did not suppress *memi-1(sb41)* embryonic lethality. This data indicated that the 3xFLAG tag did not disrupt the function of *gskl-1* (Figure 4.27).



In order to determine the location of the GSKL-2 protein, I also used CRISPR-Cas9 methods to tag this gene with Ollas. The predicted gene structure for *gskl-2* suggested a single transcript is produced by this gene. Based on the results above, indicating that the N-terminal FLAG tag did not likely disrupt GSKL-1 function, the Ollas tag was also targeted to the 5' end of *gskl-2*. 13 out of a total of 15 worms that were injected segregated Rol/Dpy in F1 generation (Table 4.6). I focussed on two jackpot broods which gave the highest numbers of Roller progeny. Using PCR, I identified the Ollas insertion in the parent of the F1 Rols and, in the next generation, a homozygous strain was identified through PCR and confirmed by sequencing.

Experimental Set	Number of total injected worms	Number of worms yielding F1 Rol/Dpy	Percentage of Rol/Dpy in Jackpot broods
I	15	13	23 and 42 %

Table 4.6: Summary of CRISPR injections to tag *gskl-2* with *Ollas* at the 5' end.

Homozygous *Ollas::gskl-2* worms appeared healthy and no embryonic lethality was observed (Figure 4.28). To test whether the Ollas insertion abrogated the function of *gskl-2*, males from *Ollas::gskl-2* were mated to *memi-1(sb41)* worms at 25°C. The *Ollas::gskl-2* males did not suppress the embryonic lethality of *memi-1(sb41)* (Figure 4.29). This indicates that insertion of Ollas did not interfere with the normal function of *gskl-2*.

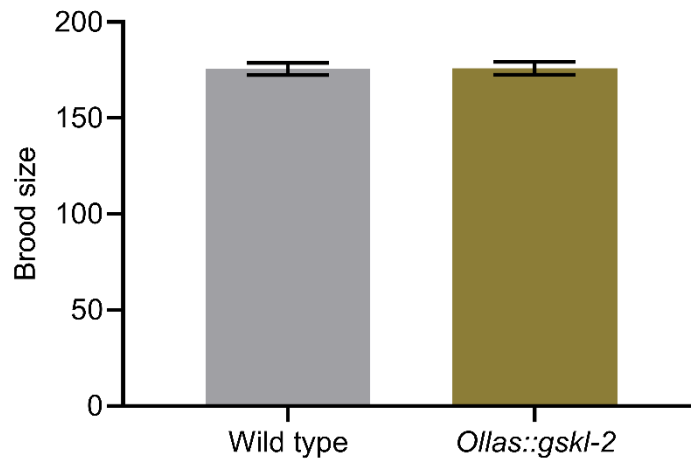


Figure 4.28: *Ollas::gskl-2* displayed no decrease in brood size. No significant difference was observed in the brood size between the wild type and *Ollas::gskl-2* worms. n = 8 for each group, scoring was done at 20°C, values are expressed as mean ± SEM.

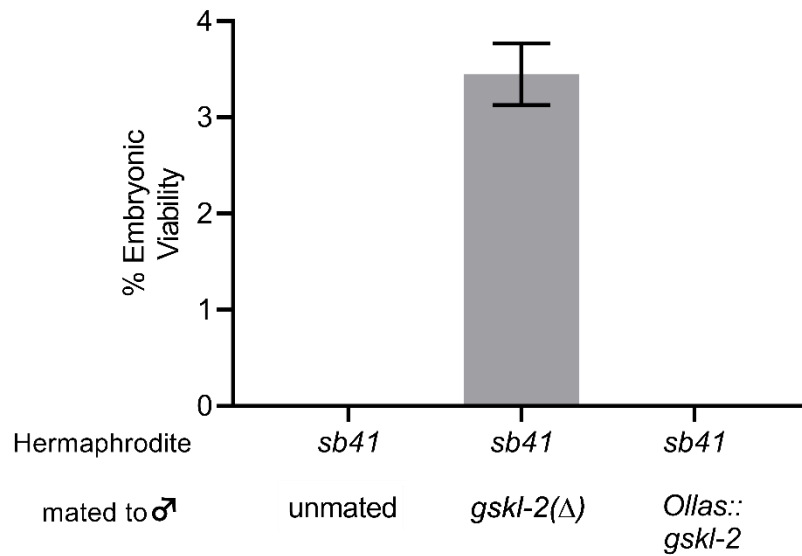
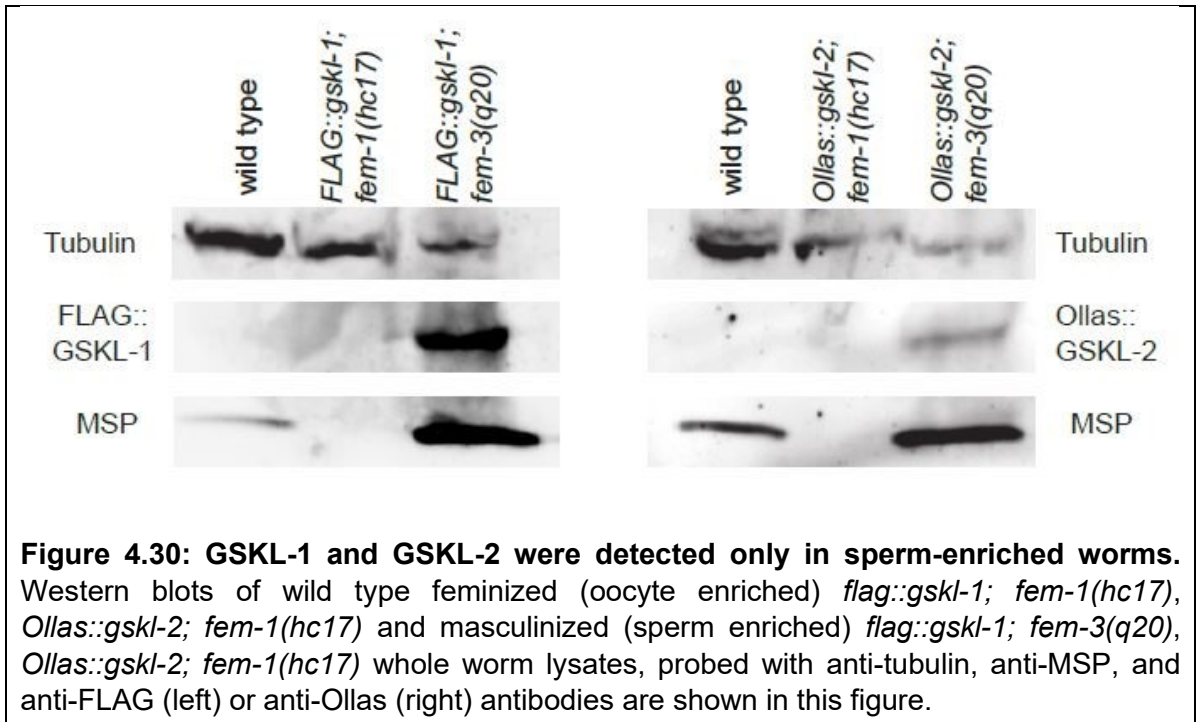


Figure 4.29: *Ollas::gskl-2* males did not suppress embryonic lethality of *memi-1(sb41)* at 25°C. *gskl-2(Δ)* males were used as positive control in this experiment. n=6 for each group.

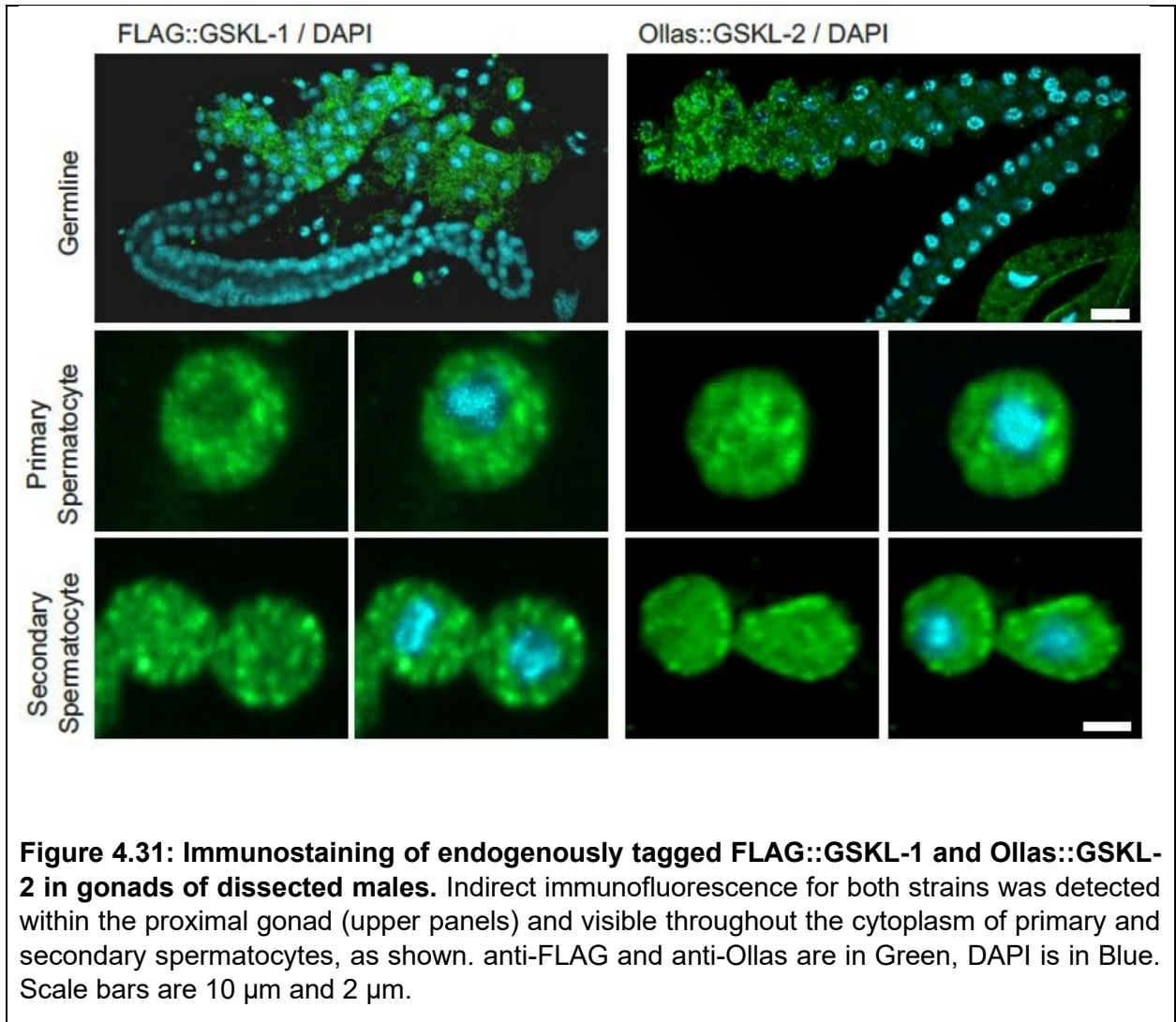
4.12 *gskl-1* and *gskl-2* are expressed only in masculinized, but not feminized, worms

The genetics experiments suggested that *gskl-1* and *gskl-2* likely have sperm functions. The tagged strains allowed a direct test of the hypothesis that these genes are expressed in the male germline of *C. elegans*. To test for sex-specific expression of GSKL-1 and GSKL-2, we used temperature-sensitive mutants that produce only sperm (*fem-3(q20gf)*) or only oocytes (*fem-1(hc17lf)*). In addition, I probed the western blot for tubulin, which is widely expressed in hermaphrodites and males, although not present in sperm. As another control, I probed for Major Sperm Protein (MSP), which is sperm-specific. Western blotting revealed that GSKL-1^{FLAG} and GSKL-2^{Ollas} were detected in sperm-only *fem-3(q20gf)* worms but not in oocyte-only *fem-1(hc17lf)* females (Figure 4.30). Both tagged proteins were not detected in wild-type hermaphrodites, although, the amount of sperm present in these worms is much lower, as shown with the decreased levels of MSP.



4.13 *gskl-1* and *gskl-2* are expressed in the male germline

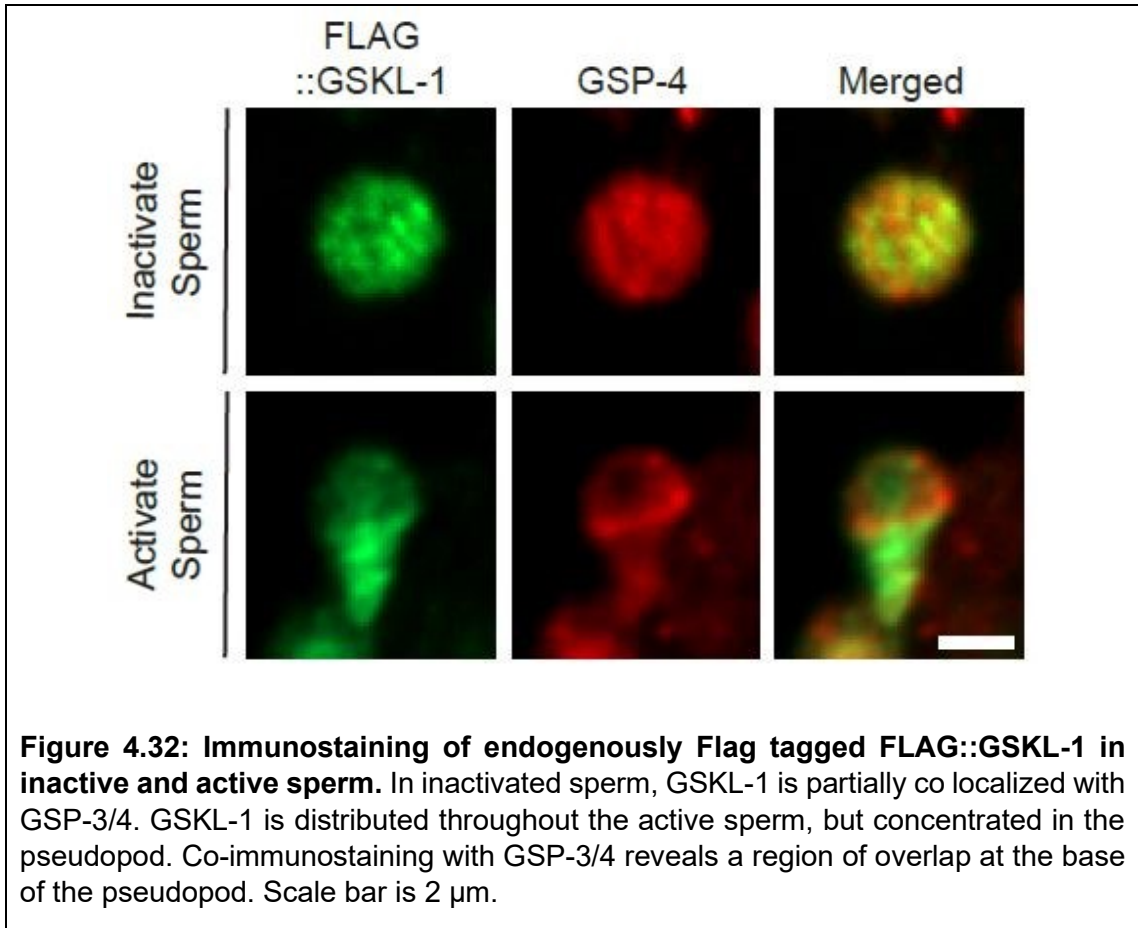
Consistent with the western blot experiments, immunostaining of endogenous GSKL-1^{FLAG} and GSKL-2^{Ollas} worms revealed strong fluorescence at multiple stages of spermatogenesis. In males, immunofluorescence was brightest in the proximal gonad, which is where spermatogenesis occurs (Figure 4.31). Immunofluorescence was also observed in the cytoplasm of primary and secondary spermatocytes, as well as spermatids (Figure 4.31). Within spermatocytes and inactive spermatids, the fluorescence appeared punctate, similar to that previously reported for GSP-3/4 (Wu et al. 2012).

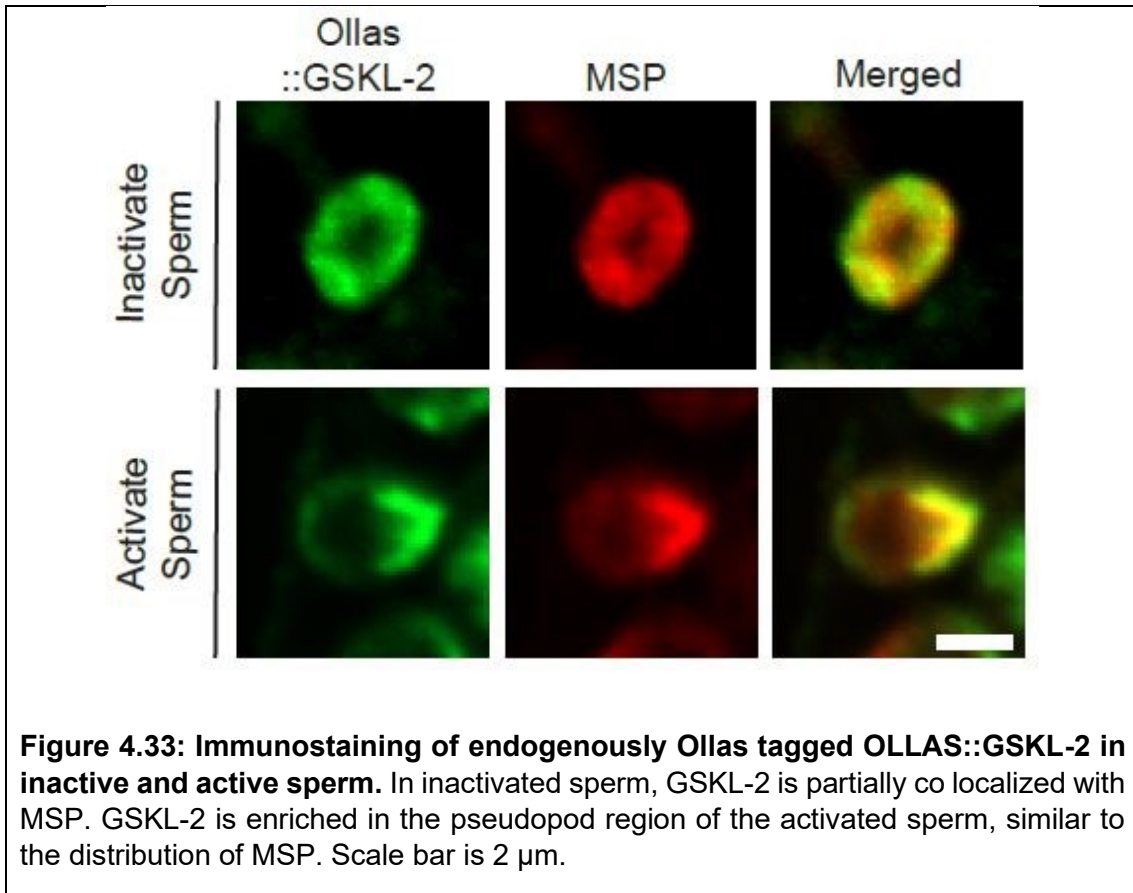


4.14 GSKL-1 and GSKL-2 localize to the pseudopod in spermatozoa

As sperm become activated to crawl, GSP-3/4 location changes from a distributed punctate pattern associated with fibrous bodies, to a restricted band at the base of the pseudopod. During this transition, MSP becomes concentrated throughout the pseudopod, overlapping with GSP-3/4 at the base (Wu et al. 2012).

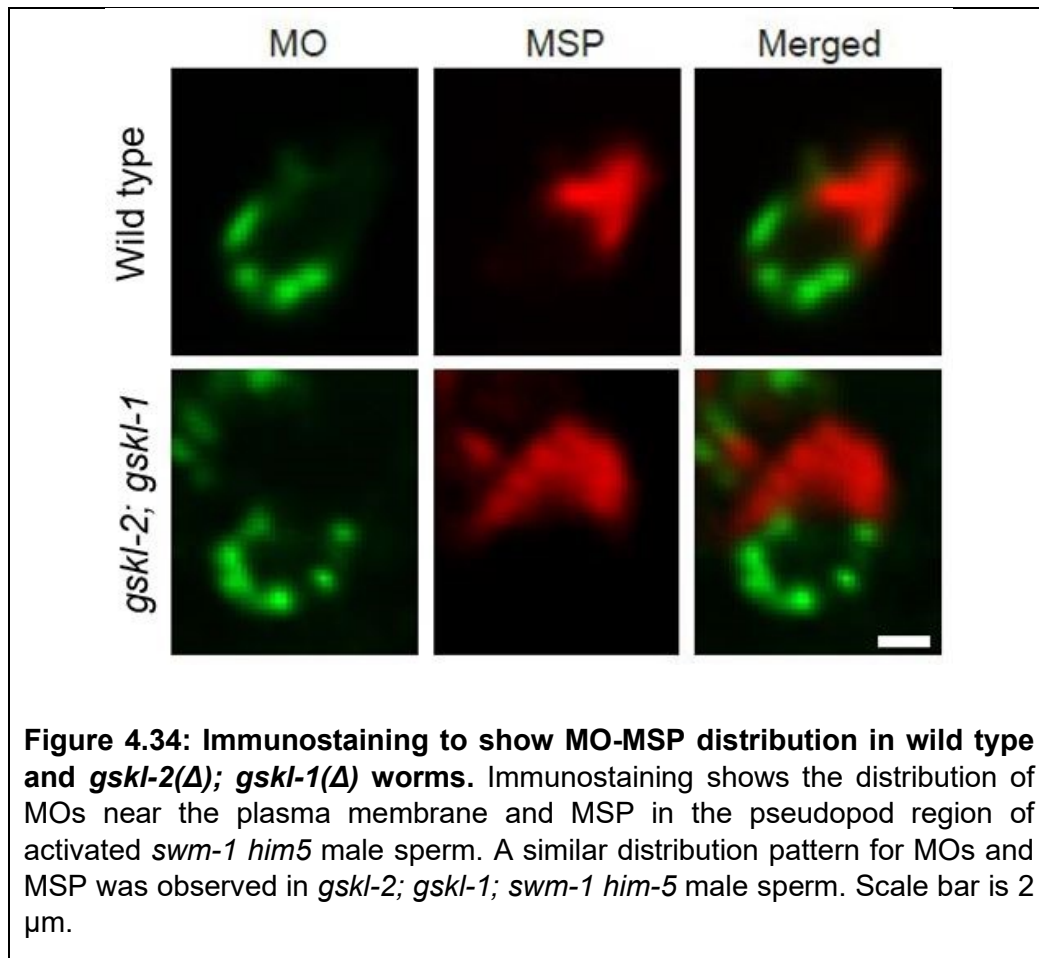
In inactive sperm from males, GSKL-1^{3XFLAG} was distributed throughout the cytoplasm, displaying a punctate pattern similar to GSP-4. However, GSP-4 only partially colocalized with GSKL-1^{3XFLAG} and, in many cases, fluorescent foci were located adjacent to GSP-4 foci (Figure 4.32). Similarly, in inactive sperm, GSKL-2^{Ollas} was distributed throughout the cytoplasm and partially colocalized with MSP (Figure 4.33). In contrast to the isotropic distribution of the tagged proteins in inactive sperm, the immunostaining revealed an asymmetric distribution for both proteins in activated sperm. In activated sperm, GSKL-2^{Ollas} and GSKL-1^{3XFLAG} immunofluorescence levels were strongest throughout the pseudopod, similar to MSP (Figure 4.32 and 4.33). Furthermore, coimmunostaining for GSP-4 revealed colocalization with GSKL-1^{3XFLAG} at the base of the pseudopod. GSKL-1^{3XFLAG} was also detected in the cell body of active sperm, whereas GSKL-2^{Ollas} was more restricted to the pseudopod. The asymmetric distribution of GSKL-1^{3XFLAG} and GSKL-2^{Ollas} in the active pseudopod is consistent with a possible role for this kinase in MSP treadmilling and sperm motility.





4.15 *gskl-1* and *gskl-2* are not required for MO-MSP distribution during sperm activation

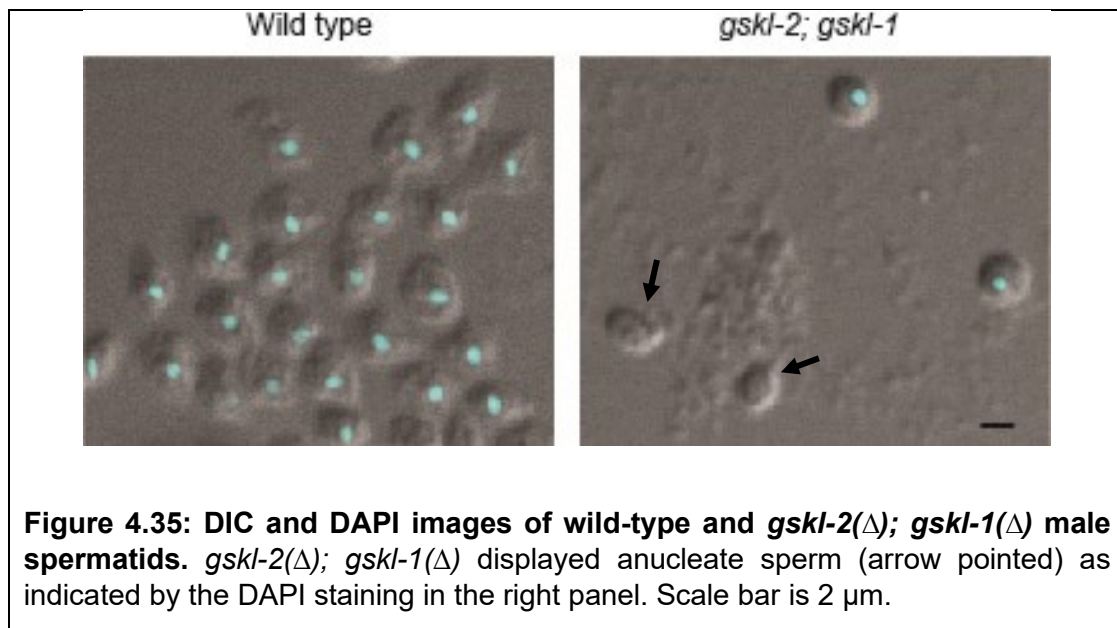
Because sperm activation also involves fusion of MOs with the membrane and a redistribution of MSP prior to pseudopod formation (Singaravelu et al. 2012), we examined these structures in inactive and active sperm (see Material and Methods). We observed a similar distribution pattern of MOs and MSP in *swm-1(me66) him-5(e1490)* male sperm and in *gskl-2(Δ); gskl-1(Δ); swm-1(me66) him-5(e1490)* male sperm (Figure 4.34). This suggested that, during sperm activation, GSKL-2 and GSKL-1 were not required for proper distribution of MOs and MSP.

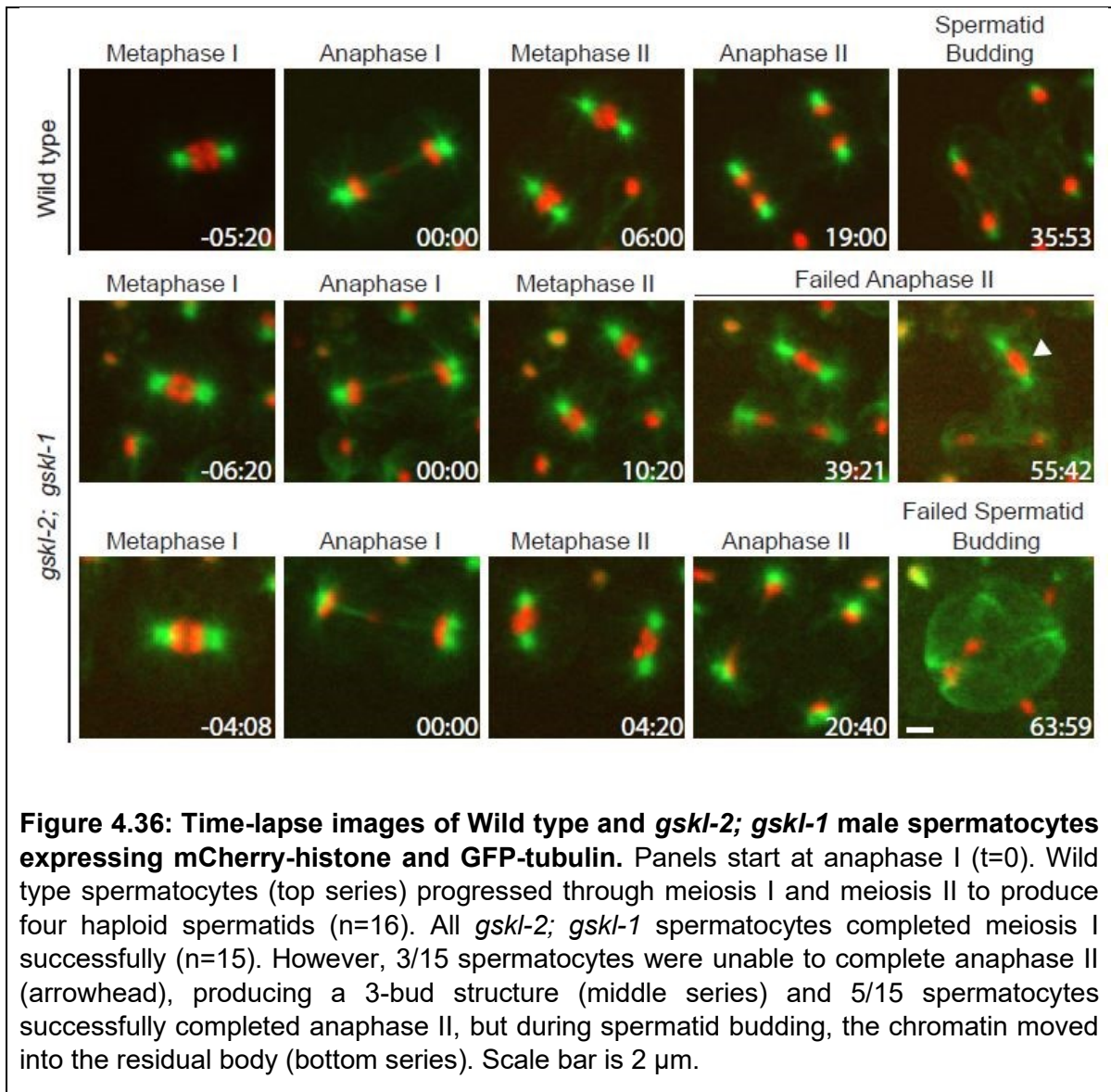


4.16 *gskl-1* and *gskl-2* are required for sister chromatid segregation and spermatid budding during male meiosis

From the above experiments, I noticed a variation in sperm size and that many sperm seemed to lack nuclei, as determined by DIC imaging (Figure 4.35). Therefore, I decided to determine the requirements of *gskl-2* and *gskl-1* in male meiosis by performing live imaging of wild-type and *gskl-2(Δ); gskl-1(Δ)* male spermatocytes

expressing GFP-tubulin (microtubules) and mCherry-histone (chromatin). In wild-type males (n=16), homologous chromosomes separated in meiosis I, and sister chromatids separated in meiosis II to generate a four-bud structure (Figure 4.36). Each bud eventually separated from the residual body to become an individual spermatid. In *gskl-2*(Δ); *gskl-1*(Δ) males (n=15), homologous chromosomes separated successfully to form secondary spermatocytes; however, one pair of sister chromatids did not separate in 3 out of 15 spermatocytes (Figure 4.36). Instead, these cells displayed an aberrant 3-bud structure that would be expected to produce one aneuploid sperm. In 12 out of 15 *gskl-2*(Δ); *gskl-1*(Δ) male spermatocytes, both homologous chromosomes and sister chromatids separated successfully to form a four-bud structure, similar to controls. However, at the time of budding, one or more sets of segregated chromosomes moved back into the residual body, resulting in the formation of an anucleate sperm (5/12; Figure 4.36). The remaining 7 out of 15 appeared as the wild-type controls.





4.17 *gskl-1* and *gskl-2* are required for female meiosis II

Because *gskl-2*(Δ); *gskl-1*(Δ) double mutants exhibited some paternal-effect embryonic lethality, we reasoned that these sperm components should also function in

the fertilized embryo. To address this, I used *gskl-2*(Δ); *gskl-1*(Δ) hermaphrodites that express GFP-tubulin (microtubules) and mCherry-histone (chromatin). Time-lapse *in utero* imaging of *gskl-2*(Δ); *gskl-1*(Δ) embryos showed that female MI spindle formation, homologous chromosome segregation, and extrusion of the first polar body were similar to wild-type fertilized embryos. However, I observed significant delays and defects in subsequent stages in a subset of mutant embryos. For example, in *gskl-2*(Δ); *gskl-1*(Δ) embryos fertilized with a nucleated sperm, 7/13 cells exhibited defects during meiosis II. Five of these samples could be timed accurately, which displayed a severe delay in the appearance of the MII spindle (17 min 52 s +/- 3.28 after anaphase I onset, as compared with 4 min 14 s +/- 0.93 in controls; $P < 0.0001$, Figure 4.37). In these cases, polar body extrusion did not occur. In all seven meiosis-defective embryos, sperm-derived centrosomal microtubules were visible even though the female meiosis II spindle persisted; normally, these microtubules do not appear prior to dissolution of the female meiotic spindle. Eventually, the MII spindle disappeared and pronuclei formed and migrated towards each other (Figure 4.38). I also observed a separate defect that occurred as the oocyte traversed the spermatheca, whereby a portion of the cell formed an oblong extension containing maternal DNA, which eventually cleaved off from the rest of the oocyte to become trapped inside the spermatheca (7/20) (Figure 4.39).

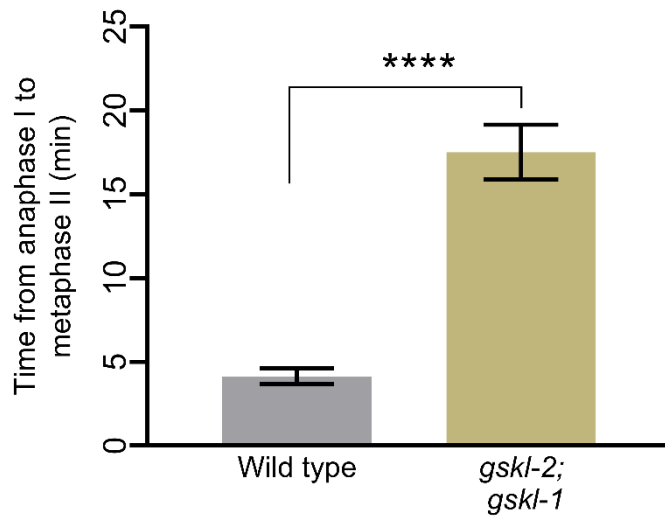
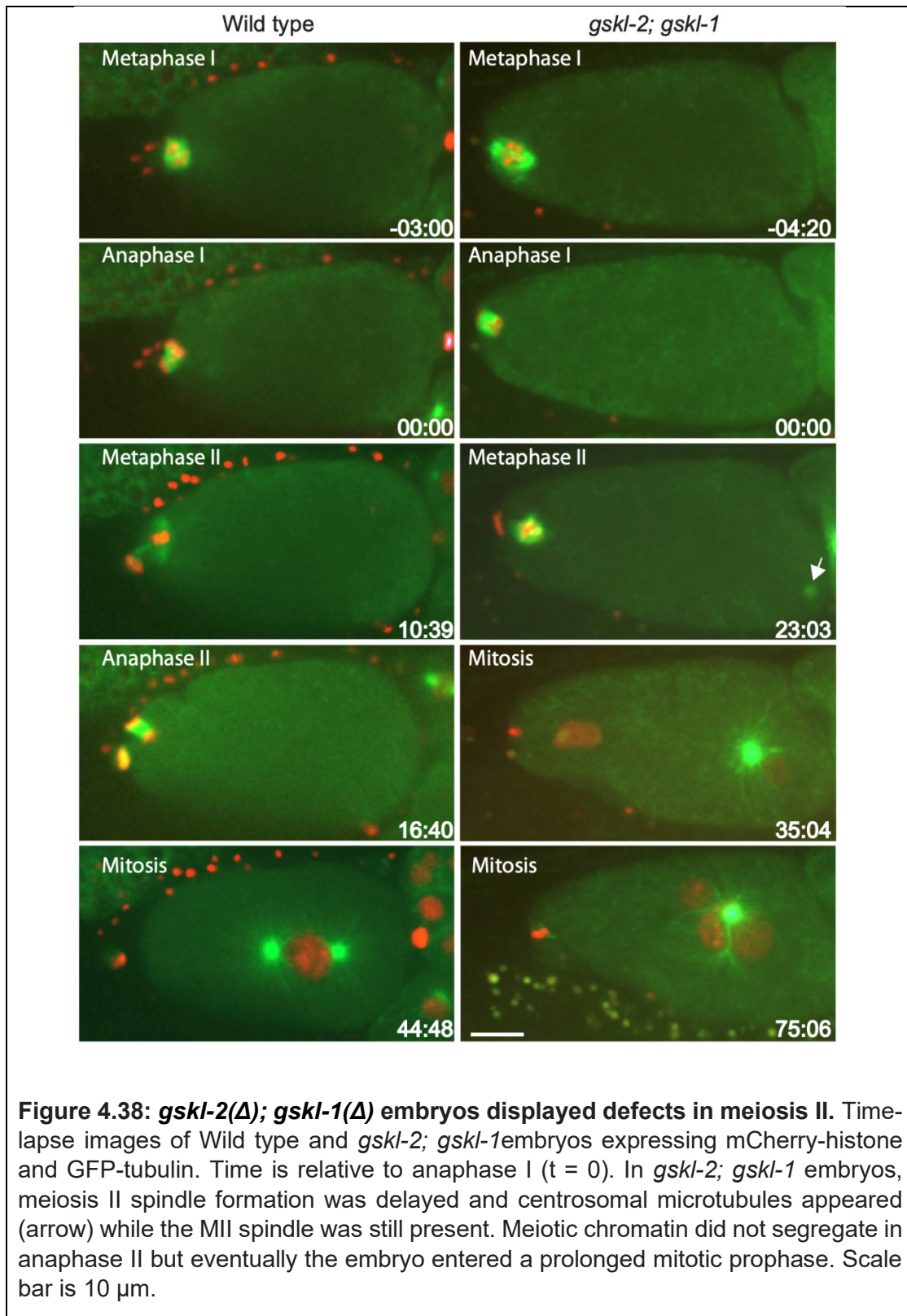


Figure 4.37: *gskl-2*(Δ); *gskl-1*(Δ) embryos exhibit a delay from the beginning of anaphase I to metaphase II. This delay is significant compared to wild type controls ($P < 0.0001$; Student's T-test), $n = 5$ for each group, error bars represent SEM.



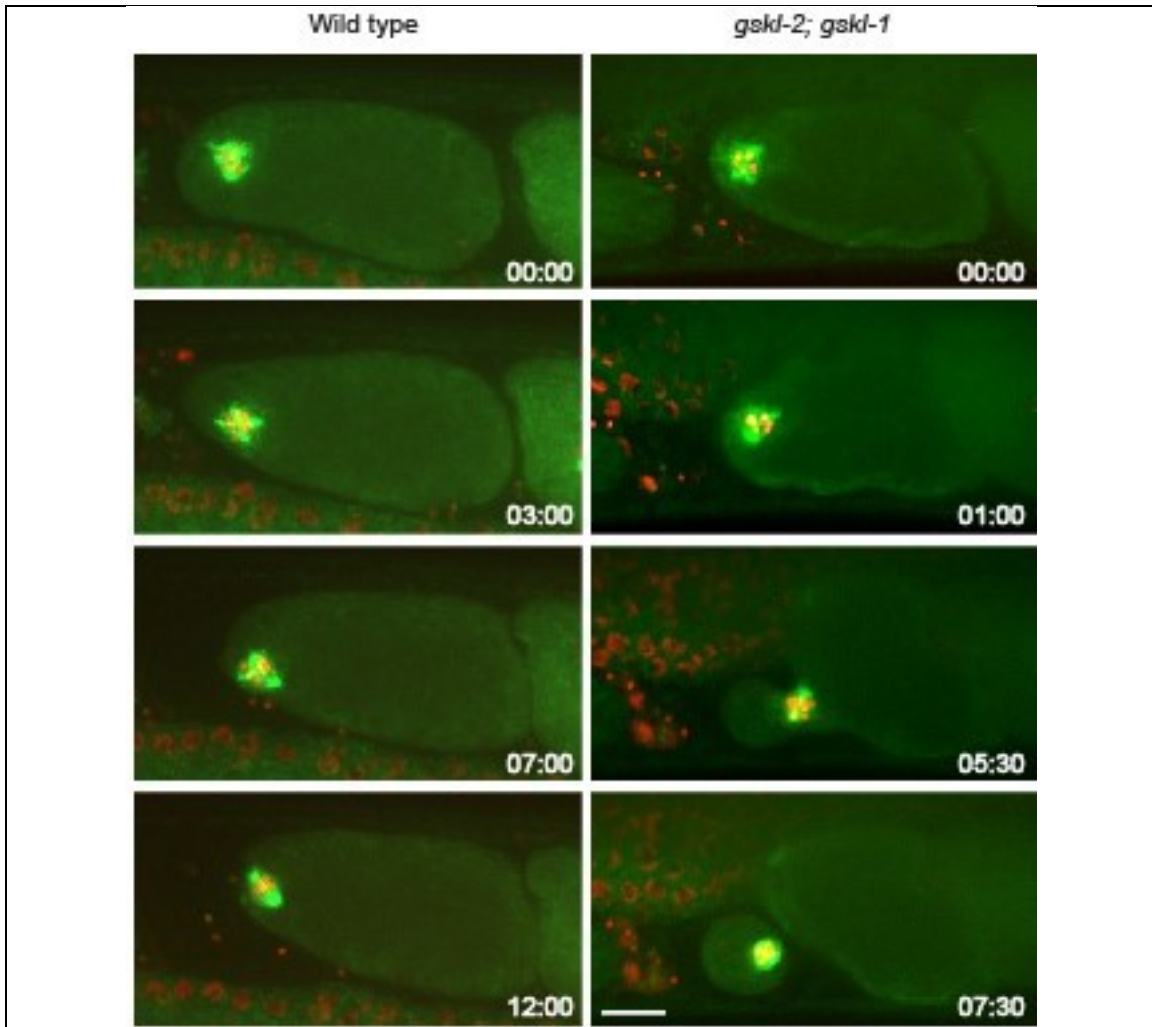
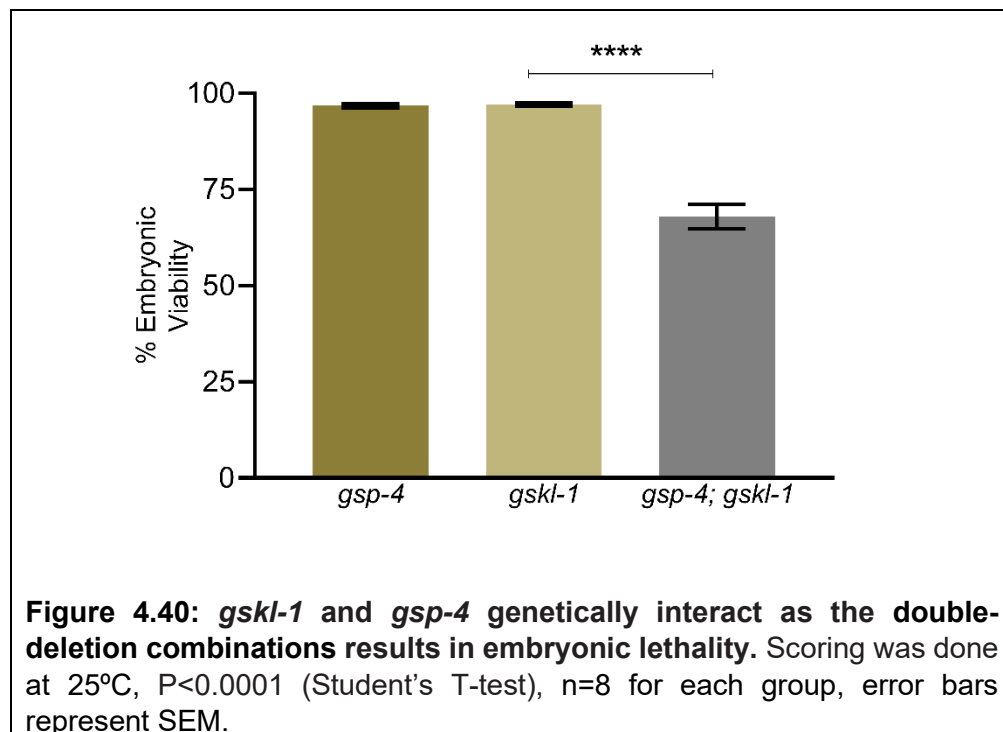


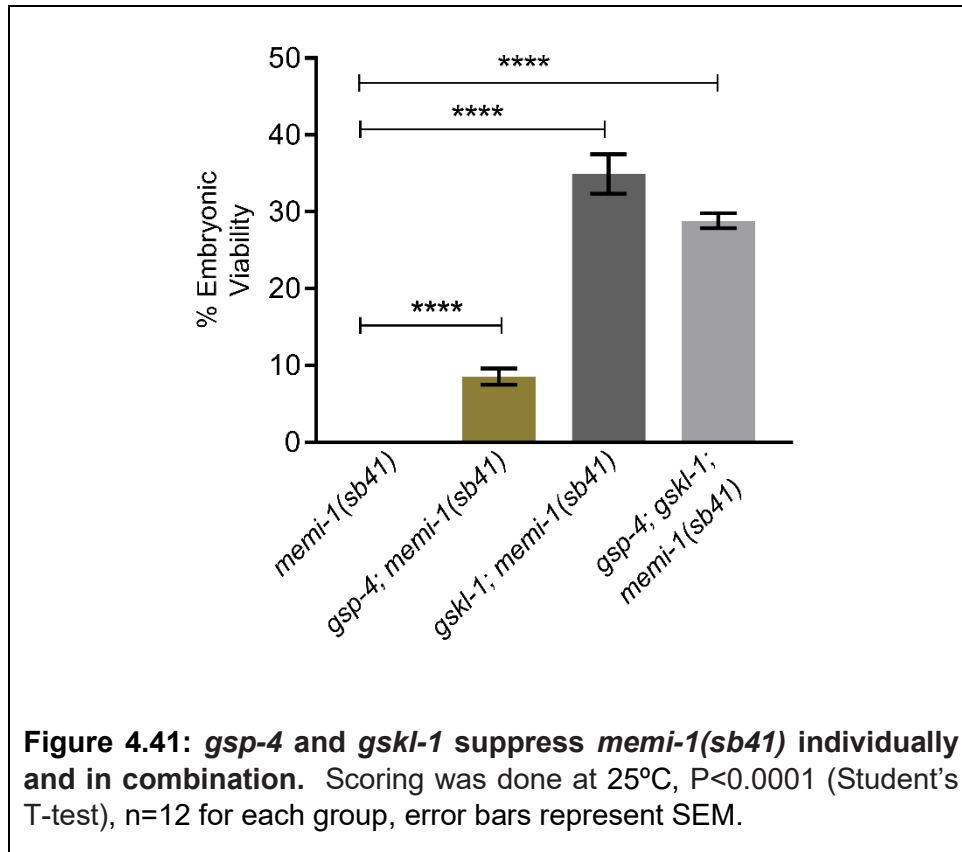
Figure 4.39: *gskl-2*(Δ); *gskl-1*(Δ) embryos displayed broken oocyte phenotypes. Time-lapse images of Wild type and *gskl-2*; *gskl-1* embryos expressing mCherry-histone and GFP-tubulin. Time is relative to entry of oocyte into the spermatheca ($t = 0$). In *gskl-2*; *gskl-1* oocyte is squeezed, and maternal chromatin gets separated from the rest of the oocyte when it tries to exit from the spermatheca. Scale bar is 10 μ m.

4.18 *gskl-1* and *gskl-2* genetically interact with *gsp-3/4* to regulate female meiosis II through the MEMI pathway

Previous work showed that reduction of both *gsp-3* and *gsp-4* (*gsp-3/4(RNAi)*) could effectively suppress *memi-1(sb41)* (Ataeian et al. 2016). The EMS genetic screen also identified *gsp-4* as one of the suppressors of *memi-1(sb41)*. I also tested *gsp-3(Δ)* and found that mutations in this gene can also suppress *memi-1(sb41)*. Data presented in this thesis showed that loss-of-function mutations in *gskl-1* or *gskl-2* can suppress *memi-1(sb41)*. In addition to all of these genes behaving in a similar way with respect to suppression of *memi-1(sb41)*, my data indicated that *gskl-1* also plays a role similar to *gsp-3/4*, with respect to sperm functions. Thus, I tested whether these two mutations enhance each other genetically. Indeed, the double-deletion strain *gsp-4(Δ); gskl-1(Δ)* exhibited 32% embryonic lethality, compared to 3% in the individual mutant strains (Figure 4.40).

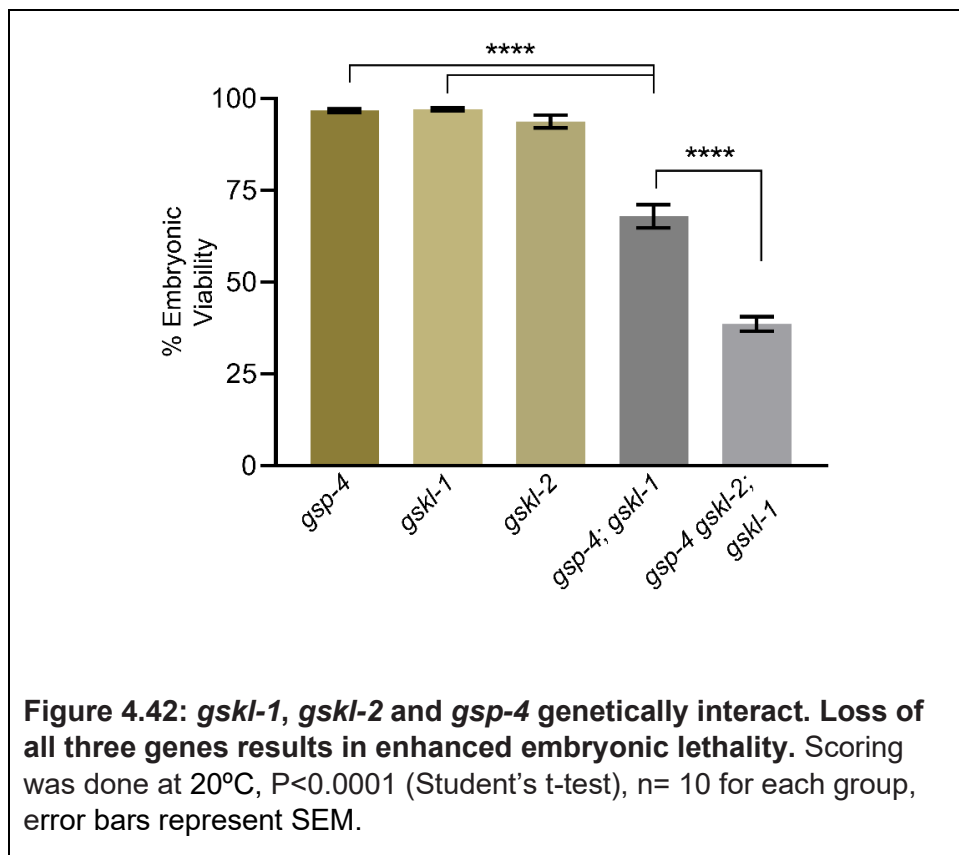


Next, I wanted to test the effect of removing *gskl-1* and *gsp-4* activity with respect to their ability to suppress *memi-1(sb41)*. For example, if the kinase and phosphatases activity oppose each other, I would predict the combination might not suppress *memi-1(sb41)*. In contrast, the combination of mutations might act synergistically and provide more suppression than expected contribution from each one individual mutation. Alternatively, the combination of these two mutations might suppress in an additive manner. *gskl-1(Δ)* and *gsp-4(Δ)* independently suppressed the maternal-effect lethality of *memi-1(sb41)* up to 34.9% and 8.5% survival, respectively, compared to 0% for *memi-1(sb41)* controls at 25°C (Figure 4.41). The *gsp-4(Δ); gskl-1(Δ); memi-1(sb41)* triple mutant exhibited 28.8% survival (Figure 4.40). However, after correcting for an expected maximum survival of only 68.9 % due to *gskl-1(Δ) gsp-4(Δ)* alone, the combination of mutations was slightly more effective at suppressing *memi-1(sb41)* than either one individually. This data is consistent with the idea that each of the GSK-3 kinases and the PP1 phosphatases contribute towards some common function, and the attenuation of this function suppresses *memi-1(sb41)*.



If *gskl-1*, *gskl-2* and *gsp-4* act within the same pathway after fertilization, it is expected that loss of these genes should cause a phenotype similar to the *memi-1/2/3(RNAi)* phenotype. We found that *gsp-4(Δ) gskl-2(Δ); gskl-1(Δ)* displayed increased embryonic lethality compared to *gskl-2(Δ); gskl-1(Δ)* (68% vs. 32% embryonic lethality; Figure 4.42). We made a strain that expressed GFP tubulin (microtubules) and mCherry-histone (chromatin) to characterize the phenotype of defective embryos *in utero*. In *gsp-4(Δ) gskl-2(Δ); GSKL-1(Δ)* embryos, 11 out of 22 embryos displayed defects during the completion of female meiosis. Four of these embryos exhibited a skipped-MII phenotype, characteristic of *memi* loss-of-function (Figure 4.43). Seven out of 11 defective embryos progressed through metaphase I but

did not complete anaphase I or release the first polar body, and they exhibited delays in forming the meiosis II spindle. These embryos were unable to progress through anaphase II and the maternal DNA formed multiple maternal nuclei. Centrosomal microtubules appeared before dissolution of the MII spindle and pronuclear migration initiated soon after the MII spindle disappeared (Figure 4.43). In addition, in 3/25 cases, the oocyte fragmented as it moved through the spermatheca, resulting in a small chromatin-containing cell that blebbed off from the oocyte, a phenotype that was also observed in the double mutant mentioned previously.



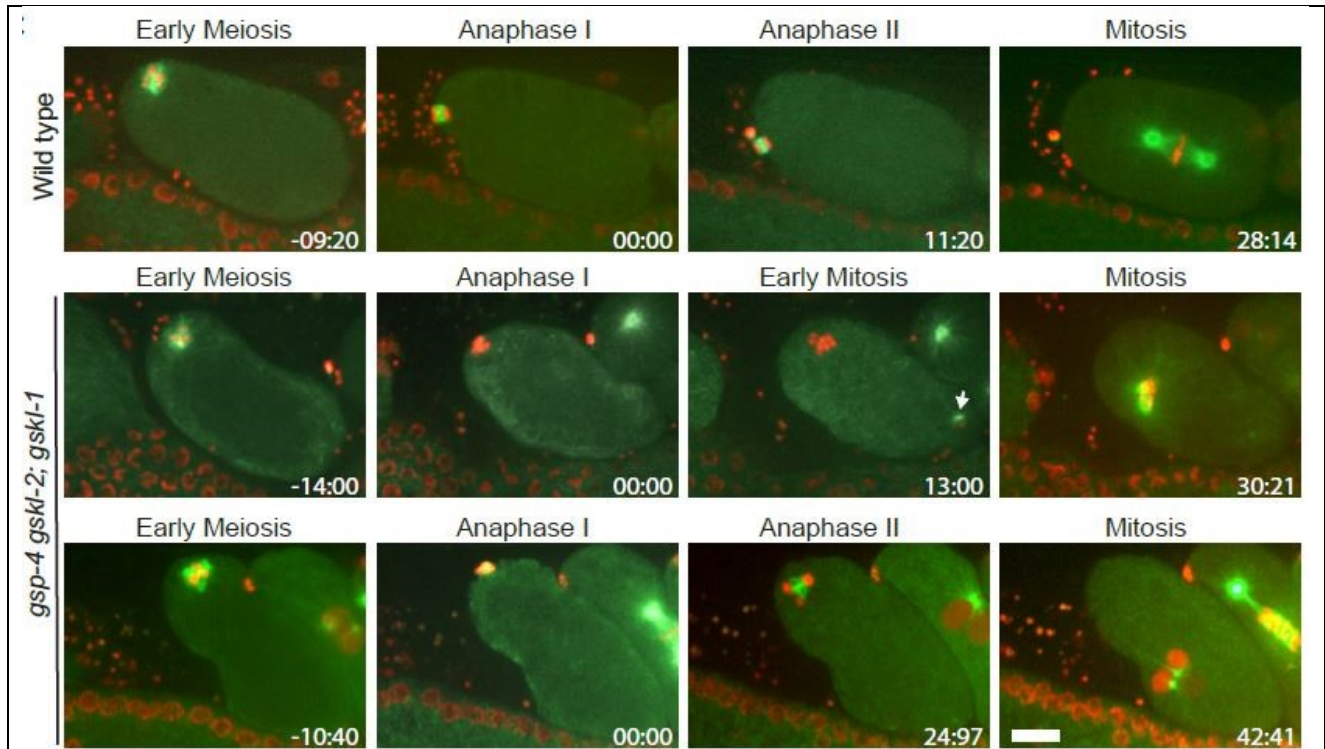


Figure 4.43: *gsp-4 gskl-2; gskl-1* embryos displayed meiotic defects. Time-lapse images of wild type (top panels) and *gsp-4 gskl-2; gskl-1* embryos expressing mCherry-histone and GFP-tubulin. The middle panel shows an example of a *gsp-4 gskl-2; gskl-1* embryo with a skipped-Meiosis II phenotype (4/22). Centrosomal microtubules are visible (arrow), the nuclear envelope does not form around meiotic chromatin, and an abnormal mitotic spindle forms. The bottom panel shows an example of a *gsp-4 gskl-2; gskl-1* embryo that did not extrude the first polar body, was delayed in meiosis II spindle formation, and did not complete anaphase II (7/22). Scale bar 10 μ m.

4.19 Summary

The identification of two paternally contributed GSK-3 family members required for early embryonic events is a major step to understand the molecular mechanism of the sperm-oocyte interactions required for development. This work has shown that sperm-specific GSKL-1/GSKL-2 play roles in sperm meiotic chromosome segregation, sperm motility, and after fertilization they involve in regulating female meiosis II through the *mei* pathway. This work has also shown that GSKL-1/GSKL-2 and GSP-3/4 work together in the same pathway and do not work counter to one another, as one could posit from that fact that these are kinases and phosphatases.

5. Discussion

5.1 Sperm-specific suppressors of *memi-1(sb41)*

The MEMI-1,2,3 proteins are exclusively maternal and functionally redundant. The MEMIs are required for the proper completion of female meiosis II and the transition to subsequent mitosis. For example, the loss of all *memi* paralogs via *memi-1/2/3(RNAi)* results in a skipped-meiosis II phenotype and abnormal mitotic cell division. Fertilization of the oocyte during female meiosis I is also required for these events, and loss of either MEMI function or an absence of fertilization result in similar phenotypes, indicating the involvement of the MEMI proteins in this post-fertilization signal. Although the MEMIs are essential for female meiosis II, the proteins must be degraded prior to mitosis, and this degradation is dependent on CUL-2 E3 ubiquitin ligase activity. The hypermorphic, gain-of-function *memi-1(sb41)* mutation interferes with the degradation of MEMI-1, and its persistence in mitosis is likely responsible for the gain-of-function mitotic phenotype (Ataeian et al. 2016).

The *memi-1(sb41)* mutation has proven to be useful for genetic screens that identify components of the post-fertilization signal for regulating female meiosis II. The rationale behind these approaches is based on the idea that the *sb41* mutation results in persistent or inappropriate MEMI activity into mitosis. Therefore, a loss or reduction of function in any gene required for MEMI activity could suppress the embryonic lethality characteristic of this mutation. These types of suppressors would behave as genetic activators of the MEMI pathway, and, thus, such suppressors would be good candidates for a sperm-specific component of the fertilization signal. Alternatively,

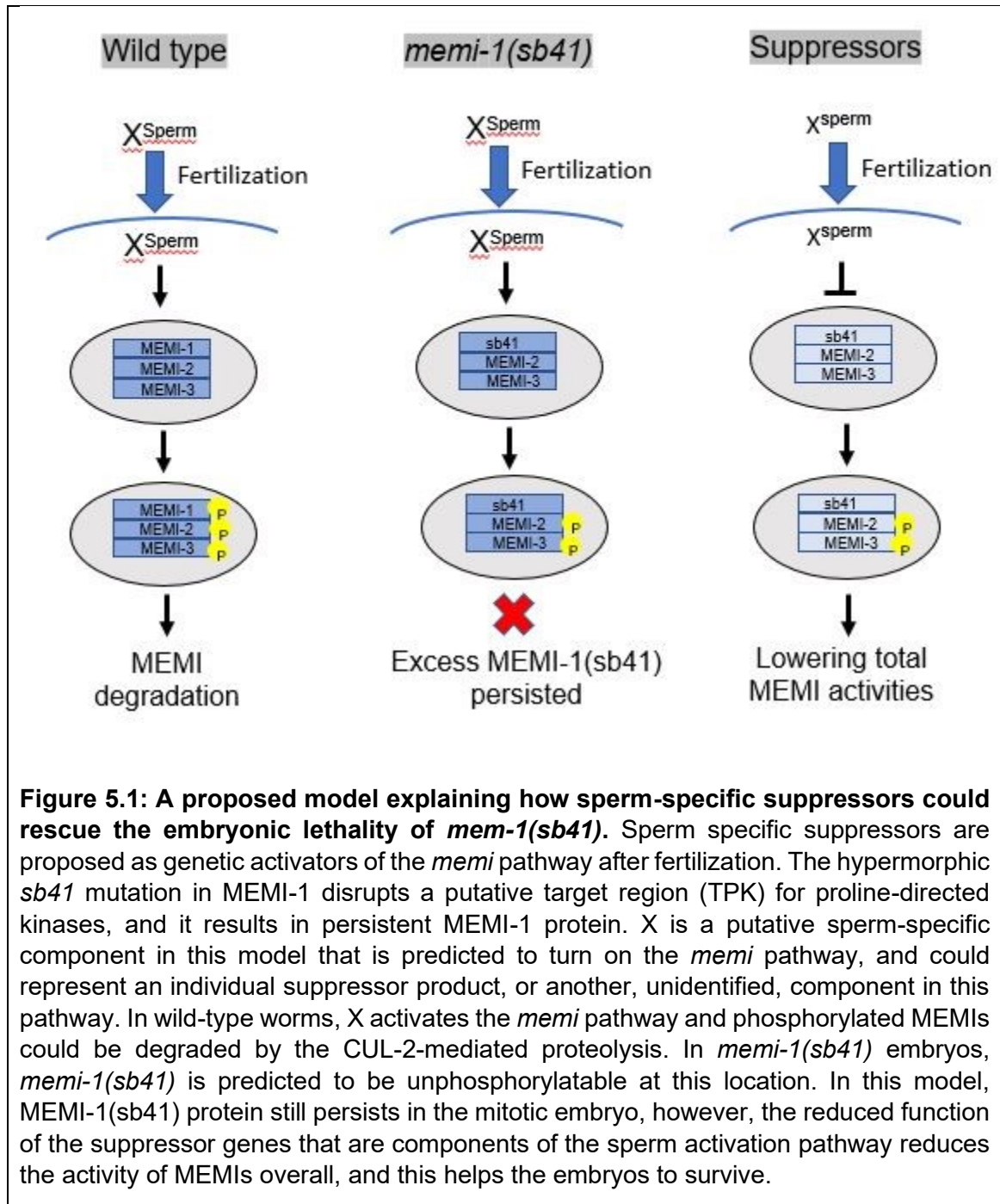
bypass suppressors that open an alternative degradation pathway could also suppress by removing the otherwise persistent MEMI-1(*sb41*) protein. Interestingly, these screens and subsequent analyses have so far identified five genes that encode sperm-specific components. These genes are *gsp-3* and *gsp-4* (PP1 phosphatases), *gskl-1* and *gskl-2* (GSK-3 kinases) and *smz-1* (a relatively uncharacterized PDZ domain-containing protein that has been shown to have a role in sperm meiosis Chu et al. 2006). Another putative suppressor, *frm-8*, also encodes a PDZ domain-containing protein. Although this gene has not been characterized, my experiments showed that *frm-8*(Δ) males suppressed *memi-1*(*sb41*) hermaphrodites after mating, suggesting that it could also encode a sperm-specific component. In addition to these sperm factors, one suppressor identified by genetic screening, and confirmed with CRISPR mutagenesis, is a maternal-specific component, *mbk-2*, which encodes mini-brain kinase.

The *memi-1*(*sb41*) mutation results in a P74S substitution that is within a target region of proline-directed kinases, such as cyclin-dependent kinase, MAPK, and GSK-3. The functionally redundant genes *memi-2* and *memi-3* also have the same putative phosphorylation site. This disruption in the proline-directed phosphorylation site might protect MEMI-1(*sb41*) from the E3 ubiquitin ligase. Persistent MEMI-1(*sb41*) protein would be expected to represent an unphosphorylated protein with respect to this site, however, there is no evidence that the P74S change in *sb41* causes any alteration in phosphorylation or protein structure. In the future, mass spectrometry could be used to show whether MEMIs are phosphorylated during the meiosis-to-mitosis transition or not. This, in turn, would help reveal the molecular mechanism of the *memi* pathway.

Suppression by the *gsp-3*(Δ), *gsp-4*(Δ), *gskl-1*(Δ), *gskl-2*(Δ), *smz-1*(Δ) and *frm-8*(Δ) males is consistent with the idea that sperm entry is required for the suppression (Ataeian et al. 2016). In the case of sperm-specific components acting as suppressors of *memi-1*(*sb41*), one possible mechanism is that they could normally be required to activate *memis* after fertilization. If this activation were reduced, then the effect of MEMI-1(*sb41*) protein persistence might be reduced, allowing some embryos to survive without changing the protein levels *per se* (Figure 5.1). Future experiments could involve examining MEMI protein levels in each of the suppressor strains, to rule out other mechanisms, for example, increased degradation rates. In addition, the interaction of identified sperm components with MEMI after fertilization needs to be done in future. Previously it was shown that anti-MEMI antibodies co-immunoprecipitated GSP-3/4, but anti-GSP-3/4 antibodies were unable to co-immunoprecipitate MEMI proteins (Ataeian et al. 2016).

In addition to the sperm-specific suppressors identified, at least one suppressor, *mbk-2*(*abc56*) could be acting as a bypass suppressor, within the fertilized one-cell cytoplasm. The maternal component MBK-2 is required to degrade different proteins during oocyte-to-embryo transition. A loss-of-function allele of *mbk-2* was previously reported to enhance maternal-effect lethality of *mei-1*, which is required for female meiotic spindle assembly during oocyte-to-embryo transition (Quintin et al. 2003). But initial data found that *mbk-2*(*abc56*) did not enhance *mei-1* embryonic lethality (Ish Jain *pers. comm.*). This data suggests that *mbk-2*(*abc56*) might not be a loss-of-function allele. In that case, *mbk-2*(*abc56*) somehow increases the activity of

mbk-2 and that increased activity of *mbk-2* may be involved in degrading *memi-1(sb41)*.



5.2 Summary of sperm phenotypes associated with loss of *gskl-1* and *gskl-2*

The screen for genetic suppressors of *memi-1(sb41)* revealed a number of genes that could participate in the post-fertilization pathway that specifies the female meiosis II cell division program. In this study, I focused on the characterization of *gskl-1*. *gskl-1* is one of seven *C. elegans* genes that encode members of the GSK-3 family of kinases. Complete loss of *gskl-1* did not cause observable phenotypes, however, by testing pairwise double-deletion combinations, I found that *gskl-1* was functionally redundant with another member of the GSK-3 family, *gskl-2*. Thus, the double deletion strain allowed a characterization of phenotypes that occur as a result of loss of GSK-3 function. Importantly, my work revealed functions for these GSK-3 genes that was previously masked by previous single-gene knock-out approaches. Specifically, I observed a number of phenotypes related to spermatogenesis and sperm motility (Table 5.1) as well as variably penetrant embryonic lethality (Table 5.2).

Sperm defects displayed by <i>gskl-2</i> (Δ); <i>gskl-1</i> (Δ) male		
Genotype \ Characteristics	Wild type	<i>gskl-2</i> (Δ); <i>gskl-1</i> (Δ)
Completed Meiosis I	Yes	Yes
Metaphse II	Yes	Yes
Sister chromatid segregation during Anaphase II	Yes	3/15 defective
Spermatid budding	Yes	5/15 defective
Pseudopod Treadmilling rates	19.6 \pm 2.4 μ m/min	8.8 \pm 2.5 μ m/min
<i>in vitro</i> sperm activation	100% within 12 minutes	20% within 30 minutes

Table 5.1: summary of phenotypes displayed by *gskl-2*(Δ); *gskl-1*(Δ) male sperm.

Embryonic defects displayed by *gskl-2*(Δ); *gskl-1*(Δ)

Genotype	Wild type	<i>gskl-2</i> (Δ); <i>gskl-1</i> (Δ)
Characteristics		
Exit from Spermatheca	Yes	7/20 displayed broken oocyte
Protrude 1 st polar body	Yes	Yes
Meiosis II spindle appear after anaphase I	4 min 14 s (avg)	17 min 52 s (avg)
Anaphase II segregation	Yes	7/13 defective (no segregation)
Protrude 2 nd polar body	Yes	No
Pronuclear migration	Yes	Yes

Table 5.2: Summary of the phenotypes displayed by *gskl-2*(Δ); *gskl-1*(Δ) embryos.

5.3 *gskl-1* and *gskl-2* expression are specific to the male germline

Immunostaining of FLAG-GSKL-1 and Ollas-GSKI-2 revealed strong fluorescence signals in the spermatogenesis zone of the male germline. I also found strong expression of these tagged GSKL-1/GSKI-2 proteins in primary spermatocytes, secondary spermatocytes and in male spermatids. In the activated male sperm, GSKL-1 was distributed in the cytoplasm of the cell body and more concentrated in the pseudopod region while GSKL-2 was located within the pseudopod only. I also observed fluorescence in the sperm of adult hermaphrodites, but no fluorescence signal was detected in the maternal germline of adult hermaphrodites. Hermaphrodites produce sperm during the L4 stage and then they switch to produce oocytes only. Therefore, in order to conclusively determine whether GSKL-1/GSKL-2 expression was restricted to the male germline, I used a feminized mutant, *fem-1(hc17)*, which results in worms that produce only oocytes, and a masculinized mutant, *fem-3(q20)*, which results in worms that produce only sperm. Western blot analysis showed that Flag tagged GSKL-1 and Ollas tagged GSKL-2 are expressed in sperm-only worms and absent in oocyte-only worms. Together, immunostaining and western blot results confirmed that GSKL-1/GSKL-2 are sperm-specific components. This is also aligned with the genetic observation that *gskl-2(Δ); gskl-1(Δ)* displayed paternal-effect embryonic lethal phenotype.

5.4 The role of *gskl-1* and *gskl-2* in sperm meiosis

In the wild-type worms, primary spermatocytes undergo the first meiotic cell division (MI) to separate homologous chromosomes, followed by a second meiotic cell division (MII) to separate sister chromatids and form four haploid spermatids (Chu and Shakes 2013). At the end of MII, the four spermatids detach from the residual body, a specialized compartment that stores the cytoplasmic contents that are not needed for fertilization or sperm function. Work presented in this thesis revealed that *gskl-1*(Δ) *gskl-2*(Δ) mutants exhibited defects during the MII phase of spermatogenesis. Specifically, 3 out of 15 spermatocytes displayed defects in sister chromatid segregation during anaphase II, in one half of the secondary spermatocyte sister chromatid were separated but in the other half it was not. Although 5/15 spermatocytes completed anaphase II successfully, the segregated chromatin came back to the residual body during spermatid budding.

Morphogenesis of the fibrous body -membranous organelle (FB-MO) complexes and proper assembly of MSP into the FBs during *C. elegans* spermatogenesis is key to making functional sperm. Assembly of MSP into FBs has been proposed to be a necessary conformational change to prevent MSP from interfering with chromosome segregation during the meiotic divisions (Price et al. 2021) and to facilitate proper segregation of MSP into mature spermatids (Nishimura and L'Hernault 2010). For example, tubulin is required for chromosome segregation during spermatogenesis, but this cytoskeletal protein is removed from the sperm during the final stages of MII.

The regulation of MSP during spermatogenesis involves two key SPE proteins. One intrinsically disordered protein, SPE-18, is required to form FBs on the membrane of MOs during the late pachytene stage of MI, and the casein-kinase, SPE-6, is required at later stages for the proper assembly of MSP into the FBs (Price et al. 2021). Many *spe* genes are also involved in regulating FB-MO morphogenesis and MSP distribution. Spermatocytes from *spe-39* mutants also arrest without forming proper residual bodies. In these *spe-39* mutants, clear MO structures were absent in spermatocytes; instead, several small vesicles were present (Zhu and L'Hernault 2003). A role for SPE-4 in residual body function was also revealed by examining various *spe-4* mutants, which exhibited arrested spermatocytes that did not form a proper residual body. Furthermore, in all these *spe-4* mutants, tubulin was abnormally distributed on the plasma membrane (Arduengo et al. 1998). Tubulin missegregation during MII was also observed in *spe-5* mutants, which arrest during spermatogenesis with four haploid nuclei (Machaca and L'Hernault 1997). Due to the mislocalization of actin filaments and the ER, loss of *spe-26* resulted in spermatogenesis arrest at MII, producing almost no functional spermatids (Varkey et al. 1995). Loss of functional *spe-15* resulted in improper segregation of mitochondria, FB-MOs and cytoskeletal proteins in budding spermatids; however, sister chromatids segregated successfully (L'Hernault et al. 1988; Kelleher et al. 2000). In wild type, ribosomes are always deposited into residual bodies (RBs) but in *spe-17* mutants, ribosomes were detected in the MOs and these mutants produced no functional spermatids (Shakes and Ward 1989b).

Paternal-effect lethal mutations may be defined as male-specific mutations that affect the development of offspring. *top-2*, *emb-27* and *emb-30* are the three genes

reported till date that show paternal-effect lethal phenotype and also show defects in chromosome segregation during spermatogenesis. *top-2* encodes the topoisomerase II that has 52% amino acid sequence identity with human topoisomerase II α . The role of *top-2* in chromosome segregation during embryonic mitosis was previously reported (Bembenek et al. 2013). Also, *top-2* induces DNA damage that occurs during the onset of zygotic genome activation in the primordial germ cells of embryos (Butuči et al. 2015). Recent studies revealed that a loss-of-function allele, *top-2(it7)* displayed paternal-effect embryonic lethality due to a failure to segregate DNA properly during sperm meiosis (Jaramillo-Lambert et al. 2016). In *top-2(it7)*, spermatocytes failed to separate homologous chromosome in anaphase I and, without forming any secondary spermatid structure, these cells enter the spermatid budding stage. The anaphase-promoting complex encoding *emb-27* and *emb-30* were originally isolated as maternal-effect lethal mutants (Cassada et al. 1981; Denich et al. 1984). Later, it was confirmed that both are responsible for paternal-effect embryonic lethality (Sadler and Shakes 2000). In *emb-27(g48)* mutants spermatocytes arrest at metaphase I (Jaramillo-Lambert et al. 2016).

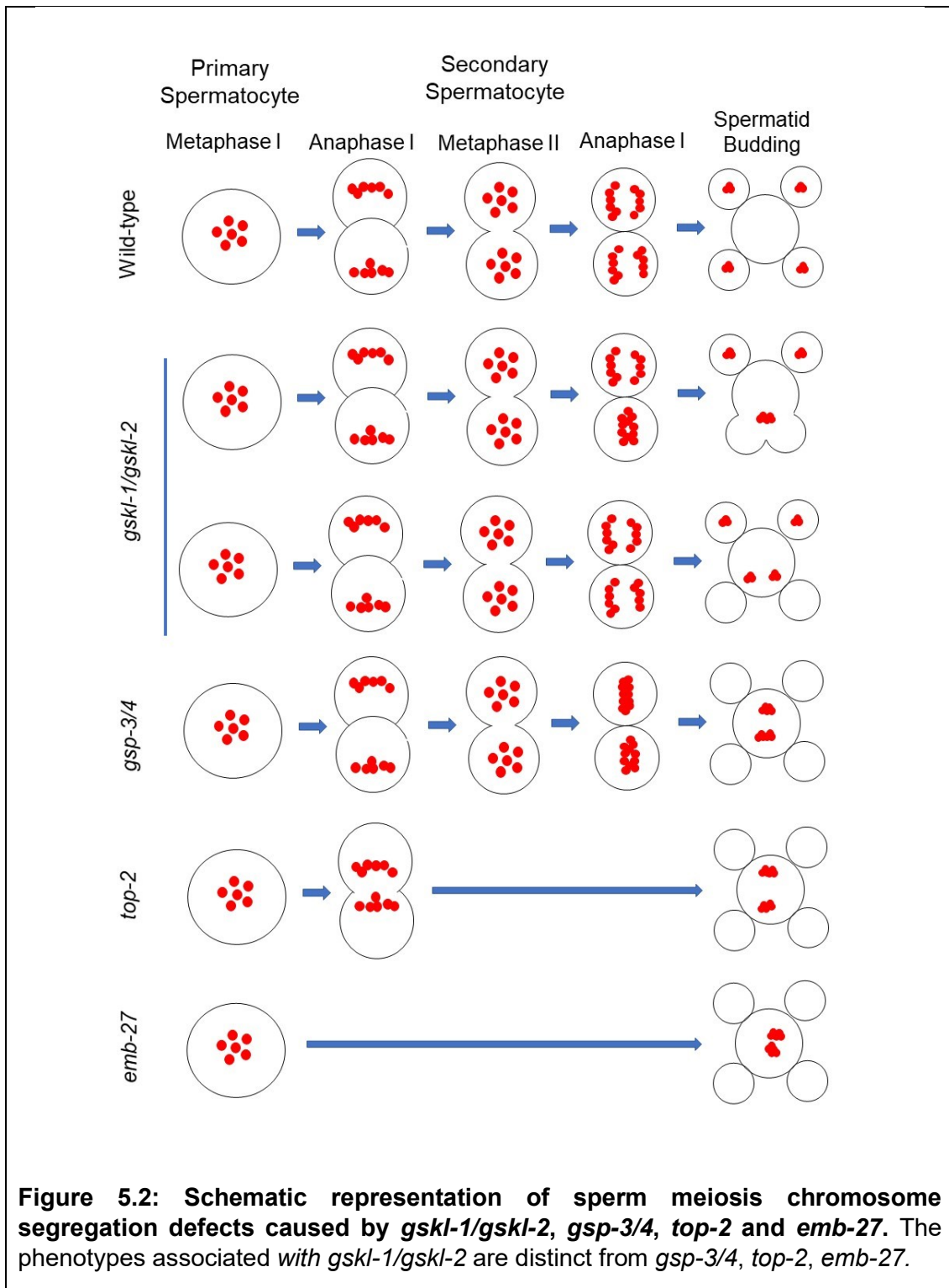
The *gskl-2(Δ); gskl-1(Δ)* mutants also exhibited defects during spermatogenesis, however, these defects were distinct from the phenotypes observed in the above mentioned paternal-effect lethal genes (Figure 5.2). First, there was no misregulation in of tubulin during spermatogenesis observed. Surprisingly, chromatin comes back to the residual body during the budding process. Also, some of the spermatocytes failed to segregate sister chromatids in only one of the two secondary spermatocyte pairs, indicating that this defect did not induce a general cell-cycle arrest. The sister chromatid

segregation defects associated with the *gskl-2*(Δ); *gskl-1*(Δ) are also distinct from the phenotypes associated with the loss of sperm-specific PP1 phosphatases *gsp-3/4* (Figure 5.2). In *gsp-3/4* mutants, spermatocytes successfully completed anaphase I and progressed to metaphase II; but, the sister chromatids failed to segregate properly at the end of anaphase II, leading to the formation of anucleate or aneuploid sperm (Wu et al. 2012).

The observed phenotypes associated with loss of GSKL-1/GSKI-2 could be due to changes in MSP. It has been suggested that MSP must be sequestered or inactivated during male meiotic cell divisions in order to prevent this sperm cytoskeletal polymer from interfering with microtubule- and actin-related functions that are, in turn, required for meiosis and spermatid budding (Varkey et al. 1993; Price et al. 2021). Therefore, the chromosome segregation and spermatocyte budding phenotypes might be related to dysregulation of MSP at these stages.

In mouse and rat, GSK-3B is expressed in type B spermatogonia and preleptotene spermatocytes, suggesting that vertebrate counterparts also play a significant role in spermatogenesis (Guo et al. 2003; Bhattacharjee et al. 2015). The precise role of vertebrate GSK-3 in spermatogenesis is still unclear. In *C. elegans*, LAB-1 preserves meiotic sister chromatid cohesion by restricting the localization of the *C. elegans* Aurora B kinase, AIR-2, during MI and MII (Tzur et al. 2012). LAB-1 locates between sister chromatids in MI, but disappears in MII, to allow sister chromatid release. Future experiments could assess the localization pattern of LAB-1 and AIR-2 in the *gskl-2*(Δ); *gskl-1*(Δ) spermatocytes. If loss of GSK-3 activity prevents LAB-1 degradation, this

would provide a molecular explanation for the lack of sister chromatid release in the spermatocytes.



5.5 The role of *gskl-1* and *gskl-2* in MSP treadmilling in activated sperm

The data presented in this thesis showed that loss of *gskl-1* and *gskl-2* affects male sperm migration. After mating, all wild-type male sperm normally reach the spermatheca within a few hours, however, mating the *gskl-2*(Δ); *gskl-1*(Δ) males indicated that many sperm do not reach the spermatheca after 12 hours. This result indicated that the mutant male sperm could have defects in guidance or motility. Further *in vitro* analysis revealed that pseudopod treadmilling rates within active sperm were significantly lower in *gskl-2*(Δ); *gskl-1*(Δ) male sperm. In a separate assay that uses a non-specific protease, Pronase to remove an inhibitory signal, 100% of wild-type spermatids became activated to crawl within 12 minutes of application. However, only 20% *gskl-2*(Δ); *gskl-1*(Δ) male sperm were activated within 30 minutes after *in vitro* Pronase treatment. All of these results indicated that the mutant spermatids were inefficient at transitioning into active crawling sperm, and that those sperm that did become active, exhibited slower pseudopod treadmilling dynamics, which is directly correlated with crawling velocity (Wu et al. 2012). Therefore, these cellular phenotypes provide an explanation for why mated male sperm are inefficient in making their way to the hermaphrodite spermatheca.

Current models for sperm activation and motility in the *Ascaris* nematode involve assembly of MSP fibres at the leading edge of the pseudopod and disassembly at the base. Because MSP filaments lack polarity (Bullock et al. 1998; Baker et al. 2002), accessory proteins are required to facilitate unidirectional growth. At the leading edge, membrane-bound MPOP (MSP polymerization organizing protein), recruits a serine/threonine kinase MPAK (MSP polymerization-activating kinase) to

phosphorylate MFP-2 (MSP fibre protein) at a threonine residue (LeClaire et al. 2003; Yi et al. 2007). Upon its phosphorylation, MFP2 associates with the MSP fibre (Yi et al. 2007). Although the mechanism is not clear, MFP2 could promote fibre polymerization by facilitating the addition of MSP subunits to the ends of filaments (Roberts and Stewart 2012). Another accessory protein, MFP-3, is important for stabilizing MSP fibres, with PP2A-induced dephosphorylation at the base of the pseudopod resulting in MFP3 release and fibre disassembly (Yi et al. 2009). Finally, MFP1 seems to be a negative regulator of assembly, whereby excess MFP1 reduces the rate of fiber elongation and inhibition of MFP1 increases polymerization rate (Buttery et al. 2003). MFP1 contains sequences similar to the MSP-fold and, thus, could co-polymerize with fibres to interfere with their elongation (Roberts and Stewart 2012).

The data from *Ascaris* indicate that phosphorylation and dephosphorylation of accessory proteins is likely key to involve *in vivo* regulation of MSP fibre dynamics. The *Ascaris* proteins seem to have homologs in *C. elegans*, and it was shown recently that *C. elegans* MFP1 and MFP2 co-localize with MSP in the pseudopod (Morrison et al. 2021). However, it is still unclear whether any of the accessory proteins play a direct role in *C. elegans* sperm motility.

The phenotypes associated with *gskl-2*(Δ); *gskl-1*(Δ) double mutants, and the subcellular location of GSKL-1/GSKL-2 in the sperm pseudopod raises the possibility that these kinases could regulate MSP dynamics. Although the targets of GSK-3 are unknown, a few MSP fibre components contain putative GSK-3 target sites. For example, the MSP monomer itself contains a consensus sequence Ser/Thr-X-X-X-Ser/Thr, where the first Ser/Thr is a target and the last Ser/Thr is a site for priming

phosphorylation (ter Haar et al. 2001). In other examples, priming is not absolutely required for GSK-3-dependent phosphorylation but it can greatly increase the efficiency of GSK-3 action (Thomas et al. 1999). Interestingly, X-ray crystallography of MSP-142 revealed that the GSK-3 consensus is within a conserved region required for MSP assembly *in vitro* (Baker et al. 2002; del Castillo-Olivares and Smith 2008). Therefore, GSKL-1/GSKL-2 could directly regulate MSP during pseudopod treadmilling. Alternatively, GSKL-1/GSKL-2 could act on accessory proteins to regulate MSP dynamics. For example, the accessory protein MFP-2 (encoded by *nsph-2* and *nsph-3.2*) also contains putative GSK-3 target sites. In this case, GSKL-1/GSKL-2 could act similarly to the serine/threonine kinase MPAK in *Ascaris*, to promote MSP assembly at the leading edge of the pseudopod.

To date, the PP1 phosphatases GSP-3/4 represent good candidate enzymes to regulate MSP dynamics and treadmilling in the *C. elegans* sperm pseudopod (Wu et al. 2012). It is tempting to speculate that the GSK-3 kinases and PP1 phosphatases could have opposite effects with respect to the assembly and disassembly of MSP fibres, similar to the *Ascaris* situation involving MPAK and PP2A, respectively. However, data presented here indicated that reduction of function of either enzyme type resulted in similar phenotypes. One simple explanation for this observation is that MSP dynamics requires a precise balance of assembly and disassembly, and any shift in this equilibrium disrupts the entire process. Another idea is that, in addition to acting on MSP and/or accessory proteins, the kinases and phosphatases could also depend on each other for their activity. In other systems, GSK-3s engage in complex regulatory networks that involve PP1 and/or PP2A phosphatases, or their respective regulatory

subunits. For example, bovine PP2A and PP1 activity in immature sperm has been correlated with increased activity of GSK-3 (Vijayaraghavan et al. 1996). GSK-3 can also phosphorylate inhibitor 2, a PP1 regulatory subunit (Lin et al. 2003), and this phosphorylation enhances PP1 catalytic activity in the motile caudal sperm in mice (Goswami et al. 2018). Although we have not identified a regulatory subunit for GSP-3/4, it is possible that a similar form of regulation occurs in *C. elegans* sperm. Alternatively, GSP-3/4 phosphatases could be a direct target of GSKL-1/GSKL-2 kinases, or *vice versa*. Having this type of interdependent regulation could allow more precise spatial regulation of MSP dynamics within the relatively small pseudopod region.

5.6 Testing *gskl-1* and *gskl-2* for their role in the *spe-8* pathway

There are five genes in the *spe-8* pathway, namely, *spe-8*, *spe-12*, *spe-19*, *spe-27* and *spe-29* which are involved in hermaphrodite specific sperm functions (Shakes and Ward 1989a; Minniti et al. 1996; Nance et al. 1999; Nance et al. 2000; Geldziler et al. 2005). Hermaphrodite sperm with a mutation in any of these mentioned genes are unable to activate, and are immotile. As a result, hermaphrodites are self-sterile. However, the hermaphrodite spermatids become active after being mated to either wild-type males or even mutated males from the *spe-8* class. Interestingly, the *spe-8* class of mutant spermatids from both males and hermaphrodites were unable to form proper pseudopods when treated with Pronase *in vitro*. This data indicated that there are two different pathways for sperm activation. Hermaphrodites sperm activation depends on the *spe-8* pathway, while male sperm activation does not. In order to

identify suppressors of *spe-27* hermaphrodite-specific sterility defects, a suppressor screen was conducted; interestingly, *spe-6(hc163)* was found as a suppressor out of that screen. The loss-of-function allele *spe-6(hc163)* not only suppressed *spe-27* but also suppressed all other genes in the *spe-8* pathway. Thus, these results indicated that the *spe-8* pathway likely functions to inhibit SPE-6 activity, and prevent sperm activation in hermaphrodites, but not males. In my experiments, I observed that the *gskl-2(Δ); gskl-1(Δ)* males produced 91% viable progeny when mated to *fog-2* females, which was higher than the viability of *gskl-2(Δ); gskl-1(Δ)* hermaphrodites (91% vs., 56% embryonic viability, and Figure 4.17). This raised the possibility that GSK-3 could be part of the *spe-8* pathway, therefore, I tested the possibility that *spe-6(hc163)* would also suppress the *gskl-2(Δ); gskl-1(Δ)* mutant embryonic viability. As *spe-6(hc163)* did not suppress the embryonic lethality of *gskl-2(Δ); gskl-1(Δ)*, I concluded that the *gskl-1/gskl-2* genes were likely not part of the *spe-8* pathway, although this experiment does not rule out the possibility that these genes act downstream of the pathway.

5.7 A possible role for *gskl-1/gskl-2* during oocyte progression through the spermatheca

In every sexually reproducing organism, the oocyte arrests at late prophase I and, before fertilization, it needs to exit this dormant state. The transition from this dormant phase to metaphase I of the oocyte is known as oocyte meiotic maturation. In *C. elegans*, the sperm sends an MSP-based diffusible signal to activate the oocyte (Miller et al. 2001). The mature oocyte is then pushed through the distal valve, into the spermatheca where it is fertilized by the sperm. Typically within two minutes, the

fertilized oocyte is pushed through the spermathecal-uterine valve, into the uterus (Kimble and Hirsh 1979; McCarter et al. 1999). During the normal progression of unfertilized oocytes through the spermatheca to the uterus, the spermatheca undergoes a series of repetitive contraction-relaxation cycles. An actin binding protein, FLN-1 activates IP3-dependent calcium signaling as soon as the oocyte enters the spermatheca (Kovacevic and Cram 2013). This in turn activates the NMY-1 (non muscle myosin I) that triggers the constriction of spermatheca to propel the embryo through the spermathecal-uterine valve. So, the maintenance of cytoplasmic Ca^{2+} might be the key for the Ca^{2+} -mediated response to the mechanical stimuli during the progression of oocyte through the spermatheca.

Upon imaging *gskl-2*(Δ); *gskl-1*(Δ) I noticed that some oocyte fragmented revealed that small cellular fragments blebbed off from the oocyte as it transitioned through the spermatheca. This defect could result from some dysregulation of contractility within the spermathecal sheath.

Calcium signalling throughout the body is dependent on calcium-selective cation channels, namely, store-operated calcium channels (SOCs). Depletion of ER Ca^{2+} leads to the activation of SOCs to refill the stores. This pathway is widely known as Store-operated Ca^{2+} entry (SOCE) (Venkatachalam et al. 2002). One of the most characterized calcium channels in the SOCE pathways is the Ca^{2+} release-activated Ca^{2+} channel (CRAC) (Parekh and Penner 1997; Parekh and Putney 2005). In *Drosophila*, *stim1* and *orai1* were identified as essential components of the CRAC channel through two separate genome-wide RNAi screen (Roos et al. 2005; Feske et al. 2006). It is well established from many works that human homologues of *stim1* and

orai1 also work as essential components of CRAC channels (Liou et al. 2005; Zhang et al. 2005; Prakriya et al. 2006; Yeromin et al. 2006). Interestingly, homologues of *stim1* and *orai1* in *C. elegans*, *stim-1* and *orai-1* are involved in regulating spermatheca contractility during the fertilization process; RNAi mediated knockdown of *stem-1* and *orai-1* in *C. elegans* is predicted to disrupt the IP3 mediated disruption of spermatheca contractility that reduced the brood size significantly (Lorin-Nebel et al. 2007).

The identification of PIEZO1 and PIEZO2 as mechano-sensitive ion channels that respond to Ca²⁺-mediated mechanical stimuli has drawn the attention of biologists to study the role of PIEZO channels in different biological processes (Coste et al. 2010; Coste et al. 2012; Alper 2017; Murthy et al. 2017; Wu et al. 2017). PIEZO1 forms a mono trimeric complex at the plasma membrane, which acts as an ion channel, which, in turn, responds to Ca²⁺-mediated mechanical stimuli, including shearing stress, static pressure and membrane stretch (Poole et al. 2014; Ranade et al. 2014; Del Marmol et al. 2018) and the function of PIEZO2 is to act as a mechano-transducer for light, touch, proprioception and breathing (Woo et al. 2014; Woo et al. 2015; Nonomura et al. 2017). *pezo-1* is the only *PIEZO* orthologue present in *C. elegans*. This receptor acts in a pathway that is parallel to *orai-1* to replenish the cell with extracellular Ca²⁺ when the cytosolic Ca²⁺ levels become low (Bai et al. 2020). As the loss of *pezo-1* displayed broken oocyte phenotype, similar to loss of effect with *gskl-1/gskl-2*, it could be possible that all these genes work in a complex network to regulate Ca²⁺ signalling. The data presented here suggests that *gskl-1/gskl-2* regulate sperm motility, possibly by regulating MSP. MSP is the key cytoskeletal protein that is not only required for locomotion but also sends the signal for oocyte maturation and gonadal sheath cell

contraction. MSP is released from the sperm by a specialised vesicle budding mechanism to provide the maturation signal (Kosinski et al. 2005). Thus, the defects in oocyte blebbing could be due to a sperm-derived defect involving *gskl-1/gskl-2* and MSP regulation. Individual knockdown of *orai-1(RNAi)* and *pezo-1(RNAi)* reduced brood size significantly and knockdown of both enhances the phenotype. To test the idea if they work together with *gskl-1/gskl-2* in the same pathway to regulate extracellular Ca^{2+} level, in future *orai-1(RNAi)* or *pezo-1(RNAi)* could be done on *gskl-2*; *gskl-1* worms to see if that enhances the phenotype.

The phenotype that I observed in the oocytes is reminiscent of a previously reported mutant phenotype that results from deletion of the *famk-1* gene (Gerson-Gurwitz et al. 2019). *famk-1* encodes an orthologue of vertebrate FAM20C, which is Golgi casein kinase (Salvi et al. 2010). Young adult *famk-1* deletion worms do not exhibit any obvious phenotypes, however, in aged hermaphrodites, the spermatheca becomes extended and part of the oocyte gets trapped inside (Gerson-Gurwitz et al. 2019). *famk-1* is predicted to involve in phosphorylating different substrates including lectins. So, it is less likely that *gskl-1/gskl-2* are involved in *famk-1* pathway.

5.8 *gskl-1* and *gskl-2* are required to complete female meiosis II after fertilization

Studies from fertilization-defective sperm in *C. elegans*, such as those involving the mutant *fer-1*, revealed that sperm entry is required to complete female meiosis II (McNally and McNally 2005). These mutant sperm can secrete the MSP-based signal for oocyte maturation, but are unable to fertilize the oocyte. In the absence of

fertilization, such MSP-stimulated meiosis-stage oocytes enter anaphase I, but they fail to extrude the first polar body. Then, they skip meiosis II and proceed directly to mitosis. These results indicate that some signal from the sperm enters the oocyte cytoplasm to promote entry into MII, rather than mitosis. At the level of sister chromatid segregation, MII and mitosis are superficially similar, however, many other differences between female meiosis and mitosis are important to consider. For example, the centrosomal microtubules appear after the completion of female meiosis II, katanin dependent meiotic spindle assembly is very different from that of mitotic spindle assembly and nuclear envelopes do not form around meiotic chromatin.

Prior to the work presented in this thesis, the only genes known to be directly involved in the fertilization-dependent signal that specifies female MI were the *memi* genes (Ataeian et al. 2016). Loss of all three paralogs of the *memi* genes results in a skipped-meiosis II phenotype. The *gskl-2*(Δ); *gskl-1*(Δ) double-deletion mutant revealed incompletely penetrant paternal-effect embryonic lethality. The reason for the variability in phenotypic severity amongst individual sperm is still unclear, but there could be some further redundancy for GSK-3 activity within the sperm and/or fertilized embryo. Though not significant, but little lower brood size was observed on *F20F4.1*(RNAi) treated *gskl-1*(*abc57*) and *gskl-1*(*abc41*) mutant worms. In future, *F20F4.1*(Δ) can be combined with the *gskl-2*(Δ); *gskl-1*(Δ) to see if that enhances the embryonic lethality of the later.

In utero time-lapse analysis revealed that 7 out of 20 oocytes that were fertilized by *gskl-2*(Δ); *gskl-1*(Δ) sperm completed anaphase I successfully as indicated by the release of first polar body. Meiosis II spindle formation was delayed in those embryos,

and they could not complete anaphase II, did not release second polar body. Prior to this study, *spe-11* was the only known sperm component that displayed a role in controlling female meiosis II in *C. elegans*, fertilization of wild-type oocytes by sperm from homozygous *spe-11* mutant males leads to abnormal zygotic development (Hill et al. 1989). However, ectopically expressing *spe-11* oocytes produce viable progeny when mated to *spe-11* mutant sperm. This suggests that SPE-11 is a sperm supplied factor which is directly involved in early embryogenesis (Browning and Strome 1996). Anaphase I chromosome collapsed together and no polar body 1 was extruded in the defective *spe-11* embryos; however, those embryos progressed through anaphase II but were unable to extrude the second polar body (McNally and McNally 2005). In addition, the *spe-11* embryos show defects in egg shell formation, such that the embryos are permeable to DAPI, whereas *gskl-2*(Δ); *gskl-1*(Δ) embryos did not have a permeable egg shell. Overall, the loss of *gskl-1* and *gskl-2* resulted in embryonic phenotypes that resembled the *spe-11* mutant embryos, though the phenotypes were not similar enough to conclude identical embryonic functions for these genes. In addition, I found that the embryonic lethality of *memi-1(sb41)* was not suppressed by a loss-of-function allele of *spe-11* (Appendix, Figure 4). Therefore, although *spe-11* might be involved in some overlapping functions that involve the GSK-3 genes, it is not likely a genetic activator of the *memi* pathway.

An intriguing correlation between the motility of individual sperm and a post-fertilization function that is essential for development has shown in this study. I have shown that the percentage of viable progeny from *fog-2* mated to *gskl-2*(Δ); *gskl-1*(Δ) males was significantly higher than the viability of double deletion hermaphrodites *gskl-*

2(Δ); *gskl-1*(Δ) due to competition amongst ejaculated male sperm to reach to the spermatheca. It was also shown that the absence of sperm before fertilization in *fog-2* did not affect the fertilization process as the *gskl-2*(Δ); *gskl-1*(Δ) males mated to older wild type hermaphrodites that have used up their cache of self sperm also produced similar percentage of viable progenies. To date, this is the first example of a paternal-effect embryonic lethal phenotype that is influenced by the outcome of pre-fertilization competition amongst sperm.

5.9 *gsp-4* and *gskl-1/gskl-2* work together to activate the *memi* pathway

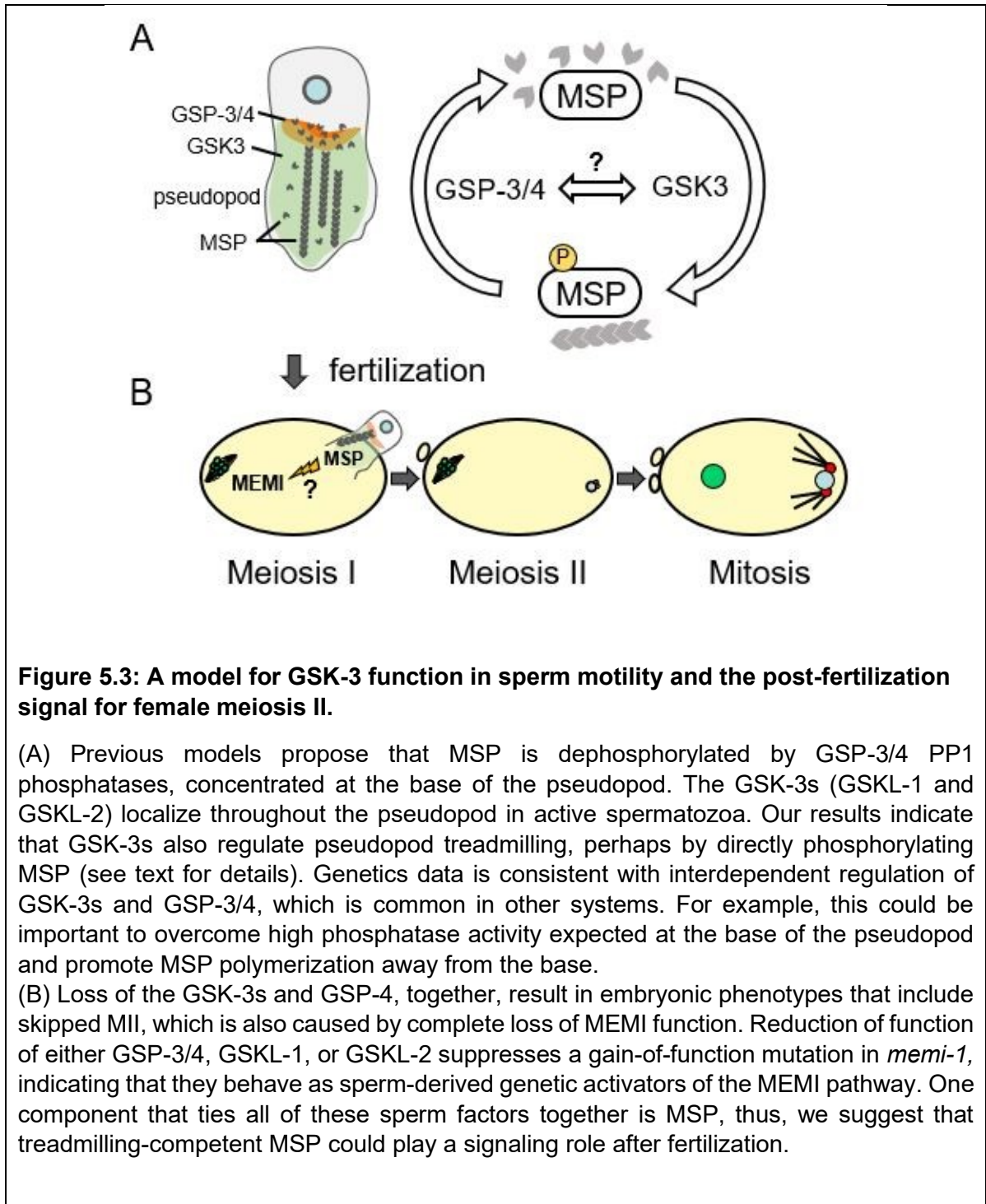
The data presented here suggest that GSKL-1/GSKL-2 kinases and GSP-3/4 phosphatases, despite having presumably opposite biochemical activities in these cells, are likely to perform at least some similar functions. For example, reduction of either GSP-3/4 phosphatase or GSKL-1/GSKL-2 kinase activity results in similar meiotic defects during male meiosis II, delayed activation of spermatids, as well as reduced sperm motility and slow pseudopod treadmilling. In addition, loss of all individual components act as suppressors of *memi-1*(*sb41*). Furthermore, the *gsp-4*(Δ); *gskl-1*(Δ) kinase/phosphatase double mutant suppressed *memi-1*(*sb41*), indicating that reducing both kinase and phosphatase activity did not cancel out individual suppression, rather the suppression increased. Finally, the *gsp-4*(Δ) *gskl-2*(Δ); *gskl-1*(Δ) triple mutant exhibited more severe embryonic lethality than the double mutants alone, and some of those defective embryos displayed a skipped-MII phenotype similar to loss of *memi-1/2/3* function. Thus, all data indicate that, perhaps unexpectedly,

reducing the activity of either GSKL-1/GSKL-2 kinases or GSP-3/4 phosphatases results in a very similar phenotypic outcome.

The model shown in Figure 5.3A explains the connection between GSKL-1/GSKL-2 and GSP-3/4, sperm motility, and possibly spermatogenesis, but it is difficult to explain how loss of either kinase or phosphatase relates to the post-fertilization function for this system, as reflected by their suppression of *memi-1(sb41)*. The *memi-(sb41)* mutation results in a P74S change, at a putative proline-directed phosphorylation site and it has been shown that MEMI-1 degradation depends on this motif. The suppression data is inconsistent with a simple mechanism involving direct phosphorylation or dephosphorylation of MEMI by GSKL-1/GSKL-2 and GSP-3/4, respectively. Instead, the common link between these genes and the MEMI pathway might be MSP itself acting in two independent pathways (Figure 5.3B). This protein has unusual properties; it is both a cytoskeletal polymer within the sperm cytoplasm and a diffusible hormone, secreted by sperm to trigger oocyte maturation. MSP could have a third function, as part of a sperm-derived signal that activates the maternal MEMI proteins to trigger female MII. This signal would function independently of the secreted MSP-based oocyte maturation signal, and be delivered into the oocyte upon fertilization. Extending the model to explain the role of these components in sperm motility, the treadmilling-competent MSP is proposed to be important for MEMI activity once MSP is internalized after oocyte-sperm fusion. In this case, reduction of phosphatase or kinase function would suppress the gain-of-function *memi-1(sb41)* mutation.

This model assumes that fertilization involves the delivery of the aforementioned cytosolic sperm proteins into the oocyte, however, I have not been able to detect any of the proteins within fertilized embryos using immunofluorescence approaches. It is possible that sperm factors diffuse rapidly within the comparatively larger volume of the oocyte, making them hard to detect, however, this aspect of the model still requires validation.

An important test of this model would be to genetically alter MSP activity, or change the relative proportion of phosphorylated MSP in a *memi-1(sb41)* background. Unfortunately, this approach is hindered by the fact that MSP is encoded by over forty paralogous genes (Burke and Ward 1983; Klass et al. 1984; Ward et. al. 1988). Future efforts will focus on assessing the phosphorylation state of MSP in the kinase and phosphatase mutant backgrounds described.



If GSKL-1/GSKL-2 kinases and GSP-3/4 phosphatases (and, by extension, treadmilling-competent MSP) are essential components of a sperm-derived signal that

triggers entry into female MII after fertilization, one would expect that the loss of such components should result in a skipped-MII phenotype, similar to a complete loss of MEMI function. Using a combination of double and triple mutants from these redundant pathways, the skipped MII phenotype was observed in many fertilized embryos, consistent with the idea that GSKL-1/GSKL-2 and GSP-3/4 are required for the transition to MII in the fertilized embryo. It is possible that some embryonic defects could be due to aneuploidy or missegregation of other components during male meiosis. However, it is reasonable to consider that the embryonic defects are specific for this pathway, since other mutations that produce anucleate or aneuploid sperm give rise to different phenotypes. For example, the paternal-effect mutants such as *emb-27* (Sadler and Shakes 2000) and *top-2* (Jaramillo-Lambert et al. 2016) form anucleate sperm that are capable of fertilization. In these mutants, the early female meiotic divisions appear normal, indicating that the post-fertilization phenotypes of *gskl-2*(Δ); *gskl-1*(Δ) double mutants are not simply a result of chromosome segregation defects during male meiosis.

In summary, this work reveals a new role for two homologs of the GSK-3 family, *gskl-1* and *gskl-2*, in sperm meiosis and sperm motility in *C. elegans*. The presented data also indicate that the GSK-3 kinases could act with GSP-3/4 PP1 phosphatases to activate the MEMI pathway for proper completion of female meiosis II after fertilization, possibly through their action on MSP, which could be an internalized activation signal.

References

1998. Genome sequence of the nematode *C. elegans*: a platform for investigating biology. *Science* **282**: 2012-2018.
- Aitken RJ, Nixon B. 2013. Sperm capacitation: a distant landscape glimpsed but unexplored. *Molecular human reproduction* **19**: 785-793.
- Alexandre H. 2001. A history of mammalian embryological research. *The International journal of developmental biology* **45**: 457-467.
- Alper SL. 2017. Genetic Diseases of PIEZO1 and PIEZO2 Dysfunction. *Current topics in membranes* **79**: 97-134.
- An N, Blumer JB, Bernard ML, Lanier SM. 2008. The PDZ and band 4.1 containing protein Frmpd1 regulates the subcellular location of activator of G-protein signaling 3 and its interaction with G-proteins. *The Journal of biological chemistry* **283**: 24718-24728.
- Anderson JL, Morran LT, Phillips PC. 2010. Outcrossing and the maintenance of males within *C. elegans* populations. *The Journal of heredity* **101 Suppl 1**: S62-74.
- Anderson P. 1995. Mutagenesis. *Methods in cell biology* **48**: 31-58.
- Arduengo PM, Appleberry OK, Chuang P, L'Hernault SW. 1998. The presenilin protein family member SPE-4 localizes to an ER/Golgi derived organelle and is required for proper cytoplasmic partitioning during *Caenorhabditis elegans* spermatogenesis. *Journal of cell science* **111 (Pt 24)**: 3645-3654.
- Arribere JA, Bell RT, Fu BX, Artiles KL, Hartman PS, Fire AZ. 2014. Efficient marker-free recovery of custom genetic modifications with CRISPR/Cas9 in *Caenorhabditis elegans*. *Genetics* **198**: 837-846.

- Ataeian M, Tegha-Dunghu J, Curtis DG, Sykes EM, Nozohourmehrabad A, Bajaj M, Cheung K, Srayko M. 2016. Maternal MEMI Promotes Female Meiosis II in Response to Fertilization in *Caenorhabditis elegans*. *Genetics* **204**: 1461-1477.
- Bae Y-K, Kim E, L'Hernault SW, Barr MM. 2009. The CIL-1 PI 5-phosphatase localizes TRP Polycystins to cilia and activates sperm in *C. elegans*. *Current biology : CB* **19**: 1599-1607.
- Baer CEa. 1827. De Ovi Mammalium et Hominis Genesi Epistolam ad Academiam Imperialem Scientiarum Petropolitanam dedit Carolus Ernestus a Baer. *Lipsiae : Sumptibus Vossii*.
- Bai X, Bouffard J, Lord A, Brugman K, Sternberg PW, Cram EJ, Golden A. 2020. *Caenorhabditis elegans* PIEZO channel coordinates multiple reproductive tissues to govern ovulation. *Elife* **9**.
- Baker AME, Roberts TM, Stewart M. 2002. 2.6Å Resolution Crystal Structure of Helices of the Motile Major Sperm Protein (MSP) of *Caenorhabditis elegans*. *Journal of molecular biology* **319**: 491-499.
- Beard SM, Smit RB, Chan BG, Mains PE. 2016. Regulation of the MEI-1/MEI-2 Microtubule-Severing Katanin Complex in Early *Caenorhabditis elegans* Development. *G3 (Bethesda, Md)* **6**: 3257-3268.
- Bembenek JN, Verbrugghe KJ, Khanikar J, Csankovszki G, Chan RC. 2013. Condensin and the spindle midzone prevent cytokinesis failure induced by chromatin bridges in *C. elegans* embryos. *Curr Biol* **23**: 937-946.

- Bhattacharjee R, Goswami S, Dey S, Gangoda M, Brothag C, Eisa A, Woodgett J, Phiel C, Kline D, Vijayaraghavan S. 2018. Isoform-specific requirement for GSK3alpha in sperm for male fertility. *Biology of reproduction* **99**: 384-394.
- Bhattacharjee R, Goswami S, Dudiki T, Popkie AP, Phiel CJ, Kline D, Vijayaraghavan S. 2015. Targeted disruption of glycogen synthase kinase 3A (GSK3A) in mice affects sperm motility resulting in male infertility. *Biology of reproduction* **92**: 65.
- Bischoff FR, Ponstingl H. 1991. Catalysis of guanine nucleotide exchange on Ran by the mitotic regulator RCC1. *Nature* **354**: 80-82.
- Bleil JD, Beall CF, Wassarman PM. 1981. Mammalian sperm-egg interaction: fertilization of mouse eggs triggers modification of the major zona pellucida glycoprotein, ZP2. *Dev Biol* **86**: 189-197.
- Blumenthal T SK. 1997. RNA processing and gene structure. In *C. elegans II* (ed. Riddle DL, et al.) *Cold Spring Harbor Laboratory Press, Cold Spring Harbor*: 117–145.
- Bollen M, Peti W, Ragusa MJ, Beullens M. 2010. The extended PP1 toolkit: designed to create specificity. *Trends Biochem Sci* **35**: 450-458.
- Bowerman B, Kurz T. 2006. Degrade to create: developmental requirements for ubiquitin-mediated proteolysis during early *C. elegans* embryogenesis. *Development (Cambridge, England)* **133**: 773-784.
- Brenner S. 1974. The genetics of *Caenorhabditis elegans*. *Genetics* **77**: 71-94.
- Brisbin S, Liu J, Boudreau J, Peng J, Evangelista M, Chin-Sang I. 2009. A role for *C. elegans* Eph RTK signaling in PTEN regulation. *Developmental cell* **17**: 459-469.

- Browning H, Strome S. 1996. A sperm-supplied factor required for embryogenesis in *C. elegans*. *Development (Cambridge, England)* **122**: 391-404.
- Bullock TL, McCoy AJ, Kent HM, Roberts TM, Stewart M. 1998. Structural basis for amoeboid motility in nematode sperm. *Nature structural biology* **5**: 184-189.
- Bürglin TR, Kuwabara PE. 2006. Homologs of the Hh signalling network in *C. elegans*. *WormBook : the online review of C elegans biology*: 1-14.
- Burkart AD, Xiong B, Baibakov B, Jiménez-Movilla M, Dean J. 2012. Ovastacin, a cortical granule protease, cleaves ZP2 in the zona pellucida to prevent polyspermy. *The Journal of cell biology* **197**: 37-44.
- Burke DJ, Ward S. 1983. Identification of a large multigene family encoding the major sperm protein of *Caenorhabditis elegans*. *Journal of molecular biology* **171**: 1-29.
- Buttery SM, Ekman GC, Seavy M, Stewart M, Roberts TM. 2003. Dissection of the *Ascaris* sperm motility machinery identifies key proteins involved in major sperm protein-based amoeboid locomotion. *Molecular biology of the cell* **14**: 5082-5088.
- Butučić M, Williams AB, Wong MM, Kramer B, Michael WM. 2015. Zygotic Genome Activation Triggers Chromosome Damage and Checkpoint Signaling in *C. elegans* Primordial Germ Cells. *Developmental cell* **34**: 85-95.
- Cassada R, Isnenghi E, Culotti M, von Ehrenstein G. 1981. Genetic analysis of temperature-sensitive embryogenesis mutants in *Caenorhabditis elegans*. *Dev Biol* **84**: 193-205.

- Cecchetelli AD, Cram EJ. 2017. Regulating distal tip cell migration in space and time. *Mech Dev* **148**: 11-17.
- Chalbi M, Barraud-Lange V, Ravaux B, Howan K, Rodriguez N, Soule P, Ndzoudi A, Boucheix C, Rubinstein E, Wolf JP et al. 2014. Binding of sperm protein Izumo1 and its egg receptor Juno drives Cd9 accumulation in the intercellular contact area prior to fusion during mammalian fertilization. *Development (Cambridge, England)* **141**: 3732-3739.
- Cheng H, Govindan JA, Greenstein D. 2008. Regulated trafficking of the MSP/Eph receptor during oocyte meiotic maturation in *C. elegans*. *Curr Biol* **18**: 705-714.
- Cheng KC, Klancer R, Singson A, Seydoux G. 2009. Regulation of MBK-2/DYRK by CDK-1 and the pseudophosphatases EGG-4 and EGG-5 during the oocyte-to-embryo transition. *Cell* **139**: 560-572.
- Chu DS, Liu H, Nix P, Wu TF, Ralston EJ, Yates JR, 3rd, Meyer BJ. 2006. Sperm chromatin proteomics identifies evolutionarily conserved fertility factors. *Nature* **443**: 101-105.
- Chu DS, Shakes DC. 2013. Spermatogenesis. *Advances in experimental medicine and biology* **757**: 171-203.
- Church DL, Guan KL, Lambie EJ. 1995. Three genes of the MAP kinase cascade, mek-2, mpk-1/sur-1 and let-60 ras, are required for meiotic cell cycle progression in *Caenorhabditis elegans*. *Development (Cambridge, England)* **121**: 2525-2535.
- Clandinin TR, DeModena JA, Sternberg PW. 1998. Inositol trisphosphate mediates a RAS-independent response to LET-23 receptor tyrosine kinase activation in *C. elegans*. *Cell* **92**: 523-533.

- Clark GF. 2013. The role of carbohydrate recognition during human sperm-egg binding. *Hum Reprod* **28**: 566-577.
- Clift D, Schuh M. 2013. Restarting life: fertilization and the transition from meiosis to mitosis. *Nature reviews Molecular cell biology* **14**: 549-562.
- Clyne RK, Katis VL, Jessop L, Benjamin KR, Herskowitz I, Lichten M, Nasmyth K. 2003. Polo-like kinase Cdc5 promotes chiasmata formation and cosegregation of sister centromeres at meiosis I. *Nature cell biology* **5**: 480-485.
- Corsi AK, Wightman B, Chalfie M. 2015. A Transparent Window into Biology: A Primer on *Caenorhabditis elegans*. *Genetics* **200**: 387-407.
- Coste B, Mathur J, Schmidt M, Earley TJ, Ranade S, Petrus MJ, Dubin AE, Patapoutian A. 2010. Piezo1 and Piezo2 are essential components of distinct mechanically activated cation channels. *Science* **330**: 55-60.
- Coste B, Xiao B, Santos JS, Syeda R, Grandl J, Spencer KS, Kim SE, Schmidt M, Mathur J, Dubin AE et al. 2012. Piezo proteins are pore-forming subunits of mechanically activated channels. *Nature* **483**: 176-181.
- Cross DA, Alessi DR, Cohen P, Andjelkovich M, Hemmings BA. 1995. Inhibition of glycogen synthase kinase-3 by insulin mediated by protein kinase B. *Nature* **378**: 785-789.
- Crowder ME, Flynn JR, McNally KP, Cortes DB, Price KL, Kuehnert PA, Panzica MT, Andaya A, Leary JA, McNally FJ. 2015. Dynactin-dependent cortical dynein and spherical spindle shape correlate temporally with meiotic spindle rotation in *Caenorhabditis elegans*. *Molecular biology of the cell* **26**: 3030-3046.

- Cuenca AA, Schetter A, Aceto D, Kempfues K, Seydoux G. 2003. Polarization of the *C. elegans* zygote proceeds via distinct establishment and maintenance phases. *Development (Cambridge, England)* **130**: 1255-1265.
- Dancheck B, Ragusa MJ, Allaire M, Nairn AC, Page R, Peti W. 2011. Molecular investigations of the structure and function of the protein phosphatase 1-spinophilin-inhibitor 2 heterotrimeric complex. *Biochemistry* **50**: 1238-1246.
- Danlasky BM, Panzica MT, McNally KP, Vargas E, Bailey C, Li W, Gong T, Fishman ES, Jiang X, McNally FJ. 2020. Evidence for anaphase pulling forces during *C. elegans* meiosis. *The Journal of cell biology* **219**.
- Das D, Chen SY, Arur S. 2020. ERK phosphorylates chromosomal axis component HORMA domain protein HTP-1 to regulate oocyte numbers. *Science advances* **6**.
- de Carvalho CE, Zaaijer S, Smolikov S, Gu Y, Schumacher JM, Colaiacovo MP. 2008. LAB-1 antagonizes the Aurora B kinase in *C. elegans*. *Genes & development* **22**: 2869-2885.
- Dean J. 2004. Reassessing the molecular biology of sperm-egg recognition with mouse genetics. *BioEssays : news and reviews in molecular, cellular and developmental biology* **26**: 29-38.
- del Castillo-Olivares A, Smith HE. 2008. Critical contact residues that mediate polymerization of nematode major sperm protein. *Journal of cellular biochemistry* **104**: 477-487.
- Del Marmol JI, Touhara KK, Croft G, MacKinnon R. 2018. Piezo1 forms a slowly-inactivating mechanosensory channel in mouse embryonic stem cells. *Elife* **7**.

- Denich KT, Schierenberg E, Isnenghi E, Cassada R. 1984. Cell-lineage and developmental defects of temperature-sensitive embryonic arrest mutants of the nematode *Caenorhabditis elegans*. *Wilhelm Roux's archives of developmental biology* **193**: 164-179.
- Denver DR, Morris K, Lynch M, Thomas WK. 2004. High mutation rate and predominance of insertions in the *Caenorhabditis elegans* nuclear genome. *Nature* **430**: 679-682.
- Detwiler MR, Reuben M, Li X, Rogers E, Lin R. 2001. Two zinc finger proteins, OMA-1 and OMA-2, are redundantly required for oocyte maturation in *C. elegans*. *Developmental cell* **1**: 187-199.
- Doble BW, Woodgett JR. 2003. GSK-3: tricks of the trade for a multi-tasking kinase. *Journal of cell science* **116**: 1175-1186.
- Doudna JA, Charpentier E. 2014. Genome editing. The new frontier of genome engineering with CRISPR-Cas9. *Science* **346**: 1258096.
- Dow MR, Mains PE. 1998. Genetic and molecular characterization of the *Caenorhabditis elegans* gene, *mel-26*, a postmeiotic negative regulator of *mei-1*, a meiotic-specific spindle component. *Genetics* **150**: 119-128.
- Drake JW, Charlesworth B, Charlesworth D, Crow JF. 1998. Rates of spontaneous mutation. *Genetics* **148**: 1667-1686.
- Duerr JS. 2013. Antibody staining in *C. elegans* using "freeze-cracking". *J Vis Exp*: 50664.

- Dumont J, Oegema K, Desai A. 2010. A kinetochore-independent mechanism drives anaphase chromosome separation during acentrosomal meiosis. *Nature cell biology* **12**: 894-901.
- Ellefson ML, McNally FJ. 2009. Kinesin-1 and cytoplasmic dynein act sequentially to move the meiotic spindle to the oocyte cortex in *Caenorhabditis elegans*. *Molecular biology of the cell* **20**: 2722-2730.
- Ellefson ML, McNally FJ. 2011. CDK-1 inhibits meiotic spindle shortening and dynein-dependent spindle rotation in *C. elegans*. *The Journal of cell biology* **193**: 1229-1244.
- Ellis RE, Stanfield GM. 2014. The regulation of spermatogenesis and sperm function in nematodes. *Seminars in cell & developmental biology* **29**: 17-30.
- Fan H-Y, Liu Z, Shimada M, Sterneck E, Johnson PF, Hedrick SM, Richards JS. 2009. MAPK3/1 (ERK1/2) in ovarian granulosa cells are essential for female fertility. *Science (New York, NY)* **324**: 938-941.
- Fan HY, Sun QY. 2004. Involvement of mitogen-activated protein kinase cascade during oocyte maturation and fertilization in mammals. *Biology of reproduction* **70**: 535-547.
- Ferrandiz N, Barroso C, Telecan O, Shao N, Kim HM, Testori S, Faull P, Cutillas P, Snijders AP, Colaiácovo MP et al. 2018. Spatiotemporal regulation of Aurora B recruitment ensures release of cohesion during *C. elegans* oocyte meiosis. *Nature communications* **9**: 834.

- Feske S, Gwack Y, Prakriya M, Srikanth S, Puppel SH, Tanasa B, Hogan PG, Lewis RS, Daly M, Rao A. 2006. A mutation in Orai1 causes immune deficiency by abrogating CRAC channel function. *Nature* **441**: 179-185.
- Fischer SE. 2010. Small RNA-mediated gene silencing pathways in *C. elegans*. *The international journal of biochemistry & cell biology* **42**: 1306-1315.
- Fischer SE, Butler MD, Pan Q, Ruvkun G. 2008. Trans-splicing in *C. elegans* generates the negative RNAi regulator ERI-6/7. *Nature* **455**: 491-496.
- Fraire-Zamora JJ, Broitman-Maduro G, Maduro M, Cardullo RA. 2011. Evidence for phosphorylation in the MSP cytoskeletal filaments of amoeboid spermatozoa. *International journal of biochemistry and molecular biology* **2**: 263-273.
- Francis R, Barton MK, Kimble J, Schedl T. 1995. *gld-1*, a tumor suppressor gene required for oocyte development in *Caenorhabditis elegans*. *Genetics* **139**: 579-606.
- Fredriksson R, Schiöth HB. 2005. The repertoire of G-protein-coupled receptors in fully sequenced genomes. *Molecular pharmacology* **67**: 1414-1425.
- Freitas MJ, Vijayaraghavan S, Fardilha M. 2016. Signaling mechanisms in mammalian sperm motility†. *Biology of reproduction* **96**: 2-12.
- Geldziler B, Chatterjee I, Singson A. 2005. The genetic and molecular analysis of *spe-19*, a gene required for sperm activation in *Caenorhabditis elegans*. *Dev Biol* **283**: 424-436.
- Gerson-Gurwitz A, Worby CA, Lee K-Y, Khaliullin R, Bouffard J, Cheerambathur D, Oegema K, Cram EJ, Dixon JE, Desai A. 2019. Ancestral roles of the Fam20C

- family of secreted protein kinases revealed in *C. elegans*. *The Journal of cell biology* **218**: 3795-3811.
- Gleason EJ, Lindsey WC, Kroft TL, Singson AW, L'Hernault S W. 2006. spe-10 encodes a DHHC-CRD zinc-finger membrane protein required for endoplasmic reticulum/Golgi membrane morphogenesis during *Caenorhabditis elegans* spermatogenesis. *Genetics* **172**: 145-158.
- Goldstein B, Hird SN. 1996. Specification of the anteroposterior axis in *Caenorhabditis elegans*. *Development (Cambridge, England)* **122**: 1467-1474.
- Gosney R, Liao W-S, Lamunyon CW. 2008. A novel function for the presenilin family member spe-4: inhibition of spermatid activation in *Caenorhabditis elegans*. *BMC developmental biology* **8**: 44-44.
- Goswami S, Korrodi-Gregorio L, Sinha N, Bhutada S, Bhattacharjee R, Kline D, Vijayaraghavan S. 2018. Regulators of the protein phosphatase PP1gamma2, PPP1R2, PPP1R7, and PPP1R11 are involved in epididymal sperm maturation. *Journal of cellular physiology*.
- Govindan JA, Cheng H, Harris JE, Greenstein D. 2006. Galphao/i and Galphas signaling function in parallel with the MSP/Eph receptor to control meiotic diapause in *C. elegans*. *Curr Biol* **16**: 1257-1268.
- Govindan JA, Nadarajan S, Kim S, Starich TA, Greenstein D. 2009. Somatic cAMP signaling regulates MSP-dependent oocyte growth and meiotic maturation in *C. elegans*. *Development (Cambridge, England)* **136**: 2211-2221.
- Grishok A. 2005. RNAi mechanisms in *Caenorhabditis elegans*. *FEBS Lett* **579**: 5932-5939.

- Guo TB, Chan KC, Hakovirta H, Xiao Y, Toppari J, Mitchell AP, Salameh WA. 2003. Evidence for a role of glycogen synthase kinase-3 beta in rodent spermatogenesis. *Journal of andrology* **24**: 332-342.
- Gusnowski EM, Srayko M. 2011. Visualization of dynein-dependent microtubule gliding at the cell cortex: implications for spindle positioning. *The Journal of cell biology* **194**: 377-386.
- Guven-Ozkan T, Nishi Y, Robertson SM, Lin R. 2008. Global transcriptional repression in *C. elegans* germline precursors by regulated sequestration of TAF-4. *Cell* **135**: 149-160.
- Guven-Ozkan T, Robertson SM, Nishi Y, Lin R. 2010. zif-1 translational repression defines a second, mutually exclusive OMA function in germline transcriptional repression. *Development (Cambridge, England)* **137**: 3373-3382.
- Harris JE, Govindan JA, Yamamoto I, Schwartz J, Kaverina I, Greenstein D. 2006. Major sperm protein signaling promotes oocyte microtubule reorganization prior to fertilization in *Caenorhabditis elegans*. *Dev Biol* **299**: 105-121.
- Harvey WW, G. Disputations touching, animals. tgo. 1981. Disputations touching the generation of animals *Blackwell Scientific*.
- Hendrickx A, Beullens M, Ceulemans H, Den Abt T, Van Eynde A, Nicolaescu E, Lesage B, Bollen M. 2009. Docking motif-guided mapping of the interactome of protein phosphatase-1. *Chem Biol* **16**: 365-371.
- Hertwig O. 1876. Beiträge zur Kenntniss der Bildung, Befruchtung und Theilung des thierischen Eies. *Morphol Jahrb* **1**, 347–434

- Herzog JA. 2018. Identifying novel suppressors of *memi-1(sb41)* and their possible roles in meiosis. *MSc thesis, Department of Biological Sciences, University of Alberta*
- Hill DP, Shakes DC, Ward S, Strome S. 1989. A sperm-supplied product essential for initiation of normal embryogenesis in *Caenorhabditis elegans* is encoded by the paternal-effect embryonic-lethal gene, *spe-11*. *Dev Biol* **136**: 154-166.
- Hodgkin J. 1987. Primary sex determination in the nematode *C. elegans*. *Development (Cambridge, England)* **101 Suppl**: 5-16.
- Hodgkin J, Horvitz HR, Brenner S. 1979. Nondisjunction Mutants of the Nematode *CAENORHABDITIS ELEGANS*. *Genetics* **91**: 67-94.
- Horvitz HR, Brenner S, Hodgkin J, Herman RK. 1979. A uniform genetic nomenclature for the nematode *Caenorhabditis elegans*. *Molecular & general genetics : MGG* **175**: 129-133.
- Huelgas-Morales G, Greenstein D. 2018. Control of oocyte meiotic maturation in *C. elegans*. *Seminars in cell & developmental biology* **84**: 90-99.
- Hunter CP, Wood WB. 1990. The *tra-1* gene determines sexual phenotype cell-autonomously in *C. elegans*. *Cell* **63**: 1193-1204.
- Italiano JE, Jr., Roberts TM, Stewart M, Fontana CA. 1996. Reconstitution in vitro of the motile apparatus from the amoeboid sperm of *Ascaris* shows that filament assembly and bundling move membranes. *Cell* **84**: 105-114.
- Jaffe LA. 1976. Fast block to polyspermy in sea urchin eggs is electrically mediated. *Nature* **261**: 68-71.

- Jan E, Motzny CK, Graves LE, Goodwin EB. 1999. The STAR protein, GLD-1, is a translational regulator of sexual identity in *Caenorhabditis elegans*. *The EMBO journal* **18**: 258-269.
- Jaramillo-Lambert A, Fabritius AS, Hansen TJ, Smith HE, Golden A. 2016. The Identification of a Novel Mutant Allele of topoisomerase II in *Caenorhabditis elegans* Reveals a Unique Role in Chromosome Segregation During Spermatogenesis. *Genetics* **204**: 1407-1422.
- Jasin M, Haber JE. 2016. The democratization of gene editing: Insights from site-specific cleavage and double-strand break repair. *DNA Repair (Amst)* **44**: 6-16.
- Jiang W, Marraffini LA. 2015. CRISPR-Cas: New Tools for Genetic Manipulations from Bacterial Immunity Systems. *Annual review of microbiology* **69**: 209-228.
- Johnson JL, Lu C, Raharjo E, McNally K, McNally FJ, Mains PE. 2009. Levels of the ubiquitin ligase substrate adaptor MEL-26 are inversely correlated with MEI-1/katanin microtubule-severing activity during both meiosis and mitosis. *Dev Biol* **330**: 349-357.
- Jones AR, Francis R, Schedl T. 1996. GLD-1, a cytoplasmic protein essential for oocyte differentiation, shows stage- and sex-specific expression during *Caenorhabditis elegans* germline development. *Dev Biol* **180**: 165-183.
- Jud MC, Czerwinski MJ, Wood MP, Young RA, Gallo CM, Bickel JS, Petty EL, Mason JM, Little BA, Padilla PA et al. 2008. Large P body-like RNPs form in *C. elegans* oocytes in response to arrested ovulation, heat shock, osmotic stress, and anoxia and are regulated by the major sperm protein pathway. *Dev Biol* **318**: 38-51.

- Kaitna S, Pasierbek P, Jantsch M, Loidl J, Glotzer M. 2002. The aurora B kinase AIR-2 regulates kinetochores during mitosis and is required for separation of homologous Chromosomes during meiosis. *Curr Biol* **12**: 798-812.
- Kamath RS, Ahringer J. 2003. Genome-wide RNAi screening in *Caenorhabditis elegans*. *Methods (San Diego, Calif)* **30**: 313-321.
- Karashima T, Sugimoto A, Yamamoto M. 2000. *Caenorhabditis elegans* homologue of the human azoospermia factor DAZ is required for oogenesis but not for spermatogenesis. *Development (Cambridge, England)* **127**: 1069-1079.
- Karsenti E. 2005. TPX or not TPX? *Molecular cell* **19**: 431-432.
- Kelker MS, Page R, Peti W. 2009. Crystal structures of protein phosphatase-1 bound to nodularin-R and tautomycin: a novel scaffold for structure-based drug design of serine/threonine phosphatase inhibitors. *Journal of molecular biology* **385**: 11-21.
- Kelleher JF, Mandell MA, Moulder G, Hill KL, L'Hernault SW, Barstead R, Titus MA. 2000. Myosin VI is required for asymmetric segregation of cellular components during *C. elegans* spermatogenesis. *Curr Biol* **10**: 1489-1496.
- Kim DY, Roy R. 2006. Cell cycle regulators control centrosome elimination during oogenesis in *Caenorhabditis elegans*. *The Journal of cell biology* **174**: 751-757.
- Kim S, Govindan JA, Tu ZJ, Greenstein D. 2012. SACY-1 DEAD-Box helicase links the somatic control of oocyte meiotic maturation to the sperm-to-oocyte switch and gamete maintenance in *Caenorhabditis elegans*. *Genetics* **192**: 905-928.
- Kimble J, Hirsh D. 1979. The postembryonic cell lineages of the hermaphrodite and male gonads in *Caenorhabditis elegans*. *Dev Biol* **70**: 396-417.

- Kimble JE, White JG. 1981. On the control of germ cell development in *Caenorhabditis elegans*. *Dev Biol* **81**: 208-219.
- Kitajima TS, Sakuno T, Ishiguro K, Iemura S, Natsume T, Kawashima SA, Watanabe Y. 2006. Shugoshin collaborates with protein phosphatase 2A to protect cohesin. *Nature* **441**: 46-52.
- Klass MR, Kinsley S, Lopez LC. 1984. Isolation and characterization of a sperm-specific gene family in the nematode *Caenorhabditis elegans*. *Mol Cell Biol* **4**: 529-537.
- Kosinski M, McDonald K, Schwartz J, Yamamoto I, Greenstein D. 2005. *C. elegans* sperm bud vesicles to deliver a meiotic maturation signal to distant oocytes. *Development (Cambridge, England)* **132**: 3357-3369.
- Kovacevic I, Cram EJ. 2013. Filamin and Phospholipase C- ϵ are required for calcium signaling in the *Caenorhabditis elegans* Spermatheca. *Worm* **2**: e25717.
- Kumsta C, Hansen M. 2012. *C. elegans* rrf-1 mutations maintain RNAi efficiency in the soma in addition to the germline. *PLoS One* **7**: e35428.
- Kutscher LM, Shaham S. 2014. Forward and reverse mutagenesis in *C. elegans*. *WormBook : the online review of C elegans biology*: 1-26.
- L'Hernault SW. 2006. Spermatogenesis. *WormBook : the online review of C elegans biology*: 1-14.
- L'Hernault SW, Arduengo PM. 1992. Mutation of a putative sperm membrane protein in *Caenorhabditis elegans* prevents sperm differentiation but not its associated meiotic divisions. *The Journal of cell biology* **119**: 55-68.

- L'Hernault SW, Shakes DC, Ward S. 1988. Developmental genetics of chromosome I spermatogenesis-defective mutants in the nematode *Caenorhabditis elegans*. *Genetics* **120**: 435-452.
- LaMunyon CW, Ward S. 1998. Larger sperm outcompete smaller sperm in the nematode *Caenorhabditis elegans*. *Proceedings Biological sciences* **265**: 1997-2002.
- Lantsch I, Yu CH, Chen YZ, Zimyanin V, Yazdkhasti H, Lindow N, Szentgyoergyi E, Pani AM, Prohaska S, Srayko M et al. 2021. Microtubule reorganization during female meiosis in *C. elegans*. *Elife* **10**.
- LeClaire LL, 3rd, Stewart M, Roberts TM. 2003. A 48 kDa integral membrane phosphoprotein orchestrates the cytoskeletal dynamics that generate amoeboid cell motility in *Ascaris* sperm. *Journal of cell science* **116**: 2655-2663.
- Lee BH, Amon A. 2003. Role of Polo-like kinase CDC5 in programming meiosis I chromosome segregation. *Science* **300**: 482-486.
- Lee MH, Ohmachi M, Arur S, Nayak S, Francis R, Church D, Lambie E, Schedl T. 2007. Multiple functions and dynamic activation of MPK-1 extracellular signal-regulated kinase signaling in *Caenorhabditis elegans* germline development. *Genetics* **177**: 2039-2062.
- Lee MH, Schedl T. 2001. Identification of in vivo mRNA targets of GLD-1, a maxi-KH motif containing protein required for *C. elegans* germ cell development. *Genes & development* **15**: 2408-2420.
- Leeuwenhoek A. 1677. Observationes, D. Anthonii Lewenhoeck, de natis e` semini genitalianimalcules. . *Phil Trans R Soc Lond B* **12**, 1040–1046

- Lin T-H, Chen Y-C, Chyan C-I, Tsay L-h, Tang TC, Jeng H-H, Lin F-M, Huang H-b. 2003. Phosphorylation by glycogen synthase kinase of inhibitor-2 does not change its structure in free state. *FEBS Letters* **554**: 253-256.
- Liou J, Kim ML, Heo WD, Jones JT, Myers JW, Ferrell JE, Jr., Meyer T. 2005. STIM is a Ca²⁺ sensor essential for Ca²⁺-store-depletion-triggered Ca²⁺ influx. *Curr Biol* **15**: 1235-1241.
- Lishko PV, Botchkina IL, Kirichok Y. 2011. Progesterone activates the principal Ca²⁺ channel of human sperm. *Nature* **471**: 387-391.
- Liu Z, Chen L, Shang Y, Huang P, Miao L. 2013. The micronutrient element zinc modulates sperm activation through the SPE-8 pathway in *Caenorhabditis elegans*. *Development (Cambridge, England)* **140**: 2103-2107.
- Lopata A. 2009. History of the egg in embryology. *J Mammal Ova Res* **26**, 2–9
- Lopez AL, 3rd, Chen J, Joo HJ, Drake M, Shidate M, Kseib C, Arur S. 2013. DAF-2 and ERK couple nutrient availability to meiotic progression during *Caenorhabditis elegans* oogenesis. *Developmental cell* **27**: 227-240.
- Lorin-Nebel C, Xing J, Yan X, Strange K. 2007. CRAC channel activity in *C. elegans* is mediated by Orai1 and STIM1 homologues and is essential for ovulation and fertility. *The Journal of physiology* **580**: 67-85.
- Lu C, Mains PE. 2007. The *C. elegans* anaphase promoting complex and MBK-2/DYRK kinase act redundantly with CUL-3/MEL-26 ubiquitin ligase to degrade MEI-1 microtubule-severing activity after meiosis. *Dev Biol* **302**: 438-447.

- Ma X, Zhao Y, Sun W, Shimabukuro K, Miao L. 2012. Transformation: how do nematode sperm become activated and crawl? *Protein & cell* **3**: 755-761.
- Machaca K, DeFelice LJ, L'Hernault SW. 1996. A novel chloride channel localizes to *Caenorhabditis elegans* spermatids and chloride channel blockers induce spermatid differentiation. *Dev Biol* **176**: 1-16.
- Machaca K, L'Hernault SW. 1997. The *Caenorhabditis elegans* spe-5 gene is required for morphogenesis of a sperm-specific organelle and is associated with an inherent cold-sensitive phenotype. *Genetics* **146**: 567-581.
- Madl JE, Herman RK. 1979. Polyploids and sex determination in *Caenorhabditis elegans*. *Genetics* **93**: 393-402.
- Maine EM. 2008. Studying gene function in *Caenorhabditis elegans* using RNA-mediated interference. *Briefings in functional genomics & proteomics* **7**: 184-194.
- Manning G. 2005. Genomic overview of protein kinases. *WormBook : the online review of C elegans biology*: 1-19.
- Marcello MR, Singaravelu G, Singson A. 2013. Fertilization. *Advances in experimental medicine and biology* **757**: 321-350.
- Martinez-Perez E, Schvarzstein M, Barroso C, Lightfoot J, Dernburg AF, Villeneuve AM. 2008. Crossovers trigger a remodeling of meiotic chromosome axis composition that is linked to two-step loss of sister chromatid cohesion. *Genes & development* **22**: 2886-2901.
- Maruyama R, Velarde NV, Klancer R, Gordon S, Kadandale P, Parry JM, Hang JS, Rubin J, Stewart-Michaelis A, Schweinsberg P et al. 2007. EGG-3 regulates

- cell-surface and cortex rearrangements during egg activation in *Caenorhabditis elegans*. *Curr Biol* **17**: 1555-1560.
- McCarter J, Bartlett B, Dang T, Schedl T. 1999. On the control of oocyte meiotic maturation and ovulation in *Caenorhabditis elegans*. *Dev Biol* **205**: 111-128.
- McNally KL, McNally FJ. 2005. Fertilization initiates the transition from anaphase I to metaphase II during female meiosis in *C. elegans*. *Dev Biol* **282**: 218-230.
- Meiselbach H, Sticht H, Enz R. 2006. Structural analysis of the protein phosphatase 1 docking motif: molecular description of binding specificities identifies interacting proteins. *Chem Biol* **13**: 49-59.
- Miao L, Vanderlinde O, Stewart M, Roberts TM. 2003. Retraction in amoeboid cell motility powered by cytoskeletal dynamics. *Science* **302**: 1405-1407.
- Mikeladze-Dvali T, von Tobel L, Strnad P, Knott G, Leonhardt H, Schermelleh L, Gönczy P. 2012. Analysis of centriole elimination during *C. elegans* oogenesis. *Development (Cambridge, England)* **139**: 1670-1679.
- Miller MA, Nguyen VQ, Lee MH, Kosinski M, Schedl T, Caprioli RM, Greenstein D. 2001. A sperm cytoskeletal protein that signals oocyte meiotic maturation and ovulation. *Science* **291**: 2144-2147.
- Miller MR, Mannowetz N, Iavarone AT, Safavi R, Gracheva EO, Smith JF, Hill RZ, Bautista DM, Kirichok Y, Lishko PV. 2016. Unconventional endocannabinoid signaling governs sperm activation via the sex hormone progesterone. *Science* **352**: 555-559.

- Minniti AN, Sadler C, Ward S. 1996. Genetic and molecular analysis of *spe-27*, a gene required for spermiogenesis in *Caenorhabditis elegans* hermaphrodites. *Genetics* **143**: 213-223.
- Mitenko NL, Eisner JR, Swiston JR, Mains PE. 1997. A Limited Number of *Caenorhabditis elegans* Genes Are Readily Mutable to Dominant, Temperature-Sensitive Maternal-Effect Embryonic Lethality. *Genetics* **147**: 1665-1674.
- Morrison KN, Uyehara CM, Ragle JM, Ward JD, Shakes DC. 2021. MFP1/MSD-1 and MFP2/NSPH-2 co-localize with MSP during *C. elegans* spermatogenesis. *MicroPubl Biol* **2021**: 10.17912/micropub.biology.000427.
- Muhlrad PJ, Ward S. 2002. Spermiogenesis Initiation in *Caenorhabditis elegans* Involves a Casein Kinase 1 Encoded by the *spe-6* Gene. *Genetics* **161**: 143-155.
- Müller-Reichert T, Greenan G, O'Toole E, Srayko M. 2010. The elegans of spindle assembly. *Cellular and Molecular Life Sciences* **67**: 2195-2213.
- Murthy SE, Dubin AE, Patapoutian A. 2017. Piezos thrive under pressure: mechanically activated ion channels in health and disease. *Nature reviews Molecular cell biology* **18**: 771-783.
- Nadarajan S, Govindan JA, McGovern M, Hubbard EJ, Greenstein D. 2009. MSP and GLP-1/Notch signaling coordinately regulate actomyosin-dependent cytoplasmic streaming and oocyte growth in *C. elegans*. *Development (Cambridge, England)* **136**: 2223-2234.

- Nance J, Davis EB, Ward S. 2000. spe-29 encodes a small predicted membrane protein required for the initiation of sperm activation in *Caenorhabditis elegans*. *Genetics* **156**: 1623-1633.
- Nance J, Minniti AN, Sadler C, Ward S. 1999. spe-12 encodes a sperm cell surface protein that promotes spermiogenesis in *Caenorhabditis elegans*. *Genetics* **152**: 209-220.
- Nasmyth K, Haering CH. 2009. Cohesin: its roles and mechanisms. *Annual review of genetics* **43**: 525-558.
- Nayak S, Santiago FE, Jin H, Lin D, Schedl T, Kipreos ET. 2002. The *Caenorhabditis elegans* Skp1-related gene family: diverse functions in cell proliferation, morphogenesis, and meiosis. *Curr Biol* **12**: 277-287.
- Nelson GA, Roberts TM, Ward S. 1982. *Caenorhabditis elegans* spermatozoan locomotion: amoeboid movement with almost no actin. *The Journal of cell biology* **92**: 121-131.
- Nelson GA, Ward S. 1980. Vesicle fusion, pseudopod extension and amoeboid motility are induced in nematode spermatids by the ionophore monensin. *Cell* **19**: 457-464.
- Nishi Y, Lin R. 2005. DYRK2 and GSK-3 phosphorylate and promote the timely degradation of OMA-1, a key regulator of the oocyte-to-embryo transition in *C. elegans*. *Dev Biol* **288**: 139-149.
- Nishi Y, Rogers E, Robertson SM, Lin R. 2008. Polo kinases regulate *C. elegans* embryonic polarity via binding to DYRK2-primed MEX-5 and MEX-6. *Development (Cambridge, England)* **135**: 687-697.

- Nishimura H, L'Hernault SW. 2010. Spermatogenesis-defective (spe) mutants of the nematode *Caenorhabditis elegans* provide clues to solve the puzzle of male germline functions during reproduction. *Developmental dynamics : an official publication of the American Association of Anatomists* **239**: 1502-1514.
- Nonomura K, Woo SH, Chang RB, Gillich A, Qiu Z, Francisco AG, Ranade SS, Liberles SD, Patapoutian A. 2017. Piezo2 senses airway stretch and mediates lung inflation-induced apnoea. *Nature* **541**: 176-181.
- O'Connell KF, Maxwell KN, White JG. 2000. The spd-2 gene is required for polarization of the anteroposterior axis and formation of the sperm asters in the *Caenorhabditis elegans* zygote. *Dev Biol* **222**: 55-70.
- Ozlü N, Srayko M, Kinoshita K, Habermann B, O'Toole E T, Müller-Reichert T, Schmalz N, Desai A, Hyman AA. 2005. An essential function of the *C. elegans* ortholog of TPX2 is to localize activated aurora A kinase to mitotic spindles. *Developmental cell* **9**: 237-248.
- Paix A, Folkmann A, Rasoloson D, Seydoux G. 2015. High Efficiency, Homology-Directed Genome Editing in *Caenorhabditis elegans* Using CRISPR-Cas9 Ribonucleoprotein Complexes. *Genetics* **201**: 47-54.
- Paix A, Folkmann A, Seydoux G. 2017. Precision genome editing using CRISPR-Cas9 and linear repair templates in *C. elegans*. *Methods (San Diego, Calif)* **121-122**: 86-93.
- Paix A, Wang Y, Smith HE, Lee CY, Calidas D, Lu T, Smith J, Schmidt H, Krause MW, Seydoux G. 2014. Scalable and versatile genome editing using linear DNAs with

- microhomology to Cas9 Sites in *Caenorhabditis elegans*. *Genetics* **198**: 1347-1356.
- Parekh AB, Penner R. 1997. Store depletion and calcium influx. *Physiological reviews* **77**: 901-930.
- Parekh AB, Putney JW, Jr. 2005. Store-operated calcium channels. *Physiological reviews* **85**: 757-810.
- Park SH, Cheong C, Idoyaga J, Kim JY, Choi JH, Do Y, Lee H, Jo JH, Oh YS, Im W et al. 2008. Generation and application of new rat monoclonal antibodies against synthetic FLAG and OLLAS tags for improved immunodetection. *Journal of immunological methods* **331**: 27-38.
- Parry JM, Velarde NV, Lefkovith AJ, Zegarek MH, Hang JS, Ohm J, Klancer R, Maruyama R, Druzhinina MK, Grant BD et al. 2009. EGG-4 and EGG-5 Link Events of the Oocyte-to-Embryo Transition with Meiotic Progression in *C. elegans*. *Curr Biol* **19**: 1752-1757.
- Patel P, Woodgett JR. 2017. Glycogen Synthase Kinase 3: A Kinase for All Pathways? *Current topics in developmental biology* **123**: 277-302.
- Phillips CM, Wong C, Bhalla N, Carlton PM, Weiser P, Meneely PM, Dernburg AF. 2005. HIM-8 Binds to the X Chromosome Pairing Center and Mediates Chromosome-Specific Meiotic Synapsis. *Cell* **123**: 1051-1063.
- Poole K, Herget R, Lapatsina L, Ngo HD, Lewin GR. 2014. Tuning Piezo ion channels to detect molecular-scale movements relevant for fine touch. *Nature communications* **5**: 3520.

- Prakriya M, Feske S, Gwack Y, Srikanth S, Rao A, Hogan PG. 2006. Orai1 is an essential pore subunit of the CRAC channel. *Nature* **443**: 230-233.
- Price KL, Presler M, Uyehara CM, Shakes DC. 2021. The intrinsically disordered protein SPE-18 promotes localized assembly of MSP in *Caenorhabditis elegans* spermatocytes. *Development (Cambridge, England)* **148**: dev195875.
- Quintin S, Mains PE, Zinke A, Hyman AA. 2003. The mbk-2 kinase is required for inactivation of MEI-1/katanin in the one-cell *Caenorhabditis elegans* embryo. *EMBO reports* **4**: 1175-1181.
- Ranade SS, Qiu Z, Woo SH, Hur SS, Murthy SE, Cahalan SM, Xu J, Mathur J, Bandell M, Coste B et al. 2014. Piezo1, a mechanically activated ion channel, is required for vascular development in mice. *Proc Natl Acad Sci U S A* **111**: 10347-10352.
- Rankin TL, Tong ZB, Castle PE, Lee E, Gore-Langton R, Nelson LM, Dean J. 1998. Human ZP3 restores fertility in Zp3 null mice without affecting order-specific sperm binding. *Development (Cambridge, England)* **125**: 2415-2424.
- Reinke V, Gil IS, Ward S, Kazmer K. 2004. Genome-wide germline-enriched and sex-biased expression profiles in *Caenorhabditis elegans*. *Development (Cambridge, England)* **131**: 311-323.
- Reinke V, Smith HE, Nance J, Wang J, Van Doren C, Begley R, Jones SJ, Davis EB, Scherer S, Ward S et al. 2000. A global profile of germline gene expression in *C. elegans*. *Molecular cell* **6**: 605-616.
- Roberts TM, Pavalko FM, Ward S. 1986. Membrane and cytoplasmic proteins are transported in the same organelle complex during nematode spermatogenesis. *The Journal of cell biology* **102**: 1787-1796.

- Roberts TM, Stewart M. 2012. Role of major sperm protein (MSP) in the protrusion and retraction of *Ascaris* sperm. *International review of cell and molecular biology* **297**: 265-293.
- Robertson S, Lin R. 2013. The oocyte-to-embryo transition. *Advances in experimental medicine and biology* **757**: 351-372.
- Rogers E, Bishop JD, Waddle JA, Schumacher JM, Lin R. 2002. The aurora kinase AIR-2 functions in the release of chromosome cohesion in *Caenorhabditis elegans* meiosis. *The Journal of cell biology* **157**: 219-229.
- Roos J, DiGregorio PJ, Yeromin AV, Ohlsen K, Lioudyno M, Zhang S, Safrina O, Kozak JA, Wagner SL, Cahalan MD et al. 2005. STIM1, an essential and conserved component of store-operated Ca²⁺ channel function. *The Journal of cell biology* **169**: 435-445.
- Rose KL, Winfrey VP, Hoffman LH, Hall DH, Furuta T, Greenstein D. 1997. The POU gene *ceh-18* promotes gonadal sheath cell differentiation and function required for meiotic maturation and ovulation in *Caenorhabditis elegans*. *Dev Biol* **192**: 59-77.
- Rosenberg SC, Corbett KD. 2015. The multifaceted roles of the HORMA domain in cellular signaling. *The Journal of cell biology* **211**: 745-755.
- Ruvkun G, Hobert O. 1998. The taxonomy of developmental control in *Caenorhabditis elegans*. *Science* **282**: 2033-2041.
- Sadler PL, Shakes DC. 2000. Anucleate *Caenorhabditis elegans* sperm can crawl, fertilize oocytes and direct anterior-posterior polarization of the 1-cell embryo. *Development (Cambridge, England)* **127**: 355-366.

- Salvi M, Cesaro L, Tibaldi E, Pinna LA. 2010. Motif analysis of phosphosites discloses a potential prominent role of the Golgi casein kinase (GCK) in the generation of human plasma phospho-proteome. *Journal of proteome research* **9**: 3335-3338.
- Schedl T, Kimble J. 1988. fog-2, a germ-line-specific sex determination gene required for hermaphrodite spermatogenesis in *Caenorhabditis elegans*. *Genetics* **119**: 43-61.
- Schleiden MJ. 1838. Beiträge zur Phylogenesis. *Müller's Archiv für Anatomie, Physiologie und wissenschaftliche Medicin*: 137-176.
- Schlesinger A, Shelton CA, Maloof JN, Meneghini M, Bowerman B. 1999. Wnt pathway components orient a mitotic spindle in the early *Caenorhabditis elegans* embryo without requiring gene transcription in the responding cell. *Genes & development* **13**: 2028-2038.
- Schubert CM, Lin R, de Vries CJ, Plasterk RH, Priess JR. 2000. MEX-5 and MEX-6 function to establish soma/germline asymmetry in early *C. elegans* embryos. *Molecular cell* **5**: 671-682.
- Schwann T. 1839. Mikroskopische Untersuchungen über die Uebereinstimmung in der Struktur und dem Wachsthum der Thiere und Pflanzen. *Neue Not Geb Nat Heilk.*
- Severson AF, Ling L, van Zuylen V, Meyer BJ. 2009. The axial element protein HTP-3 promotes cohesin loading and meiotic axis assembly in *C. elegans* to implement the meiotic program of chromosome segregation. *Genes & development* **23**: 1763-1778.
- Shakes DC, Ward S. 1989a. Initiation of spermiogenesis in *C. elegans*: a pharmacological and genetic analysis. *Dev Biol* **134**: 189-200.

- Shakes DC, Ward S. 1989b. Mutations that disrupt the morphogenesis and localization of a sperm-specific organelle in *Caenorhabditis elegans*. *Developmental Biology* **134**: 307-316.
- Shakes DC, Wu J-c, Sadler PL, LaPrade K, Moore LL, Noritake A, Chu DS. 2009. Spermatogenesis-Specific Features of the Meiotic Program in *Caenorhabditis elegans*. *PLOS Genetics* **5**: e1000611.
- Shi Y. 2009. Serine/threonine phosphatases: mechanism through structure. *Cell* **139**: 468-484.
- Shirayama M, Soto MC, Ishidate T, Kim S, Nakamura K, Bei Y, van den Heuvel S, Mello CC. 2006. The Conserved Kinases CDK-1, GSK-3, KIN-19, and MBK-2 Promote OMA-1 Destruction to Regulate the Oocyte-to-Embryo Transition in *C. elegans*. *Curr Biol* **16**: 47-55.
- Sijen T, Fleenor J, Simmer F, Thijssen KL, Parrish S, Timmons L, Plasterk RH, Fire A. 2001. On the role of RNA amplification in dsRNA-triggered gene silencing. *Cell* **107**: 465-476.
- Singaravelu G, Chatterjee I, Rahimi S, Druzhinina MK, Kang L, Xu XZ, Singson A. 2012. The sperm surface localization of the TRP-3/SPE-41 Ca²⁺-permeable channel depends on SPE-38 function in *Caenorhabditis elegans*. *Dev Biol* **365**: 376-383.
- Smardon A, Spoerke JM, Stacey SC, Klein ME, Mackin N, Maine EM. 2000. EGO-1 is related to RNA-directed RNA polymerase and functions in germ-line development and RNA interference in *C. elegans*. *Curr Biol* **10**: 169-178.

- Smith JR, Stanfield GM. 2011. TRY-5 is a sperm-activating protease in *Caenorhabditis elegans* seminal fluid. *PLoS Genet* **7**: e1002375.
- Srayko M, Buster DW, Bazirgan OA, McNally FJ, Mains PE. 2000. MEI-1/MEI-2 katanin-like microtubule severing activity is required for *Caenorhabditis elegans* meiosis. *Genes & development* **14**: 1072-1084.
- Srayko M, O'Toole E T, Hyman AA, Müller-Reichert T. 2006. Katanin disrupts the microtubule lattice and increases polymer number in *C. elegans* meiosis. *Curr Biol* **16**: 1944-1949.
- Stanfield GM, Villeneuve AM. 2006. Regulation of sperm activation by SWM-1 is required for reproductive success of *C. elegans* males. *Curr Biol* **16**: 252-263.
- Stitzel ML, Seydoux G. 2007. Regulation of the oocyte-to-zygote transition. *Science* **316**: 407-408.
- Stricker SA. 1999. Comparative biology of calcium signaling during fertilization and egg activation in animals. *Dev Biol* **211**: 157-176.
- Sun XH, Zhu YY, Wang L, Liu HL, Ling Y, Li ZL, Sun LB. 2017. The Catsper channel and its roles in male fertility: a systematic review. *Reproductive biology and endocrinology : RB&E* **15**: 65.
- ter Haar E, Coll JT, Austen DA, Hsiao HM, Swenson L, Jain J. 2001. Structure of GSK3beta reveals a primed phosphorylation mechanism. *Nature structural biology* **8**: 593-596.
- Thomas GM, Frame S, Goedert M, Nathke I, Polakis P, Cohen P. 1999. A GSK3-binding peptide from FRAT1 selectively inhibits the GSK3-catalysed phosphorylation of axin and beta-catenin. *FEBS Lett* **458**: 247-251.

- Thompson O, Edgley M, Strasbourger P, Flibotte S, Ewing B, Adair R, Au V, Chaudhry I, Fernando L, Hutter H et al. 2013. The million mutation project: a new approach to genetics in *Caenorhabditis elegans*. *Genome research* **23**: 1749-1762.
- Trebichalská Z, Holubcová Z. 2020. Perfect date-the review of current research into molecular bases of mammalian fertilization. *Journal of assisted reproduction and genetics* **37**: 243-256.
- Tzur YB, Egydio de Carvalho C, Nadarajan S, Van Bostelen I, Gu Y, Chu DS, Cheeseman IM, Colaiacovo MP. 2012. LAB-1 targets PP1 and restricts Aurora B kinase upon entrance into meiosis to promote sister chromatid cohesion. *PLoS biology* **10**: e1001378.
- Urio F, Nkya S, Rooks H, Mgya JA, Masamu U, Zozimus Sangeda R, Mmbando BP, Brumat M, Mselle T, Menzel S et al. 2020. F cell numbers are associated with an X-linked genetic polymorphism and correlate with haematological parameters in patients with sickle cell disease. *British journal of haematology* **191**: 888-896.
- Varkey JP, Jansma PL, Minniti AN, Ward S. 1993. The *Caenorhabditis elegans* spe-6 gene is required for major sperm protein assembly and shows second site non-complementation with an unlinked deficiency. *Genetics* **133**: 79-86.
- Varkey JP, Muhlrud PJ, Minniti AN, Do B, Ward S. 1995. The *Caenorhabditis elegans* spe-26 gene is necessary to form spermatids and encodes a protein similar to the actin-associated proteins kelch and scruin. *Genes & development* **9**: 1074-1086.

- Venkatachalam K, van Rossum DB, Patterson RL, Ma HT, Gill DL. 2002. The cellular and molecular basis of store-operated calcium entry. *Nature cell biology* **4**: E263-272.
- Verlhac MH, de Pennart H, Maro B, Cobb MH, Clarke HJ. 1993. MAP kinase becomes stably activated at metaphase and is associated with microtubule-organizing centers during meiotic maturation of mouse oocytes. *Dev Biol* **158**: 330-340.
- Vijayaraghavan S, Stephens DT, Trautman K, Smith GD, Khatra B, da Cruz e Silva EF, Greengard P. 1996. Sperm Motility Development in the Epididymis is Associated with Decreased Glycogen Synthase Kinase-3 and Protein Phosphatase 1 Activity1. *Biology of reproduction* **54**: 709-718.
- Von Stetina JR, Orr-Weaver TL. 2011. Developmental control of oocyte maturation and egg activation in metazoan models. *Cold Spring Harb Perspect Biol* **3**: a005553-a005553.
- Wakula P, Beullens M, Ceulemans H, Stalmans W, Bollen M. 2003. Degeneracy and function of the ubiquitous RVXF motif that mediates binding to protein phosphatase-1. *The Journal of biological chemistry* **278**: 18817-18823.
- Wang M, Lin L, Shi Y, He L, Wang C, Zhu J. 2020. Structure of the FERM domain of a neural scaffold protein FRMPD4 implicated in X-linked intellectual disability. *The Biochemical journal* **477**: 4623-4634.
- Ward S. 1986. The asymmetric localization of gene products during the development of *Caenorhabditis elegans* spermatozoa. . In *Gametogenesis and the Early Embryo*, J Gall, ed (New York: AR Liss), pp 55–75.

- Ward S, Argon Y, Nelson GA. 1981. Sperm morphogenesis in wild-type and fertilization-defective mutants of *Caenorhabditis elegans*. *The Journal of cell biology* **91**: 26-44.
- Ward S, Burke DJ, Sulston JE, Coulson AR, Albertson DG, Ammons D, Klass M, Hogan E. 1988. Genomic organization of major sperm protein genes and pseudogenes in the nematode *Caenorhabditis elegans*. *Journal of molecular biology* **199**: 1-13.
- Ward S, Carrel JS. 1979. Fertilization and sperm competition in the nematode *Caenorhabditis elegans*. *Developmental Biology* **73**: 304-321.
- Ward S, Hogan E, Nelson GA. 1983. The initiation of spermiogenesis in the nematode *Caenorhabditis elegans*. *Dev Biol* **98**: 70-79.
- Wassarman PM, Litscher ES. 2008. Mammalian fertilization: the egg's multifunctional zona pellucida. *The International journal of developmental biology* **52**: 665-676.
- Watanabe Y, Nurse P. 1999. Cohesin Rec8 is required for reductional chromosome segregation at meiosis. *Nature* **400**: 461-464.
- Wei Y, Reveal B, Reich J, Laursen WJ, Senger S, Akbar T, Iida-Jones T, Cai W, Jarnik M, Lilly MA. 2014. TORC1 regulators Iml1/GATOR1 and GATOR2 control meiotic entry and oocyte development in *Drosophila*. *Proc Natl Acad Sci U S A* **111**: E5670-E5677.
- Whitten SJ, Miller MA. 2007. The role of gap junctions in *Caenorhabditis elegans* oocyte maturation and fertilization. *Dev Biol* **301**: 432-446.
- Woo SH, Lukacs V, de Nooij JC, Zaytseva D, Criddle CR, Francisco A, Jessell TM, Wilkinson KA, Patapoutian A. 2015. Piezo2 is the principal

- mechanotransduction channel for proprioception. *Nature neuroscience* **18**: 1756-1762.
- Woo SH, Ranade S, Weyer AD, Dubin AE, Baba Y, Qiu Z, Petrus M, Miyamoto T, Reddy K, Lumpkin EA et al. 2014. Piezo2 is required for Merkel-cell mechanotransduction. *Nature* **509**: 622-626.
- Woodgett JR. 1990. Molecular cloning and expression of glycogen synthase kinase-3/factor A. *The EMBO journal* **9**: 2431-2438.
- Wu J, Lewis AH, Grandl J. 2017. Touch, Tension, and Transduction - The Function and Regulation of Piezo Ion Channels. *Trends Biochem Sci* **42**: 57-71.
- Wu JC, Go AC, Samson M, Cintra T, Mirsoian S, Wu TF, Jow MM, Routman EJ, Chu DS. 2012. Sperm development and motility are regulated by PP1 phosphatases in *Caenorhabditis elegans*. *Genetics* **190**: 143-157.
- Xia W, Wolfe MS. 2003. Intramembrane proteolysis by presenilin and presenilin-like proteases. *Journal of cell science* **116**: 2839-2844.
- Yang HY, Mains PE, McNally FJ. 2005. Kinesin-1 mediates translocation of the meiotic spindle to the oocyte cortex through KCA-1, a novel cargo adapter. *The Journal of cell biology* **169**: 447-457.
- Yeromin AV, Zhang SL, Jiang W, Yu Y, Safrina O, Cahalan MD. 2006. Molecular identification of the CRAC channel by altered ion selectivity in a mutant of Orai. *Nature* **443**: 226-229.
- Yi K, BATTERY SM, Stewart M, Roberts TM. 2007. A Ser/Thr kinase required for membrane-associated assembly of the major sperm protein motility apparatus in the amoeboid sperm of *Ascaris*. *Molecular biology of the cell* **18**: 1816-1825.

- Yi K, Wang X, Emmett MR, Marshall AG, Stewart M, Roberts TM. 2009. Dephosphorylation of major sperm protein (MSP) fiber protein 3 by protein phosphatase 2A during cell body retraction in the MSP-based amoeboid motility of *Ascaris* sperm. *Molecular biology of the cell* **20**: 3200-3208.
- Zarkower D. 2006. Somatic sex determination. *WormBook : the online review of C elegans biology*: 1-12.
- Zevian SC, Yanowitz JL. 2014. Methodological considerations for heat shock of the nematode *Caenorhabditis elegans*. *Methods (San Diego, Calif)* **68**: 450-457.
- Zhang SL, Yu Y, Roos J, Kozak JA, Deerinck TJ, Ellisman MH, Stauderman KA, Cahalan MD. 2005. STIM1 is a Ca²⁺ sensor that activates CRAC channels and migrates from the Ca²⁺ store to the plasma membrane. *Nature* **437**: 902-905.
- Zhu GD, L'Hernault SW. 2003. The *Caenorhabditis elegans* spe-39 gene is required for intracellular membrane reorganization during spermatogenesis. *Genetics* **165**: 145-157.

Appendix

1. List of Primers

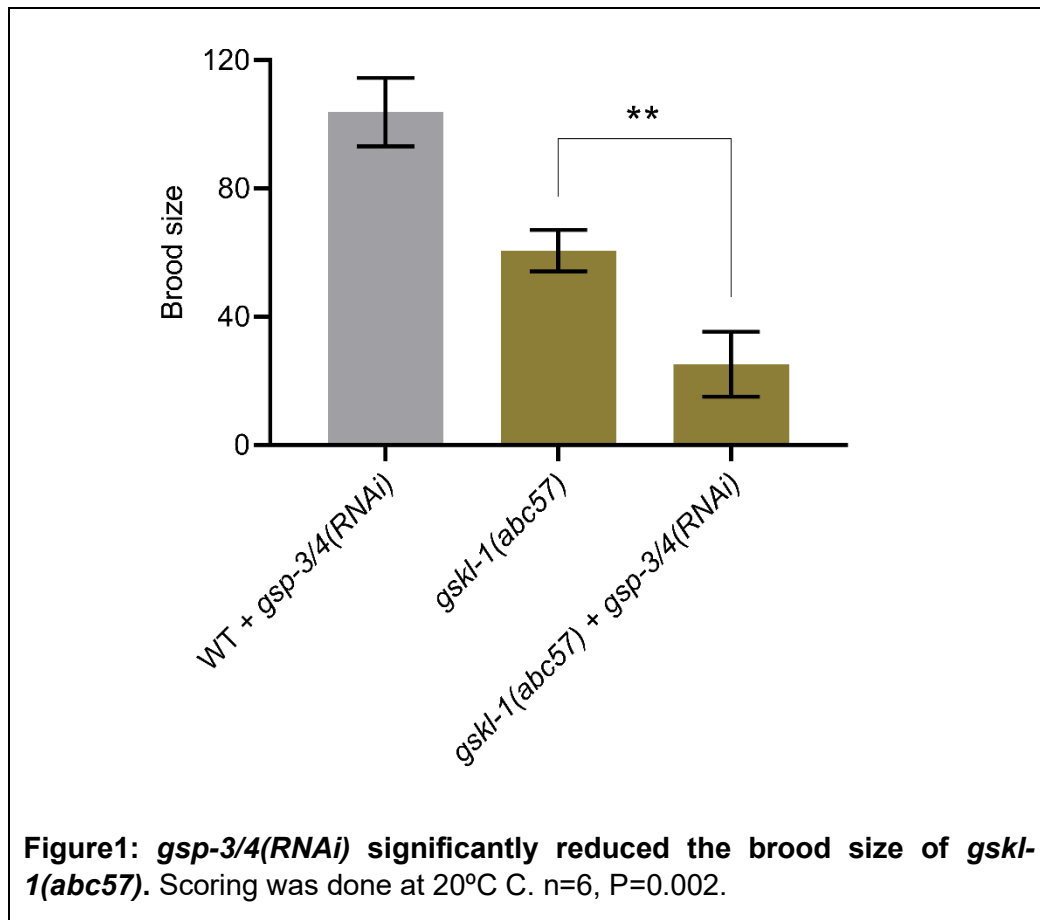
Primer name	Sequence	Annealing temperature
abc57 F1	CGG AAA CAC GCA ACT AGT GAA	56°C
abc41 F1	GCA ATT TGT GTG GCG TTT G	56°C
abc51 F1	TCC AAA TTG TGT TGA TAA CTG G	56°C
abc59 F1	TTT TCA GAT ATC CTA CAG ACG	56°C
R03D7.5(tm4146) Fwd1	ACG TGC CAC ATC GAA CGA TT	56°C
R03D7.5(tm4146) Rev1	CGC GCG TGT GTA CTT CTC GT	56°C
C44H4.6(tm5959) Fwd1	GTC GAG AAC TTA CCA TCA TG	56°C
C44H4.6(tm5959) Rev1	GCC TTC GAA TGC CGA GTG AA	56°C
F21F3.2(tm4021) Fwd1	GCA CGT TCA ACG CTG ACT CT	56°C
F21F3.2(tm4021) Rev1	ATG CTA ACC GGG ATA AGA GT	56°C
gsk3(tm1237) Fwd1	ATG GAT CAT TCG GAG TGG TA	56°C
gsk3(tm1237) Rev1	GAG ATC AAT CGC TTC AGC AG	56°C
Y106G6D.4(tm4165) Fwd1	CTA CGG ATG TTC ACA GCT TA	56°C
Y106G6D.4(tm4165) Rev1	GCC CAT TCT TGG TTC TCA GT	56°C
gsk3(tm2223/+) Fwd1	GCC CGG CAC TAT TCG AAG CA	56°C
gsk3(tm2223/+) Rev1	CGT CGG CGT ATA CTC GAT AA	56°C
gsp4(tm5415) Fwd1	GAC GAA AGT ACA GAC CAT GT	56°C
gsp4(tm5415) Rev1	ATT CTT GCG ACG GAC ACG AG	56°C
RB1034 deletion F1	ACG TCT CCC GAT TTC ACA GC	56°C
RB1034 deletion R1	AAA GGA GGC CAA GGC AGA AG	56°C
RB1034 F1	ACC GAT GTC TGT TGA AAG CC	58°C
RB1034 R1	CGA TCT CTT TGG AAA CTC GC	58°C

gsk-3(tm1237) F-2	CGT ACT ACG ATC AGA AAG TG	56°C
gsk-3(tm1237) R-2	CCG AGA CGT CGG CGT ATA CT	56°C
F21F3.2(tm4021) F-2	AGC TTA GCA CGT TCA ACG CT	56°C
F21F3.2(tm4021) R-2	CGA TCG TCA GAG CTG TCC TC	56°C
gsp-3 F Primer 1	TAC GAT TCT TGC GAC GGA CG	56°C
gsp-3 R primer 1	TCT CAT TTG GTT GGT TGG TTG G	56°C
tm2789 F Primer 1	AAA GAC CTG GCC GCG TCA CA	56°C
tm2789 R Primer 1	AGT ACG GAT GAG TGA GAA TC	56°C
tm3228 F Primer 1	GCA GAA GCA TGG GTT CCG AG	56°C
tm3228 R Primer 1	CAC ATC ACT TGA CCT TGC GA	56°C
R03D7.5 Cas9 Digest F1	CGG CAA AGA AAC AAA GTG TCG	56°C
R03D7.5 Cas9 Digest R1	AAA GTG TAG AGC TTT GCG TCG	56°C
R03D7.5 Crispr Nested F1	TAG AAA TCT CTC TGA AAT CAA	56°C
R03D7.5 Crispr Nested R1	TAA AAT TCG CCA TTA TTC TTG	56°C
swm-1 F. Primer	TGC ATC GTT GCT GTT GCT ACC	56°C
swm-1 R. Primer	TGC ATC TGA GTC CAT GAC G	56°C
swm-1 sequencing primer	TGA GGA GCT GGT ATC GTG C	56°C
swm-1 sequence primer2	ATG TGA AGC CAA TGA GGA GC	56°C
smz tm3228-EF1	GCA GAA GCA TGG GTT CCG AG	60°C
smz tm3228-ER1	CAC ATC ACT TGA CCT TGC GA	60°C
smz tm3228-IF1	CGA GAT CTG TAT CGA TAT GG	60°C
smz tm3228-IR1	TGC GAA GAG CTT TTC CCT CA	60°C
3XFLAG-I for R03D7.5-F	GAC TAC AAA GAC CAT GAC GGT G	56°C
gsp-3(tm1647) F1	CCT CCA TCC AAC AGA ATG CA	56°C
gsp-3(tm1647) F2	CAT GCT TTC CTT GTC GTA CG	56°C

gsp-3(tm1647) R1	GAA ACT ATT CAG CCC GCG TT	56°C
gsp-3(tm1647) R2	AGC CCG CGT TTT CAG GGG AT	56°C
spe-11 screening F1	TCC GTC AAC CGG CAA ATA A	56°C
spe-11 screening R4	AGC TCC AAA GAA CCT CAG AAC	56°C
spe-11 screening F2	CTC CTG CTT CCT GAT ACA ATC C	56°C
spe-11 screening R2	GTC GGG TTA CCT GCT TTC TT	56°C
F1_Ola	AGC TCG GAC CAC GTC TCA TG	58.5°C
R1_gska3_Ola	ATT TGG TGG TTG GAT TCT GTG C	58.5°C
F3_gska3	ATC AAG ATG CCC TAG TTA GGA G	58.5°C
mbk-2 cr_screen F1	CAG GTA ATC AAG GCA TTC GAT C	56°C
mbk-2 cr_screen R1	ATG TGG CCG TGC AAT AAC GTG	56°C
mbk-2 cr Sequencing	CAA GTG CAT CAC GTT TGA GC	56°C
SphI RE Control F1	ATG ACA CCG CAT TCC TGA AG	56°C
SphI RE Control R1	TGG TGC GTT CAT CAC CGA C	56°C
ceh-18 F1	CCA CAC CAG TTT CCA CAA ATG	56°C
ceh18 R1	TAT AGA TCC GAG CAG CCG TC	56°C
frm-8 deletion F1	AAT TTG GAA TCA GCT CAC GG	56°C
frm-8 deletion R1	AGC CAC CAT TTT GAA TTT CG	56°C

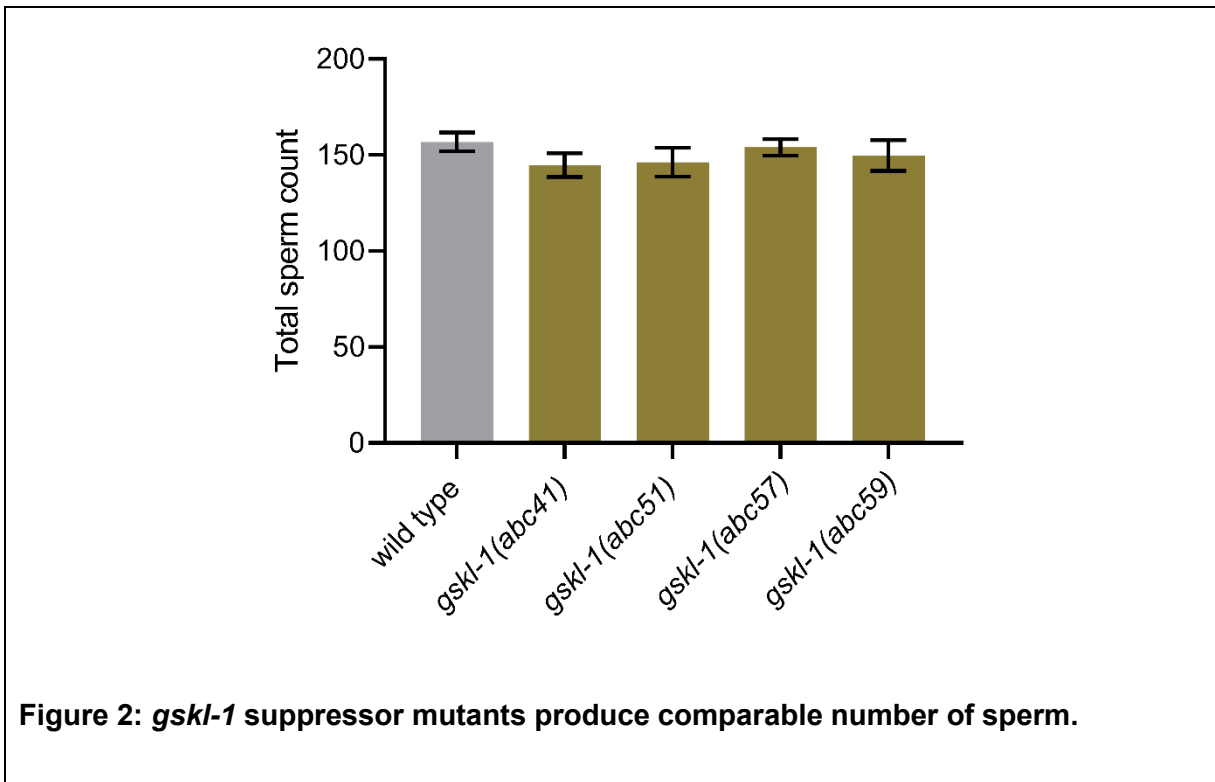
2. Effect of *gsp-3/4(RNAi)* on *gskl-1* suppressor mutants

In order to test the genetic interaction between *gsp-3/4* and *gskl-1*, I initially did *gsp-3/4(RNAi)* on *gskl-1(abc57)* and *gskl-1(abc41)* suppressor mutants. The suppressor mutant *abc57* showed a significantly lower brood size when treated with *gsp-4* dsRNA by feeding, in comparison to *gsp-4(RNAi)* alone. Due to a low sample size, it was not possible to make a conclusion about the brood size of *abc41* with *gsp-4(RNAi)*.



3. Sperm numbers are not decreased in *gskl-1* suppressor mutants

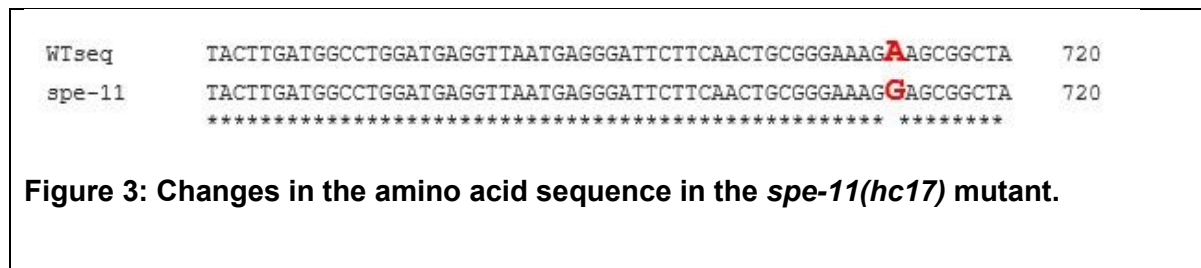
All four *gskl-1* suppressor mutants produced small but significantly lower brood size. I used the *gskl-1(abc57)* and *gskl-1(abc41)* hermaphrodites labelled with mCherry::histone to count their total sperm number. Young worms were picked into 7 μ l of egg buffer containing 5 mM tetramisole hydrochloride. This was done to immobilize the worms prior to imaging. Once the worms stopped moving (typically 10 minutes), the cover slip was inverted onto a 2% agarose pad. Fluorescent images of 14 planes, spaced 0.5 μ m apart using a 60X oil (NA 1.42) objective lens with an Olympus IX81 spinning disc confocal inverted microscope. Then images were analyzed to count the sperm numbers on the basis of fluorescence signal.



4. *spe-11* does not suppress *memi-1(sb41)*

Prior to this study, *spe-11* was the only known sperm component that displayed a role in controlling female meiosis II in *C. elegans*. The *gskl-2(Δ); gskl-1(Δ)* defective embryos resulted in embryonic phenotypes that resembled the *spe-11* mutant embryos; however, the phenotypes were not similar enough to conclude identical embryonic functions for these genes.

Next, I sought to determine if the loss of *spe-11* suppresses *memi-1(sb41)*. In order to do this experiment, I obtained *spe-11(hc17)* allele from the CGC. I found that *spe-11(hc17)* causes a A712G missense mutation. This *spe-11(hc17)* mutation causes paternal-effect lethality at 25°C. Hence, I did this experiment at 20°C.



I used *memi-1(sb41)* males to mate to *spe-11(hc17)* hermaphrodites. From the F1 trans heterozygotes, I picked up 60 mCherry positive worms and transferred them to 20°C to test for suppression. I found 4 of them were homozygous for both *spe-11(hc17)* and *memi-1(sb41)*. None of them produced any viable progeny.

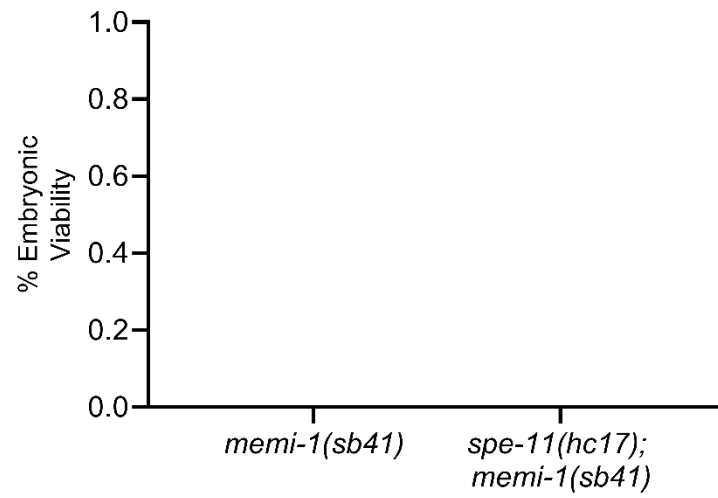


Figure 4: *spe-11(hc17)* does not suppress *memi-1(sb41)* at 20°C.

5. Knockdown of MFP-2 by RNAi does not suppress *memi-1(sb41)*

The phenotypes associated with *gskl-2*(Δ); *gskl-1*(Δ) double mutants, and the subcellular location of GSKL-1/GSKL-2 in the sperm pseudopod raises the possibility that these kinases could regulate MSP dynamics. My data indicates that treadmilling competent MSP might be required for the post-fertilization signal to activate the MEMI pathway. MSP has the target site for GSKL-1/GSKI-2 and these kinases might directly phosphorylate MSP. In that case, knockdown of MSP by RNAi should suppress the *memi-1(sb41)*. Unfortunately, this idea is not possible to test as MSP has more than 40 genes.

The data from *Ascaris* indicate that phosphorylation and dephosphorylation of accessory proteins is likely key to involve *in vivo* regulation of MSP fibre dynamics. The *Ascaris* proteins seem to have homologs in *C. elegans*, and it was shown recently that *C. elegans* MFP1 and MFP2 co-localize with MSP in the pseudopod (Morrison et. al. 2021). The accessory protein MFP-2 (encoded by *nsph-2* and *nsph-3.2*) also contains putative GSK-3 target sites. I did *nsph-2*(RNAi) and *nsph-3*(RNAi) on *memi-1(sb41)* worms to see if that would suppress *memi-1(sb41)*. I put young L4 *memi-1(sb41)* worms on RNAi plates and I found no significant suppression at 25°C.

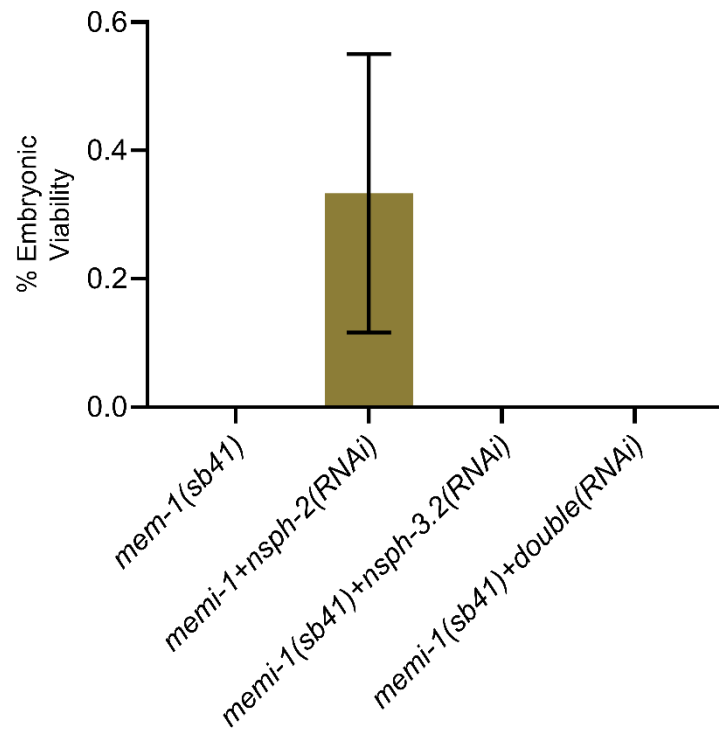
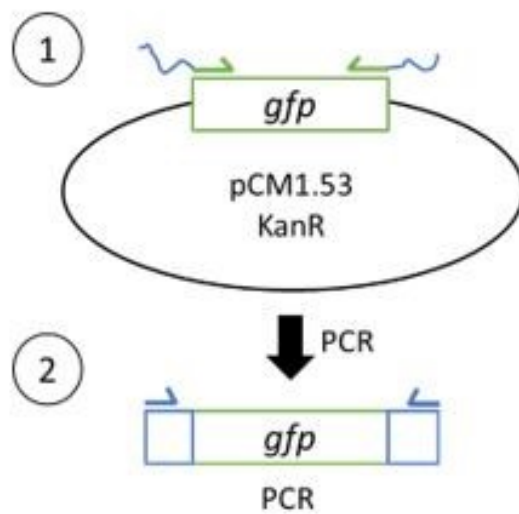


Figure 5: Knockdown of MFP by RNAi does not suppress *memi-1(sb41)*.

6. Preparing *gfp* repair template for Crispr injection

In order to prepare repair template to insert *gfp* at the 5 prime end of *gskl-1*, I extracted pCM1.53 DNA. Then, I amplified *gfp* with the primers that had *gskl-1* overhangs as displayed (1). Subsequently, nested primers were used to amplify *gskl-1* with *gfp* as displayed (2).



7. Sperm purification from males

There is no evidence currently available supporting the idea that MSP is phosphorylated in activated sperm. In order to test this, I used *swm-1* mutant males, which contain constitutively active sperm. I followed the standard protocol of sperm isolation with some modification (Miller. 2006). Briefly, worms were grown in 10 large “egg” plates, which contain normal OP50 mixed with fresh egg. When worms reached the dauer stage, I washed them off and made a concentrated stock of 30 ml of worms. This was distributed equally in 10 new large plates and kept at 20°C. After one day to allow worms to reach the adult stage, I washed those worms off from those plates and made a concentrated stock of 15 ml. Then that stock was transferred through a 35 µm filter to collect only males. Hermaphrodites can not pass through the 35 µm filter due to their larger size.

The worms were ruptured using a French press at 7000 psi, however, it destroyed not only the worms, but also the sperm. As an alternative to the French press, the worms were grown again as in the previous paragraph, but subjected to chopping with razor blades. Then the sperm suspension was passed through 5 µm filters to collect the sperm. Next, the sperm suspension was centrifuged at 13000 g for 5 minutes to collect the sperm pellet. The supernatant was discarded and the remaining suspension was centrifuged one more time at 3500 g. Then the tube with the sperm pellet was dipped into liquid nitrogen for 15 seconds and the sample was stored at -80°C. This sample can be used for mass spectrometry analysis.